Advances
in Clinical and Experimental Medicine

WROCLAW
MEDICAL UNIVERSITY

Advances
in Clinical and Experimental Medicine

Editorial Policy

Contents

Bioavailability of ursolic/oleanolic acid, with therapeutic potential in chronic diseases and cancer

Vasile Staicu[A,B,D], Justinian-Andrei Tomescu[C,E], Ioan Calinescu[E,F]

Department of Bioresources and Polymer Sciences, Faculty of Chemical Engineering and Biotechnologies, National University of Science and Technology, Bucharest, Romania

A – research concept and design; B – collection and/or assembly of data; C – data analysis and interpretation;
D – writing the article; E – critical revision of the article; F – final approval of the article

Address for correspondence
Vasile Staicu
E-mail: vasile.staicu@yahoo.ro

Abstract

This study focused on describing the bioavailability of ursolic/oleanolic acids (UA/OA) and the methods to increase it, so that these 2 bioactive compounds can have therapeutic and preventive effects in chronic diseases and cancer. Ursolic/oleanolic acids are natural compounds that have been known since the 19th century. They are very widespread and offer special benefits for human health — especially that their high absorbability makes them suitable for use in therapeutic and preventive treatment. One of the important aspects of their bioavailability is related to their interaction with other bioactive compounds or drugs. In chronic diseases and cancer, UA/OA may affect the absorption of other nutrients and interact with bioactive compounds. By increasing the bioavailability of UA/OA with various technical processes, especially using nanocarriers and nanoparticles, these compounds can affect collagen production, contributing to maintaining skin elasticity and preventing the appearance of wrinkles. Today, UA/OA are frequently used to treat many conditions, ranging from chronic to metabolic.

Key words: cancer, chronic diseases, bioavailability, ursolic acid, oleanolic acid

Introduction

Bioavailability is defined as the percentage (fraction) of an orally administered, unchanged dose of a drug that has reached the bloodstream (systemic circulation) or, more simply: bioavailability, is the fraction of an orally administered drug that reaches the systemic circulation.

Wagner[1] defined bioavailability as a drug-specific, orally administered parameter that defines both the amount of active substance released from the drug and absorbed into the bloodstream (systemic circulation) and the rate at which the active substance is released and absorbed.

The World Health Organization (WHO) defines bioavailability as the amount of absorbable (potential) active substance, while the U.S. Food and Drug Administration (FDA)[2,3] as the amount of active substance that is released, absorbed and reaches the internal organ, the site of action, and manifests its therapeutic effect. The American Pharmaceutical Association (APA)[4] describes bioavailability as the amount of active substance absorbed unchanged. Therefore, bioavailability is seen as both the amount of active substance released and absorbed, and the rate at which the active substance is released and absorbed, getting to the site of action, thus manifesting its therapeutic effect. This parameter is a key step in ensuring the biological efficacy of bioactive food compounds or oral medicines. Food bioactive compounds, whether from plant or animal sources, must be bioavailable to exert beneficial effects on human health.

Numerous plant compounds provide multiple benefits for human health, among which ursolic/oleanolic acids (UA/OA) play an important role. One of the essential aspects of UA/OA is their bioavailability, i.e., the ability to be efficiently absorbed, used and eliminated by the body. Despite its pentacyclic structure, the UA/OA molecule can be embedded in lipid nanoparticles to ensure its transport and digestion in the small intestine, metabolism in the liver, entry into the systemic circuit, and interaction with other substances.

Ursolic and oleanolic acids are primarily absorbed in the small intestine and can subsequently circulate throughout the body, reaching all tissues and organs. This is due to the entry of these compounds into the systemic and enterohepatic circulation. The enterohepatic communication pathway is essential for the UA/OA to reach different organs, and exert beneficial effects in various diseases. Low oral bioavailability, demonstrated in some clinical studies, is a major reason why new drugs researched and proposed for approval fail to reach the market.

In this article, we reviewed the practical ways of incorporating UA/OA into inorganic/organic structures and nanoparticles to increase their absorption (bioavailability). Natural plant compounds are an important source of raw materials for obtaining drugs and food supplements with antitumor effect, with a selective mechanism of action and minimal side effects. Ursolic acid and its isomer, OA, are 2 natural compounds with multiple health benefits. The chemical structure of UA/OA is pentacyclic triterpenic, with the following formula: $C_{30}H_{48}O_3$ (Fig. 1).[5]

Plants rich in UA

Ursolic acid is found in the peel of many fruits, especially apples, but also in herbs such as rosemary, lavender, thyme, sage, marigolds, etc. Oleanolic acid is found in large quantites in rosemary, lavender, sage, and olive. Table 1[6-10] shows that:

– The best represented plant family in terms of the UA/OA presence is Lamiaceae-Labiatae (66%);

– The highest amounts of UA are found in marigold flowers, rosemary, sage, and lavender (aerial parts);

– The highest amounts of OA are found in olives (leaves and fruits) and *Silphium trifoliatum* leaves (rich in UA and OA; Fig. 2).[11]

Discussion

The presence of UA/OA in fruits and plants offers the potential for a wide range of therapeutic effects due to a unique quality of these compounds, namely their bioavailability. This parameter of UA/OA has a significant impact on the use of this compounds in therapeutic and preventive purposes.
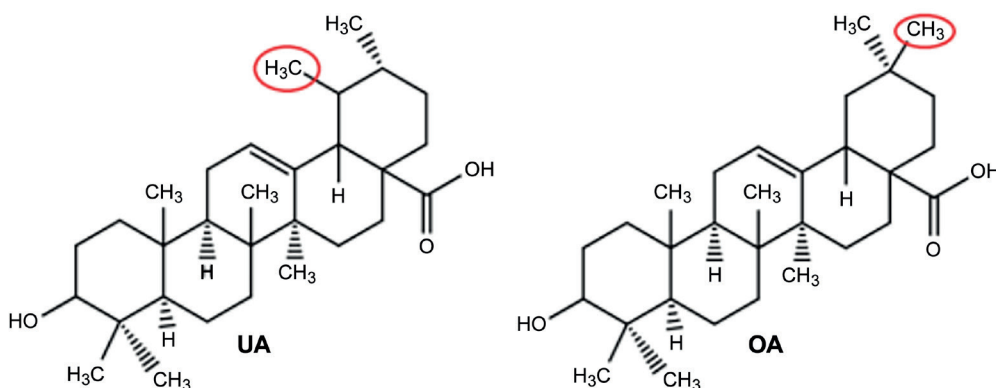
Fig. 1. Chemical structure of ursolic/oleanolic acid, isomers differentiated by the position of the methyl group[5]

Table 1. Natural sources for UA and OA [mg/g dw][1]

Plan species	Family	Plant part	OA [mg/g dw]	UA [mg/g dw]	Reference
Marigold, *calendula officinalis*	Compositae	flowers	–	20.5	[6]
Whorled Rosinweeds, *Silphium trifoliatum*	Asteraceae	leaves	22.0	15.5	[6]
Lavender, *lavandula angustifolia*	Lamiaceae, Labiatae	aerial parts	4.5	15.9	[7]
Lemon balm, *mellisa officinalis*	Lamiaceae, Labiatae	aerial parts	1.6	6.7	[7]
Basil, *ocimum basilicum*	Lamiaceae, Labiatae	aerial parts	–	3.0	[7]
Marjoram, *origanum majorana*	Lamiaceae, Labiatae	aerial parts	1.9	6.6	[7]
Oregano, *origanum vulgare*	Lamiaceae, Labiatae	aerial parts	–	2.8	[7]
Sage, *salvia officinalis*	Lamiacea, Labiatae	aerial parts	6.7	18	[7]
Thyme, *thymus vulgaris*	Lamiaceae, Labiatae	aerial parts	3.7	9.4	[7]
Mountain savory, winter savory, *satureja montana*	Lamiaceae, Labiatae	aerial parts	1.4	4.9	[7]
Black elderberry, *sambucus nigra*	Adoxaceae	leaves bark	1.2 0.8	5.8 3.2	[7]
Olive, *olea europaea*	Oleaceae	leaves fruits bark	31.0 21.0 9.8	3.8	[7]
Apple, *malus domestica*	Rosaceae	the peel of the fruit	–	9.4	[8]
Deulkkae, Korean perilla, japanese basil, *Perilla frutescens*	Lamiaceae, Labiatae	aerial parts	2.33	3.59	[9]
Rosemary, *rosmarinus officinalis*	Lamiaceae, Labiatae	aerial parts	7.98	16.06	[10]

UA – ursolic acid; OA – oleanolic acid; DW – dry weight.

Fig. 2. *Silphium trifoliatum* (whorled rosinweed)[7]

Oral bioavailability (F%) is the fraction of a medicine that reaches the systemic circulation.[8] Bioavailability of orally administered drugs is one of the most important properties in drug design and development. High oral bioavailability consistently reduces the amount of drug administered to achieve the desired pharmacologic effect, and poor oral bioavailability can result in decreased efficacy and unpredictable response to drug administration.[12,13]

In the context of dietary supplements, herbs and other nutrients, where the route of administration is typically oral, bioavailability refers to the amount or percentage of the ingested dose that is absorbed.[14] A significant amount of the active ingredient is broken down during digestion when herbal supplements are taken orally. The acidic environment in the stomach, digestive enzymes and gut microbes break down nutrients. As a result, only a small fraction of the ingested nutrients become available for absorption and used by cells.[15]

Bioavailability studies have shown that UA/OA are absorbed primarily in the small intestine. Once in the systemic circuit, these biocompounds can circulate and reach various tissues of the human body, including the liver, skin and muscles. The highly bioavailable form in which UA/OA is administered must be the form that makes them easy for the body to use. The molecular details of how UA/OA are absorbed in the body can be clarified by conducting several studies regarding their oral administration. A practical possibility would be the absorption of UA/OA directly from the ethanolic extract on natural carbonic adsorbents (herbal medicinal charcoal) or their adsorption into the molecular lattice of natural biopolymers (such as lignans in flaxseed meal) using the molecular imprinting method.[16–18] Natural polymers have a much higher adsorption capacity and specificity in ethanol than in water at pH 7.0. Another practical way to increase the bioavailability of UA/OA

is to incorporate them into a nanocarrier lipid fraction (liposomes), which facilitates the transport and digestion of these compounds in the small intestine and their metabolism in the liver, since digestion in the stomach degrades these compounds due to the acidic environment of the stomach, digestive enzymes and intestinal microbes. In this case, only a part of the total compounds that we ingest becomes available for their metabolism in the intestine and the liver, and thus for absorption and use at the cellular level. Liposomes make the UA/OA easy to use by the organism. Another practical way is to get some UA/OA inclusion complexes with hydrophilic semisynthetic cyclodextrins, which represent a possibility to increase the aqueous solubility and to optimize the pharmacokinetic properties of the guest molecule.[19] Another theoretical and practical possibility is the derivatization of UA/OA by a condensation reaction (at the COOH group, C_{28}) with a primary amino group present in the structure of 3-R-4-amino-mercapto-1,2,4-triazoles and the use of gold nanoparticles as transporters, for the compounds thus produced.[20] Finally, triazole derivatives of triterpenic acids (UA/OA) bioconjugated with gold particles are obtained, with a cytotoxic effect on malignant melanoma cell lines. Another practical possibility by which a maximum bioactivity of UA/OA can be obtained, with the minimum amount of triterpenes used, is the use of inorganic nanostructures (complex nanostructures, composites, silicon oxide, titanium oxide, etc.) for the incorporation (adsorption) of UA/OA. The inorganic nanostructures have a large surface area, inhibit bacterial growth, are stable, have low toxicity, and are capable of activating many molecules.[21–24] As indicated above,[20] in addition to bioavailability, research has also focused on how UA/OA act in the body. In this regard, studies have found that UA/OA have anti-inflammatory, antioxidant and anti-cancer properties. They can help lower blood cholesterol and fat levels by influencing lipid metabolism. These multiple effects make UA/OA potential allies in the prevention and treatment of cancer, cardiovascular disease and chronic inflammation, in cosmetic applications (these compounds can influence collagen production, helping maintain skin elasticity and prevent the appearance of wrinkles), and sometimes as ingredients in the food industry.[25–29] The bioavailability of UA/OA is a crucial aspect in understanding and exploiting their benefits and their ability to be efficiently absorbed, circulate in the body and interact with other substances. This demonstrates remarkable potential for improving human health. Laboratory studies have shown that UA/OA may inhibit the growth of cancer cells in several types of cancer, including stomach, colon, pancreatic, and liver cancer.[30,31] Ursolic/oleanolic acids inhibit the viability and proliferation of cancer cells, prevent their migration and metastasis, and induce their apoptosis. Both in vitro and in vivo studies indicate that UA/OA are promising anti-cancer agents that may prevent

carcinogenesis at every step. Furthermore, cancers at all stages are susceptible to the UA/OA activity. The anti-tumorigenic effect of UA/OA on gastric, colon, pancreatic, and liver cancers, as well as the mechanisms underlying this process, have already been presented.[30] Furthermore, other authors have showed the antitumor effects of UA/OA in vitro with gastric cancer cell line BGC-823.[31]

Ursolic/oleanolic acids induce apoptosis, inhibit cancer cell proliferation and prevent tumor growth and metastasis. Nanoformulations with UA/OA and their bioavailability have a very good inhibitory effect preventing tumor growth and metastasis.[32] Zou et al.[32] reviewed the great potential of UA as a drug candidate in the field of cancer therapy in terms of suppressing tumor initiation, progression and metastasis.

Due to their cytotoxicity against cancer cell cultures, the group of triterpenoid derivatives of UA/OA is considered a promising anticancer drug. In addition, due to their various pharmacological activities, including antiangiogenic, anti-inflammatory and antioxidant effect and their ability to improve cell differentiation, they are more than just an anticancer drug. The group of triterpenoid derivatives of UA/OA is indicated and suitable for future modern anticancer strategies. Furthermore, they are considered essential parts of human nutrition due to their chemopreventive potential to combat the development of cancer.[33] Ursolic acid is a promising biomolecule with anti-inflammatory and analgesic activity, in applications with anti-arthritic potential, as presented in the study by Ahmad et al.[34] In this study, formulations and evaluations of nanostructured lipid carriers with *Ocimum sanctum* L. (holy basil) were described, for a transdermal application, improved in UA, in anti-arthritic treatment.

The *Ocimum sanctum* leaf extract was prepared by the extraction method with supercritical CO_2. Various surfactants (Tween 80), solid lipids (glyceryl monostearate) and liquid lipids (Capryol-90) have been used to prepare nanostructures loaded with *Ocimum sanctum* (Fig. 3; visual representation of the technological flow).[35,36] The resulting nanoparticles facilitate the transport of *Ocimum sanctum* through tissues via passive or active targeting. Passive targeting involves diffusion into transdermal tissue, while active targeting involves conjugation of ligands (mannitol) to nanoparticles for greater specificity and absorption at the site of inflammation. The results demonstrated the efficiency of treatment with lipid nanostructures compared to the standard formulation with diclofenac topical gel, in antiarthritic applications.

Conclusions

The bioavailability of UA/OA can be shaped by their interactions with other substances or bioactive compounds, such as certain receptors or proteins in the body, which can modify or amplify the effects of UA/OA. For instance,
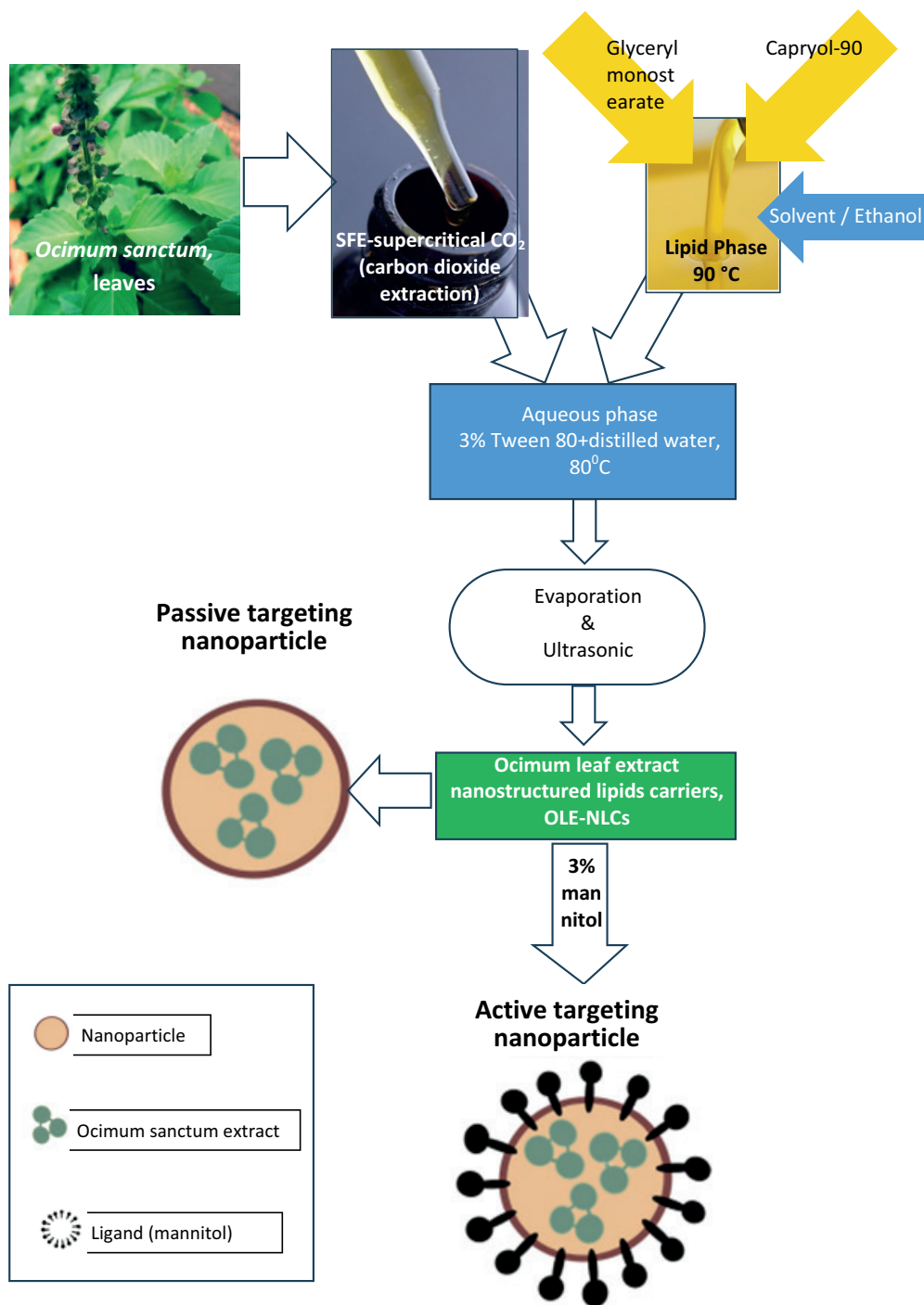
Fig. 3. Obtaining lipid nanostructures loaded with *Ocimum sanctum* leaf extract[35,36]

interactions with plant flavones can create synergies that enhance human health benefits by increasing the antioxidant, anti-inflammatory and anticancer activity of these plant compounds. The availability of these acids in the body creates promising perspectives in the fields of human health. It is essential to continue research to fully understand their potential and to develop practical applications in medicine. Establishing the optimal dosage of UA/OA is essential for their use in long-term treatment programs. Additional studies may provide guidance on appropriate dosing and can evaluate side effects and potential interactions of UA/OA with other substances and metabolites.

ORCID iDs

Vasile Staicu ⓘ https://orcid.org/0000-0003-4409-1146
Justinian-Andrei Tomescu ⓘ https://orcid.org/0000-0002-3412-631X
Ioan Calinescu ⓘ https://orcid.org/0000-0003-4141-6697

References

1. Wagner JG. *Biopharmaceutics and Relevant Pharmacokinetics*. Washington, D.C, USA: Drug Intelligence Publications; 1971. ISBN:978-0-914768-18-0.
2. U.S. Food and Drug Administration (FDA). Guidance for Industry: Immediate Release Solid Oral Dosage Forms, Scale-Up and Post-Approval Changes: Chemistry, Manufacturing and Controls, In Vitro Dissolution Testing and in Vivo Bioequivalence Documentation. Rockville, USA: U.S. Food and Drug Administration (FDA); 1995. https://www.fda.gov/media/70949/download.

3. U.S. Food and Drug Administration (FDA). Guidance for Industry: Dissolution Testing of Immediate Release Solid Oral Dosage Forms. Rockville, USA: U.S. Food and Drug Administration (FDA); 1997. https://www.fda.gov/media/70936/download.

4. United States Pharmacopoeial Convention. *The United States Pharmacopoeia*. 30th ed. Rockville, USA: US Pharmacopoeial Convention Inc. 2007.

5. Gudoityte E, Arandarcikaite O, Mazeikiene I, Bendokas V, Liobikas J. Ursolic and oleanolic acids: Plant metabolites with neuroprotective potential. *Int J Mol Sci*. 2021;22(9):4599. doi:10.3390/ijms22094599

6. Kowalski R. Studies of selected plant raw materials as alternative sources of triterpenes of oleanolic and ursolic acid types. *J Agric Food Chem*. 2007;55(3):656–662. doi:10.1021/jf0625858

7. Jäger S, Trojan H, Kopp T, Laszczyk MN, Scheffler A. Pentacyclic triterpene distribution in various plants: Rich sources for a new group of multi-potent plant extracts. *Molecules*. 2009;14(6):2016–2031. doi:10.3390/molecules14062016

8. Ludeña-Huaman MA, Ramos-Inquiltupa DA. Determination of the content of ursolic and oleanolic acid in the cuticular wax of fruits of different species of Rosaceae. *Rev Colomb Quim*. 2019;48(2):15–20. doi:10.15446/rev.colomb.quim.v48n2.77046

9. Staicu V. Separation and purification of plant extracts by removal of chlorophyll, xanthophylls and pigments using mineral adsorbents in liquid chromatography (CLS). *Curr Trends Eng Sci*. 2023;3(6):1046. doi:10.54026/CTES/1046

10. Staicu V. Extracte vegetale si valorificarea lor. Obtinerea compusilor bioactivi din deseuri vegetale si plante medicinale cu ajutorul ultrasunetelor si microundelor, Facultatea de inginerie chimica si biotehnologii [doctoral thesis]. Bucharest, Romania: National University of Science and Technology; 2023.

11. Kowalska G, Baj T, Kowalski R, Hanif MA. Characteristics of selected *Silphium* species as alternative plants for cultivation and industry with particular emphasis on research conducted in Poland: A review. *Sustainability*. 2022;14(9):5092. doi:10.3390/su14095092

12. Hinderliter P, Saghir SA. Pharmacokinetics. In: Wexler P, ed. *Encyclopedia of Toxicology*. 3rd ed. London, UK: Academic Press; 2014:352. ISBN:978-0-12-386455-0.

13. Parii S, Nicolae E, Ungureanu A, Parii E, Valica V. Current aspects in the bioavailability of drugs [in Romanian]. *Revista Farmaceutica a Moldovei*. 2016;1–4:[no pages given].

14. Duan JZ. Pharmacokinetics of oral absorbtion. In: Shargel L, Yu ABC, eds. *Applied Biopharmaceutics and Pharmacokinetics*. 7th ed. New York, USA: McGraw-Hill Education; 2016:177–204. ISBN:978-0-07-182964-9.

15. Lee MK. Liposomes for enhanced bioavailability of water-insoluble drugs: In vivo evidence and recent approaches. *Pharmaceutics*. 2020;12(3):264. doi:10.3390/pharmaceutics12030264

16. Martín-Esteban A. Molecularly imprinted polymers: New molecular recognition materials for selective solid-phase extraction of organic compounds. *Fresenius J Anal Chem*. 2001;370(7):795–802. doi:10.1007/s002160100854

17. Sánchez-Barragán I, Costa-Fernández JM, Pereiro R, et al. Molecularly imprinted polymers based on iodinated monomers for selective room-temperature phosphorescence optosensing of fluoranthene in water. *Anal Chem*. 2005;77(21):7005–7011. doi:10.1021/ac050400a

18. Kim SH, Jun CD, Suk K, et al. Gallic acid inhibits histamine release and pro-inflammatory cytokine production in mast cells. *Toxicol Sci*. 2006;91(1):123–131. doi:10.1093/toxsci/kfj063

19. Soica C, Oprean C, Borcan F, et al. The synergistic biologic activity of oleanolic and ursolic acids in complex with hydroxypropyl-γ-cyclodextrin. *Molecules*. 2014;19(4):4924–4940. doi:10.3390/molecules19044924

20. Mioc M, Soica C. HeteroTerA: Proiect: Sinteza si evaluarea de noi bioconjugati de nanoparticule de aur-triazol-triterpene, utilizate ca agenti activi in melanomul malign. Contract PD, 2020. Proiect PN III-P1-1.1-PD-2019-1078. Timişoara, Romania: Victor Babeş University of Medicine and Pharmacy; 2020. http://old.umft.ro.heterotera_931. Accessed August 15, 2024.

21. Petrişor G, Motelica L, Truşcă RD, et al. The antimicrobial potency of mesoporous silica nanoparticles loaded with *Melissa officinalis* extract. *Pharmaceutics*. 2024;16(4):525. doi:10.3390/pharmaceutics16040525

22. Low SS, Lim CN, Yew M, et al. Recent ultrasound advancements for the manipulation of nanobiomaterials and nanoformulations for drug delivery. *Ultrason Sonochem*. 2021;80:105805. doi:10.1016/j.ultsonch.2021.105805

23. Low SS, Yew M, Lim CN, et al. Sonoproduction of nanobiomaterials: A critical review. *Ultrason Sonochem*. 2022;82:105887. doi:10.1016/j.ultsonch.2021.105887

24. Ealia AM, Saravanakumar MP. A review on the classification, characterisation, synthesis of nanoparticles and their application. *IOP Conf Ser Mater Sci Eng*. 2017;263:032019. doi:10.1088/1757-899X/263/3/032019

25. Stielow M, Witczyńska A, Kubryń N, Fijałkowski Ł, Nowaczyk J, Nowaczyk A. The bioavailability of drugs: The current state of knowledge. *Molecules*. 2023;28(24):8038. doi:10.3390/molecules28248038

26. Maisto M, Piccolo V, Novellino E, et al. Optimization of ursolic acid extraction in oil from Annurca apple to obtain oleolytes with potential cosmeceutical application. *Antioxidants (Basel)*. 2023;12(2):224. doi:10.3390/antiox12020224

27. Rein MJ, Renouf M, Cruz-Hernandez C, Actis-Goretta L, Thakkar SK, Da Silva Pinto M. Bioavailability of bioactive food compounds: A challenging journey to bioefficacy. *Br J Clin Pharmacol*. 2013;75(3):588–602. doi:10.1111/j.1365-2125.2012.04425.x

28. Wang L, Yin Q, Liu C, Tang Y, Sun C, Zhuang J. Nanoformulations of ursolic acid: A modern natural anticancer molecule. *Front Pharmacol*. 2021;12:706121. doi:10.3389/fphar.2021.706121

29. Ayeleso T, Matumba M, Mukwevho E. Oleanolic acid and its derivatives: Biological activities and therapeutic potential in chronic diseases. *Molecules*. 2017;22(11):1915. doi:10.3390/molecules22111915

30. Pięt M, Paduch R. Ursolic and oleanolic acids as potential anticancer agents acting in the gastrointestinal tract. *Mini Rev Org Chem*. 2018;16(1):78–91. doi:10.2174/1570193X15666180612090816

31. Xiao S, Wang W, Liu Y. Research progress on extraction and separation of active components from loquat leaves. *Separations*. 2023; 10(2):126. doi:10.3390/separations10020126

32. Zou J, Lin J, Li C, et al. Ursolic acid in cancer treatment and metastatic chemoprevention: From synthesized derivatives to nanoformulations in preclinical studies. *Curr Cancer Drug Targets*. 2019;19(4): 245–256. doi:10.2174/1568009618666181016145940

33. Laszczyk M. Pentacyclic triterpenes of the lupane, oleanane and ursane group as tools in cancer therapy. *Planta Med*. 2009;75(15): 1549–1560. doi:10.1055/s-0029-1186102

34. Ahmad A, Abuzinadah MF, Alkreathy HM, Banaganapalli B, Mujeeb M. Ursolic acid rich *Ocimum sanctum* L leaf extract loaded nanostructured lipid carriers ameliorate adjuvant induced arthritis in rats by inhibition of COX-1, COX-2, TNF-α and IL-1: Pharmacological and docking studies. *PLoS One*. 2018;13(3):e0193451. doi:10.1371/journal.pone.0193451

35. Almatroodi SA, Alsahli MA, Almatroudi A, Rahmani AH. *Ocimum sanctum*: Role in diseases management through modulating various biological activity. *Pharmacogn J*. 2020;12(5):1198–1205. doi:10.5530/pj.2020.12.168

36. Chen Q, Tan Qian Lin K, Yow Li-Wen NS, Heng S, Hui C, Chon Mun Ping A. Nanotechnology: A better diagnosis and treatment strategy for brain tumour? *J Young Invest*. 202AD;25(3):33–47. https://www.jyi.org/2022-march/2022/3/1/nanotechnology-a-better-diagnosis-and-treatment-strategy-for-brain-tumour. Accessed August 15, 2024.

Safety and efficacy of acetylcholinesterase inhibitors for Alzheimer's disease: A systematic review and meta-analysis

Yaqi Gao[1,2,A,D–F], Yulin Liu[1,B,C], Yanfang Li[1,B,E]

[1] College of Nursing, Hebi Polytechnic, Henan, China

[2] College of Health Care, Sehan University, Yeongam, South Korea

A – research concept and design; B – collection and/or assembly of data; C – data analysis and interpretation;
D – writing the article; E – critical revision of the article; F – final approval of the article

Address for correspondence
Yaqi Gao
E-mail: yaqigao01@hotmail.com

Conflict of interest
None declared

Abstract

Alzheimer's disease (AD) affects millions of people worldwide. The most commonly used drugs are acetylcholinesterase inhibitors, i.e., donepezil, galantamine and rivastigmine, which increase levels of acetylcholine. However, the exact efficacy and safety of acetylcholinesterase inhibitors in the treatment of AD is still unclear. The main objective of the current study was to determine the exact safety and efficacy profile of acetylcholinesterase inhibitors in the treatment of AD by conducting a systematic review and meta-analysis of clinical trials according to the Preferred Reporting Items for Systematic Reviews and Meta-Analyses (PRISMA) guidelines. We conducted a web-based literature search of PubMed and clinical trial websites using relevant keywords. Data were extracted from eligible records and pooled as mean difference (MD) or risk ratio (RR) values with their 95% confidence interval (95% CI) using Review Manager software (v. 5.3 for Windows). Heterogeneity was calculated using χ^2 and I^2 tests. The standard mean difference (SMD) was −0.33 [−0.52, −0.13] for donepezil, −0.48 [−0.58, −0.38] for galantamine and −0.65 [−1.06, −0.23] for rivastigmine, indicating a significant effect of these drugs on cognitive outcomes. Here we show the significant effects of all available acetylcholinesterase inhibitors on cognitive function in patients with AD. However, further studies are needed to draw valid conclusions about the effects of acetylcholinesterase inhibitors on functional outcomes and adverse events.

Key words: Alzheimer's disease, galantamine, donepezil, rivastigmine, acetylcholinesterase inhibitors

Introduction

Alzheimer's disease (AD) is a neurodegenerative disease that affects millions of peoples across the globe. Many researchers have documented the abnormal aggregation of β-amyloid in the brains of patients with AD. This abnormal aggregation leads to the activation of various inflammatory and oxidative stress signaling pathways, ultimately leading to neuronal degeneration. Structural and functional abnormalities have been observed in specific regions of the brain, particularly the hippocampus and prefrontal cortex, in patients with AD.[1–3] Mitochondrial dysfunctions also play a significant role in the neurodegenerative diseases, including AD. Tanaka et al. reviewed the functions of mitochondria in the central nervous system (CNS) and their alterations in neurodegenerative diseases.[4]

In normal brain physiology, there is a balance between excitatory and inhibitory neurotransmitters. The major excitatory neurotransmitter in the CNS is glutamate, while the major inhibitory neurotransmitter is gamma-aminobutyric acid (GABA). Glutamate acts on NMDA receptors, while GABA acts on GABA receptors. In neurodegenerative diseases, levels of excitatory neurotransmitters increase, leading to excitotoxicity.[5]

There are a number of mechanisms involved in the pathogenesis of AD. Oxidative stress is one of the major mechanisms involved in the development of AD. Under normal physiological conditions, reactive oxygen species (ROS), reactive nitrogen species (RNS), etc., are generated in mitochondria and scavenged by endogenous antioxidant enzymes such as glutathione, superoxide dismutase (SOD), catalase, etc. Overall, there is balance between generation of reactive species and anti-oxidant enzymes. However, the imbalance (increase in level of reactive species and decrease in level of endogenous antioxidant enzymes) results in the activation of oxidative stress signaling pathways.[6,7]

Increased oxidative stress results in the alteration of the mitochondrial membrane potential.[8,9] The altered mitochondrial potential causes increased expression of apoptotic proteins such as BAX and decreased expression of anti-apoptotic proteins such as Bcl-2. This imbalance activates the caspase-dependent and caspase-independent pathways, which ultimately leads to cell death.[10–15]

Reports in the literature have indicated cognitive dysfunctions in patients with AD.[15–20] The exact etiology of AD is unclear; however, it is known that there is an impairment of central cholinergic neurons in patients with AD.[21] Common AD-associated neuropsychiatric symptoms include depression, anxiety, agitation, aggression, and apathy.[22–24] Currently, very few drugs are available for the AD treatment. The majority of available drugs inhibit the enzyme cholinesterase, which is responsible for degradation of acetylcholine into choline and acetic acid. Inhibition of cholinesterase results in the increased level of acetylcholine. The well-known cholinesterase inhibitors used to treat AD are donepezil, rivastigmine and galantamine.[25] These have been used alone and in combination with memantine.[26] However, the exact efficacy and safety of acetylcholinesterase inhibitors in the treatment of AD is still unclear.

Objectives

The main objective of this study was to determine the exact safety and efficacy profile of acetylcholinesterase inhibitors in the treatment of AD by conducting systematic review and meta-analysis of clinical studies according to the Preferred Reporting Items for Systematic Reviews and Meta-Analyses (PRISMA) guidelines. The overall estimate measure was calculated in terms of standard mean difference (SMD) for continuous data, whereas the odds ratio (OR) or relative risk was calculated for dichotomous data to examine overall safety and efficacy of acetylcholinesterase inhibitors in clinical trials.

Materials and methods

Search strategy

Relevant studies were searched in PubMed from inception to October 2022. The followings MeSH terms were used: "Alzheimer disease" or "AD," "donepezil," "galantamine," and "rivastigmine," with a proper use of Boolean operators.

Selection criteria

The studies were selected based on inclusion and exclusion criteria. The inclusion criteria were as follows: 1) double-blind randomized clinical trials (RCTs) testing at least 1 acetylcholinesterase inhibitor; 2) treatment duration at least 52 weeks; 3) one of the cognitive, functional changes or adverse events were reported. Both sexes and all age groups were included. Non-randomized clinical trials, case reports, case series, narrative reviews, and meta-analyses were excluded. Studies published in languages other than English were also excluded. Two authors (YG and YL) screened the studies based on titles and abstracts. The full text of selected studies was downloaded into a folder. The quality assessment of each study was also assessed to reduce the risk of bias in the estimate of effects.

Data extraction

Data from selected studies were extracted by 2 authors (YG and YL) into a suitable Excel spreadsheet. The columns of Excel spreadsheets were as follows: authors and type of the study.

Data analysis

All data were analyzed using Rev Man 5 (Cochrane Collaboration, London, UK). For continuous data, the overall estimate was calculated as the SMD with 95% confidence interval (95% CI). For dichotomous data, overall estimate was calculated as ORs. The SMD was preferred to the mean difference (MD) due to variations among scales used for cognitive and functional outcomes between the studies. Dichotomous data were in terms of adverse events; therefore, OR was preferred. Heterogeneity was assessed using the Cochran's Q statistic and I^2 tests. The random effects model was used due to variations among included studies. The inverse variance method was used for continuous data and the Mantel–Haenszel method was used for dichotomous data.

Results

Selection of studies

A total of 2,300 studies were found in PubMed, which were further screened based on inclusion and exclusion criteria. A total of 16 studies were selected for quantitative analysis regarding efficacy of acetylcholinesterase inhibitors, while 15 studies were found relevant regarding safety of acetylcholinesterase inhibitors. Of the 16 studies, 6 were related to donepezil,[27–32] 6 were related to galantamine[33–37] and the remaining 4 studies were related to rivastigmine.[38–42] Among the 15 studies related to safety, 9[17–31,43–46] were related to donepezil and the remaining 6 were related to galantamine.[33–38] The flow of study selection is presented in Fig. 1. The characteristics of the included studies are provided in Table 1.

Efficacy of acetylcholinesterase inhibitors

The efficacy of individual acetylcholinesterase inhibitors is compiled below.

Donepezil

Cognitive function

The SMD was found to be −0.33 [−0.52, −0.13], indicating a significant effect of donepezil on cognitive outcome. The forest plot along with the pooled effect, i.e., SMD, is presented in Fig. 2A. The heterogeneity between studies was 38%, as indicated by the I^2 statistic.
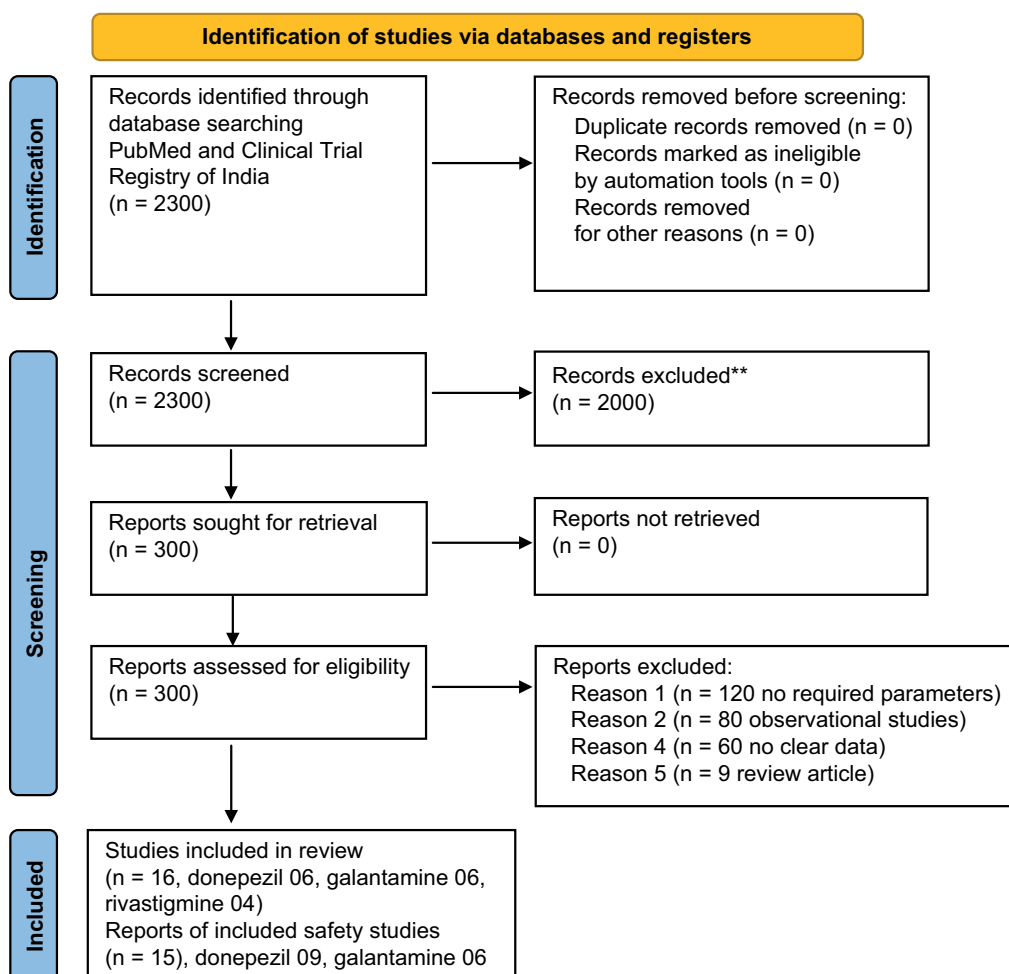
Fig. 1. Selection of studies as per the Preferred Reporting Items for Systematic Reviews and Meta-Analyses (PRISMA) guidelines

Table 1. Characteristics of included studies

Authors and year of publication	Location	Age years (M ±SD)	Total sample size	Disease severity	Duration [weeks]
Haig et al., 2014[28]	USA	70.3 ±7.94 (placebo) 70.5 ±8.31 (drug)	63 (placebo) 60 (drug)	mild to moderate	12
Johannsen et al., 2006[29]	Denmark	71.4 ±9.3 74.1 ±7.6	103 (placebo) 99 (drug)	mild to moderate	12
Maher-Edward et al., 2011[30]	UK	71.6 ±6.72 (placebo) 71.1 ±8.39	61 (placebo) 67 (drug)	mild to moderate	24
Seltzer, 2004[31]	USA	73.3 ±8.8 (placebo) 73.3 ±9.6	57 (placebo) 96 (drug)	mild to moderate	24
Tune et al., 2003[32]	USA	72.2 ±9.57 (placebo) 73.7 ±5.25 (drug)	14 (placebo) 14 (drug)	mild to moderate	24
Brodaty et al., 2005[33]	Australia	–	296 (placebo) 296 (drug)	mild to moderate	6 months
Raskind et al., 2000[34]	USA	–	207 (placebo) 202 (drug)	mild to moderate	6 months
Rockwood, 2001[35]	USA, Canada, UK, South Africa, Australia, and New Zealand	74.6 ±0.68 75.2 ±0.45	120 (placebo) 239 (drug)	patients with probable Alzheimer's disease	3 months
Gault et al., 2016[44]	USA	73.2 ±7.39 (placebo) 75.1 ±7.75 (drug)	104 (placebo) 76 (drug)	mild to moderate	24
Jia et al., 2017[45]	China	70.0 ±9.57 71.6 ±8.56	156 (placebo) 157 (drug)	severe	24
Tariot et al., 2001[46]	USA	85.9 ±9.25 85.4 ±8.5	105 (placebo) 103 (drug)	mild to moderate	24
Black et al., 2007[47]	Canada	78.0 ±8.04 (placebo) 78.0 ±8.20	167 (placebo) 176 (drug)	severe	24
Gault et al., 2015[48]	USA	73.6 ±8.23 73.9 ±7.92	68 (placebo) 68 (drug)	mild to moderate	12
Homma et al., 2008[49]	Japan	79.7 ±7.5 76.9 ±7.9	102 (placebo) 92 (drug)	severe	24
Winblad et al., 2006[50]	Sweden	85.3 ±5.9 84.5 ±6.0	120 (placebo) 128 (drug)	severe	24
Feldman et al., 2001[51]	Canada	74.0 ±11 73.2 ±10	146 (placebo) 144 (drug)	moderate to severe	24

M ±SD – mean ± standard deviation.

Functional outcome

The effects of donepezil on the functional outcomes were also found to be significant compared to the control group, as indicated by the SMD values, i.e., 0.24 [0.12, 0.36]. The forest plot together with the pooled effect is shown in Fig. 2B. No heterogeneity between studies was found, as indicated by the I^2 statistic.

Adverse events

The overall OR was found to be 1.22 [0.98, 1.52], indicating a non-significant association of donepezil with adverse events. The forest plot together with the pooled effect is shown in Fig. 2C. No heterogeneity between studies was found.

Galantamine

Cognitive function

The SMD was found to be −0.48 [−0.58, −0.38], indicating a significant improvement in cognitive functions in patients with AD compared to the control group. The forest plot together with pooled effect is shown in Fig. 3A. The heterogeneity between studies was 29%, as indicated by the I^2 statistic.

Functional outcomes

The effect of galantamine on functional outcome was not significant, as indicated by the SMD, i.e., 0.17 [−0.08, 0.43]. The forest plot together with the pooled effect is shown in Fig. 3B. However, the heterogeneity between studies was very high (83%) (Fig. 3B).[29,47,48]
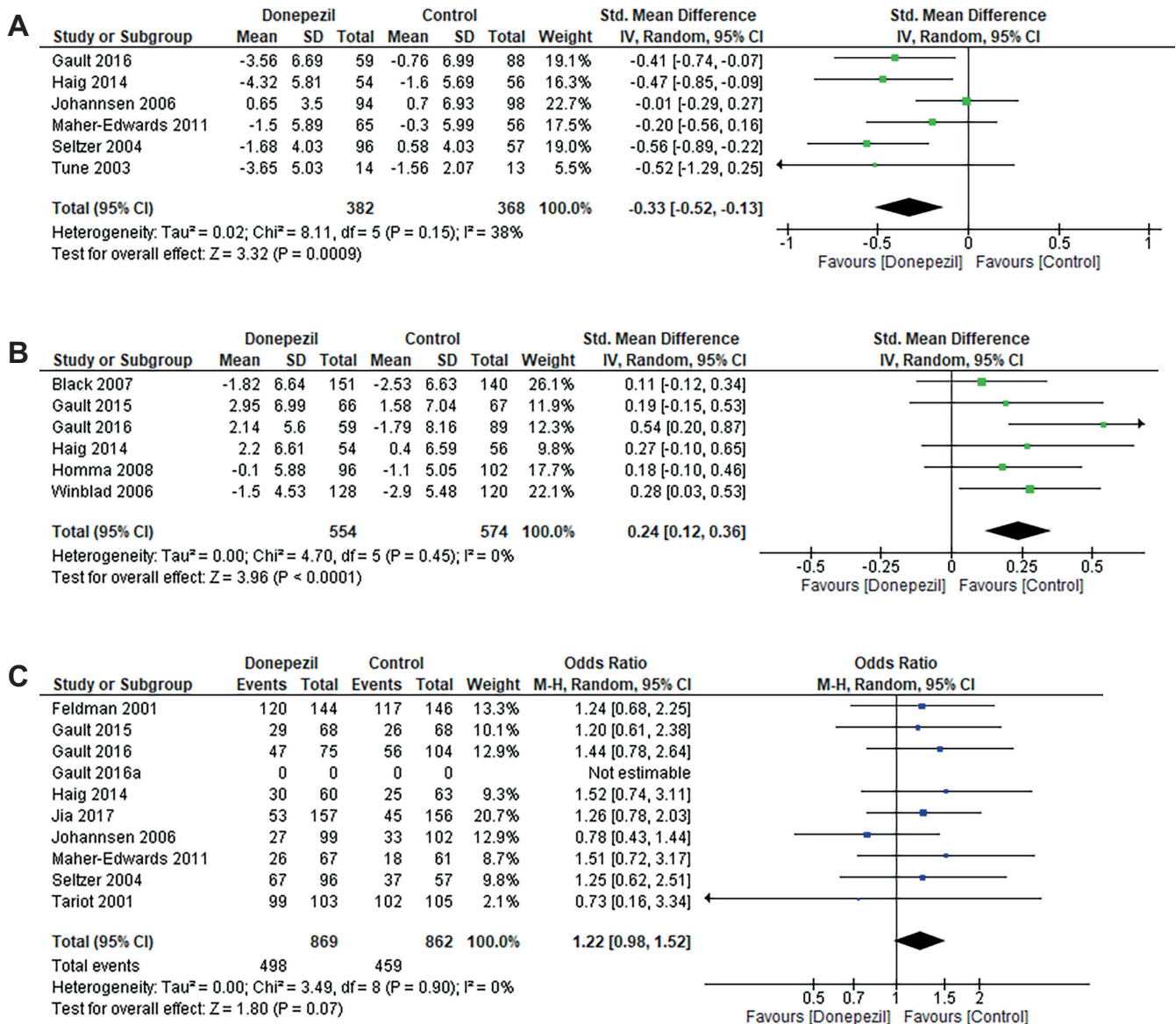
Fig. 2. Effect of donepezil. A. Forest plot + pooled effect on cognitive outcomes, standard mean difference (SMD) with 95% confidence interval (95% CI); B. Forest plot + pooled effect on functional outcomes, SMD with 95% CI; C. Forest plot + pooled effect on adverse events, odds ratio (OR) with 95% CI

Adverse events

The overall OR was found to be 2.34 [1.35, 4.08], indicating a significant association. The forest plot together with the pooled effect is shown in Fig. 3C. The heterogeneity between studies was 73%, as indicated by the I^2 statistic.

Rivastigmine

Cognitive function

The overall estimate, i.e., SMD, was found to be −0.65 [−1.06, −0.23], indicating a significant improvement in cognitive functions in the rivastigmine group compared to the control group. The forest plot together with the pooled effect is shown in Fig. 4. The heterogeneity between studies was very high, i.e., 92% (I^2 statistic).

We did not find sufficient studies for meta-analysis regarding functional outcomes and adverse events related to rivastigmine.

Overall, the results of our meta-analysis showed that all available acetylcholinesterase inhibitors, i.e., donepezil, galantamine and galantamine, significantly improved cognitive functions in patients with AD. However, the results for galantamine and rivastigmine should be considered with caution due to high heterogeneity of the included studies. Therefore, physicians could consider any of the available acetylcholinesterase inhibitors to improve cognitive function in patients with AD. Nonetheless, only the donepezil group showed a significant improvement in functional outcome. There is also insufficient data on rivastigmine in terms of functional outcomes and adverse events.
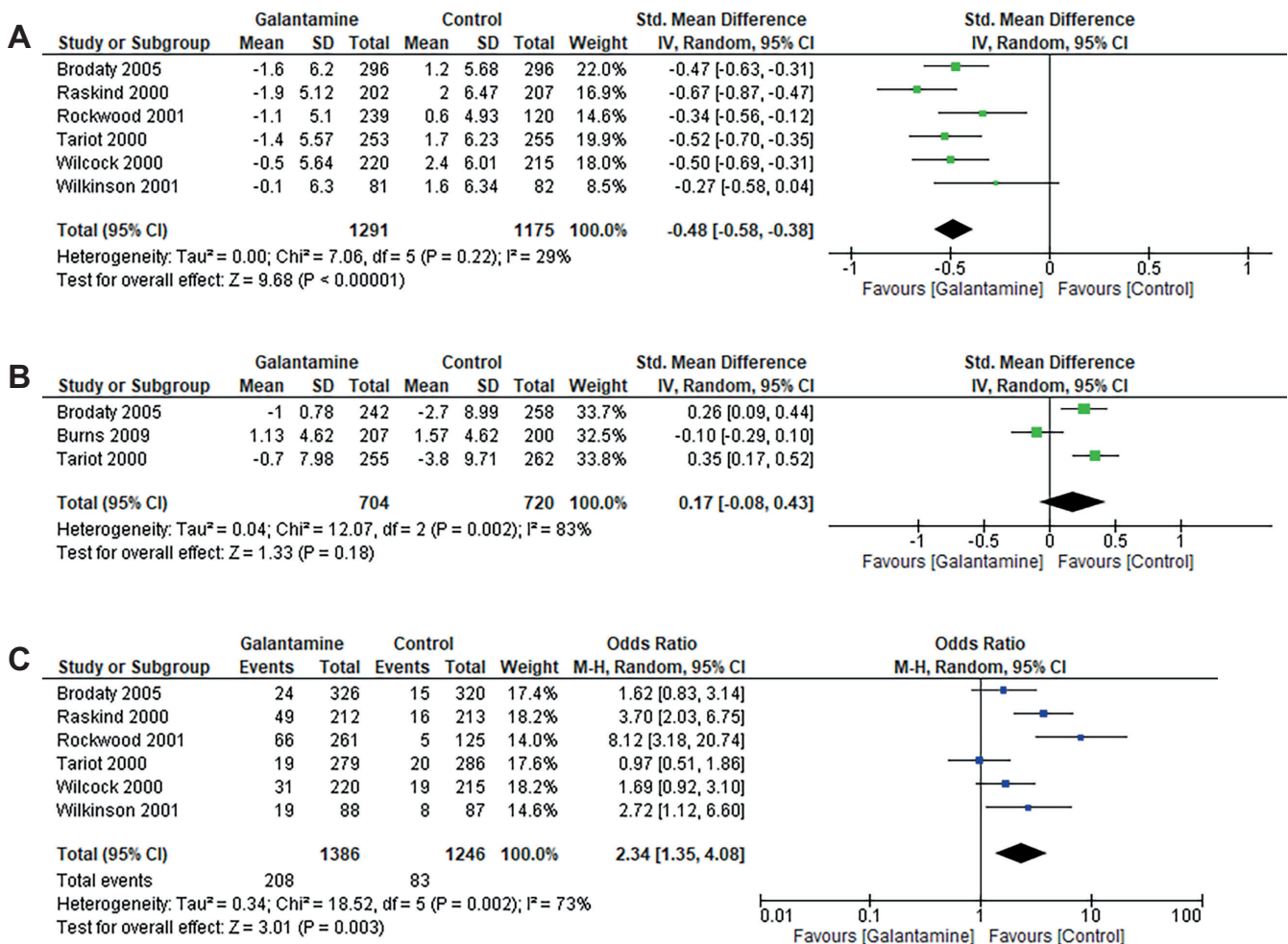
Fig. 3. Effect of galantamine. A. Forest plot + pooled effect on cognitive outcomes, standard mean difference (SMD) with 95% confidence interval (95% CI); B. Forest plot + pooled effect on functional outcomes, SMD with 95% CI; C. Forest plot + pooled effect on adverse events, odds ratio (OR) with 95% CI
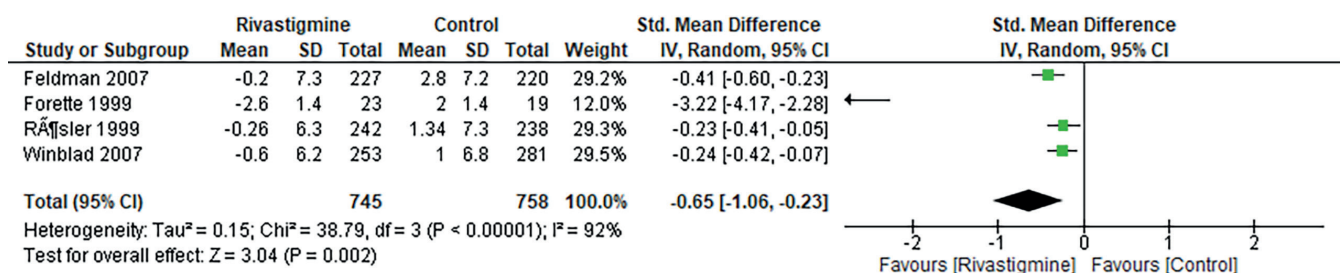
Fig. 4. Effect of rivastigmine on cognitive outcomes (forest plot + pooled effect), standard mean difference (SMD) with 95% confidence interval (95% CI)

Discussion

Despite significant advances in our understanding of the CNS structure and function, the discovery and clinical development of novel medications for many CNS disorders has proven difficult.[53–58] Alzheimer's disease is a CNS disorder that worsens over time.[59,60]

The diagnosis of AD relies mainly on behavioral assessment. Many studies are ongoing to identify specific peripheral biomarkers.[61] The etiology of AD is also unclear.[62] In AD, cells that produce and use acetylcholine are damaged. Acetylcholinesterase is one of the important enzymes that breakdowns acetylcholine into acetic acid and choline in the synaptic cleft. Acetylcholine is a major neurotransmitter that has many important roles, including cognition. It has been observed that the level of acetylcholine is decreased in patients with AD.[50–65] Therefore, drugs that can increase acetylcholine levels are useful in the management of patients with AD. Regulatory authorities across the globe have approved acetylcholinesterase inhibitors for the treatment of patients with AD. Tacrine, donepezil, galantamine, and rivastigmine are

well-known acetylcholinesterase inhibitors approved for the management of patients with AD. However, tacrine has been withdrawn from the market due to its adverse reactions, particularly hepatotoxicity. Recently, monoclonal antibodies have also been approved for the treatment of AD, but their exact role is unclear.[66,67] The efficacy and safety of acetylcholinesterase is also not known so far. Therefore, there is need of updated meta-analysis to find out exact profile of these inhibitors. Meta-analysis is a quantitative analysis that helps to draw a valid conclusion from clinical studies which helps the clinicians to make the right treatment decision.[68–70]

We conducted a meta-analysis of clinical studies to determine the exact role of acetylcholinesterase inhibitors in the treatment of AD. We have found significant differences between the donepezil and placebo groups, between the galantamine and placebo groups and between the rivastigmine and placebo groups. The results of the current meta-analysis have shown significant improvement in cognitive functions of patients with AD in the donepezil, galantamine and rivastigmine groups compared with the control groups. To the best of our knowledge, very few meta-analyses have been conducted so far to examine the efficacy and safety profile of available acetylcholinesterase inhibitors. Kobayashi et al. have conducted a Bayesian network meta-analysis to compare the efficacy and safety of cholinesterase inhibitors in patients with mild-to-moderate AD.[71] The results of the analysis also indicated the significant efficacy of acetylcholinesterase inhibitors on cognitive functions of patients with mild-to-moderate AD. The effects on functional outcome and adverse events are different across the acetylcholinesterase inhibitors. Donepezil has shown a significant effect on functional outcome in patients with AD, whereas galantamine has shown nonsignificant effects. Furthermore, donepezil was not significantly associated with adverse events, whereas galantamine was significantly associated with adverse events. The meta-analysis of RCTs of galantamine in schizophrenia was conducted by Koola et al. and reported significant cognitive improvement.[72]

The results of a meta-analysis conducted by Lanctôt et al. reported modest efficacy of acetylcholinesterase inhibitors and significantly higher rates of adverse events and treatment discontinuation. Cognitive outcomes were reported from randomized, double-blind, placebo-controlled, parallel-group trials of currently marketed cholinesterase inhibitors (ChEIs; donepezil, rivastigmine and galantamine) administered at therapeutic doses for at least 12 weeks. The proportions of participants who responded, experienced adverse events, discontinued treatment for any reason, or discontinued treatment due to adverse events were determined. Treatment with ChEIs produces a small but considerable therapeutic effect, as well as small but considerably increased rates of adverse events and treatment discontinuation.[73] Dou et al. conducted a network meta-analysis to compare the safety and efficacy of ChEIs and memantine in AD. The results of their analysis indicated a beneficial effect of acetylcholinesterase inhibitors on cognition, function and global changes, but not on neuropsychiatric symptoms. They observed that the severity of the disease and its clinical symptoms may have a major impact on the treatment selection.[74]

As only studies that show a substantial difference are usually published, some completed researches were not released and therefore could not be included in the meta-analysis, which could lead to publication bias. Meta-analyses of other treatments, such as like glucagon-like peptide-1 receptor agonists and negative allosteric modulators of 5-hydroxytryptamine 2A receptors, were also conducted by the researchers across the globe.[75,76]

Our meta-analysis showed that all 3 acetylcholinesterase inhibitors now in use, i.e., donepezil, galantamine and galantamine, significantly enhance patients' cognitive abilities. However, given to the substantial heterogeneity among the included trials, caution should be exercised in interpreting the results of galantamine and rivastigmine. To improve cognition of patients with AD, physicians can prescribe any of the currently approved acetylcholinesterase inhibitors. However, patients in the donepezil group showed considerable improvement in functional outcomes. Functional outcomes and adverse events are not adequately covered by the available data on rivastigmine. Therefore, in our opinion, based on current clinical evidence, among the available acetylcholinesterase inhibitors, donepezil should be considered by the physicians in the management of patients with AD unless contraindicated.

Limitations

We included only studies published in English. We also searched only 1 database, i.e., PubMed, for relevant studies. The heterogeneity among studies was quite high. There is a risk of publication bias in all the meta-analyses presented, but this could not be determined due to the small number of studies. The analysis was based on the strength of the drugs; dosage forms were not analyzed due to data unavailability. All available acetylcholinesterase inhibitors are effective in improving cognitive function, but further RCTs are required to find out the exact effects of available acetylcholinesterase inhibitors on functional outcomes or other AD parameters.

Conclusions

A meta-analysis of clinical data was conducted for the current study to determine the precise function of acetylcholinesterase inhibitors in the management of AD. We observed significant differences between the donepezil and placebo groups, the galantamine and placebo groups, and the rivastigmine and placebo groups. According to the current meta-analysis, donepezil, galantamine and rivastigmine significantly improved the cognitive abilities of patients with AD when compared to control groups. Based on current clinical evidence, donepezil has shown

significant improvement in cognitive and functional outcomes. We also found non-significant association of donepezil with adverse events. However, more RCTs are required to test the effects of galantamine and rivastigmine, particularly on functional outcomes and adverse events.

ORCID iDs

Yaqi Gao https://orcid.org/0009-0005-8709-8323
Yulin Liu https://orcid.org/0009-0005-4740-869X
Yanfang Li https://orcid.org/0009-0009-1792-887X

References

1. Battaglia S, Thayer JF. Functional interplay between central and autonomic nervous systems in human fear conditioning. *Trends Neurosci.* 2022;45(7):504–506. doi:10.1016/j.tins.2022.04.003

2. Battaglia S, Orsolini S, Borgomaneri S, Barbieri R, Diciotti S, Di Pellegrino G. Characterizing cardiac autonomic dynamics of fear learning in humans. *Psychophysiology.* 2022;59(12):e14122. doi:10.1111/psyp.14122

3. Yan W, Peng YR, Van Zyl T, et al. Cell atlas of the human fovea and peripheral retina. *Sci Rep.* 2020;10(1):9802. doi:10.1038/s41598-020-66092-9

4. Tanaka M, Szabó Á, Spekker E, Polyák H, Tóth F, Vécsei L. Mitochondrial impairment: A common motif in neuropsychiatric presentation? The link to the tryptophan–kynurenine metabolic system. *Cells.* 2022;11(16):2607. doi:10.3390/cells11162607

5. Battaglia S, Di Fazio C, Vicario CM, Avenanti A. Neuropharmacological modulation of N-methyl-D-aspartate, noradrenaline and endocannabinoid receptors in fear extinction learning: Synaptic transmission and plasticity. *Int J Mol Sci.* 2023;24(6):5926. doi:10.3390/ijms24065926

6. Praticò D. Evidence of oxidative stress in Alzheimer's disease brain and antioxidant therapy: Lights and shadows. *Ann N Y Acad Sci.* 2008;1147(1):70–78. doi:10.1196/annals.1427.010

7. Perry G, Raina AK, Nunomura A, Wataya T, Sayre LM, Smith MA. How important is oxidative damage? Lessons from Alzheimer's disease. *Free Radic Biol Med.* 2000;28(5):831–834. doi:10.1016/S0891-5849(00)00158-1

8. Kshirsagar S, Sawant N, Morton H, Reddy AP, Reddy PH. Protective effects of mitophagy enhancers against amyloid beta-induced mitochondrial and synaptic toxicities in Alzheimer disease. *Hum Mol Genet.* 2022;31(3):423–439. doi:10.1093/hmg/ddab262

9. Perez Ortiz JM, Swerdlow RH. Mitochondrial dysfunction in Alzheimer's disease: Role in pathogenesis and novel therapeutic opportunities. *Br J Pharmacol.* 2019;176(18):3489–3507. doi:10.1111/bph.14585

10. Erekat NS. Apoptosis and its therapeutic implications in neurodegenerative diseases. *Clin Anat.* 2022;35(1):65–78. doi:10.1002/ca.23792

11. Dhiman A, Sharma R, Singh RK. Target-based anticancer indole derivatives and insight into structure–activity relationship: A mechanistic review update (2018–2021). *Acta Pharm Sin B.* 2022;12(7):3006–3027. doi:10.1016/j.apsb.2022.03.021

12. Bamberger ME, Landreth GE. Inflammation, apoptosis, and Alzheimer's disease. *Neuroscientist.* 2002;8(3):276–283. doi:10.1177/1073858402008003013

13. Obulesu M, Lakshmi MJ. Apoptosis in Alzheimer's disease: An understanding of the physiology, pathology and therapeutic avenues. *Neurochem Res.* 2014;39(12):2301–2312. doi:10.1007/s11064-014-1454-4

14. Takuma K, Yan SS, Stern DM, Yamada K. Mitochondrial dysfunction, endoplasmic reticulum stress, and apoptosis in Alzheimer's disease. *J Pharmacol Sci.* 2005;97(3):312–316. doi:10.1254/jphs.CPJ04006X

15. Bayer AU, Keller ON, Ferrari F, Maag KP. Association of glaucoma with neurodegenerative diseases with apoptotic cell death: Alzheimer's disease and Parkinson's disease. *Am J Ophthalmol.* 2002;133(1):135–137. doi:10.1016/S0002-9394(01)01196-5

16. Stern Y, Hesdorffer D, Sano M, Mayeux R. Measurement and prediction of functional capacity in Alzheimer's disease. *Neurology.* 1990;40(1):8–14. doi:10.1212/WNL.40.1.8

17. Chen ST, Sultzer DL, Hinkin CH, Mahler ME, Cummings JL. Executive dysfunction in Alzheimer's disease: Association with neuropsychiatric symptoms and functional impairment. *J Neuropsychiatry Clin Neurosci.* 1998;10(4):426–432. doi:10.1176/jnp.10.4.426

18. Perry RJ, Hodges JR. Relationship between functional and neuropsychological performance in early Alzheimer disease. *Alzheimer Dis Assoc Didord.* 2000;14(1):1–10. doi:10.1097/00002093-200001000-00001

19. Caro J, Ward A, Ishak K, et al. To what degree does cognitive impairment in Alzheimer's disease predict dependence of patients on caregivers? *BMC Neurol.* 2002;2(1):6. doi:10.1186/1471-2377-2-6

20. Pereira FS, Yassuda MS, Oliveira AM, Forlenza OV. Executive dysfunction correlates with impaired functional status in older adults with varying degrees of cognitive impairment. *Int Psychogeriatr.* 2008;20(6):1104. doi:10.1017/S1041610208007631

21. Inestrosa NC, Sagal JP, Colombres M. Acetylcholinesterase interaction with Alzheimer amyloid β. *Subcell Biochem.* 2005;38:299–317. doi:10.1007/0-387-23226-5_15

22. Pless A, Ware D, Saggu S, Rehman H, Morgan J, Wang Q. Understanding neuropsychiatric symptoms in Alzheimer's disease: Challenges and advances in diagnosis and treatment. *Front Neurosci.* 2023;17:1263771. doi:10.3389/fnins.2023.1263771

23. Fan P, Miranda O, Qi X, Kofler J, Sweet RA, Wang L. Unveiling the enigma: Exploring risk factors and mechanisms for psychotic symptoms in Alzheimer's disease through electronic medical records with deep learning models. *Pharmaceuticals.* 2023;16(7):911. doi:10.3390/ph16070911

24. Liu M, Xie X, Xie J, et al. Early-onset Alzheimer's disease with depression as the first symptom: A case report with literature review. *Front Psychiatry.* 2023;14:1192562. doi:10.3389/fpsyt.2023.1192562

25. Doody RS, Stevens JC, Beck C, et al. Practice parameter: Management of dementia (an evidence-based review). Report of the Quality Standards Subcommittee of the American Academy of Neurology. *Neurology.* 2001;56(9):1154–1166. doi:10.1212/WNL.56.9.1154

26. Koola MM. Galantamine-memantine combination in the treatment of Alzheimer's disease and beyond. *Psychiatry Res.* 2020;293:113409. doi:10.1016/j.psychres.2020.113409

27. Rogers SL, Friedhoff LT. The efficacy and safety of donepezil in patients with Alzheimer's disease: Results of a US multicentre, randomized, double-blind, placebo-controlled trial. *Dementia.* 1996;7(6):293–303. doi:10.1159/000106895

28. Haig GM, Pritchett Y, Meier A, et al. A randomized study of H3 antagonist ABT-288 in mild-to-moderate Alzheimer's dementia. *J Alzheimers Dis.* 2014;42(3):959–971. doi:10.3233/JAD-140291

29. Johannsen P, Salmon E, Hampel H, et al. Assessing therapeutic efficacy in a progressive disease: A study of donepezil in Alzheimer's disease. *CNS Drugs.* 2006;20(4):311–325. doi:10.2165/00023210-200620040-00005

30. Maher-Edwards G, Dixon R, Hunter J, et al. SB-742457 and donepezil in Alzheimer disease: A randomized, placebo-controlled study. *Int J Geriatr Psychiatry.* 2011;26(5):536–544. doi:10.1002/gps.2562

31. Seltzer B. Efficacy of donepezil in early-stage Alzheimer disease: A randomized placebo-controlled trial. *Arch Neurol.* 2004;61(12):1852. doi:10.1001/archneur.61.12.1852

32. Tune L, Tiseo PJ, Ieni J, et al. Donepezil HCl (E2020) maintains functional brain activity in patients with Alzheimer disease: Results of a 24-week, double-blind, placebo-controlled study. *Am J Geriatr Psychiatry.* 2003;11(2):169–177. doi:10.1097/00019442-200303000-00007

33. Brodaty H, Corey-Bloom J, Potocnik FCV, Truyen L, Gold M, Damaraju CRV. Galantamine prolonged-release formulation in the treatment of mild to moderate Alzheimer's disease. *Dement Geriatr Cogn Disord.* 2005;20(2–3):120–132. doi:10.1159/000086613

34. Raskind MA, Peskind ER, Wessel T, Yuan W; the Galantamine USA – Study Group. Galantamine in AD: A 6-month randomized, placebo-controlled trial with a 6-month extension. *Neurology.* 2000;54(12):2261–2268. doi:10.1212/WNL.54.12.2261

35. Rockwood K. Effects of a flexible galantamine dose in Alzheimer's disease: A randomised, controlled trial. *J Neurol Neurosurg Psychiatry.* 2001;71(5):589–595. doi:10.1136/jnnp.71.5.589

36. Tariot PN, Solomon PR, Morris JC, et al. A 5-month, randomized, placebo-controlled trial of galantamine in AD. *Neurology.* 2000;54(12):2269–2276. doi:10.1212/WNL.54.12.2269

37. Wilcock GK, Lilienfeld S, Gaens E. Efficacy and safety of galantamine in patients with mild to moderate Alzheimer's disease: Multicentre randomised controlled trial. *BMJ.* 2000;321(7274):1445–1445. doi:10.1136/bmj.321.7274.1445

38. Wilkinson D, Murray J; the Galantamine Research Group. Galantamine: A randomized, double-blind, dose comparison in patients with Alzheimer's disease. *Int J Geriat Psychiatry*. 2001;16(9):852–857. doi:10.1002/gps.409

39. Feldman HH, Lane R; on behalf of the Study 304 Group. Rivastigmine: A placebo controlled trial of twice daily and three times daily regimens in patients with Alzheimer's disease. *J Neurol Neurosurg Psychiatry*. 2007;78(10):1056–1063. doi:10.1136/jnnp.2006.099424

40. Forette F, Anand R, Gharabawi G. A phase II study in patients with Alzheimer's disease to assess the preliminary efficacy and maximum tolerated dose of rivastigmine (Exelon®). *Eur J Neurol*. 1999;6(4):423–429. doi:10.1046/j.1468-1331.1999.640423.x

41. Rosler M, Anand R, Cicin-Sain A, et al. Efficacy and safety of rivastigmine in patients with Alzheimer's disease: International randomised controlled trial. *BMJ*. 1999;318(7184):633–640. doi:10.1136/bmj.318.7184.633

42. Winblad B, Grossberg G, Frolich L, et al. IDEAL: A 6-month, double-blind, placebo-controlled study of the first skin patch for Alzheimer disease. *Neurology*. 2007;4(4 Suppl 1):S14–S22. doi:10.1212/01.wnl.0000281847.17519.e0

43. Feldman H, Gauthier S, Hecker J, Vellas B, Subbiah P, Whalen E. A 24-week, randomized, double-blind study of donepezil in moderate to severe Alzheimer's disease. *Neurology*. 2001;57(4):613–620. doi:10.1212/WNL.57.4.613

44. Gault LM, Lenz RA, Ritchie CW, et al. ABT-126 monotherapy in mild-to-moderate Alzheimer's dementia: Randomized double-blind, placebo and active controlled adaptive trial and open-label extension. *Alzheimers Res Ther*. 2016;8(1):44. doi:10.1186/s13195-016-0210-1

45. Jia J, Wei C, Jia L, et al. Efficacy and safety of donepezil in Chinese patients with severe Alzheimer's disease: A randomized controlled trial. *J Alzheimers Dis*. 2017;56(4):1495–1504. doi:10.3233/JAD-161117

46. Tariot PN, Cummings JL, Katz IR, et al. A randomized, double-blind, placebo-controlled study of the efficacy and safety of donepezil in patients with Alzheimer's disease in the nursing home setting. *J Am Geriatr Soc*. 2001;49(12):1590–1599. doi:10.1111/j.1532-5415.2001.49266.x

47. Black SE, Doody R, Li H, et al. Donepezil preserves cognition and global function in patients with severe Alzheimer disease. *Neurology*. 2007;69(5):459–469. doi:10.1212/01.wnl.0000266627.96040.5a

48. Gault LM, Ritchie CW, Robieson WZ, Pritchett Y, Othman AA, Lenz RA. A phase 2 randomized, controlled trial of the α7 agonist ABT-126 in mild-to-moderate Alzheimer's dementia. *Alzheimers Dement (N Y)*. 2015;1(1):81–90. doi:10.1016/j.trci.2015.06.001

49. Homma A, Imai Y, Tago H, et al. Donepezil treatment of patients with severe Alzheimer's disease in a Japanese population: Results from a 24-week, double-blind, placebo-controlled, randomized trial. *Dement Geriatr Cogn Disord*. 2008;25(5):399–407. doi:10.1159/000122961

50. Winblad B, Kilander L, Eriksson S, et al. Donepezil in patients with severe Alzheimer's disease: Double-blind, parallel-group, placebo-controlled study. *Lancet*. 2006;367(9516):1057–1065. doi:10.1016/S0140-6736(06)68350-5

51. Burns A, Bernabei R, Bullock R, et al. Safety and efficacy of galantamine (Reminyl) in severe Alzheimer's disease (the SERAD study): A randomised, placebo-controlled, double-blind trial. *Lancet Neurol*. 2009;8(1):39–47. doi:10.1016/S1474-4422(08)70261-8

52. Tariot P. Current status and new developments with galantamine in the treatment of Alzheimer's disease. *Exp Opin Pharmacother*. 2001;2(12):2027–2049. doi:10.1517/14656566.2.12.2027

53. Singh RK, Devi S, Prasad DN. Synthesis, physicochemical and biological evaluation of 2-amino-5-chlorobenzophenone derivatives as potent skeletal muscle relaxants. *Arab J Chem*. 2015;8(3):307–312. doi:10.1016/j.arabjc.2011.11.013

54. Singh RK, Prasad DN, Bhardwaj TR. Synthesis in vitro/in vivo evaluation and in silico physicochemical study of prodrug approach for brain targeting of alkylating agent. *Med Chem Res*. 2013;22(11):5324–5336. doi:10.1007/s00044-013-0537-0

55. Singh RK, Prasad DN, Bhardwaj TR. Synthesis, physicochemical and kinetic studies of redox derivative of bis(2-chloroethylamine) as alkylating cytotoxic agent for brain delivery. *Arab J Chem*. 2015;8(3):380–387. doi:10.1016/j.arabjc.2012.11.005

56. Singh RK, Prasad DN, Bhardwaj TR. Design, synthesis and in vitro cytotoxicity study of benzodiazepine-mustard conjugates as potential brain anticancer agents. *J Saudi Heart Assoc*. 2017;21(Suppl 1):S86–S93. doi:10.1016/j.jscs.2013.10.004

57. Singh RK, Prasad DN, Bhardwaj TR. Design, synthesis, chemical and biological evaluation of brain targeted alkylating agent using reversible redox prodrug approach. *Arab J Chem*. 2017;10(3):420–429. doi:10.1016/j.arabjc.2013.12.008

58. Tanaka M, Török N, Vécsei L. Novel pharmaceutical approaches in dementia. In: Riederer P, Laux G, Nagatsu T, Le W, Riederer C, eds. *NeuroPsychopharmacotherapy*. Cham, Switzerland: Springer International Publishing; 2022:2803–2820. doi:10.1007/978-3-030-62059-2_444

59. Bayraktar Y, Isik E, Isik I, et al. Analyzing of Alzheimer's disease based on biomedical and socio-economic approach using molecular communication, artificial neural network, and random forest models. *Sustainability*. 2022;14(13):7901. doi:10.3390/su14137901

60. Orso B, Lorenzini L, Arnaldi D, et al. The role of hub and spoke regions in theory of mind in early Alzheimer's disease and frontotemporal dementia. *Biomedicines*. 2022;10(3):544. doi:10.3390/biomedicines10030544

61. Török N, Tanaka M, Vécsei L. Searching for peripheral biomarkers in neurodegenerative diseases: The tryptophan–kynurenine metabolic pathway. *Int J Mol Sci*. 2020;21(24):9338. doi:10.3390/ijms21249338

62. Tanaka M, Toldi J, Vécsei L. Exploring the etiological links behind neurodegenerative diseases: Inflammatory cytokines and bioactive kynurenines. *Int J Mol Sci*. 2020;21(7):2431. doi:10.3390/ijms21072431

63. El-Tallawy HN, Saadeldin HM, Ezzeldin AM, et al. Genetic, clinical, and biochemical aspects of patients with Alzheimer disease. *Egypt J Neurol Psychiatry Neurosurg*. 2022;58(1):24. doi:10.1186/s41983-022-00455-z

64. Tanaka M, Vécsei L. Editorial of Special Issue "Crosstalk between Depression, Anxiety, and Dementia: Comorbidity in Behavioral Neurology and Neuropsychiatry." *Biomedicines*. 2021;9(5):517. doi:10.3390/biomedicines9050517

65. Carrera-González MDP, Cantón-Habas V, Rich-Ruiz M. Aging, depression and dementia: The inflammatory process. *Adv Clin Exp Med*. 2022;31(5):469–473. doi:10.17219/acem/149897

66. Kurkinen MT. Lecanemab (Leqembi) is not the right drug for patients with Alzheimer's disease. *Adv Clin Exp Med*. 2023;32(9):943–947. doi:10.17219/acem/171379

67. Kurkinen MT. Donanemab: Not two without a third. *Adv Clin Exp Med*. 2023;32(10):1085–1087. doi:10.17219/acem/172673

68. Thakur M, Datusalia AK, Kumar A. Use of steroids in COVID-19 patients: A meta-analysis. *Eur J Pharmacol*. 2022;914:174579. doi:10.1016/j.ejphar.2021.174579

69. Srivastava R, Kumar A. Use of aspirin in reduction of mortality of COVID-19 patients: A meta-analysis. *Int J Clin Pract*. 2021;75(11). doi:10.1111/ijcp.14515

70. Vitalakumar D, Sharma A, Kumar A, Flora S. Neurological manifestations in COVID-19 patients: A meta-analysis. *ACS Chem Neurosci*. 2021;12(15):2776–2797. doi:10.1021/acschemneuro.1c00353

71. Kobayashi H, Ohnishi T, Nakagawa R, Yoshizawa K. The comparative efficacy and safety of cholinesterase inhibitors in patients with mild-to-moderate Alzheimer's disease: A Bayesian network meta-analysis. *Int J Geriat Psychiatry*. 2016;31(8):892–904. doi:10.1002/gps.4405

72. Koola MM, Looney SW, Hong H, Pillai A, Hou W. Meta-analysis of randomized controlled trials of galantamine in schizophrenia: Significant cognitive enhancement. *Psychiatry Res*. 2020;291:113285. doi:10.1016/j.psychres.2020.113285

73. Lanctôt KL, Herrmann N, Yau KK, et al. Efficacy and safety of cholinesterase inhibitors in Alzheimer's disease: A meta-analysis. *Can Med Assoc J*. 2003;169(6):557–564. PMID:12975222. PMCID:PMC191283.

74. Dou KX, Tan MS, Tan CC, et al. Comparative safety and effectiveness of cholinesterase inhibitors and memantine for Alzheimer's disease: A network meta-analysis of 41 randomized controlled trials. *Alzheimers Res Ther*. 2018;10(1):126. doi:10.1186/s13195-018-0457-9

75. Bi Z, Wang L, Wang W. Evaluating the effects of glucagon-like peptide-1 receptor agonists on cognitive function in Alzheimer's disease: A systematic review and meta-analysis. *Adv Clin Exp Med*. 2023;32(11):1223–1231. doi:10.17219/acem/161734

76. Chen Y, Sun J, Yang Z, Bi H. Efficacy and safety of negative allosteric modulators of 5-hydroxytryptamine 2A receptors in the treatment of Alzheimer's disease psychosis: A systematic review and meta-analysis. *Adv Clin Exp Med*. 2023;32(10):1089–1098. doi:10.17219/acem/161159

Depressive disorders in children with chronic kidney disease treated conservatively

Katarzyna Kiliś-Pstrusińska[1,A–F], Anna Medyńska[1,A–F], Piotr Adamczyk[2,B,E,F], Beata Leszczyńska[3,B,E,F], Maria Szczepańska[4,B,E,F], Marcin Tkaczyk[5,B,E,F], Anna M. Wasilewska[6,B,E,F], Katarzyna Zachwieja[7,B,E,F], Ilona Zagożdżon[8,B,E,F], Krzysztof Kujawa[9,C–F], Natalia W. Dryjańska[10,B,D–F]

[1] Clinical Department of Pediatric Nephrology, Wroclaw Medical University, Poland

[2] Department of Pediatrics, Faculty of Medical Sciences in Katowice, Medical University of Silesia, Poland

[3] Department of Pediatrics and Nephrology, Medical University of Warsaw, Poland

[4] Clinic of Pediatrics, Nephrology and Endocrinology, Medical University of Silesia, Zabrze, Poland

[5] Nephrology Division, Polish Mother's Memorial Hospital Research Institute, Łódź, Poland

[6] Department of Pediatrics and Nephrology, Medical University of Białystok, Poland

[7] University Children's Hospital, Jagiellonian University Medical College, Cracow, Poland

[8] Department of Pediatric Nephrology and Hypertension, Medical University of Gdansk, Poland

[9] Statistical Analysis Centre, Wroclaw Medical University, Poland

[10] Department of Pediatric Nephrology, University Hospital in Wroclaw, Poland

A – research concept and design; B – collection and/or assembly of data; C – data analysis and interpretation;
D – writing the article; E – critical revision of the article; F – final approval of the article

Address for correspondence
Katarzyna Kiliś-Pstrusińska
E-mail: katarzyna.kilis-pstrusinska@umw.edu.pl

Abstract

Background. Children with chronic kidney disease (CKD) experience a lot of mental and emotional stress, which can lead to the development of depressive disorders. The prevalence of depressive disorders in CKD children is estimated to be between 7% and 35%.

Objectives. The aim of our study was to analyze the prevalence and characteristics of depression and depressive symptoms in children and adolescents with CKD treated conservatively.

Materials and methods. The cross-sectional, multicenter study was conducted in 73 CKD children aged 8–18 and in 92 of their parents. To assess the mental wellbeing of CKD children, Kovacs's Children's Depression Inventory 2 (CDI2) was used as CDI2: Self-Report and CDI2: Parent Form.

Results. The majority of CKD children acquired medium scores in CDI2, 11% of participants reported symptoms suggesting depressive disorder, and among them 8.2% met the criteria for depression. A significant relationship was found between age and interpersonal problems, age at CKD diagnosis, and total score and ineffectiveness, CKD duration and total score/emotional problems. Depressive symptoms were associated with the stage of CKD, and they differed significantly between stages III and IV. We noticed the child–parent disagreement on reported depressive symptoms. Parents perceive their children's mental state as worse than the children themselves.

Conclusions. There is a problem of depression in children with CKD treated conservatively. Variables associated with depressive symptoms in CKD children treated conservatively require further study. Key factors predisposing to the development of depression seem to be age at the time of diagnosis, disease duration, and progression of CKD from stage III to IV. Disparities between depressive symptoms self-reported by CKD children and their parents' assessment require further analysis. However, these disparaties indicate that the final diagnosis of the occurrence of depressive disorders should be based on a multidimensional assessment of the patient's situation.

Key words: children, chronic kidney disease, depressive disorders, Kovacs's Children's Depression Inventory 2

1190

K. Kiliś-Pstrusińska et al. Depressive disorders in children with CKD

Background

Chronic kidney disease (CKD) significantly impacts children's quality of life. As a disease with no definitive cure, CKD requires children to receive long-term medication, regular examinations and hospitalizations.[1] Children with CKD experience an increased amount of psychological stress.[2,3] The disease may also influence patients' mental and emotional health, which can result in symptoms of depression and anxiety.[4,5]

According to DSM-5 criteria for children and adolescents, clinical depression (major depressive disorder (MDD)) is characterized as a combination of depressed mood or loss of interest or pleasure lasting most of the day, nearly every day for 2 weeks or longer. It must be accompanied by 4 or more additional symptoms and cause clinically significant distress or impairment.[6] Depression in the presence of chronic somatic disease may also influence how the patient perceives a disease and whether they will adhere to medical recommendations. Finally, it may be connected to CKD progression and all-cause mortality.

In the adult population, the prevalence of interview-diagnosed depression amounts to 22.8% of patients with end-stage CKD and 26.5% of those with CKD stages 1–5.[7] According to World Health Organization (WHO), around 10% of children and adolescents have a mental disorder, and 3% develop a depressive disorder.[8] In a study conducted by Kogon et al., 7% of children and adolescents with CKD met the study criteria for depression, and 5% reported elevated depressive symptoms.[9] Based on other data, the prevalence of depressive disorders in CKD children is estimated to be 7–35%.[10–12]

Although the problem of depressive disorders in the pediatric population is now increasingly discussed, data on their prevalence and specificity in CKD children treated conservatively are scarce. Most of the data relate to the entire group of patients with CKD, regardless of the disease stage.[13,14] Still, the inclusion of dialysis and transplant patients and patients with a range of kidney function may result in diluted findings. Another problem may be the use of proper tools to measure depression. These should be standardized and adapted to the studied group.

Objectives

The aim of the study was to analyze the prevalence and characteristics of depression and depressive symptoms in children and adolescents with CKD treated conservatively.

Materials and methods

Study design and sample

This paper describes the results of a cross-sectional, multicenter study of children with CKD treated conservatively, recruited from 8 pediatric nephrology centers in Poland. The study protocol adhered to the Declaration of Helsinki and was approved by the Ethics Committee of Wroclaw Medical University, Wrocław, Poland (approval No. KB-490/2021). The study was conducted among patients and their parents/caregivers between September 2021 and May 2022. Written informed consent was obtained from all study participants (73 CKD children and 92 of their parents).

Inclusion criteria

Inclusion criteria for children were as follows: 1) age 7–18 years, 2) stage II of CKD or higher according to the Kidney Disease Outcomes Quality Initiative (KDOQI)[15] based on the estimated glomerular filtrationm rate (eGFR) measured with the Schwartz formula at the time of the study,[16] 3) conservative treatment of CKD, 4) CKD diagnosed at least 3 months before the beginning of the study, and 5) informed consent. Exclusion criteria for children were: 1) history of severe to profound intellectual disability, 2) transplantation, 3) cancer diagnosis, 4) hospitalization within 14 days before inclusion in the study, 5) a significant life event unrelated to their kidney disease in the past 30 days, such as losing a family member.

Data sources

A medical chart review was performed to obtain the following information: primary diagnosis of kidney disease, additional non-renal comorbidities, patient's age at CKD diagnosis and CKD stage at diagnosis, current stage of CKD, disease duration, current number of medications taken by the child, family structure, and parents' opinions on their children's observed changes in appetite and sleep problems over the past 6 months. Recent data on body weight and height, presence of hypertension, blood hemoglobin, serum creatinine, and albumin values were also included in the analysis.

Patients and their parents who agreed to participate in the study were required to complete Children's Depression Inventory 2 (CDI2). The questionnaire was used to assess the prevalence, severity and specificity of depression in CKD children.[17] The CDI2 is an assessment tool to measure the cognitive, affective and behavioral signs of depressive symptoms in youths aged 7–18 years.[17] The full-length CDI2: Self-Report is a 28-item assessment that yields a total score (TS), 2 scale scores (emotional problems (EP) and functional problems (FP)), and 4 subscale scores: negative mood/physical symptoms, interpersonal problems, ineffectiveness, and negative self esteem. Raw scores are converted to T-scores. T-scores of 40–59 were defined as medium, and a total T-score of 60–64 as elevated. A total score ≥65 identifies potentially depressed individuals and we used it as the threshold defining the presence of depression. The test was based

on experiences over the past 2 weeks and the test time was approx. 15 min. CDI2: Parent (CDI:P) form consists of 17 items that correspond to the self-report version and are suitably rephrased. Parent assessment yields a TS and 2 scale scores (EP and FP). The CDI2 has been translated into many languages, including Polish, and was standardized for the Polish population.[18] The reliability of CDI2: Self-Report Polish version has been reported to range from 0.84 to 0.87 (Cronbach's α coefficient) and the validity has been established at the level of 0.66. The reliability of the CDI2: Parent Form Polish version has been evaluated at the level of 0.82–0.86 and the validity of 0.74. In the current study, the CDI2 was used in paper-and-pencil format.

The differences in Kovacs's score between the children's assessment and their parents' assessment were analyzed using the t-test for matched pairs. The concordance of the differences between the child's assessment and the parents' assessment with a normal distribution (t-test for matched pairs assumption) was checked using the Shapiro–Wilk test (TS: W = 0.99, p = 0.650, EP: W = 0.98, p = 0.507, FP: W = 0.98, p = 0.476).

Statistical analyses

Participants' clinical and psychosocial characteristics were summarized using median and interquartile range (IQR) or count and proportions for continuous and categorical variables, respectively. Comparisons of clinical parameters between the 2 groups were made using a Mann–Whitney U test. Categorical data were analyzed using Fisher's exact tests. Relationships between continuous variables were analyzed using Spearman's rank correlation analysis. To evaluate the link between CKD stage and CDI results, Kruskal–Wallis one-way analysis of variance by ranks was used, followed by the post hoc Dunn's test with Bonferroni's correction. To determine the association of high Kovacs's scale scores (>59) with selected clinical parameters, logistic regression was performed. The compliance with the assumption of non-collinearity was checked using the variable inflation factor (VIF), which was smaller than 1.8 for each of the predictors (much less than 5, which was considered the threshold value). The assumption of linear relationships between numerical predictors and the log odds was checked using Box–Tidwell test, in which all the predictors met this assumption (p > 0.1 for all the predictors). A p-value <0.05 was considered statistically significant.

Results

Participants

The study included 73 children with CKD aged 8–18, treated conservatively, and 92 parents (62 women and 30 men; in 19 cases, both parents completed the CDI2: parent form). Characteristics of the patients are shown in Tables 1,2. The median age for CKD diagnosis was 2 years (Q1 = 1.0, Q3 = 8.0) and 9 years for the disease duration. At the time of the study, the median age was 13 years (Q1 = 11.0, Q3 = 16.0); 12 (16.43%) children presented with CKD stage II, 30 (41.1%) with stage III, 24 (32.88%) with stage IV, and 7 (9.59%) with stage V (pre-dialysis end-stage renal disease). In the last 6 months, parents did not notice any of their child's sleep-related changes. In almost all cases (93.15%), no change in appetite was observed by the parents.

Table 1. Characteristics of the patients with CKD

Characteristics of the patients		n	%
Sex	male	38	52
	female	35	48
Underlying disease	CAKUT	33	45.2
	glomerulonephritis	4	5.5
	post AKI	7	9.6
	other	29	39.7
Comorbidities	no	28	38.4
	yes	45	61.6
CKD stage at diagnosis	I	11	15.1
	II	30	41.1
	III	25	34.2
	IV	7	9.6
Family	full	54	74.0
	incomplete	19	26.0
Siblings	no	17	23.3
	1	38	52.0
	2	11	15.1
	3	3	4.1
	4	1	1.4
	5	3	4.1
Change in appetite	no	68	93.2
	yes	5	6.8
Arterial hypertension	no	39	53.4
	yes	34	46.6

CKD – chronic kidney disease; CAKUT – congenital anomalies of kidney and urinary tract; AKI – acute kidney injury.

Table 2. Anthropometric and biochemical parameters of patients with CKD

Parameter	Median (1st quartile–3rd quartile)	Min–max
Body mass [percentiles]	30 (7–67)	0.1–98
Height [percentiles]	16 (4–46)	0.1–85
BMI [percentiles]	52 (19–84)	0.1–98
Hemoglobin [g/dL]	12.3 (11.6–13.7)	8.5–16.4
Albumin [g/L]	44 (42–46.68)	35–53
Drugs [number]	6 (3–10)	0–16

CKD – chronic kidney disease; BMI – body mass index.

1192

K. Kiliś-Pstrusińska et al. Depressive disorders in children with CKD

Main results

Results of Kovacs's test in CKD children are shown in Tables 3,4. Collected data indicate that most children with CKD have acquired medium scores (according to Kovacs, points ranging from 40–59), which correspond to the typical severity of depressive symptoms in children of the same sex and of similar age (Polish standardization group). In the studied group, 8 children scored 60 points or more, 2 children were in the range of 60–64 and 6 children had 65 points and above. It indicates that within the studied group, 11% of participants presented with symptoms suggesting depressive disorder and 8.2%

Table 3. Results of the Kovacs' test in the group of patients with CKD (n = 73)

CDI2 category score	Median (1st quartile–3rd quartile)	Min–max
Total score	49.5 (42–55)	21–74
Emotional problems	47.5 (40.5–50.5)	27–73
Negative mood/physical symptoms	48.5 (39–55)	34–74
Negative self esteem	48 (38.5–53.5)	33–68
Functional problems	52 (44.5–57.5)	26–79
Ineffectiveness	50 (42–58)	27–79
Interpersonal problems	45 (44–58)	43–72

CKD – chronic kidney disease ; CDI2 – Children's Depression Inventory 2.

Table 4. Results of Kovacs's test (total score) in the group of children with CKD according to the CKD stage

CKD	Median (1st quartile–3rd quartile)	Min–max
Stage II (n = 12)	46.5 (40.5–54)	36–69
Stage III (n = 30)	44.5 (39–54)	21–71
Stage IV (n = 24)	54 (49–58)	36–74
Stage V (n = 9)	50.5 (48–56)	28–63

CKD – chronic kidney disease.
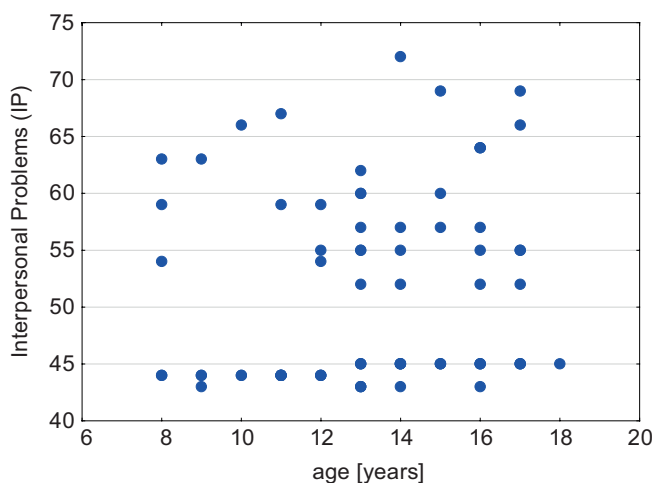
Table 5. The results of the logistic regression of the score in Kovacs' test (high (>59) compared to low (≤ 59)) on the selected explanatory variables

Explanatory variable	Coefficient	SE	z	p-value
Intercept	−4.15	3.01	−1.38	0.168
Age [years]	0.03	0.20	0.17	0.869
Disease duration [years]	0.02	0.11	0.22	0.828
Height [percentiles]	0.00	0.02	−0.06	0.956
BMI [percentiles]	−0.02	0.01	−1.23	0.217
Current CKD staging [1–5]	0.56	0.51	1.10	0.272
Family status [modelled: "complete"]	−0.31	0.86	−0.36	0.718
Sex [modelled: "woman"]	0.82	0.83	0.98	0.328

SE – standard error; z – test value.

were potentially depressed. Using the logistic regression model, no statistically significant differences were found in patients who scored >59 and ≤59 for the following traits: sex, age at the time of the study, duration of the disease, current CKD staging, family status (complete family or non-complete family), height, and body mass index (BMI) percentile (Table 5). The data from this patient subgroup were analyzed qualitatively. In the group of 8 children, there were more girls (5) than boys (3). Chronic kidney disease was diagnosed in early childhood, and in most cases the length of the disease exceeded 10 years. In 5 cases, children's weight and height were below the 10th percentile.

The associations between the Kovacs's test scores and clinical traits are shown in Table 6. The analysis showed a statistically significant positive correlation between patients' age and Interpersonal Problems (IP) score (Fig. 1), and statistically significant negative correlation between the age of CKD diagnosis and TS, ineffectiveness trait (Fig. 2), and, at the limit of statistical significance, negative mood/physical symptoms trait. The duration of CKD positively correlated
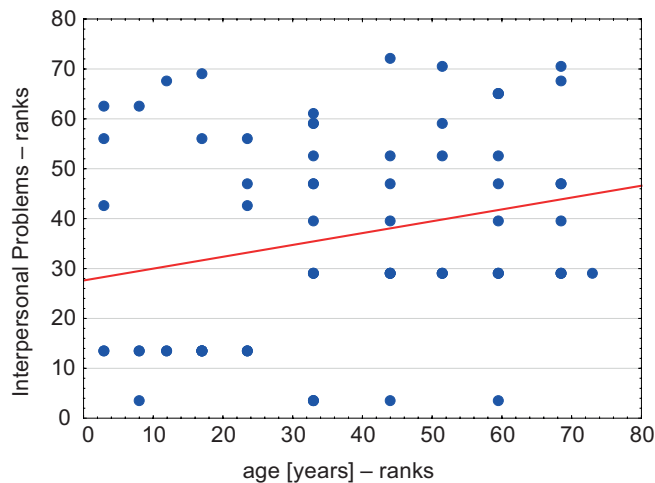
Fig. 1. Results of Spearman's correlation analysis between patients' age and results of interpersonal problems subscale scores (r = 0.24, p = 0.041). Left – original data, right – ranked data
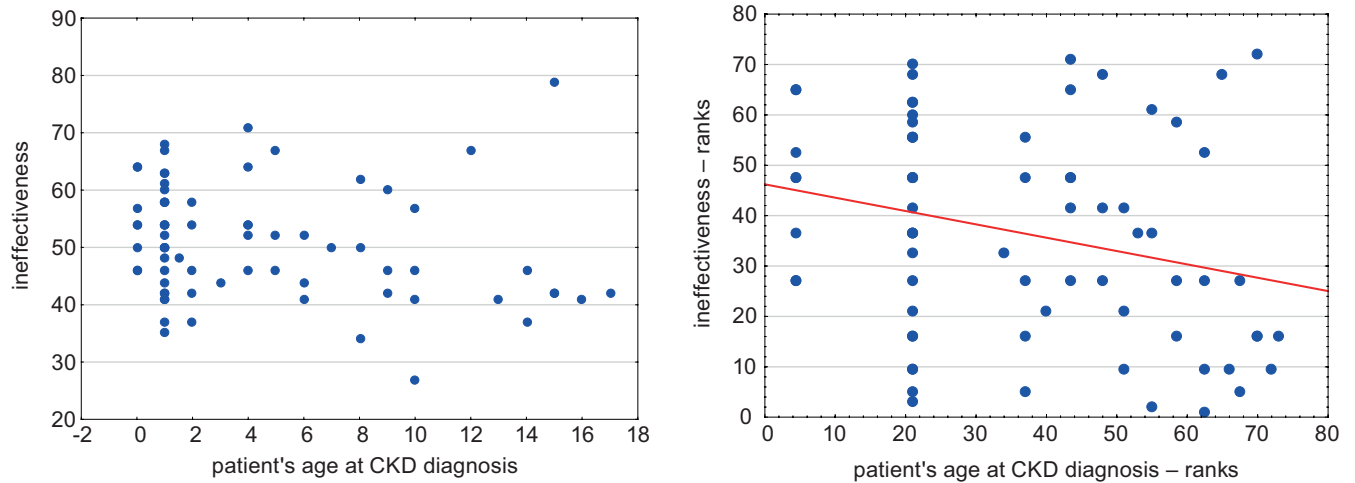
Fig. 2. Results of Spearman's correlation analysis between patients' age at chronic kidney disease (CKD) diagnosis and results of ineffectiveness subscale scores (r = −0.26, p = 0.026). Left – original data, right – ranked data
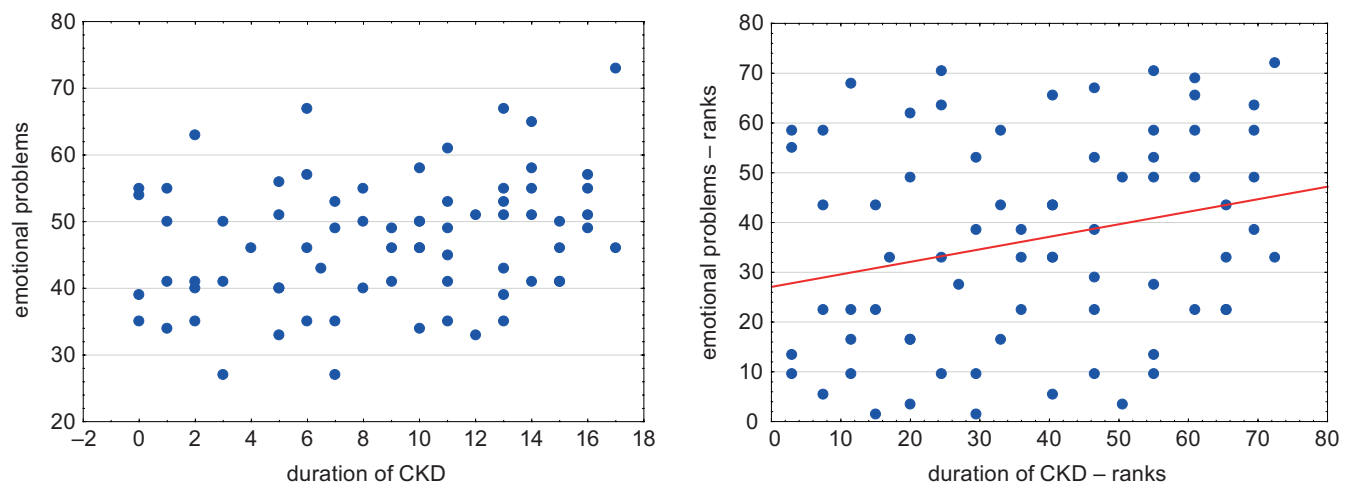
Fig. 3. Results of Spearman's correlation analysis between duration of chronic kidney disease (CKD) diagnosis and results of emotional problems scale scores (r = 0.25, p = 0.032). Left – original data, right – ranked data
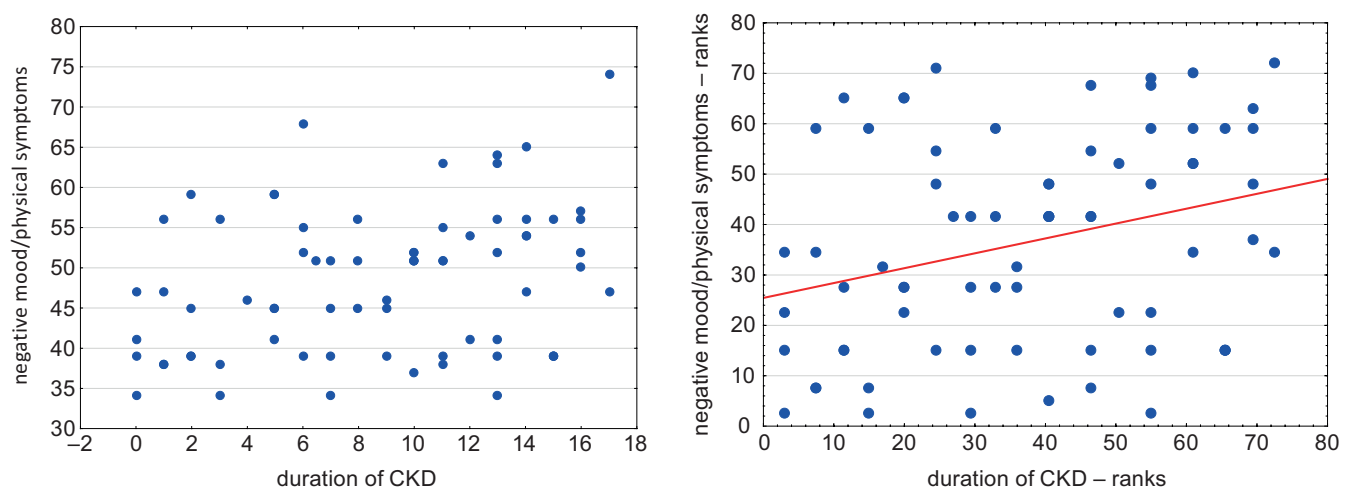
Fig. 4. Results of Spearman's correlation analysis between duration of chronic kidney disease (CKD) diagnosis and results of negative mood/physical symptoms subscale scores (r = 0.30, p = 0.012). Left – original data, right – ranked data

Table 6. The relationship between results of Child Depression Inventory 2 (CDI2) test and clinical parameters in CKD children

Parameter	Total score	Emotional problems	Negative mood/physical symptoms	Negative self-esteem	Functional problems	Ineffectiveness	Interpersonal problems
Age[1]	0.02 (0.863)	0.19 (0.105)	0.15 (0.206)	0.09 (0.479)	−0.09 (0.431)	−0.19 (0.112)	0.24 (0.041)
Patient's age at CKD diagnosis[1]	−0.22 (0.061)	−0.19 (0.112)	−0.23 (0.050)	−0.19 (0.101)	−0.22 (0.067)	−0.26 (0.026)	0.02 (0.898)
Duration of CKD[1]	0.21 (0.092)	0.25 (0.032)	0.30 (0.012)	0.16 (0.177)	0.14 (0.222)	0.14 (0.230)	0.07 (0.547)
Gender[2]	−0.07 (0.946)	0.92 (0.356)	0.54 (0.589)	−0.01 (0.996)	−0.49 (0.624)	−0.16 (0.875)	0.51 (0.608)
Current stage of CKD[3]	9.68 (0.046)	11.21 (0.024)	8.94 (0.062)	7.10 (0.131)	6.20 (0.185)	2.82 (0.588)	5.58 (0.334)
Body mass [percentiles][1]	−0.05 (0.666)	−0.08 (0.534)	−0.07 (0.581)	−0.08 (0.533)	0.03 (0.801)	0.01 (0.939)	−0.06 (0.637)
Body height [percentiles][1]	−0.12 (0.309)	−0.15 (0.197)	−0.18 (0.137)	−0.12 (0.332)	−0.08 (0.492)	−0.04 (0.770)	−0.10 (0.408)
BMI [percentiles][1]	0.003 (0.979)	0.03 (0.812)	0.04 (0.713)	0.01 (0.959)	−0.02 (0.870)	−0.01 (0.917)	−0.04 (0.723)
Serum creatinine[1]	0.19 (0.117)	0.10 (0.392)	0.22 (0.068)	−0.02 (0.879)	0.15 (0.223)	0.05 (0.658)	0.14 (0.254)
Hemoglobin[1]	−0.09 (0.446)	−0.03 (0.795)	−0.06 (0.625)	−0.09 (0.467)	−0.07 (0.559)	−0.01 (0.951)	−0.08 (0.507)
Albumin[1]	−0.10 (0.384)	−0.01 (0.956)	−0.07 (0.535)	−0.02 (0.865)	−0.14 (0.245)	−0.04 (0.761)	−0.20 (0.085)
Number of drugs[1]	0.13 (0.291)	0.07) (0.569)	0.18 (0.127)	−0.08 (0.495)	0.08 (0.492)	0.07 (0.550)	−0.03 (0.787)

CKD – chronic kidney disease; BMI – body mass index; [1,2,3] tests used; p-value is given in parentheses; p < 0.05 in bold; [1] The Spearman's rank-order correlation (correlation coefficient r_S); [2] Mann–Whitney test with correction for continuity (U-value); [3] analysis of variance (ANOVA) Kruskal–Wallis test by ranks (H-value).

with EP and negative mood/physical symptoms traits (Fig. 3,4). There was a positive correlation between the age of diagnosis and the ineffectiveness trait. A statistically significant correlation between the current stage of chronic kidney disease (CKD) and TS and EP was found. Analysis of multiple (two-sided) comparisons showed a significant difference between CKD stage III and IV (z = 2.88; p = 0.040 for TS and z = 3.14; p = 0.017), with higher scores noted in patients with CKD stage IV (Fig. 5). Slightly above the threshold for statistical significance was a link between the current CKD stage and a negative mood/physical symptoms trait, with the analysis of multiple (two-sided) comparisons showing marginal statistical significance between stages III and IV of CKD (Dunn's test: z = 2.76; p = 0.057) (Table 7). In addition, lower height was associated with increased emotional problems and a more negative mood.

A comparative overview of the results of Kovacs's test for children and their parents is shown in Table 8. A statistically significant difference was found within the TS (parental mean score 54.56 ±10.18, child's 49.00 ±10.62, t = 4.92, degree of freedom (df) = 70 p < 0.001), and trait-related subscales of EP (parental mean score 52.57 ±10.21, child's 47.13 ±9.58, t = 4.67, df = 71, p < 0.001) and FP (parental mean score 54.74 ±9.95, child's score 50.96 ±10.04, t = 3.40, df = 71, p = 0.001) (Fig. 6). In the case where both
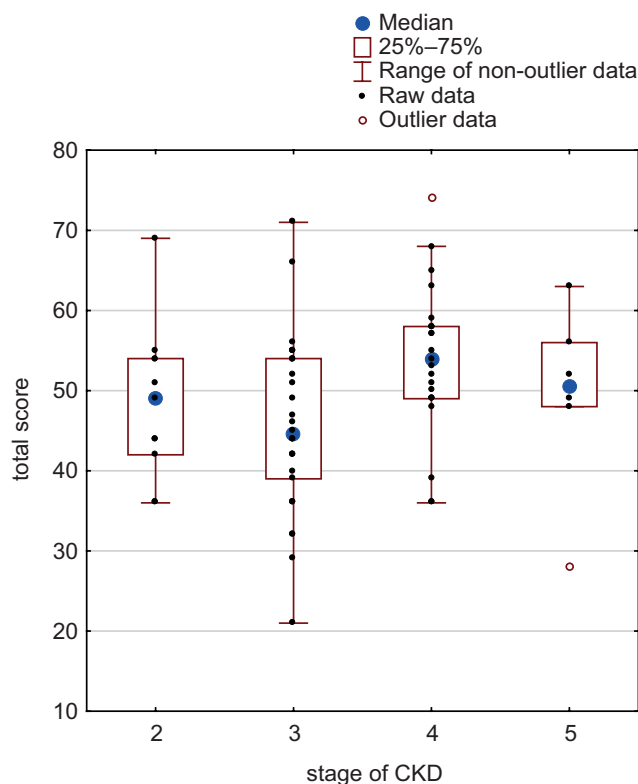
Fig. 5. Total score in regard to the current stage of chronic kidney disease (CKD)

Table 7. The results of Dunn's post hoc test of the differences in the negative mood/physical symptoms trait scores between the current chronic kidney disease (CKD) stages

CKD stage	1	2	3	4	5
1	–	1.0000	1.0000	1.0000	1.0000
2	0.1371	–	1.0000	0.4191	1.0000
3	0.1215	0.0556	–	0.0575	1.0000
4	0.8702	2.0345	2.7617	–	1.0000
5	0.5420	0.8715	1.0328	0.6621	–

1–5: CKD stages, right-top part: p-values, left-bottom part: z-values

Table 8. Comparative summary of Child Depression Inventory 2 (CDI2) results in a group of chronic kidney disease (CKD) children (CDI2: Self-Report) and their parents (CDI2: Parent Form)

Results of CDI2	Children with CKD (n = 73)		Parents (n = 92)
	median (1st quartile–3rd quartile)	min–max	median (1st quartile–3rd quartile)
Total score	49.5 (42–55)	21–74	55 (47–60)
Emotional problems	47.5 (40.5–50.5)	27–73	52 (44–60.5)
Functional problems	52 (44.5–57.5)	26–79	52.5 (50–59.5)
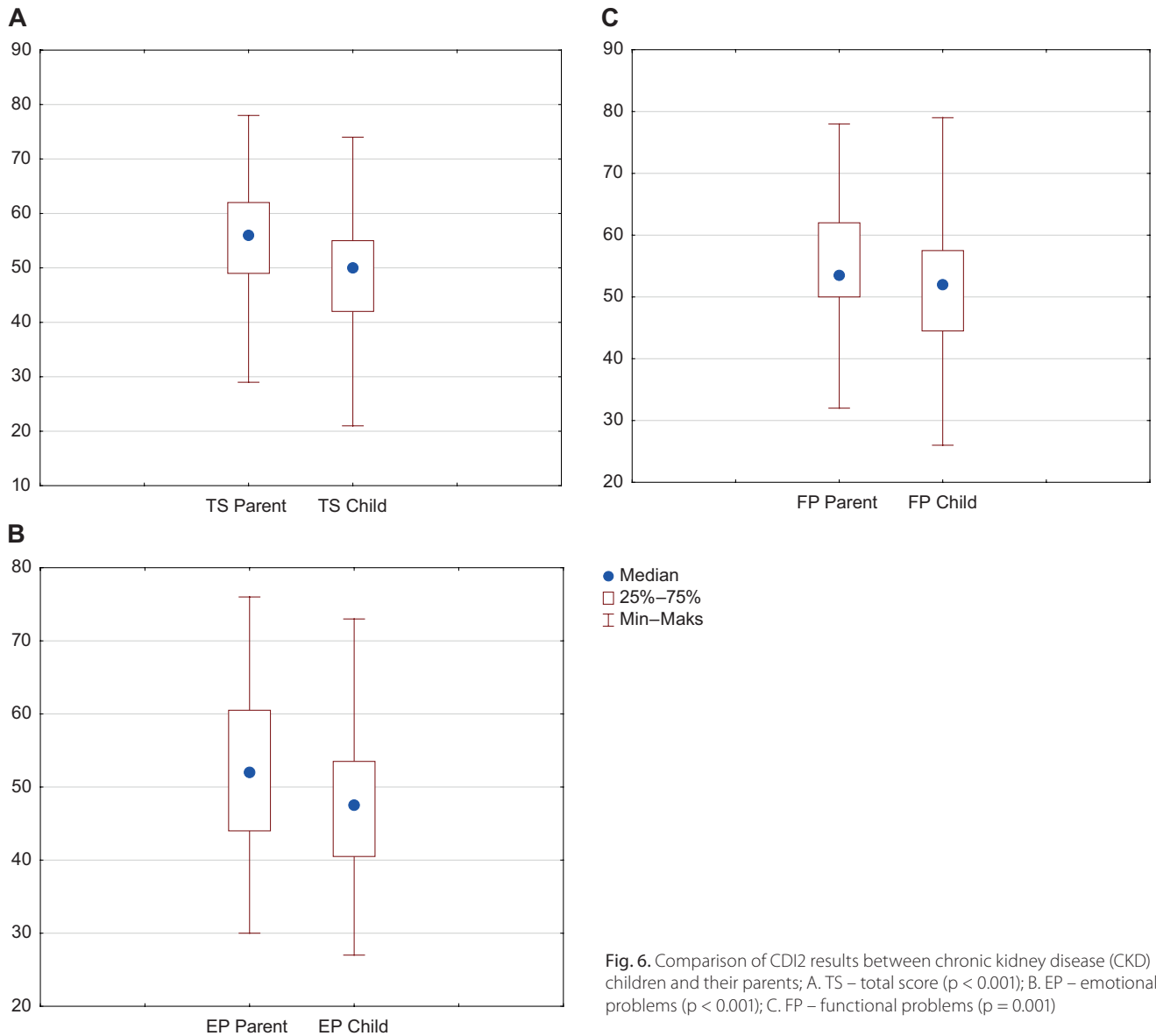
Fig. 6. Comparison of CDI2 results between chronic kidney disease (CKD) children and their parents; A. TS – total score (p < 0.001); B. EP – emotional problems (p < 0.001); C. FP – functional problems (p = 0.001)

parents assessed the severity of their child's depressive symptoms, no difference between female and male parents was found (TS – t-test for matched pairs: |t| = 0.62, df = 19, p = 0.542, EP – Wilcoxon test for matched pairs: Z = 0.16, N = 14, p = 0.875, FP – t-test for matched pairs: |t| = 0.33, df = 19, p = 0.747).

Discussion

The CDI used in this study was based on self-report of depressive symptoms that the patient experiences or has experienced lately.

The study did not show that the vast majority of CKD children treated conservatively presented with emotional difficulties associated with depression. Only 2 study participants (2.7%) had elevated results on the Kovacs's test (total T-score 60−64), and 6 (8.2%) met the criteria of depression (total T-score ≥65). Our results are in line with the analysis carried out by Stahl et al.[14] concerning psychiatric disorders in CKD children based on the parent-reported diagnoses. As a part of the baseline assessment, 345 children completed CDI2, and among them, only 2.3% met the screening threshold for clinically significant depressive symptoms. In another study, 7% of CKD children and adolescents (median GFR 41.6 mL/min/1.73 m^2 (1st quartile (Q1) = 31.9, 3rd quartile (Q3) = 53.6)) met the study criteria for depression, and 5% reported elevated depressive symptoms in CDI.[9] In some works, the percentage of children with CKD and depression is higher. However, most studies on depression/anxiety and health-related quality of life (HRQoL) in children with CKD focus on severe CKD, end-stage renal disease (ESRD) and kidney transplantation patients, with less emphasis on patients with mild-to-moderate CKD.[7,12,19,20] The study groups were different in age and heterogeneous in terms of the type of CKD treatment. For example, in the study on 71 patients with CKD aged 8–25 years (among them, 3% on dialysis and 25% with functioning transplant), depression was identified in 12 (17%) patients.[13] In addition, different instruments were used for the diagnosis of depressive disorders in the abovementioned study, such as CDI2 and Beck Depression Inventory (BDI). Furthermore, it cannot be ruled out that some self-reported variables could be subject to information bias, as patients may under- or overreport symptoms. We cannot also exclude other confounders (e.g., personality traits). Different factors may mediate the development of depressive disorders.[21–24] However, research on these potential factors is inconclusive.

In our study, no association between the presence of general depressive symptoms (TS, EP, FP, and 3 of 4 subscale scores) and the patient's age was found. However, we stated a positive correlation between the age and the interpersonal problems subscale results. Other authors report that the period of early adolescence may represent a particularly

formative and vulnerable time in the development of mood and interpersonal skills. We also revealed that the patient's age at CKD diagnosis may be linked to depressive symptoms. The younger the age of diagnosis, the more probable that general depressive symptoms will occur and lower effectiveness will be perceived. Our results indicate that implementation of proper psychological care from the moment of the diagnosis is necessary. It is also worth noting that a lack of effectiveness might result from "learned helplessness". It is a phenomenon observed when humans have been conditioned to expect pain, suffering or discomfort without a way to escape it.[25] Lack of efficiency can also be connected with overprotective parenting styles and the elimination of the child's daily chores to alleviate the burden of illness. However, this area requires further research.

Our study has shown a link between depressive symptoms (EP and negative mood/physical symptoms) and the duration of the disease. It may indicate the negative impact of chronic disease-associated difficulties on a child's emotional functioning. This suggestion is proven right by the significant difference in depressive symptoms between the III and IV stages of CKD. Our observations indicate a lack of patients' adaptation to CKD, which may be caused by insufficient access to psychological care in Poland. Results of the study by Kogon et al. also indicated that having a diagnosis of CKD for a more extended period may be associated with a higher likelihood of depression.[12] The authors speculated that the burden and stress of living with CKD increases over time and may worsen a child's ability to adjust. However, in the other paper, Kogon et al.[13] found that CKD duration was not related to depression. In addition, their result showed that eGFR was unrelated to depression. Our observations vary. We found a relationship between depressive disorders and the current stage of CKD, regarding emotional problems in particular. The analysis showed statistically significant differences between children with III and IV stage of CKD with more advanced disturbances declared by patients with CKD stage IV. Our data are consistent with the observations of Stahl et al.,[14] who noted a trend toward increased prevalence of depression with advancing CKD stage. Also, Roumelioti et al. showed that the severity of CKD was associated with lower quality of life ratings and increased reporting of weakness, fatigue and daytime sleepiness.[26] The last symptoms may be masks of depression. An association between the level of renal dysfunction and emotional-behavioral problems seems to be real. Intensifying metabolic disorders, deterioration in body functioning and medical complications, hospitalizations, need for aid from parents or caregivers, and change in interpersonal relations on the child–parent axis may lead to emotional burdens. Johnson et al.[27] presented a fascinating hypothesis that biological factors inherent to progressive CKD are likely to disrupt endocrine and neurological transmitters and influence mood and emotional functioning. The authors rightly advocate research into the potential mechanisms of that relationship.

According to the literature, a child's gender may be connected with depression, with girls presenting depressive and anxious symptoms more often than boys.[21,23] Our study did not find such a link. However, in the group of 8 children with the highest TS, girls had a 5:3 advantage.

The results of our study did not show a significant relationship between constitutional parameters and the occurrence of depressive symptoms. The literature highlights short stature as a predisposing factor for depression and low HRQoL scores.[28,29] In our research, such a tendency has only emerged. In the group of 8 children with the highest TS, 5 patients had height below the 10th percentile. Although our group of CKD children treated conservatively represents one of the largest samples to examine this research question, it is a relatively small sample size to detect some correlations and links. It is commonly repeated that obesity is related to depression, but this statement is not fully supported by research findings.[30,31] Three out of 8 longitudinal studies reported associations between obesity and subsequent depression in female children and adolescents only, and 3 out of 9 studies obtained evidence in favor of the other direction. In our work, we did not notice such a relationship. However, in the study by Kogon et al.,[13] the presence of depression was significantly associated with the presence of obesity, defined as BMI ≥95th percentile. Probably, the dissimilarity of our observations is due to the fact that by adopting the same criteria as in the work of Kogon et al., obesity occurred in only 11% of our study participants, while in our study in as much as 30%.

In our research, we found significant differences between the results of parent-reported and self-report instruments that identified depression, both in the overall assessment and in the areas of emotional and functional problems. Parents were more likely than patients with CKD to perceive their children as depressed. Ten parents (13.7%) assessed their children as meeting the criteria for depression, and an additional 15 (20.6%) rated their children as at risk of elevated depressive symptoms. In the patients' self-assessment, the percentages were 8.2% and 2.7%, respectively. Similar observations were made by Stahl et al.[14] In their study, among the 346 children with CKD, 8 (2.3%) met the screening threshold for clinically significant depression symptoms, and 26 (7.5%) had a parent-reported depression diagnosis. Discordant parent and child reporting is common.[32–34] Also, in our work on the quality of life of children with CKD,[35] we found that parents describe their child's HRQoL as lower than children themselves. Various factors come into play: dissimilar experiences, different reference systems and levels of adaptation to the disease.[36] Parents of children with CKD feel more stress and depression caused by the burden of their child's disease and the responsibility of CKD management.[37] Our results may reflect the children's tendency to emphasize the positive aspects of adaptation.[38] On the other hand, parents may be more reliable in identifying the most strongly affected areas of their children's functioning and the so-called "hidden morbidities".[39] Therefore, a dyadic child–parent approach to assessing pediatric outcomes is necessary and may provide unique information about the children's risk factors for depression and resilience to it.

A divergent assessment of CKD children's emotional and behavioral status by patients and their parents may have serious consequences, including lack of cooperation in proper therapy, demotivation for self-reliance and parental overprotection. It should also be noted that some disorders may be dynamic and change over time. The focus of children and adolescents on "here and now" and the absence of recent symptoms is likely to result in misclassification and false negative diagnoses of depressive symptoms. Thus, each case of divergence in assessing potential depressive disorders requires an individual approach and specialized psychiatric assessment. Moreover, as shown in the study by Boyd et al.[40] on the patterns of parent-youth reports of HRQoL among young people aged 7–20 with mood disorders, not only the pattern of parent low-youth low assessment of HRQoL but also of parent low-youth high assessment was associated with a more impaired clinical presentation, i.e., at-risk for worse mood symptoms and suicidal ideation.

Limitations

Our study has some limitations. The study group was relatively small, although it is one of the largest in the available literature and is strictly defined. It consisted of CKD children treated only conservatively, according to the same standards.

The depressive disorders in CKD children were scored based on a self-rating scale and did not include a structured interview, which could lead to under- or overreporting of depression. However, the same validated tool was applied to all participants. Kovacs's test is considered one of the best for assessing depression. Disparities of results shown as opposed to other articles (in which different measuring scales were used) indicate that further research is needed to establish proper screening methods for depression in children with CKD.

Our analysis excluded parent-related variables that may also influence a child's emotional state, such as parents' age, education, work, and economic status, the presence of chronic diseases, and the emotional state of parents themselves.

The literature points to nursing care and peer support as potential factors protecting from developing depression.[41,42] We did not consider these variables. However, this field of research on children with CKD might prove vital.

Conclusions

To sum up, the problem of depression in children with CKD treated conservatively exists and psychological

assistance should be included as a standard of care of young people with CDK. Screening in this area should be carried out considering the assessment of the patient and their parents/caregivers. The final diagnosis of the occurrence of depressive disorders must be based on a multidimensional assessment of the patient's situation. Factors connected to the prevalence of depressive symptoms in CKD children treated conservatively require further research. Establishing such factors may create an "anti-depressive" targeted psychological care which could be introduced in pediatric nephrology clinics, with specific interventions tailored to particular subgroups. Age at the time of the diagnosis and duration of the disease seem to be crucial factors determining the risk of depression. During the course of CKD, progression from stage III to stage IV is strongly linked to the worsening of the psychological state, especially regarding emotional problems. Understanding the extent to which time with a diagnosis of CKD affects the mental health of our patients will allow healthcare providers to determine when patients are most in need of psychosocial support and when interventions may be most effective.

Disparities between children's self-reports and their parents' assessments are an essential area of future research. Considering the role that parents play in children's development and treatment, child–parent disagreement may influence how parents respond to children's healthcare and emotional needs, which may impact the children's adaptation over time. The additional cost of conducting a more in-depth assessment of adaptation outcomes can be offset by implementing the most effective clinical interventions.

ORCID IDs

Katarzyna Kiliś-Pstrusińska https://orcid.org/0000-0001-7352-6992
Anna Medyńska https://orcid.org/0000-0001-8191-045X
Piotr Adamczyk https://orcid.org/0000-0001-9557-221X
Beata Leszczyńska https://orcid.org/0000-0001-6811-4934
Maria Szczepańska https://orcid.org/0000-0002-6772-1983
Marcin Tkaczyk https://orcid.org/0000-0003-1753-7560
Anna M. Wasilewska https://orcid.org/0000-0003-0257-4422
Katarzyna Zachwieja https://orcid.org/0000-0002-1949-5096
Ilona Zagożdżon https://orcid.org/0000-0002-6435-7776
Krzysztof Kujawa https://orcid.org/0000-0003-2812-4702
Natalia W. Dryjańska https://orcid.org/0009-0003-1875-8397

References

1. Becherucci F, Roperto RM, Materassi M, Romagnani P. Chronic kidney disease in children. *Clin Kidney J*. 2016;9(4):583–591. doi:10.1093/ckj/sfw047

2. Dotis J, Pavlaki A, Printza N, et al. Quality of life in children with chronic kidney disease. *Pediatr Nephrol*. 2016;31(12):2309–2316. doi:10.1007/s00467-016-3457-7

3. Ruidiaz-Gómez KS, Higuita-Gutiérrez LF. Impact of chronic kidney disease on health-related quality of life in the pediatric population: Meta-analysis. *J Pediatr (Rio J)*. 2021;97(5):478–489. doi:10.1016/j.jped.2020.10.013

4. Gerson AC, Wentz A, Abraham AG, et al. Health-related quality of life of children with mild to moderate chronic kidney disease. *Pediatrics*. 2010;125(2):e349–e357. doi:10.1542/peds.2009-0085

5. Moreira JM, Bouissou Morais Soares CM, Teixeira AL, Simões E Silva AC, Kummer AM. Anxiety, depression, resilience and quality of life in children and adolescents with pre-dialysis chronic kidney disease. *Pediatr Nephrol*. 2015;30(12):2153–2162. doi:10.1007/s00467-015-3159-6

6. Regier DA, Kuhl EA, Kupfer DJ. The DSM-5: Classification and criteria changes. *World Psychiatry*. 2013;12(2):92–98. doi:10.1002/wps.20050

7. Palmer S, Vecchio M, Craig JC, et al. Prevalence of depression in chronic kidney disease: Systematic review and meta-analysis of observational studies. *Kidney Int*. 2013;84(1):179–191. doi:10.1038/ki.2013.77

8. World Health Organization (WHO). Improving the mental and brain health of children and adolescents. Geneva, Switzerland: World Health Organization (WHO): 2022. https://www.who.int/activities/improving-the-mental-and-brain-health-of-children-and-adolescents. Accessed June 15, 2023.

9. Kogon AJ, Matheson MB, Flynn JT, et al. Depressive symptoms in children with chronic kidney disease. *J Pediatr*. 2016;168:164–170.e1. doi:10.1016/j.jpeds.2015.09.040

10. Bakr A, Amr M, Sarhan A, et al. Psychiatric disorders in children with chronic renal failure. *Pediatr Nephrol*. 2007;22(1):128–131. doi:10.1007/s00467-006-0298-9

11. Garralda ME, Jameson RA, Reynolds JM, Postlethwaite RJ. Psychiatric adjustment in children with chronic renal failure. *J Child Psychol Psychiatry*. 1988;29(1):79–90. doi:10.1111/j.1469-7610.1988.tb00691.x

12. Kogon AJ, Vander Stoep A, Weiss NS, Smith J, Flynn JT, McCauley E. Depression and its associated factors in pediatric chronic kidney disease. *Pediatr Nephrol*. 2013;28(9):1855–1861. doi:10.1007/s00467-013-2497-5

13. Kogon AJ, Kim JY, Laney N, et al. Depression and neurocognitive dysfunction in pediatric and young adult chronic kidney disease. *Pediatr Nephrol*. 2019;34(9):1575–1582. doi:10.1007/s00467-019-04265-z

14. Stahl JL, Wightman AG, Flythe JE, Weiss NS, Hingorani SR, Stoep AV. Psychiatric diagnoses in children with CKD compared to the general population. *Kidney Med*. 2022;4(6):100451. doi:10.1016/j.xkme.2022.100451

15. National Kidney Foundation. K/DOQI clinical practice guidelines for chronic kidney disease: Evaluation, classification, and stratification. *Am J Kidney Dis*. 2002;39(2 Suppl 1):S1–S266. PMID:11904577.

16. Schwartz GJ, Muñoz A, Schneider MF, et al. New equations to estimate GFR in children with CKD. *J Am Soc Nephrol*. 2009;20(3):629–637. doi:10.1681/ASN.2008030287

17. Kovacs M. Children's Depression Inventory (CDI and CDI 2). In: Cautin RL, Lilienfeld SO, eds. *The Encyclopedia of Clinical Psychology*. Hoboken, USA: Wiley; 2015:1–5. doi:10.1002/9781118625392.wbecp419

18. Wrocławska-Warchala E, Wujcik R, Kovacs M. *Zestaw kwestionariuszy do diagnozy depresji u dzieci i młodzieży CDI 2TM*. Warsaw, Poland: Pracownia Testów Psychologicznych Polskiego Towarzystwa Psychologicznego; 2017. ISBN:978-83-63545-40-6.

19. White C, McDonnell H. Psychosocial distress in patients with end-stage kidney disease. *J Renal Care*. 2014;40(1):74–81. doi:10.1111/jorc.12054

20. Berney-Martinet S, Key F, Bell L, Lépine S, Clermont M, Fombonne E. Psychological profile of adolescents with a kidney transplant. *Pediatr Transplant*. 2009;13(6):701–710. doi:10.1111/j.1399-3046.2008.01053.x

21. Kiliś-Pstrusińska K, Medyńska A, Adamczak P, et al. Anxiety in children and adolescents with chronic kidney disease: Multicenter national study results. *Kidney Blood Press Res*. 2013;37(6):579–587. doi:10.1159/000355738

22. Abrão RO, Lopes M, Silva GJS, Ferraro AA, Koch VH. Study of the association between generic and disease-specific quality of life and behavior problems in pediatric patients with chronic kidney disease stage 3 or higher and the quality of life and mental health of their primary caregivers. *Pediatr Nephrol*. 2021;36(10):3201–3210. doi:10.1007/s00467-021-04986-0

23. Loevaas MES, Sund AM, Patras J, et al. Emotion regulation and its relation to symptoms of anxiety and depression in children aged 8–12 years: Does parental gender play a differentiating role? *BMC Psychol*. 2018;6(1):42. doi:10.1186/s40359-018-0255-y

24. Martinsen KD, Rasmussen LMP, Wentzel-Larsen T, et al. Change in quality of life and self-esteem in a randomized controlled CBT study for anxious and sad children: Can targeting anxious and depressive symptoms improve functional domains in schoolchildren? *BMC Psychol*. 2021;9(1):8. doi:10.1186/s40359-021-00511-y

25. Pryce CR, Azzinnari D, Spinelli S, Seifritz E, Tegethoff M, Meinlschmidt G. Helplessness: A systematic translational review of theory and evidence for its relevance to understanding and treating depression. *Pharmacol Ther*. 2011;132(3):242–267. doi:10.1016/j.pharmthera.2011.06.006

26. Roumelioti ME, Wentz A, Schneider MF, et al. Sleep and fatigue symptoms in children and adolescents with CKD: A cross-sectional analysis from the Chronic Kidney Disease in Children (CKiD) study. *Am J Kidney Dis*. 2010;55(2):269–280. doi:10.1053/j.ajkd.2009.09.021

27. Johnson RJ, Gerson AC, Harshman LA, et al. A longitudinal examination of parent-reported emotional-behavioral functioning of children with mild to moderate chronic kidney disease. *Pediatr Nephrol*. 2020;35(7):1287–1295. doi:10.1007/s00467-020-04511-9

28. Rosenkranz J, Reichwald-Klugger E, Oh J, Turzer M, Mehls O, Schaefer F. Psychosocial rehabilitation and satisfaction with life in adults with childhood-onset of end-stage renal disease. *Pediatr Nephrol*. 2005;20(9):1288–1294. doi:10.1007/s00467-005-1952-3

29. Broyer M, Le Bihan C, Charbit M, et al. Long-term social outcome of children after kidney transplantation. *Transplantation*. 2004;77(7):1033–1037. doi:10.1097/01.TP.0000120947.75697.8B

30. Mühlig Y, Antel J, Föcker M, Hebebrand J. Are bidirectional associations of obesity and depression already apparent in childhood and adolescence as based on high-quality studies? A systematic review. *Obes Rev*. 2016;17(3):235–249. doi:10.1111/obr.12357

31. Lister NB, Baur LA, Felix JF, et al. Child and adolescent obesity. *Nat Rev Dis Primers*. 2023;9(1):24. doi:10.1038/s41572-023-00435-4

32. Silva N, Crespo C, Carona C, Bullinger M, Canavarro MC. Why the (dis)agreement? Family context and child–parent perspectives on health-related quality of life and psychological problems in paediatric asthma. *Child Care Health Dev*. 2015;41(1):112–121. doi:10.1111/cch.12147

33. Upton P, Lawford J, Eiser C. Parent–child agreement across child health-related quality of life instruments: A review of the literature. *Qual Life Res*. 2008;17(6):895–913. doi:10.1007/s11136-008-9350-5

34. De Los Reyes A, Lerner MD, Keeley LM, et al. Improving interpretability of subjective assessments about psychological phenomena: A review and cross-cultural meta-analysis. *Rev Gen Psychol*. 2019;23(3):293–319. doi:10.1177/1089268019837645

35. Kiliś-Pstrusińska K, Medyńska A, Chmielewska IB, et al. Perception of health-related quality of life in children with chronic kidney disease by the patients and their caregivers: Multicentre national study results. *Qual Life Res*. 2013;22(10):2889–2897. doi:10.1007/s11136-013-0416-7

36. Davis E, Nicolas C, Waters E, et al. Parent-proxy and child self-reported health-related quality of life: Using qualitative methods to explain the discordance. *Qual Life Res*. 2007;16(5):863–871. doi:10.1007/s11136-007-9187-3

37. Lima AGT, Sales CCDS, Serafim WFDL. Burden, depression and anxiety in primary caregivers of children and adolescents in renal replacement therapy. *J Bras Nefrol*. 2019;41(3):356–363. doi:10.1590/2175-8239-jbn-2018-0039

38. Oeffinger D, Gorton G, Bagley A, et al. Outcome assessments in children with cerebral palsy. Part I: Descriptive characteristics of GMFCS levels I to III. *Dev Med Child Neurol*. 2007;49(3):172–180. doi:10.1111/j.1469-8749.2007.00172.x

39. Varni JW, Burwinkle TM, Lane MM. Health-related quality of life measurement in pediatric clinical practice: An appraisal and precept for future research and application. *Health Qual Life Outcomes*. 2005;3(1):34. doi:10.1186/1477-7525-3-34

40. Boyd RC, Jones JD, Makol BA, De Los Reyes A, Hatkevich CE, Benton TD. Parent-youth convergence (and divergence) in reports about pediatric quality of life. *Qual Life Res*. 2023;32(9):2551–2560. doi:10.1007/s11136-023-03423-z

41. Goldschmidt T, Petersen L, Booley S, Roman NV. Perspectives of nurturance within the parent–child relationship in resource-constrained families. *Child Care Health Dev*. 2021;47(4):494–500. doi:10.1111/cch.12861

42. Hooper SR, Johnson RJ, Gerson AC, et al. Overview of the findings and advances in the neurocognitive and psychosocial functioning of mild to moderate pediatric CKD: Perspectives from the Chronic Kidney Disease in Children (CKiD) cohort study. *Pediatr Nephrol*. 2022;37(4):765–775. doi:10.1007/s00467-021-05158-w

Comparison of different treatment regimens and analysis of prognostic factors in secondary hemophagocytic lymphohistiocytosis in adults: A single-center retrospective study

Xing Wu[1,A,D–F], Changfeng Man[1,B,C,F], Wanying Cheng[1,B,C,F], Guangli Yin[2,C,F], Jiayu Huang[1,B,F], Jujuan Wang[2,C,F], Xin Gao[2,B,F], Tian Tian[2,B,F], Limin Duan[2,C,F], Ji Xu[2,C,F], Hongxia Qiu[2,A,D–F]

[1] Department of Hematology, The First Affiliated Hospital of Nanjing Medical University, Jiangsu Province Hospital, China
[2] Department of Geriatrics, The First Affiliated Hospital of Nanjing Medical University, Jiangsu Province Hospital, China

A – research concept and design; B – collection and/or assembly of data; C – data analysis and interpretation;
D – writing the article; E – critical revision of the article; F – final approval of the article

Address for correspondence
Hongxia Qiu
E-mail: qhx9805@126.com

Abstract

Background. Hemophagocytic lymphohistiocytosis (HLH) is a life-threatening disease caused by immune hyperactivation. The overall survival (OS) of adults with secondary HLH remains suboptimal and new treatment strategies are needed.

Objectives. This study aimed to compare the efficacy of different regimens in the treatment of secondary HLH in adults and analyze the prognostic factors affecting patient survival.

Materials and methods. The clinical data of 245 adults with secondary HLH admitted to our hospital from January 2016 to October 2021 were analyzed retrospectively. The patients were divided into 3 groups according to different treatment regimens: corticosteroids therapy + chemotherapy + supportive treatment group (JHZ group), chemotherapy + supportive treatment group (HZ group) and corticosteroids therapy + supportive treatment group (JZ group). The clinical efficacy was compared among the 3 groups after treatment, and progression-free survival (PFS) and overall survival (OS) were calculated. Additionally, risk factors associated with prognosis were also analyzed with Cox regression analysis.

Results. The objective response rate (ORR) in the JHZ group was higher than that in the HZ group and JZ group, but there was no significant difference between the 3 groups. Also, the patients in the JHZ group had the longest OS and median PFS. Further Cox regression analysis suggested that hyperbilirubinemia was an independent risk factor for OS in secondary HLH patients.

Conclusions. A combination of corticosteroids therapy, chemotherapy and supportive therapy is superior to the other 2 regimens in the clinical benefit in the treatment of secondary HLH in adults, and thus may be a preferred and feasible treatment regimen. Moreover, hyperbilirubinemia was a risk factor for prognosis that has crucial guiding significance for clinical treatment of patients with secondary HLH.

Key words: supportive treatment, hyperbilirubinemia, chemotherapy, secondary hemophagocytic lymphohistiocytosis, corticosteroids therapy

Background

Hemophagocytic lymphohistiocytosis (HLH) can be triggered by primary (genetic factors) or secondary (nongenetic factors) causes. Primary HLH is usually inherited in an autosomal recessive pattern,[1] with a high incidence in young children, being relatively rare in clinical practice but showing high mortality. However, HLH is not a pediatric-specific disease and may occur at any age. According to current studies, the incidence of secondary HLH in adults accounts for about 40% cases of HLH.[2] The causes of secondary HLH include infections, autoimmune diseases and malignancies,[3] but the pathogenesis of secondary HLH in adults has not been clarified. Adult patients with secondary HLH mainly present with symptoms of fever, organomegaly (lymphadenopathy, hepatomegaly or splenomegaly), neurological dysfunction, and liver dysfunction or coagulopathy (such as jaundice or bruising). Unfortunately, its clinical manifestations and laboratory parameters lack specificity, so it is difficult to diagnose it rapidly and treat it fully using immunosuppressive agents or chemotherapy in clinical practice. Moreover, the therapeutic effect of current treatment modalities on secondary HLH in adults is poor, and the prognosis is unsatisfactory.

There are no treatment regimens specifically developed for secondary HLH in adults, and most drugs used to treat HLH in adults are based on the HLH-94 or the HLH-2004 treatment protocols. Etoposide, dexamethasone and cyclosporin A are recommended in the HLH-94 protocol and have presented some efficacy.[1] HLH-2004 is a modification based on HLH-94, with basic treatment using etoposide, dexamethasone and cyclosporine A, and additionally with maximum supportive treatment (such as broad-spectrum antibiotics and gastric mucosal protective agents).[4] Etoposide is a chemotherapeutic drug for malignant tumors, which ablates T cells involved in the pathophysiology of HLH.[5,6] The mechanism of etoposide may induce normal apoptosis of interleukin (IL)-2-activated lymphocytes in HLH patients.[7] In a retrospective study of children with HLH associated with EBV infection, the 2.5-year survival rate was significantly higher in children who received etoposide at 4 weeks compared to children who did not.[8]

Many case reports have confirmed that a combination of chemotherapy and corticosteroid therapy has a certain alleviating effect on secondary HLH in adults. Considering the toxic effect of chemotherapeutic drugs on patients may outweigh their benefits, some researchers tried to use corticosteroids combined with supportive therapy to treat adult HLH.[9] Results showed clinical benefits and minimized toxic effect of chemotherapeutic drugs on patients.

Most existing studies on the treatment of secondary HLH in adults are case reports, and there is a lack of comprehensive and systematic analysis of the clinical efficacy of different treatment regimens in adult patients with secondary HLH.

Objectives

We aimed to preliminarily explore the preferred and feasible clinical treatment options for secondary HLH in adults by comparing different treatment options. Furthermore, we analyzed the related factors affecting the prognosis of patients using Cox regression analysis.

Materials and methods

Participants

This is a single-center retrospective study. Two hundred and forty-five adult patients with secondary HLH admitted to The First Affiliated Hospital of Nanjing Medical University, Jiangsu Province Hospital from January 2016 to October 2021 were selected as the study participants. They were divided into 3 groups according to different treatment regimens: corticosteroids therapy + chemotherapy + supportive therapy group (JHZ group) (n = 56), chemotherapy + supportive therapy group (HZ group) (n = 108) and corticosteroids therapy + supportive therapy group (JZ group) (n = 81). Informed consent was given by all patients. This study was approved by the Ethics Committee of The First Affiliated Hospital of Nanjing Medical University, Jiangsu Province Hospital (approval No. 2019-SR-446).

Inclusion and exclusion criteria

All patients satisfying the HLH-2004 diagnostic criteria[10] were selected: 1) age >18 years, with molecular diagnosis of HLH or diagnosis of X-linked lymphoproliferative syndrome; or 2) the presence of at least 3 of the following 4 criteria: fever lasting more than 7 days, body temperature >38.5°C; splenomegaly; cytopenias affecting ≥2 lineages (hemoglobin <90 g/L, platelets <100 × 10^9/L, absolute neutrophil count <1.0 × 10^9/L); hepatitis; and the presence of at least 1 of the following 4 criteria: hemophagocytosis in bone marrow, spleen or lymph node; elevated serum ferritin (≥500 μg/L); elevated soluble IL-2 receptor (sCD25) (≥2,400 U/mL); low or absent NK cell activity; and 3) other supporting evidence: hypertriglyceridemia (triglyceride level ≥ 3 mmol/L); hypofibrinogenemia (fibrinogen <1.5 g/L); hyponatremia.

Exclusion criteria were as follows: 1) patients with incomplete medical records and imaging data; 2) early patients; 3) patients treated with immune checkpoint inhibitors, but with no specific name and dose provided; 4) patients with 2 or more malignant tumors.

Treatment methods

In chemotherapy, etoposide injection (VP-16) (KPC Pharmaceuticals, Inc., Yunnan, China; 2 mL: 40 mg, batch No. H53021752) was infused intravenously (iv.).

The injection was diluted with sodium chloride injection to reach a concentration not exceeding 0.25 mg/mL. The iv. infusion was performed for no less than 30 min per time. The dose and frequency of infusion was as follows: at weeks 1 and 2: 150 mg/m^2 – twice a week; at weeks 3 to 8: 150 mg/m^2 – once a week.

In corticosteroids therapy, dexamethasone tablets (Guangdong South Land Pharmaceutical Co., Ltd., Zhanjiang, China), 0.75 mg, batch No. H44024618) were selected with the dose of 10 mg/(m^2·d) (daily dose of drug per square meter of body surface area) in weeks 1 and 2, 5 mg/(m^2·d) in weeks 3 and 4, 2.5 mg/(m^2·d) in weeks 5 and 6, and 1.25 mg/(m^2·d) in week 7. Finally, the drug was discontinued in week 8.

Supportive therapy included active prevention and treatment of infection, blood transfusion therapy, enhancing immunity, and nutritional support.

Efficacy outcome measures

Objective response rate (ORR) refers to the proportion of patients whose tumor lesion volume shrink to the expected range and can maintain the minimum time required, which is the sum of complete response (CR) rate and partial response (PR) rate. Specifically, target lesion status was assessed according to RECIST 1.1 criteria[11]: complete response (CR) – disappearance of all target lesions; partial response (PR) – at least a 30% decrease in the sum diameter of target lesions; progressive disease (PD) – at least a 20% increase in the sum diameter of target lesions; stable disease (SD) – response between PR and PD.

Overall survival (OS) is the time from the start of treatment to death, while progression-free survival (PFS) is the time from the start of treatment to the 1st recurrence/metastasis of the tumor or death of the patient. These 2 measures were mainly used to assess the clinical benefit of patients.

Statistical analyses

Experimental data were analyzed using IBM SPSS 22.0 (IMB Corp., Armonk, USA) software. The Shapiro–Wilk test was used to determine whether the continuous data conformed to normal distribution. The continuous data with non-normal distribution was expressed as median (interquartile range (IQR)) and analyzed using Kruskal–Wallis test. The categorical variables were expressed as incidence and percentage, and the difference between the 2 groups was assessed using the χ^2 or Fisher's exact tests. Progression-free survival and OS were described using the Kaplan–Meier method with the log-rank method for testing, and Bonferroni correction was used to control I-type error. Cox regression analysis was used to analyze independent risk factors for prognosis. For the Cox regression assumptions: 1) the martingale residuals test was used to test the proportional hazards assumption[12];

2) the linearity assumption was utilized to determine whether the logarithm of the survival function was linear with respect to the continuous variable; 3) variance inflation factor (VIF) and tolerance (that is, the proportion of residuals obtained when regression analysis is performed on the other independent variables with each independent variable as the dependent variable) was used to test for multicollinearity between variables. A p-value <0.05 was considered statistically significant.

Results

Basic characteristics of patients

Two hundred and forty-five adult patients with secondary HLH were divided into 3 groups according to different treatment regimens: corticosteroids therapy + chemotherapy + supportive therapy group (JHZ group) (n = 56), chemotherapy + supportive therapy group (HZ group) (n = 108) and corticosteroids therapy + supportive therapy group (JZ group) (n = 81). Combining the results showed in Supplementary Fig. 1 and Supplementary Table 1, it was determined that the age values of the groups did not follow a normal distribution. Therefore, the Kruskal–Wallis test was used for analysis. There were no statistically significant differences between the 3 groups in general data such as age (p = 0.296), sex (p = 0.370), pathological type (infection-related, tumor-related, immune disease-related; p = 0.115), and smoking history (p = 0.913) (Table 1).

Therapeutic efficacy in the 3 groups

In the JHZ group, 23 patients had CR, 16 patients PR, 12 patients SD, and 5 patients PD, with an ORR of 69.64%. In the HZ group, including 43 patients had CR, 19 patients PR, 39 patients SD and 7 patients PD, with ORR of 57.41%. Finally, in the JZ group, there were 26 patients with CR, 17 patients with PR, 37 patients with SD, and 1 patient with PD, with ORR of 53.09%. The ORR (%) in the JHZ group was higher than that in the other 2 groups, but there was no significant difference in the efficacy among the 3 treatment regimens (p = 0.0.143) (Table 2).

Prognostic analysis of patients in the 3 groups

Patients were followed up after treatment. The JHZ group was superior to the other 2 groups in terms of OS (p = 0.003). Also, the median PFS of the JHZ group (49 months) was significantly longer than that of the HZ group (29 months) and JZ group (26 months) (p < 0.001), suggesting that patients had the longest interval from the start of receiving treatment to the development of disease progression or patient death in the JHZ group (Fig. 1A,B).

Table 1. Basic characteristics of 245 adults with secondary hemophagocytic lymphohistiocytosis

Variable		JHZ group (n = 56)	HZ group (n = 108)	JZ group (n = 81)	H/F/χ^2	p-value
Age [years]		53.5 (34.5, 63.50)	57.5 (44.0, 65.0)	57.0 (45.0, 66.0)	2.432	0.296[a]
Sex (male/female)		34/22	74/34	48/33	1.990	0.370[b]
Pathological type	infection-related	25	63	39	7.418	0.115[b]
	tumor-related	17	31	20		
	immune disease-related	14	14	22		
Smoking history (no/yes)		19/37	36/72	25/56	0.182	0.913[b]
ECOG score	<2	34	55	39	2.230	0.328[b]
	≥2	22	53	42		
Malignant pleural effusion (no/yes)		39/17	79/29	60/21	0.351	0.839[b]
PD-L1 expression (positive/negative)		17/39	22/86	18/63	2.134	0.344[b]
EGFR gene mutation (positive/negative)		9/47	36/72	26/55	5.911	0.052[b]
Brain metastasis (no/yes)		11/45	38/70	22/59	4.523	0.104[b]
Surgical treatment (no/yes)		22/34	45/63	29/52	0.668	0.716[b]
Immune-related adverse events (no/yes)		37/19	76/32	67/14	5.658	0.059[b]
History of hormone therapy (no/yes)		42/14	80/28	50/31	4.171	0.124[b]
Antibiotic history (no/yes)		41/15	81/27	51/30	3.469	0.177[b]
Serum albumin	low	29	41	33	2.976	0.226[b]
	high	27	67	48		
Serum calcium	low	28	41	33	2.239	0.327[b]
	high	28	67	48		
Platelet content	<30×10⁹/L	25	63	45	2.864	0.239[b]
	≥30×10⁹/L	31	45	36		
Fibrinogen	<1.0 g/L	27	67	47	2.895	0.235[b]
	≥1.0 g/L	29	41	34		
Hyperbilirubinemia	≤17.1 μmol/L	35	56	43	1.814	0.404[b]
	>17.1 μmol/L	21	52	38		

Data are expressed as median (interquartile range) or number. [a] Kruskal–Wallis test; [b] χ^2 test; JHZ group – hormone therapy + chemotherapy + supportive therapy; HZ group – chemotherapy + supportive therapy; JZ group – hormone therapy + supportive therapy.

Table 2. Comparison of efficacy among the 3 groups

Variable	JHZ group (n = 56)	HZ group (n = 108)	JZ group (n = 81)	χ^2	p-value
CR	23 (41.07%)	43 (39.81%)	26 (32.10%)	1.559	0.459
PR	16 (28.57%)	19 (17.59%)	17 (20.99%)	2.663	0.264
SD	12 (21.43%)	39 (36.11%)	37 (45.68%)	8.463	0.015
PD	5 (8.93%)	7 (6.48%)	1 (1.23%)	5.323	0.070[#]
ORR (%)	39 (69.64%)	62 (57.41%)	43 (53.09%)	3.895	0.143

The data are n (%) and analyzed with χ^2 or Fisher's exact tests; [#] p-value was analyzed with Fischer's exact test; JHZ group – hormone therapy + chemotherapy + supportive therapy; HZ group – chemotherapy + supportive therapy; JZ group – hormone therapy + supportive therapy; CR – complete response; PR – partial response; SD – stable disease; PD – progressive disease; ORR – objective response rate.

Prognostic factors affecting overall survival

First, the results of univariate Cox regression analysis showed that 8 potential variables (age, pathological type, Eastern Cooperative Oncology Group (ECOG) score, serum albumin, serum calcium, platelets content, fibrinogen, and hyperbilirubinemia) were associated with poor prognosis in adults with secondary HLH. For the Cox regression assumptions, ECOG score and serum calcium did not satisfy the proportional hazards assumption (Supplementary Table 2). No significant violation of the linearity assumption was found for the continuous variable (age) (Supplementary Fig. 2). In addition, Supplementary Table 3 showed that there was no multicollinearity problem between the predictors. Therefore, variable screening was performed using the best subset algorithm with Bayesian information criterion (BIC)
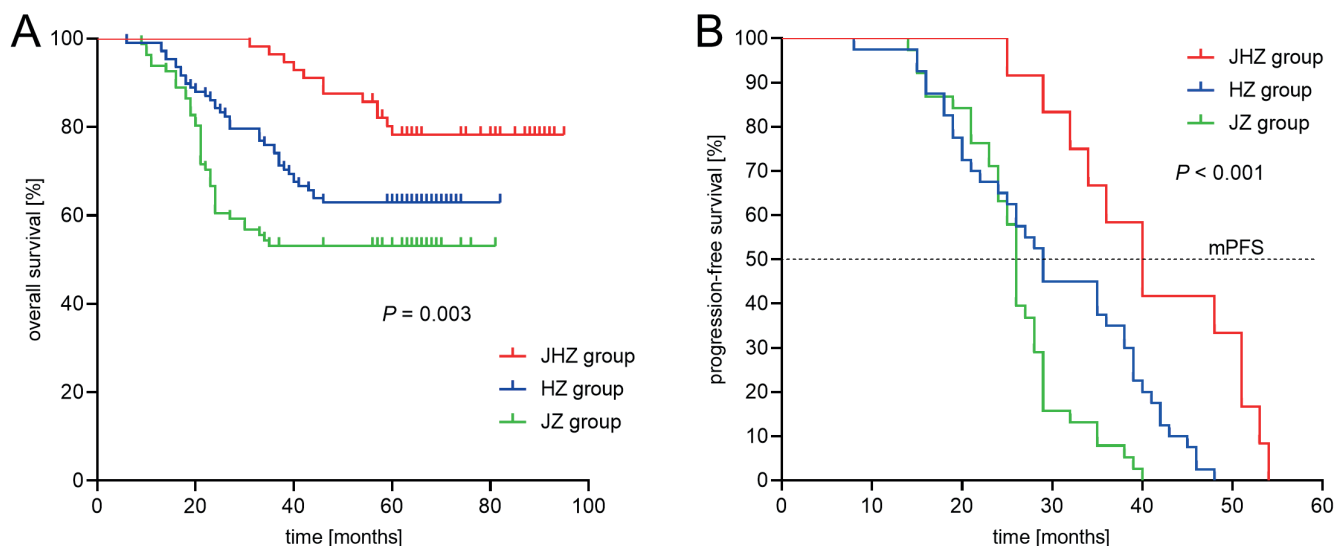
Fig. 1. Kaplan–Meier analysis of prognosis adults with secondary hemophagocytic lymphohistiocytosis (HLH) after treatment. A. Overall survival (OS); 12 (21.43%) in JHZ (hormone therapy + chemotherapy + supportive therapy) group (n = 56) were dead; 40 (37.04%) in HZ (chemotherapy + supportive therapy) group (n = 108) were dead; 38 (46.91%) in JZ (hormone therapy + supportive therapy) group (n = 81) were dead; B. Progression-free survival (PFS)

Table 3. Univariate and multivariate Cox regression analysis of factors affecting overall survival (OS)

Variable		Univariate analysis		Multivariate analysis	
		HR (95% CI)	p-value	HR (95% CI)	p-value
Age		1.166 (1.139–1.193)	<0.001	1.220 (1.170–1.260)	<0.001
Sex		0.851 (0.549–1.319)	0.471	–	–
Pathological type	infection-related	1.000	–	1.000	–
	tumor-related	13.705 (7.903–23.769)	<0.001	3.170 (1.700–5.890)	<0.001
	immune disease-related	2.472 (1.218–5.017)	0.012	5.090 (2.120–12.200)	<0.001
Smoking history		0.963 (0.621–1.493)	0.866	–	–
ECOG score		3.401 (2.173–5.323)	<0.001	–	–
Malignant pleural effusion		0.870 (0.538–1.407)	0.570	1.000 (0.610–1.650)	0.992
PD-L1 expression		0.825 (0.261–2.608)	0.743	–	–
EGFR gene mutation		0.750 (0.484–1.163)	0.198	–	–
Brain metastasis		0.746 (0.481–1.156)	0.190	–	–
Surgical treatment		0.989 (0.649–1.508)	0.959	–	–
Immune-related adverse events		0.989 (0.620–1.578)	0.963	1.380 (0.830–2.300)	0.212
History of hormone therapy		0.807 (0.503–1.297)	0.376	–	–
History of antibiotic history		0.848 (0.531–1.353)	0.488	–	–
Serum albumin		2.719 (1.692–4.369)	<0.001	1.040 (0.520–2.110)	0.906
Serum calcium		0.398 (0.25–0.636)	<0.001	–	–
Platelet content		0.430 (0.275–0.672)	<0.001	–	–
Fibrinogen		0.445 (0.282–0.703)	0.001	0.950 (0.480–1.850)	0.869
Hyperbilirubinemia		9.532 (5.458–16.647)	<0.001	2.590 (1.280–5.260)	0.008

ECOG – Eastern Cooperative Oncology Group; 95% CI – 95% confidence interval; HR – hazard ratio.

as the criterion, and the variables entered into the multivariate analysis were age, pathological type, malignant pleural effusion, immune-related adverse events, serum albumin, fibrinogen, and hyperbilirubinemia. The multivariate analysis showed that age (hazard ratio (HR) = 1.220, 95% confidence interval (95% CI): 1.170–1.260; p < 0.001),

pathological type (tumor-related: HR = 3.170, 95% CI: 1.700–5.890; p < 0.001; immune disease-related adverse events: HR = 5.090, 95% CI: 1.120–12.200; p < 0.001) and hyperbilirubinemia (HR = 2.590, 95% CI: 1.280–5.260; p = 0.008) were independent risk factors for OS in adults with secondary HLH (Table 3).

Discussion

Hemophagocytic lymphohistiocytosis is characterized by excessive activation of macrophages and lymphocytes, which leads to excessive secretion of proinflammatory cytokines, resulting in tissue infiltration, organ failure and inflammation.[13] Secondary HLH is more common in adults and is associated with factors such as infection, tumors, rheumatic diseases, immunotherapy, pregnancy, organ and hematopoietic stem cell transplantation, and metabolic diseases.[14] In adult patients, secondary HLH is life-threatening and has a poor prognosis, and background diseases have the greatest impact on the disease prognosis.[15] Hemophagocytic lymphohistiocytosis secondary to malignant tumors has the worst prognosis,[14] and is mainly treated to deal with the primary tumors.[16] However, many patients often have difficulty tolerating chemotherapy when complicated with HLH, which is one of the reasons for the poor prognosis of tumor-related HLH.[17] Hemophagocytic lymphohistiocytosis induced by Epstein–Barr virus (EBV) infection is the most common non-tumor-related HLH. A clinical study by Zhang et al.[18] found higher EBV DNA load to be an independent poor predictor of OS. Therefore, effective anti-infective therapy is critical for HLH secondary to infection. In a case report by Jongbloed et al.,[19] an adult female patient with HLH secondary to herpes simplex virus 2 infection was successfully treated with acyclovir (for anti-infection), immunoglobulins (for enhancing immunity) and dexamethasone (for anti-inflammation).

In this study, the ORR was higher than 50% in all 3 groups. Although ORR in the JHZ group was higher than in the HZ and JZ groups, the results suggested no significant difference in the efficacy among the 3 groups. Additionally, patients in the JHZ group had better OS and significantly longer median PFS compared with the other 2 groups. Our results are consistent with previous studies. Etoposide induces the normalization of lymphocyte apoptosis,[7] and dexamethasone has anti-inflammatory effects. The combination of these 2 drugs inhibits the excessive immune response to a certain extent and effectively relieves immune disorders in the body. Supportive therapy, including anti-infection, enhancing immunity and other treatments, is important for the treatment of the primary disease and prolonging OS of patients. Wei et al.[20] used etoposide combined with dexamethasone to treat 37 adult patients with secondary HLH, and the results showed that the ORR of the treated cases was as high as 45.9%, which was basically consistent with our results. Yoon et al.[21] treated 81 adult patients with secondary HLH not associated with malignancy with HLH-94 protocol, 18 with dexamethasone + cyclosporine, and 23 with dexamethasone alone. The results revealed that 43 patients treated with HLH-94 protocol achieved CR at 4 weeks after treatment and 38 patients achieved CR at 8 weeks and later. We believe

that secondary HLH in adults is a disease with complex etiology, diverse clinical manifestations and poor prognosis. Early diagnosis and early treatment are important measures to improve the prognosis, and active treatment is the key to improving the prognosis. Based on the comparison of 3 treatment regimens, a combination of corticosteroids therapy, chemotherapy and supportive therapy showed better clinical benefit for adult secondary HLH than the other 2 treatment regimens, and may be a priority and feasible treatment regimen. Our experience is to use etoposide in combination with glucocorticoids early to control inflammation, and then administer targeted chemotherapy when the condition is stable.

In terms of prognostic factors, Cox regression analysis suggested that age, pathological type (tumor-related and immune disease-related) and hyperbilirubinemia were independent risk factors for OS in adults with secondary HLH. In a clinical study, Trottestam et al.[22] found that older patients were more likely to develop secondary HLH after HLH-94 treatment. However, the patients in that study were younger (2–134 months), whereas the present study examined secondary HLH in adults, with a median age exceeding 50 years. In addition, there are no other studies confirming age or pathological type as a prognostic risk factor for secondary HLH in adults. Further multicenter, multi-sample, clinical randomized controlled trials are needed to confirm this. Yoon et al.[21] also suggested that age and hyperbilirubinemia were associated with poor OS in a multivariate analysis of EBV-HLH subgroups. In the study by Yu et al.,[23] hyperbilirubinemia or jaundice had a significant correlation with adverse outcomes in lymphoma-associated HLH. Cattaneo et al.[24] in their multivariate analysis confirmed that HLH patients with hyperbilirubinemia had a higher risk of mortality.

All of the above findings are consistent with our own. Bilirubin is a waste product of heme metabolism in red blood cells, mainly derived from hemoglobin. Hyperbilirubinemia occurs when the liver's capacity to metabolize and convert bilirubin is reduced due to liver injury. This leads to an inadequate elimination of bilirubin from the body, allowing it to accumulate in the blood and ultimately causing a significant increase in blood bilirubin levels.[25] Hyperbilirubinemia is extremely harmful to the human body. The accumulation of a substantial amount of bilirubin, which has inherent toxicity, results in severe jaundice and poses a potential life-threatening risk. Therefore, when adult patients with secondary HLH develop hyperbilirubinemia, active treatment should be administered to prolong OS.

Limitations

Due to the limitation of objective conditions such as time constrains, the number of samples in the JHZ group was too small, and more samples should be included for investigation in the future.

Conclusions

Early diagnosis and treatment are important measures to improve the prognosis of adult patients with secondary HLH, a disease with complex etiology, diverse symptoms and poor prognosis. The combination of corticosteroids, chemotherapy and supportive therapies may be the preferred and feasible treatment regimen for this disease. Hyperbilirubinemia can serve as an important indicator to predict the disease prognosis in clinical practice.

Supplementary data

The Supplementary materials are available at https://doi.org/10.5281/zenodo.10065347. The package includes the following files:

Supplementary Table 1. Analysis of normal distribution for continuous variable (age).

Supplementary Table 2. Supremum test for proportional hazards assumption

Supplementary Table 3. Tests of non-multicollinearity.

Supplementary Fig. 1. Q-Q figures of the normal distribution analysis of the age values.

Supplementary Fig. 2. The relationship between log-hazard function and age.

Data availability

The datasets generated and/or analyzed during the current study are available from the corresponding author on reasonable request.

Consent for publication

Not applicable.

ORCID iDs

Xing Wu https://orcid.org/0009-0001-3979-5280
Changfeng Man https://orcid.org/0000-0003-3369-8882
Wanying Cheng https://orcid.org/0000-0002-2955-2939
Guangli Yin https://orcid.org/0000-0002-6422-8763
Jiayu Huang https://orcid.org/0000-0001-5195-1330
Jujuan Wang https://orcid.org/0000-0002-9653-1652
Xin Gao https://orcid.org/0009-0001-3527-4162
Tian Tian https://orcid.org/0000-0003-3237-3744
Limin Duan https://orcid.org/0000-0002-6642-7643
Ji Xu https://orcid.org/0009-0008-3255-8128
Hongxia Qiu https://orcid.org/0000-0002-6348-4888

References

1. Henter JI, Aricò M, Egeler RM, et al. HLH-94: A treatment protocol for hemophagocytic lymphohistiocytosis. *Med Pediatr Oncol*. 1997; 28(5):342–347. doi:10.1002/(SICI)1096-911X(199705)28:5<342::AID-MPO3>3.0.CO;2-H
2. Ramos-Casals M, Brito-Zerón P, López-Guillermo A, Khamashta MA, Bosch X. Adult haemophagocytic syndrome. *Lancet*. 2014;383(9927): 1503–1516. doi:10.1016/S0140-6736(13)61048-X
3. Schram AM, Berliner N. How I treat hemophagocytic lymphohistiocytosis in the adult patient. *Blood*. 2015;125(19):2908–2914. doi:10.1182/blood-2015-01-551622
4. Henter J, Horne A, Aricó M, et al. HLH-2004: Diagnostic and therapeutic guidelines for hemophagocytic lymphohistiocytosis. *Pediatr Blood Cancer*. 2007;48(2):124–131. doi:10.1002/pbc.21039
5. Johnson TS, Terrell CE, Millen SH, Katz JD, Hildeman DA, Jordan MB. Etoposide selectively ablates activated T cells to control the immunoregulatory disorder hemophagocytic lymphohistiocytosis. *J Immunol*. 2014;192(1):84–91. doi:10.4049/jimmunol.1302282
6. La Rosée P, Horne A, Hines M, et al. Recommendations for the management of hemophagocytic lymphohistiocytosis in adults. *Blood*. 2019;133(23):2465–2477. doi:10.1182/blood.2018894618
7. Fadeel B, Orrenius S, Henter J. Induction of apoptosis and caspase activation in cells obtained from familial haemophagocytic lymphohistiocytosis patients. *Br J Haematol*. 1999;106(2):406–415. doi:10.1046/j.1365-2141.1999.01538.x
8. Imashuku S, Kuriyama K, Sakai R, et al. Treatment of Epstein–Barr virus-associated hemophagocytic lymphohistiocytosis (EBV-HLH) in young adults: A report from the HLH studyl center. *Med Pediatr Oncol*. 2003;41(2):103–109. doi:10.1002/mpo.10314
9. Chen EC, Stefely JA, Dey BR, Dzik WH. Chemotherapy-sparing treatment of haemophagocytic lymphohistiocytosis with intravenous immunoglobulins and corticosteroids. *BMJ Case Rep*. 2020;13(5): e234490. doi:10.1136/bcr-2020-234490
10. Parikh SA, Kapoor P, Letendre L, Kumar S, Wolanskyj AP. Prognostic factors and outcomes of adults with hemophagocytic lymphohistiocytosis. *Mayo Clin Proc*. 2014;89(4):484–492. doi:10.1016/j.mayocp.2013.12.012
11. Eisenhauer EA, Therasse P, Bogaerts J, et al. New response evaluation criteria in solid tumours: Revised RECIST guideline (version 1.1). *Eur J Cancer*. 2009;45(2):228–247. doi:10.1016/j.ejca.2008.10.026
12. Danieli C, Bossard N, Roche L, et al. Performance of two formal tests based on martingales residuals to check the proportional hazard assumption and the functional form of the prognostic factors in flexible parametric excess hazard models. *Biostatistics*. 2017;18(3):505–520. doi:10.1093/biostatistics/kxw056
13. Rosado FGN, Kim AS. Hemophagocytic lymphohistiocytosis: An update on diagnosis and pathogenesis. *Am J Clin Pathol*. 2013;139(6):713–727. doi:10.1309/AJCP4ZDKJ4ICOUAT
14. Lehmberg K, Nichols KE, Henter JI, et al. Consensus recommendations for the diagnosis and management of hemophagocytic lymphohistiocytosis associated with malignancies. *Haematologica*. 2015; 100(8):997–1004. doi:10.3324/haematol.2015.123562
15. Otrock ZK, Eby CS. Clinical characteristics, prognostic factors, and outcomes of adult patients with hemophagocytic lymphohistiocytosis. *Am J Hematol*. 2015;90(3):220–224. doi:10.1002/ajh.23911
16. Tamamyan GN, Kantarjian HM, Ning J, et al. Malignancy-associated hemophagocytic lymphohistiocytosis in adults: Relation to hemophagocytosis, characteristics, and outcomes. *Cancer*. 2016;122(18): 2857–2866. doi:10.1002/cncr.30084
17. Humblet-Baron S, Franckaert D, Dooley J, et al. IL-2 consumption by highly activated CD8 T cells induces regulatory T-cell dysfunction in patients with hemophagocytic lymphohistiocytosis. *J Allergy Clin Immunol*. 2016;138(1):200–209.e8. doi:10.1016/j.jaci.2015.12.1314
18. Zhang J, Qin S, Jin Z, et al. The clinical significance and prognostic role of whole-blood Epstein–Barr virus DNA in lymphoma-associated hemophagocytic lymphohistiocytosis. *J Clin Immunol*. 2023; 43(6):1302–1310. doi:10.1007/s10875-023-01493-9
19. Jongbloed EM, Hermans MAW, Wabbijn M, van Kampen JJA, van Laar JAM. HLH caused by an HSV-2 infection: A case report and review of the literature. *Neth J Med*. 2020;78(5):282–285. PMID:33093253.
20. Wei L, Yang L, Cong J, et al. Using etoposide + dexamethasone-based regimens to treat nasal type extranodal natural killer/T-cell lymphoma-associated hemophagocytic lymphohistiocytosis. *J Cancer Res Clin Oncol*. 2021;147(3):863–869. doi:10.1007/s00432-020-03376-7
21. Yoon JH, Park SS, Jeon YW, et al. Treatment outcomes and prognostic factors in adult patients with secondary hemophagocytic lymphohistiocytosis not associated with malignancy. *Haematologica*. 2019;104(2):269–276. doi:10.3324/haematol.2018.198655
22. Trottestam H, Horne A, Aricò M, et al. Chemoimmunotherapy for hemophagocytic lymphohistiocytosis: Long-term results of the HLH-94 treatment protocol. *Blood*. 2011;118(17):4577–4584. doi:10.1182/blood-2011-06-356261

23. Yu JT, Wang CY, Yang Y, et al. Lymphoma-associated hemophago-cytic lymphohistiocytosis: Experience in adults from a single insti-tution. *Ann Hematol*. 2013;92(11):1529–1536. doi:10.1007/s00277-013-1784-3

24. Cattaneo C, Oberti M, Skert C, et al. Adult onset hemophagocytic lym-phohistiocytosis prognosis is affected by underlying disease and coex-isting viral infection: Analysis of a single institution series of 35 patients. *Hematol Oncol*. 2017;35(4):828–834. doi:10.1002/hon.2314

25. Jordan M, Locatelli F, Allen C, et al; NI-0501-04 Study Group. A novel targeted approach to the treatment of hemophagocytic lympho-histiocytosis (HLH) with an anti-interferon gamma (IFNy) monoclo-nal antibody (mAb), NI-0501: First results from a pilot phase 2 study in children with primary HLH. *Blood*. 2015;126(23):LBA-3. doi:10.1182/blood.V126.23.LBA-3.LBA-3

Study on regulating AQP1, AQP3, AQP4, 5-HT, NOS1 in slow transit constipation rats by Liqi Tongbian mixture

Min Liu[1,A,C,D], Jianyong Chen[1,A,B], Chenger Zhan[1,A,C,F], Shuwen Wu[1,A,E],
Zhaolin Zhang[1,B,C,E], Chenyang Wang[2,A,C], Linlin Shi[1,A,B], Dongya Chen[1,A,D]

[1] Department of Gastroenterology, Zhejiang Hospital of Integrated Traditional Chinese and Western Medicine, Hangzhou, China

[2] Department of Computer Science and Technology, Changchun University of Science and Technology, China

A – research concept and design; B – collection and/or assembly of data; C – data analysis and interpretation;
D – writing the article; E – critical revision of the article; F – final approval of the article

Address for correspondence
Min Liu
E-mail: 416792904@qq.com

Abstract

Background. Liqi Tongbian is a traditional Chinese medicine (TCM) preparation that contains herbs that may treat slow transit constipation (STC). *Atractylodes macrocephala*, *Astragalus membranaceus*, *Fructus aurantii*, radish seed, uncooked *Polygonum multiflorum*, and *Agastache rugosa* were included in the formula for their unique qualities. The control of water transfer in the colon is greatly influenced by aquaporin 3 (AQP3).

Objectives. Based on this, the Liqi Tongbian mixture was used to detect the concentrations of aquaporins (AQPs), 5-HT and nitrix oxide synthase 1 (NOS1) in STC rats, and explore its effect, in order to provide a theoretical basis for the remedy of STC with TCM.

Materials and methods. Zhejiang University of Traditional Chinese Medicine provided 32 three-week-old Sprague Dawley rats of SPF-grade. The pairs licensed under SYXK (Zhejiang) 2021–0012 were kept at 20–25°C and humidity of 50–65%. The compound diphenoxylate caused constipation in the control, model, Liqi laxative (LQTB), and mosapride groups. The Liqi laxative rats were administered a mixture of traditional Chinese herbs after modeling, while mosapride was given to the other group. The levels of 5-HT, NOS1 and AQPs were tested in the feces and intestinal tissues.

Results. Comparing the condition of rat feces, it was found that the model group had significantly lower overall bulk, score and particles within 24 h compared to the control group. In comparison to mosapride, LQTB performed better. The model group had higher levels of 5-HT and NOS1 in intestinal tissue, while the LQTB and mosapride groups had decreased levels of these AQPs. LQTB had lower levels of AQP1, AQP3 and AQP4 than mosapride, while the model group had higher levels of these AQPs.

Conclusions. Liqi Tongbian mixture works better than mosapride in improving constipation symptoms in rats with STC, and its mechanism is related to regulating the level of intestinal AQPs and neurotransmitters.

Key words: 5-hydroxytryptamine, nitric oxide synthase, Liqi Tongbian mixture, slow transit constipation, aquaporins

Background

Slow transit constipation (STC) is a common type of constipation caused by the slow transmission of intestinal contents, mainly manifested as poor defecation, reduced frequency and dry stool.[1] In recent years, with the change of people's lifestyle and dietary structure, the incidence rate of STC has increased year by year, so the research on STC has become important in recent years.[2] At present, the pathogenesis of STC is not fully understood. Some researchers have demonstrated that STC is closely related to intestinal aquaporins (AQPs) and 5-hydroxytryptamine (5-HT) immunoreactivity[3,4] Aquaporin is an important protein that exists widely in mammals to regulate the balance of intracellular and extracellular water. Among them, AQP1, AQP3 and AQP4 are mostly found in gastrointestinal tract and digestive system. Mammals' digestive systems contain aquaporins, including AQP1, AQP3 and AQP4, which regulate water balance within and outside cells. The intricate relationship between AQPs and the gastrointestinal tract suggests a potential link to STC, a condition characterized by sluggish intestinal content transport. While the specific pathways are unknown, studies are being conducted to investigate the role of AQPs in STC. The process of intestinal water transport and play a regulatory role in constipation to some extent.[5]

5-hydroxytryptamine is also widely distributed in the intestines and is a common secretory messenger and neurotransmitter. The 5-HT immunoreactivity is usually enhanced in the intestines of patients with constipation.[6] In addition to 5-HT, nitric oxide synthase 1 (NOS1) is also an important regulatory factor in intestinal diseases.[7,8] Sailer showed that the concentration of NOS1 in intestinal tissue of patients with constipation is notably higher compared to the normal concentration.[9] Therefore, AQPs, 5-HT and NOS1 can be used as important indices to assess STC. At present, the drugs for the STC treatment mainly include gastrointestinal motility regulators and laxatives, but long-term use has great side effects, which will not only cause water and electrolyte disorders, but also lead to gastrointestinal damage.[10] The syndrome differentiation of traditional Chinese medicine (TCM) in the remedy of STC has the advantages of few side effects and remarkable effectiveness.

Qi is a core concept in TCM: not only the basic substance that makes up the human body, but also the driving force that maintains the vital activities of the human body. Liqi Tongbian mixture contains *Atractylodes macrocephala*, *Astragalus membranaceus*, *Fructus aurantii*, radish seed, raw *Polygonum multiflorum*, and *Agastache rugosa*. Among them, *Atractylodes macrocephala* has the effect of invigorating spleen, replenishing qi and promoting diuresis. *Astragalus* invigorates spleen and qi. *Fructus Aurantii* breaks qi, eliminating accumulation and removing ruffians. Radish seeds have been found to promote qi and

aid in digestion. Raw *Polygonum multiflorum* has the effect of moistening intestines and relieving constipation, and *Agastache rugosa* removes dampness. The combination of various medicines plays the role of regulating qi and invigorating the spleen and reaching the 6 viscera.

Objectives

Liqi Tongbian mixture was used to detect the concentrations of AQPs, 5-HT and NOS1 in STC rats, and to explore its effect to provide a theoretical basis for the treatment of STC with TCM.

Materials and methods

Animals

Thirty-two 3-week-old Sprague Dawley rats of SPF-grade were purchased from the Animal Experiment Center of Zhejiang University of Traditional Chinese Medicine (Hangzhou, China). License for the use of laboratory animals was SYXK (Zhejiang) 2021-0012. The rats were kept in cages with 2 rats in each cage, in the animal center laboratory of our hospital, at a temperature of 20–25°C and a relative humidity of 50–65%. The experiment was approved by the Animal Ethics Committee of Zhejiang University of Traditional Chinese Medicine (approval No. I ACUC-20220905-05).

Grouping and modeling

A total of 32 rats were fed adaptively for 1 week and randomly divided into control group (n = 8), model group 2 mL of normal saline was used in the model group (n = 8), Liqi laxative group (LQTB, n = 8), and mosapride group (n = 8). Slow transit constipation rat models were prepared by intragastric administration of compound diphenoxylate except the control group. The suspension of compound diphenoxylate was prepared with 10 mg/kg of compound diphenoxylate and 2 mL of normal saline. The rats were fed with water normally, rested for 1 day after 6 days of gavage, and continued to gavage for 21 days. After 24 h of gastric perfusion, the fecal particles and wet weight of each subgroup of rats were counted. If the number of stool particles and wet weight of stool of rats decreased, the divergence was statistically notable, indicating that the model was successful. If the number of fecal particles and fecal wet weight of rats decreased, the difference was statistically significant, indicating that the model was successful. Therefore, we did not further verify the success of the model through hematoxylin and eosin (H&E) staining or immunohistochemistry.

Drug intervention

After modeling, the control subgroup and model subgroup were given normal saline by gavage. Rats in the LQTB subgroup were given 30 g of *Astragalus root*, 12 g of *Atractylodes macrocephala*, 12 g of radish seed, 10 g of stir-fried *Fructus aurantii*, betel nut, and *Agastache rugosa*. A total of 6 g of raw *Polygonum multiflorum* was soaked in pure water, decocted twice and concentrated to 1 g/mL after filtering. Processed *Polygonum multiflorum* was stored in 4°C and heated to 37°C. With reference to the equivalent dose converted from the body surface area of humans and animals, 18.75 g/(kg) of the Liqi Tongbian mixture was administered by gavage. The rats in the mosapride subgroup were treated with 1.35 mg/(kg/d)[3] mosapride (Chengdu Kanghong Pharmaceutical Group Co., Ltd, Chengdu, China). Liqi Tongbian mixture and *Mosapride aqueous* solution was administered by gavage for 21 days according to the equivalent dose converted from human and animal body surface areas.

Record of fecal granules and wet weight of rats

The fecal granules and wet weight of rats in each subgroup were recorded at the time of modeling and within 24 h after intragastric treatment for 21 days, and the feces of rats were scored. Scoring standard of rat feces was as follows: When the rats' defecation presents scattered dry ball like stool, which was difficult to be discharged – 1 point. When the stool was segmented and sausage-shaped – 2 points. When the feces were sausage-like, with cracks on the surface – 3 points. When the stool was sausage-like or snake-like, smooth and soft – 4 points. When the stool was soft, appeared lump, and the edge was clear – 5 points. When the stool was soft, with rough edges or pasty stool – 6 points. When the stool was watery and had no solid component – 7 points.

Detection of 5-HT and NOS1 concentrations in intestinal tissues of rats

The intestinal ileum tissue of rats was taken. The tissue was washed with pre-cooled phosphate-buffered saline (PBS) and cut into homogenate. The supernatant was centrifuged from homogenate and underwent enzyme-linked immunosorbent assay (ELISA) detection.

Detection of AQPs in intestinal tissues of rats

Rat intestinal tissues were taken and total proteins were extracted by 10% sodium dodecyl sulfate-polyacrylamide gel electrophoresis (SDS-PAGE). The protein was transferred to polyvinylidene fluoride (PVDF) membrane using semi-dry method. The PVDF membrane was placed in 5% skimmed milk powder at room temperature and sealed for 2 h, added the primary antibody and secondary antibody for binding, incubated for 2 h. Glyceraldehyde 3-phosphate dehydrogenase (GAPDH) was used as the internal reference protein. The color-developing solution was used for color development, and then absorbance analysis was performed.

Statistical analyses

The data from each group were statistically analyzed using GraphPad Prism v. 8.0.2 (GraphPad Software, San Diego, USA) and IBM SPSS software v. 25 (IBM Corp., Armonk, USA). The measurement data were reported as the median (1st quartile (Q1) and 3rd quartile (Q3)). The normality of the distribution was tested using the Kolmogorov–Smirnov test. Since all the distributions were normal, the Brown–Forsythe test was used to establish the equality of variances, and then significant differences between multiple groups were analyzed using the Kruskal–Wallis test. Dunn's post hoc test was used for multiple comparisons. If $p < 0.05$, the data divergence was statistically notable. All tests in this study were bilateral.

Results

Comparison of stool condition of rats

There was no mortality among the rats tested. In 24 h, the model group had significantly lower total fecal bulk, score and particles than the control group. The LQTB subgroup outperformed the mosapride subgroup regarding these measures (Fig. 1A–C, Table 1).

Comparison of 5-HT and NOS1 contents in rat intestinal tissue

Compared with the control group, the concentrations of 5-HT and NOS1 in the intestinal tissues of rats in the model group were notably increased. Compared with the model group, the concentrations of 5-HT and NOS1 of rats in the LQTB group and the mosapride group were notably reduced. The concentrations of 5-HT and NOS1 were lower in LQTB group compared to the mosapride group (Fig. 2A,B, Table 1).

Comparison of AQPs content in rat intestinal tissue

Compared with the control group, the concentrations of AQP1, AQP3 and AQP4 in the intestinal tissues of rats in the model group were notably increased; the concentrations of AQP1, AQP3 and AQP4 in the intestinal tissues of rats in the LQTB group and the mosapride group notably decreased compared to the model subgroup. The concentrations of AQP1, AQP3 and AQP4 were lower in the LQTB group compared to the mosapride group (Fig. 3, Table 1).

1212

M. Liu et al. Regulating slow transit constipation in rats
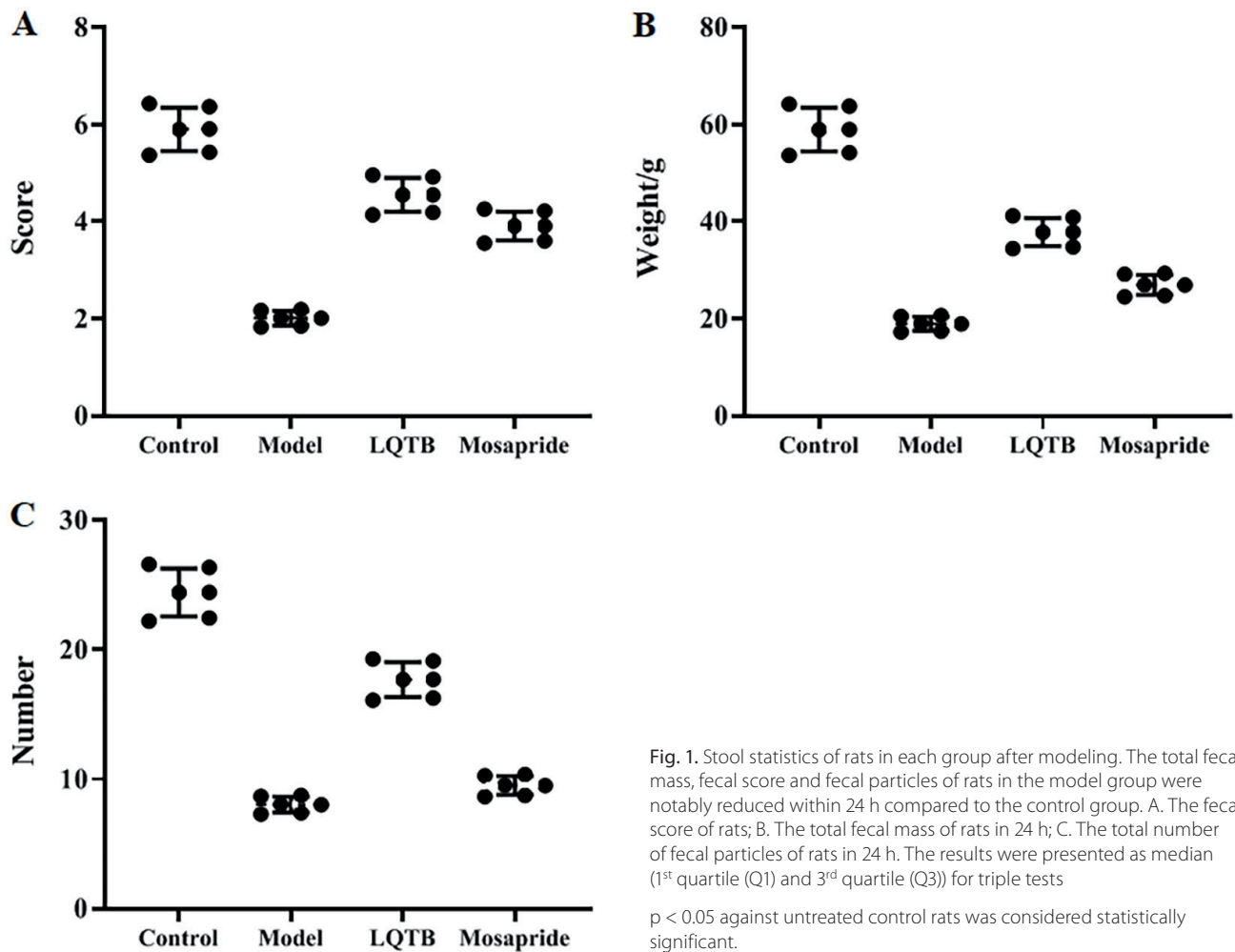
Fig. 1. Stool statistics of rats in each group after modeling. The total fecal mass, fecal score and fecal particles of rats in the model group were notably reduced within 24 h compared to the control group. A. The fecal score of rats; B. The total fecal mass of rats in 24 h; C. The total number of fecal particles of rats in 24 h. The results were presented as median (1st quartile (Q1) and 3rd quartile (Q3)) for triple tests

p < 0.05 against untreated control rats was considered statistically significant.
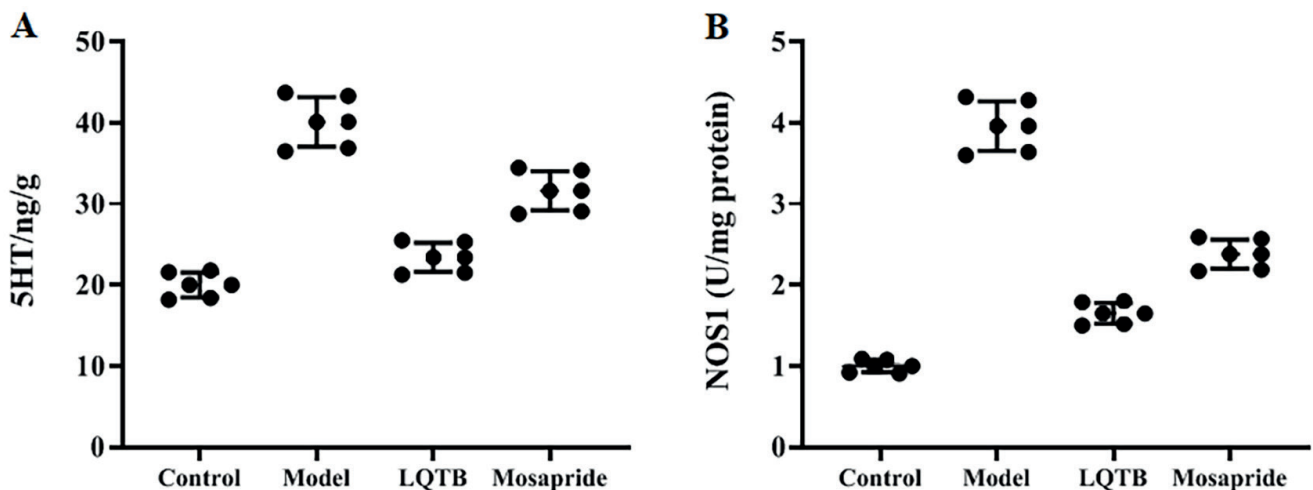
Fig. 2. Detection results of 5-HT and nitrix oxide synthase 1 (NOS1) concentrations in rat intestinal tissues. The concentrations of (A) 5-HT and (B) NOS1 in intestinal tissues of rats were compared with the control group. The results were presented as median (1st quartile (Q1) and 3rd quartile (Q3)) for triple tests

p < 0.05 against untreated control rats was considered statistically significant.

Discussion

The lesion of constipation is located in the large intestine, which is also closely related to the dysfunction of the viscera. From the perspective of TCM, the remedy should start with the spleen, liver, kidney, and lung.[11] In this study, Liqi Tongbian mixture was used to treat STC in rats.

Rat is a common animal model for studying STC.[7] In this experiment, the STC rat model was prepared by intragastric administration of compound diphenoxylate, and the feces
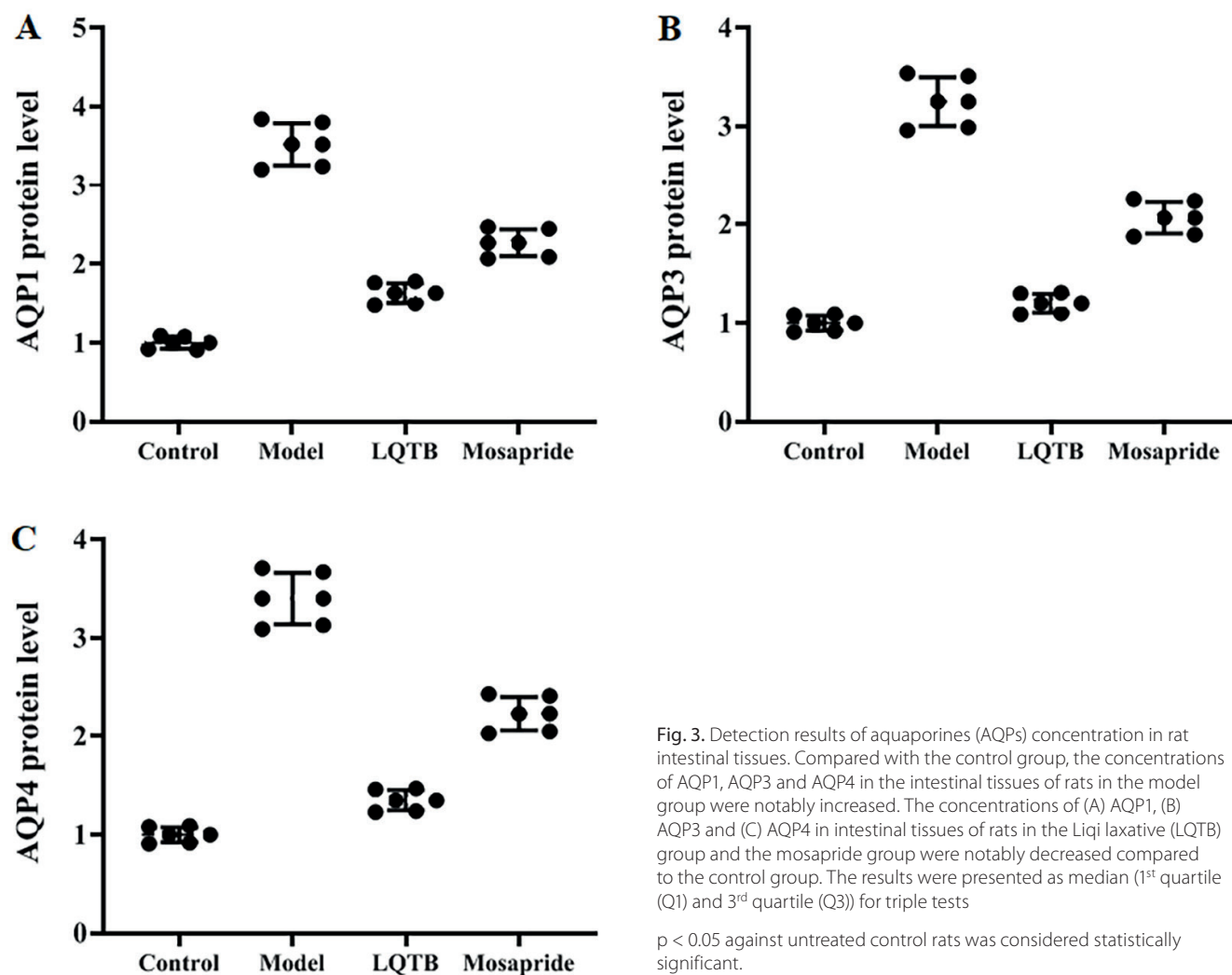
Fig. 3. Detection results of aquaporines (AQPs) concentration in rat intestinal tissues. Compared with the control group, the concentrations of AQP1, AQP3 and AQP4 in the intestinal tissues of rats in the model group were notably increased. The concentrations of (A) AQP1, (B) AQP3 and (C) AQP4 in intestinal tissues of rats in the Liqi laxative (LQTB) group and the mosapride group were notably decreased compared to the control group. The results were presented as median (1st quartile (Q1) and 3rd quartile (Q3)) for triple tests

$p < 0.05$ against untreated control rats was considered statistically significant.

Table 1. Comparison of all studied groups

Variables	Control (n = 6)	Model (n = 6)	LQTB (n = 6)	Mosapride (n = 6)	p-value*
Total fecal mass	58.96 (53.63–64.23)	18.96 (17.24– 20.66)	37.84 (34.42–41.22)	26.95 (24.52–39.36)	p < 0.001
Fecal score	5.90 (5.37–6.43)	2.01 (1.83–2.19)	4.55 (4.14–4.96)	3.91 (3.56–4.26)	p < 0.001
Fecal particles	24.42 (22.21–26.61)	8.03 (7.31–8.75)	8.69 (7.91–9.47)	9.51 (8.65–10.37)	p < 0.001
5-HT	20.01 (18.20–21.80)	40.12 (36.49–43.71)	23.41 (21.29–25.51)	31.63 (28.77–34.47)	p < 0.001
NOS1	1 (0.91–1.09)	3.96 (3.60–4.32)	1.65 (1.50–1.80)	2.38 (2.17–2.59)	p < 0.001
AQP1	1 (0.91–1.09)	3.52 (3.20–3.84)	1.63 (1.48–1.78)	2.27 (2.07–2.47)	p < 0.001
AQP3	1 (0.91–1.09)	3.25 (2.96–3.54)	1.20 (1.09–1.31)	2.07 (1.88–2.28)	p < 0.001
AQP4	1 (0.91–1.09)	3.4 (3.09–3.71)	1.35 (1.23–1.47)	2.22 (2.03–2.43)	p < 0.001

Data were present as median (Q1 and Q3); *p-value was generated from Kruskal–Wallis test. There was a significant difference among all groups in Dunn's test; LQTB – Liqi laxative; NOS1 – nitrix oxide synthase 1; AQP – aquaporine.

of the rats were observed after treatment with Liqi Tongbian mixture to assess the constipation of the rats. It was found that the total fecal mass of rats in the model group was notably reduced, which was related to the absorption of water by the intestine of rats. The boosted absorption of water by the intestinal tissue of rats after the model establishment led to the decrease of the fecal weight of rats, which resulted in constipation in rats. At the same time, the number of particles in the rat defecation decreased notably, indicating that the smooth muscle contraction of the rat fecal intestine was weakened and constipation occurred. Chen et al.[12] have exhibited that the key factor causing STC is insufficient intestinal motility. 5-hydroxy-tryptamine receptor agonists can promote the release

1214

M. Liu et al. Regulating slow transit constipation in rats

of acetylcholine to stimulate the gastrointestinal tract and promote intestinal motility. Mosapride is a 5-HT receptor agonist that is widely used in clinical practice.[13] Therefore, we selected the positive control of mosapride in this study.

The onset of STC is closely related to the relaxation of intestinal smooth muscle. There are 3 types of NOS – NOS1, NOS2 and NOS3 – which are distributed in the intestinal nervous system of vascular endothelial cells (VECs) as the "gut brain". It is mainly composed of intestinal neurons and intestinal glial cells. Among them, NOS1 is the main intestinal inhibitory neurotransmitter. Increasing the content of NOS1 in the intestine inhibits the contraction of intestinal smooth muscle and reduces the spontaneous rhythmic contraction of colonic circular muscle.[14] Usually, the increase of NOS in the intestinal tissue of patients with STC leads to the substantial increase of nitric oxide (NO) in colon tissue, which weakens intestinal motility.[9] In addition to NO and NOS, 5-HT is abnormally expressed in intestinal tissues of STC patients. 5-hydroxytryptamine, also known as serotonin, is an indole derivative, which can also enhance the contraction of blood vessels and smooth muscles. Kuang et al.[15] have demonstrated that the enhancement of 5-HT immunoreactivity is one of the main factors leading to gastrointestinal motility disorder. In this study, the concentrations of 5-HT and NOS1 in intestinal tissues of rats were measured. It was found that the concentrations of 5-HT and NOS1 in the intestinal tissue of rats in the model group, the LQTB group and the mosapride group were notably higher than those in the control group, indicating that the rats had constipation symptoms after the use of mosapride. Slow transit constipation (STC) is associated with relaxation of intestinal smooth muscle, NOS (NOS1, NOS2 and NOS3) levels, and abnormal 5-hydroxytryptamine (5-HT) production in intestinal tissue. The concentrations of 5-HT and NOS1 of rats in the LQTB and the mosapride groups were notably reduced, indicating that the constipation symptoms of STC rats were notably improved after the treatment with the Liqi Tongbian mixture. Its mechanism may be related to the reduction of 5-HT and NOS1, which regulates the intestinal smooth muscle of rats.

At present, more than a dozen kinds of AQPs have been found, among which constipation-related AQPs mainly include AQP1, AQP3 and AQP4. Aquaporin 1 is a common AQPs widely expressed in the digestive system, which allows water molecules to pass freely but is not permeable to other ions and small molecules.[16] Aquaporin 3 is mainly distributed on the surface of colonic mucosal epithelial cells. It has been confirmed that the increase of AQP3 leads to spasm of intestinal smooth muscle, thus enhancing intestinal water absorption, reducing intestinal peristalsis frequency and causing constipation.[17] Aquaporin 4 is also one of the common AQPs that cause STC. This kind of AQPs is present in the absorption epithelial cells, mainly participates in the intestinal absorption and has a certain regulatory effect on constipation.[18] The concentrations of AQP1, AQP3 and AQP4 were lower in the LQTB group. This shows that the use of Liqi Tongbian mixture can effectively regulate AQPs in the intestine of rats, thereby improving the constipation symptoms of rats, and the improvement effect is better than mosapride. Mosapride is a gastrointestinal motility drug, which mainly improves constipation by stimulating gastrointestinal peristalsis. Modern pharmacological research[18] shows that *Atractylodes macrocephala* can not only promote intestinal peristalsis, but also increase intestinal water content.

Limitations

It is important to note that this study has several limitations. First, the results are from an animal model, so extrapolation to humans may not be obvious. The study also focused on molecular markers and did not investigate alternative causes or variables of STC. More studies, including clinical trials, are needed to prove that the Liqi Tongbian combination works in humans and to understand its effects on STC. The study did not examine long-term effects or adverse outcomes, so generalizing the results to chronic conditions or prolonged use is risky.

Conclusions

Liqi Tongbian mixture can improve the constipation symptoms of STC rats by regulating the expression of AQPs and by improving the relaxation of intestinal smooth muscle of rats by regulating the concentrations of 5-HT and NOS1. Toxic and side effects of TCM on STC have not been discussed in this study. They will be explored in subsequent experiments.

Supplementary files

The Supplementary materials are available at https://doi.org/10.5281/zenodo.10460804. The package includes the following files:

Supplementary Table 1. The independent-samples median test results of total fecal volume in rats.

Supplementary Table 2. The independent-samples median test results of fecal score in rats.

Supplementary Table 3. The independent-samples median test results of fecal particles in rats.

Supplementary Table 4. The independent-samples median test results of 5HT in rats.

Supplementary Table 5. The independent-samples median test results of NOS1 in rats.

Supplementary Table 6. The independent-samples median test results of AQP1 in rats.

Supplementary Table 7. The independent-samples median test results of AQP3 in rats.

Supplementary Table 8. The independent-samples median test results of AQP4 in rats.

Data availability

The datasets generated and/or analyzed during the current study are available from the corresponding author on reasonable request.

Consent for publication

Not applicable.

ORCID iDs

Min Liu https://orcid.org/0009-0003-4697-9357
Chenger Zhan https://orcid.org/0009-0008-6235-2841

References

1. Wang Y, Lu R, Shi J, Zhao S, Jiang X, Gu X. CircORC2 is involved in the pathogenesis of slow transit constipation via modulating the signalling of miR-19a and neurotensin/motilin. *J Cell Mol Med.* 2021;25(8): 3754–3764. doi:10.1111/jcmm.16211
2. Black CJ, Ford AC. Chronic idiopathic constipation in adults: Epidemiology, pathophysiology, diagnosis and clinical management. *Med J Aust.* 2018;209(2):86–91. doi:10.5694/mja18.00241
3. Zhan Y, Tang X, Xu H, Tang S. Maren pills improve constipation via regulating AQP3 and NF-κB signaling pathway in slow transit constipation in vitro and in vivo. *Evid Based Complement Alternat Med.* 2020;2020:9837384. doi:10.1155/2020/9837384
4. Israelyan N, Del Colle A, Li Z, et al. Effects of serotonin and slow-release 5-hydroxytryptophan on gastrointestinal motility in a mouse model of depression. *Gastroenterology.* 2019;157(2):507–521.e4. doi:10.1053 /j.gastro.2019.04.022
5. Zhu X, Shen W, Wang Y, Jaiswal A, Ju Z, Sheng Q. Nicotinamide adenine dinucleotide replenishment rescues colon degeneration in aged mice. *Sig Transduct Target Ther.* 2017;2(1):17017. doi:10.1038/sigtrans.2017.17
6. He L, Tan J, Hu Q, et al. Non-contact measurement of the surface displacement of a slope based on a smart binocular vision system. *Sensors.* 2018;18(9):2890. doi:10.3390/s18092890
7. Zhan Y, Wen Y, Zhang LL, et al. Paeoniflorin improved constipation in the loperamide-induced rat model via TGR5/TRPA1 signaling-mediated 5-hydroxytryptamine secretion. *Evid Based Complement Alternat Med.* 2021;2021:6076293. doi:10.1155/2021/6076293
8. Garcia-Barcelo M, King SK, Miao X, et al. Application of HapMap data to the evaluation of 8 candidate genes for pediatric slow transit constipation. *J Pediatr Surg.* 2007;42(4):666–671. doi:10.1016/j.jpedsurg. 2006.12.014
9. Sailer M. Chronische Obstipation. *Chirurg.* 2022;93(1):103–112. doi:10. 1007/s00104-021-01399-5
10. Cao Y, Zhong F, Wen Q, et al. Effect of electroacupuncture on gastrointestinal motility in rats with slow transit constipation based on GDNF methylation modification [in Chinese]. *Zhen Ci Yan Jiu.* 2022; 47(2):141–147. doi:10.13702/j.1000-0607.20210253
11. Wang L, Wu F, Hong Y, Shen L, Zhao L, Lin X. Research progress in the treatment of slow transit constipation by traditional Chinese medicine. *J Ethnopharmacol.* 2022;290:115075. doi:10.1016/j.jep.2022. 115075
12. Chen Z, Feng J, Hu S, et al. *Bacillus subtilis* promotes the release of 5-HT to regulate intestinal peristalsis in STC mice via bile acid and its receptor TGR5 pathway. *Dig Dis Sci.* 2022;67(9):4410–4421. doi:10.1007/ s10620-021-07308-4
13. Park YS, Sung KW. Gastroprokinetic agent, mosapride inhibits 5-HT$_3$ receptor currents in NCB-20 cells. *Korean J Physiol Pharmacol.* 2019; 23(5):419. doi:10.4196/kjpp.2019.23.5.419
14. Mercado NM, Zhang G, Ying Z, Gómez-Pinilla F. Traumatic brain injury alters the gut-derived serotonergic system and associated peripheral organs. *Biochim Biophy Acta Mol Bas Dis.* 2022;1868(11):166491. doi:10.1016/j.bbadis.2022.166491
15. Kuang H, Zhang C, Zhang W, et al. Electroacupuncture improves intestinal motility through exosomal miR-34c-5p targeting SCF/ c-kit signaling pathway in slow transit constipation model rats. *Evid Based Complement Alternat Med.* 2022;2022:8043841. doi:10.1155 /2022/8043841
16. Kalita A, Das M, Baro MR, Das B. Exploring the role of aquaporins (AQPs) in LPS induced systemic inflammation and the ameliorative effect of Garcinia in male Wistar rat. *Inflammopharmacology.* 2021; 29(3):801–823. doi:10.1007/s10787-021-00832-9
17. Yu L, Yang X, Guan W, et al. Analysis of key genes for slow transit constipation based on RNA sequencing. *Int J Gen Med.* 2022;15:7569–7579. doi:10.2147/IJGM.S380208
18. Cao Y, He Y, Wei C, et al. Aquaporins alteration profiles revealed different actions of senna, sennosides, and sennoside A in diarrhea-rats. *Int J Mol Sci.* 2018;19(10):3210. doi:10.3390/ijms19103210

BVES-AS1 suppresses the colorectal cancer progression via the miR-1269a/b-SVEP1-PI3K/AKT axis

Jianguo Yang[A–F], Qican Deng[B,C,F], Zhenzhou Chen[B,C,F], Yajun Chen[D–F], Zhongxue Fu[A,D–F]

Department of Gastrointestinal Surgery, The First Affiliated Hospital of Chongqing Medical University, China

A – research concept and design; B – collection and/or assembly of data; C – data analysis and interpretation;
D – writing the article; E – critical revision of the article; F – final approval of the article

Address for correspondence
Zhongxue Fu
E-mail: fzx19990521@126.com

Conflict of interest
None declared

Abstract

Background. Numerous studies have indicated the engagement of long non-coding RNA (lncRNA) in various cancer types, including colorectal cancer (CRC). However, the functional and mechanistic roles of lncRNAs in CRC remain largely elusive.

Objectives. The aim of this study was to explore the function and mechanism of lncRNA *BVES-AS1* in CRC.

Materials and methods. The expression levels of *BVES-AS1* were validated in CRC tissues and paired normal samples using quantitative real-time polymerase chain reaction (qPCR) Subsequently, the biological functions of *BVES-AS1* in CRC cells were investigated both in vitro and in vivo. Various experimental techniques such as western blot, fluorescence in situ hybridization, RNA-sequencing (RNA-seq), biotin-labeled miRNA pulldown assay, dual-luciferase reporter gene assay, and RNA-protein immunoprecipitation (RIP) assay were employed to elucidate the potential mechanism of *BVES-AS1*.

Results. The findings of this study demonstrated that *BVES-AS1* expression was downregulated in CRC tissues compared to normal tissues, and its expression level was associated with tumor infiltration and tumor-nodule-metastasis (TNM) stage. Furthermore, *BVES-AS1* was found to suppress CRC cell proliferation, migration and metastasis both in vitro and in vivo. Mechanistically, *BVES-AS1* acted as a sponge for *miR-1269a* and *miR-1269b*, thereby regulating *SVEP1*. Additionally, the silencing of *SVEP1* activated the *PI3K/AKT* pathway.

Conclusions. These results suggest that *BVES-AS1* plays a crucial role in the progression of CRC through the m*iR-1269a/b-SVEP1-PI3K/AKT* axis, providing new insights into the therapeutic strategies for CRC.

Key words: miRNA, *PI3K/AKT*, colorectal cancer, *BVES-AS1*, *SVEP1*

1218

J. Yang et al. BVES-AS1 suppresses the colorectal cancer

Background

Colorectal cancer (CRC) is the 2nd leading cause of cancer-related deaths. The number of cancer-related deaths caused by CRC accounts for 9.4% of all cancers.[1,2] Local recurrence, metastasis and resistance to therapy are still the main reasons for cancer-related death in CRC.[3,4] At present, the mechanisms of tumorigenesis and metastasis in CRC remain unknown. Thus, clarifying the tumorigenesis, metastasis and therapeutic resistance potential molecular mechanisms of CRC is imperative.

Studies have indicated that lncRNAs can regulate CRC by serving as scaffolds, signals, decoys, or guide molecules to interact with mRNA, chromatin, miRNA, or protein.[5,6] It has been reported that lncRNAs participate in the proliferation, migration, invasion, and apoptosis processes of CRC. For example, *DLGAP1-AS2* mediates the ubiquitination of *Trim21* and the degradation of *ELOA* to promote CRC cell proliferation and metastasis.[7] LncRNAs can not only drive the progression of CRC as oncogenes but also drive the progression of CRC as tumor suppressor genes. *LINC01559* expression was downregulated in CRC. *LINC01559* overexpression inhibited CRC cell growth and invasive capacity by sponging the *miR-106b-5p* to regulate *PTEN* expression.[8] In addition, lncRNAs can also act as effective diagnostic biomarkers and early screening indicators of CRC.[9–11]

SVEP1 is a multi-structural domain extracellular matrix protein composed of Sushi, Von Willebrand factor type A, epidermal growth factor (EGF) and pentraxin domain-containing protein 1.[12] Studies have suggested that *SVEP1* plays a vital function in cell adhesion, normal lymphatic vessel development and epidermal differentiation.[13–16] *SVEP1* and its alternative splice forms may regulate the invasive ability of breast cancer cells within the bone wall niche.[17] A recent study revealed that *SVEP1* levels in hepatocellular carcinoma (HCC) tissues were significantly downregulated, and high *SVEP1* expression was correlated with better progression. Mechanistically, *SVEP1* regulated the invasion and metastasis of HCC cells through the *PI3K/ATK* pathway.[18,19] However, the function of *SVEP1* in CRC remains unknown.

LncRNA *BVES-AS1*, located in the q21 region of chromosome 6, is the antisense strand of the protein-coding gene *BVES*. *BVES-AS1* has been found to have prognostic value in triple-negative breast cancer, with higher expression correlating with improved overall survival.[20] A previous study indicated that *BVES-AS1* expression was downregulated in colon cancer and can serve as a prognostic marker for colon cancer patients. However, the exact mechanism by which *BVES-AS1* affects colon cancer is still not fully understood.[21] In our previous analysis using The Cancer Genome Atlas (TCGA) database, we observed that the expression of *BVES-AS1* in CRC tissues was significantly lower than that in paracancerous tissues. Further bioinformatic analysis revealed a significant positive correlation between *BVES-AS1* and *SVEP1* in CRC tissues. *SVEP1* has been shown to exhibit tumor suppression effects in various cancers. Therefore, we hypothesize that *BVES-AS1* may regulate the biological functions of CRC through its interaction with *SVEP1*.

Objectives

The purpose of this study was to investigate the role of *BVES-AS1* in CRC and the mechanism by which *BVES-AS1* regulates *SVEP1*.

Materials and methods

Clinical samples

Colorectal cancer and paired paracancerous tissues were collected from patients who underwent radical surgery at the First Affiliated Hospital of Chongqing Medical University (Chongqing, China) between September 2020 and March 2021. A total of 96 CRC patients were included. The collected samples were immediately placed in liquid nitrogen for freezing and then transferred to a –80°C refrigerator for permanent storage. The clinical data of CRC patients were obtained by consulting the electronic medical record system. All included patients were confirmed to have adenocarcinoma or mucinous adenocarcinoma by pathological examination and received no neoadjuvant therapy (including chemoradiotherapy, targeted therapy or immunotherapy). In addition, patients had no other malignancies. This research protocol was reviewed and approved by the Medical Ethics Committee of the First Affiliated Hospital of Chongqing Medical University (approval No. 2020-358) and informed consent was obtained from all the study participants.

Cell culture and transfection

Cell culture and transfection were conducted as previously reported. The human CRC cell lines SW620, HT-29, LoVo, and SW480 were acquired from the Cell Bank of the Chinese Academy of Sciences (Shanghai, China). The normal colonic epithelial cell NCM460 line was obtained from the American Type Culture Collection (ATCC; Rockville, USA). SW620, HT-29, SW480, and NCM460 cells were cultured with DMEM (Gibco, Waltham, USA), and the F12 medium (Gibco) was used to culture LoVo cells. All media were replenished with 10% fetal bovine serum (FBS; Biological Industries, Kibbutz Beit-Haemek, Israel) and 1% penicillin-streptomycin (Gibco). Small interfering RNA (siRNAs), mimics and plasmids were designed and synthesized by (RiboBio, Guangzhou, China) and transfected into SW480 and HT-29 cells using Lipofectamine 3000 (Lipo3000; Invitrogen, Waltham, USA). Lentiviruses of control and overexpression human *BVES-AS1* were

packaged by HanBio (Shanghai, China). Stable overexpression of *BVES-AS1* CRC cells after lentivirus transfection was screened with puromycin (MedChemExpress, Monmouth Junction, USA). The siRNA and mimic sequences are shown in Supplementary Table 1.

RNA extraction and quantitative real-time PCR

The RNA extraction procedure was performed as previously described. Total RNA was extracted from CRC tissues and cells with RNAiso Plus (Takara, Shiga, Japan). A Nanodrop 2000 (Thermo Fisher Scientific, Waltham, USA) was used to analyze the extracted RNA concentration and quality. The RT Reagent Kit and SYBR Green Kit (Takara) were used for reverse transcription (RT) and quantitative real-time polymerase chain reaction (qPCR) detection, respectively. Specific stem-loop primers were designed for the reverse transcription of microRNA (Tsingke, Beijing, China). Glyceraldehyde 3-phosphate dehydrogenase (*GAPDH*) and *U6* were used as internal controls for mRNA and miRNA, respectively. The sequences of all primers are described in Supplementary Table 2. The relative RNA expression was calculated using the $2^{-\Delta\Delta Ct}$ method.

RNA sequencing and bioinformatics analysis

RNA-sequencing (RNA-Seq) data for CRC patients were obtained from the TCGA database (portal.gdc.cancer.gov/) in March 2021. A total of 602 cases were downloaded, of which 554 were derived from CRC and 48 cases from normal colorectal tissue. The differentially expressed lncRNAs and mRNAs were filtered using the "edgeR" packages of R software (R Foundation for Statistical Computig, Vienna, Austria) with |log2foldchange|≥2 and p < 0.05. The correlation of lncRNA-mRNA or mRNA-mRNA was verified using Spearman's correlation analysis. The miRNAs targeting lncRNAs were predicted using the Lncbase (www.microrna.gr/LncBase) and miRDB (www.mirdb.org/) databases. The TargetScan (www.targetscan.org) database was used to predict the binding between mRNA and miRNA. RNA sequencing of the HT-29 vector group and *BVES-AS1* group was conducted using Illumina (Personalbio, Nanjing, China). A human genome reference was constructed based on GRCh38/hg38 of the UCSC. The R software package was used to perform the cluster and differential gene analyses. The differential mRNA was screened with |log2foldchange|≥1 and p < 0.05.

Cell Counting Kit-8 assay

The Cell Counting Kit-8 (CCK-8) assay was performed according to previously described methods.[7] A total of 3,000 logarithmic growth stage CRC cells were inoculated in a 96-well plate. Ten microliters of CCK-8 solution (APEx-BIO, Houston, USA) were added at 0 h, 24 h, 48 h, and 72 h, and then incubated at 37°C for 2 h. The optical density (OD) values were measured at 450 nm using a spectrophotometer Multiskan MK3 (Thermo Fisher Scientific).

EdU assay

The 5-ethynyl-2'-deoxyuridine (EdU) assay was performed according to the manufacturer's protocol of the EdU Cell Proliferation Kit (Beyotime Biotechnology, Shanghai, China). Colorectal cancer cells were seeded into 96-well plates and maintained for 24 h. After adding 50 mM EdU solution to the culture plates, the cells were cultured at 5% CO_2 and 37°C for 2 h. After fixing the cells with 4% paraformaldehyde (PFA), the cells were permeabilized with 1% Triton X-100. Azide 594 and Hoechst 33342 were used for cell staining. Photographs were taken with a fluorescence microscope (model TE2000; Nikon Corp., Tokyo, Japan).

Wound healing assay

Colorectal cancer cells were seeded into 6-well plates and maintained until more than 90% of the cell density was reached. A sterile pipette tip formed a manual scratch on the bottom of the culture plate. Phosphate-buffered saline (PBS) was used to wash the culture plates, and the exfoliated cells were removed. Serum-free Dulbecco's modified Eagle's medium (DMEM) was used to culture cells. A microscope (model TS2; Nikon Corp.) was used to take pictures at 0 h and 24 h.

Transwell assay

The transwell assay was conducted as previously reported.[7] The cells were resuspended in serum-free DMEM. The upper chamber of the transwell (Corning Company, Corning, USA) was inoculated with 200 μL of cell suspension, while the DMEM with 15% FBS was added to lower chamber. After 48 h of incubation at 5% CO_2 and 37°C, 4% PFA was used to fix cells, and 1% crystal violet (Beyotime Biotechnology) was used to stain cells. In the transwell invasion assay, Matrigel (BD Biosciences, Franklin Lakes, USA) was used to cover the Transwell upper chamber before inoculating resuspended cells.

Western blot

The protein extraction and western blot analysis were based on a previous report.[7] The primary antibodies including the following: rabbit *E-cadherin* antibody (#3195, Cell Signaling Technology (CST), Danvers, USA), rabbit *PI3K* antibody (#4257; CST), rabbit *N-cadherin* antibody (#13116; CST), rabbit *P-PI3K* antibody (#17366; CST), rabbit *vimentin* antibody (#5741; CST), rabbit *AKT* antibody (#2938; CST), rabbit *p-AKT* antibody (#13038; CST), and

rabbit *SVEP1* antibody (R&D Biosystems, Minneapolis, USA). Rabbit *GAPDH* antibody was purchased from Proteintech (Wuhan, China). The analysis was performed using an electrochemoluminescence (ECL) detection system (Bio-Rad, Hercules, USA).

Apoptosis assay

The Annexin-V-FITC apoptosis detection kit (Thermo Fisher Scientific) was used for the flow cytometry apoptosis assay. The centrifuged cells were resuspended in flow cytometry binding buffer (100 µL), and Annexin V/FITC (5 µL) and propidium iodide (PI; 5 µL) were used for staining. Apoptotic cells were detected using flow cytometry (CytoFLEX, Pasadena, USA).

Fluorescence in situ hybridization

The fluorescence in situ hybridization (FISH) kit (RiboBio) and *BVES-AS1* probe with Cy3 labeling (GenePharma, Shanghai, China) were used for the FISH assay. According to the protocol, Cy3-labeled *BVES-AS1* probes were incubated with CRC cells for 16 h at 37°C. Different concentrations of saline sodium citrate buffer solution was used to wash CRC cells. The nuclei of CRC cells were stained with DAPI (4′,6-diamidino-2-phenylindole). A laser confocal microscope (model LSM700; Carl Zeiss, Oberkochen, Germany) was performed to take photographs.

Dual-luciferase gene reporter assay

BVES-AS1 and *SVEP1* 3'-untranslated region (3'-UTR) sequences wild-type (WT) and mutant (Mut), which contain *miR-1269a* and *miR-1269b* binding sites, were constructed on the pSI-Check2 plasmid vector (Hanbio, Shanghai, China). The *miR-1269a* mimics, *miR-1269b* mimics and negative control (NC) mimics were cotransfected with WT and Mut dual-luciferase gene reporter plasmids into CRC cells using Lipo3000. Luciferase activity was detected after 48 h of transfection.

Biotin-labeled miRNA pulldown assay

Biotin-coupled *miR-1269a* mimics, *miR-1269b* mimics and NC mimics were designed and made by Sangon Biotech (Shanghai, China). Colorectal cancer cells were lysed after the biotin-labeled *miR-1269a* mimics, *miR-1269b* mimics and NC mimics were transfected for 48 h. Simultaneously, washed streptavidin magnetic beads (Invitrogen) were blocked at 4°C for 2 h The cell lysate was added to the washed magnetic beads and incubated in the mixed solution for 12–16 h at 4°C. After washing streptavidin magnetic beads 5 times, 500 µL of TRIzol was added to extract the RNA that specifically interacts with miRNA. Finally, the relative expression of enriched RNA was measured with qPCR.

RNA-binding protein immunoprecipitation assay

The RIP Kit (MilliporeSigma, St. Louis, USA) was applied for RIP assays. Briefly, RIP lysis solution was used to collect and lyse CRC cells. Anti-*AGO2* antibody (Proteintech and normal rabbit *IgG* (MilliporeSigma) were added into the lysate, and the mixture was incubated at 4°C for 12–16 h with rotation. Subsequently, 30 µL of Protein A/G Magnetic Bead was added and incubated with rotation for 6 h at 4°C. After washing, the enriched RNA was extracted using the TRIzol reagent.

Xenografts in mice

The procedure of xenografts in mice was described in a previous study.[7] Briefly, 4–6-week-old female BALB/c nude mice were provided by Ensiweier Biotechnology Ltd. (Chongqing, China) and housed in an environment free of specific pathogenic bacteria. Ten mice were randomly assigned into 2 groups; 200 µL (5×10^6) of HT-29 cells stably overexpressing *BVES-AS1* or empty vector was injected subcutaneously into the right axilla of nude mice. The long axes and short axes of subcutaneous tumors were measured on days 5, 10, 15, 20, and 25 after injection, and the formula: V = (width2+long)/2 was used to calculate the subcutaneous tumor volume. The mice were sacrificed on the 25th day after tumor injection. The subcutaneous tumors were extracted from the nude mice and weighed, and the mass and volume of the tumors were measured. Tumors were fixed in a 4% formalin solution for hematoxylin & eosin (H&E) staining and immunohistochemistry (IHC). All animal experiments were conducted according to the protocol approved by the Animal Experimental Research Ethics Committee of Chongqing Medicine University (approval No. IACUC-CQMU-2022-0019).

Immunohistochemistry

The standard methods of IHC have been described in a previous study by Lu et al.[22] Briefly, the collected samples were fixed with a 4% formaldehyde solution. After embedding in paraffin, they were cut into 4-µm sections. After dewaxing and hydration, the tissue sections were placed into 3% hydrogen peroxide to block the endogenous peroxidase activity. Anti-*SVEP1* antibody (R&D Biosystems) and anti-*Ki 67* antibody (Proteintech) solutions were added to the sections and incubated for 12–16 h at 4°C with anti-*SVEP1* antibody and anti-*Ki 67* antibody. The brown precipitates produced by 3,3′-diaminobenzidine (DAB) visualized the results. Finally, the sections were restained using hematoxylin. Immunohistochemistry images were obtained using a microscope (Olympus BX51; Olympus Corp., Tokyo, Japan).

Statistical analyses

Statistical analysis was conducted using GraphPad Prism 8 (GraphPad Software, San Diego, USA) and IBM SPSS statistical software v. 25.0 (IBM Corp., Armonk, USA). All experiments were performed independently in triplicate, with each independent assay containing at least 3 samples. Mean ± standard deviation (M ±SD) was used to describe normally distributed data. Normality of the data was assessed using the Shapiro–Wilk test (Supplementary Table 5), and the homogeneity of variance was tested using the Levene's test (Supplementary Table 7). For non-normally distributed paired samples, Wilcoxon signed rank analysis was

conducted. Student's t-test was used to compare 2 samples with normal distribution, while one-way analysis of variance (ANOVA) followed by Dunnett's post hoc test was applied to compare 3 or more samples with normal distribution and homogeneity of variance. If the data did not follow a normal distribution or heterogeneous variance, or the sample size was less than 9, the Mann–Whitney U test was performed to examine the data of 2 groups, and the Kruskal–Wallis test followed by Dunnett's post hoc test was used for the difference analysis of 3 or more groups (Supplementary Table 6). Spearman's correlation coefficient analysis was performed to evaluate the association between genes. The relationship between *BVES-AS1* and
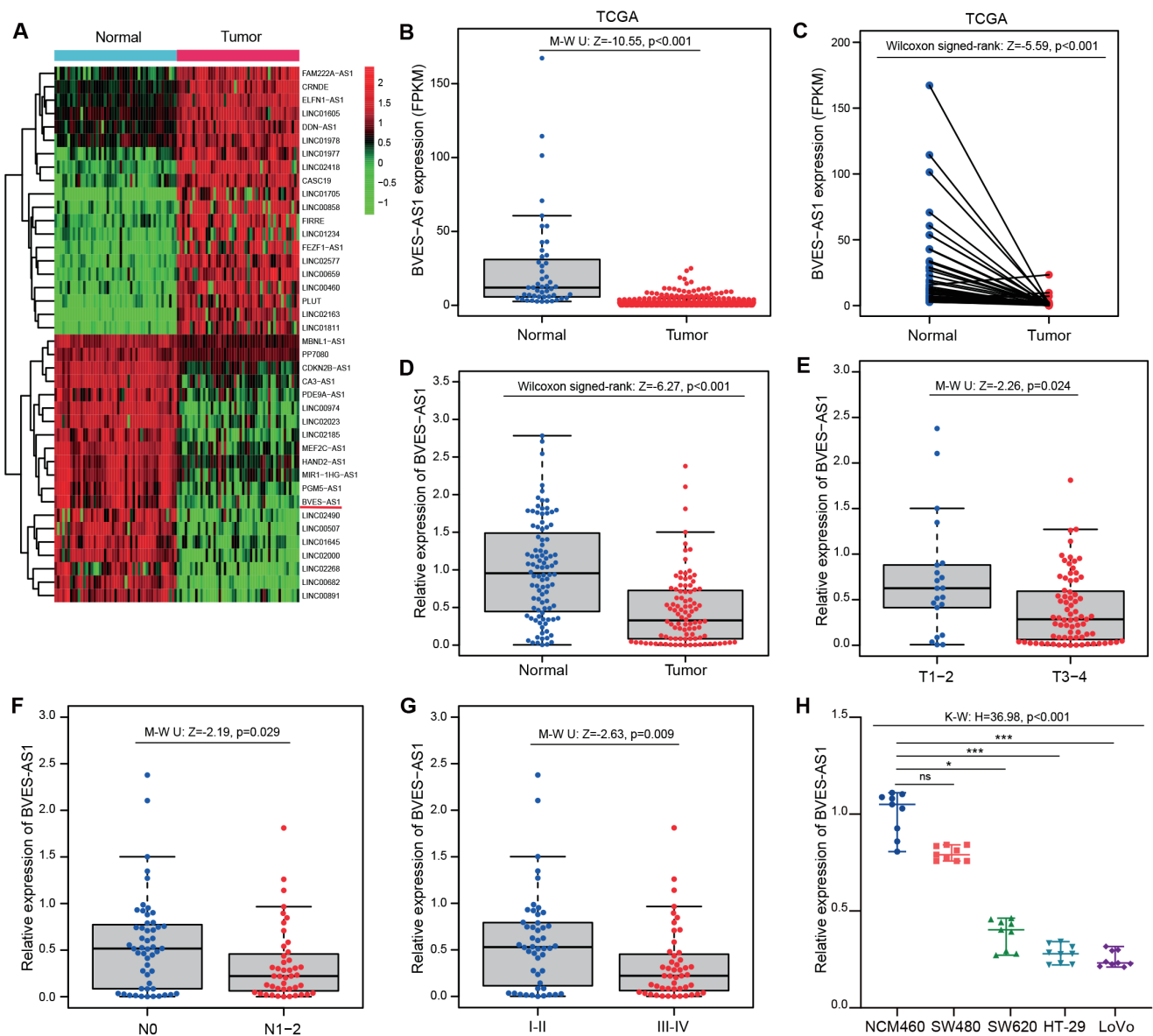
Fig. 1. Expression and clinical significance of *BVES-AS1* in colorectal cancer (CRC). A. Cluster heatmap showing the top 20 upregulated and top 20 downregulated LncRNAs of CRC and paired normal tissues in The Cancer Genome Atlas (TCGA) dataset ("edgeR" package of R, n = 47); B. TCGA database was used to analyze the *BVES-AS1* expression level in 554 CRC and 48 normal tissues (Mann–Whitney U test); C. Expression of *BVES-AS1* in CRC tissues and matched normal tissues in the TCGA database (Wilcoxon signed-rank, n = 47); D. Expression of *BVES-AS1* in CRC tissues and paired adjacent tissues (Wilcoxon signed-rank, n = 96); E–G. Expression of *BVES-AS1* was estimated according to T stage, lymph node metastasis and pathological stage (Mann–Whitney U test, n = 96); H. Expression of *BVES-AS1* in colonic epithelial cells and 4 CRC cell lines (Kruskal–Wallis test with Dunn's post hoc test, n = 9, *p < 0.05, **p < 0.01, ***p < 0.001). Data are presented as median with range. All assays were conducted in triplicate

the baseline clinical characteristics of CRC patients was analyzed using the χ^2 or Fisher's exact test. A p-value of less than 0.05 (p < 0.05) was considered statistically significant.

Results

BVES-AS1 is downregulated in CRC and related to pathological stage

The bioinformatics analysis of TCGA data revealed 720 lncRNAs that were upregulated, and 293 lncRNAs that were downregulated in CRC tissue based on |log2fold change|≥2 and p < 0.05. The clustering heatmap showed the dysregulated genes in 47 paired CRC and normal colorectal tissues (Fig. 1A). The differential expression gene analysis showed that *BVES-AS1* expression in para-cancerous tissue was significantly higher than that in CRC tissue (Fig. 1B,C). The 96 CRC tissues and paracancerous tissues were gleaned and analyzed. The results showed that *BVES-AS1* expression in CRC tissues was significantly downregulated compared with that in paracancerous tissues (Fig. 1D). The clinical baseline analysis of CRC patients indicated that *BVES-AS1* expression was closely associated with the tumor infiltration (p = 0.024), lymph node positivity (p = 0.029) and tumor-nodule-metastasis (TNM) stage (p = 0.009) (Fig. 1E–G, Supplementary Table 3). Furthermore, *BVES-AS1* was significantly downregulated in LoVo, HT29, SW480, and SW620 cells compared with NCM460 cells (Fig. 1H).

BVES-AS1 inhibits CRC cell proliferation and invasion in vitro

The previous results indicated that *BVES-AS1* expression was downregulated in HT-29 cells, but relatively high in SW480 cells (Fig. 1H). Hence, SW480 and HT-29 cells were used in subsequent studies. To elucidate the effect of *BVES-AS1* on CRC biological function, HT-29 and SW480 cells with stable overexpression of *BVES-AS1* and vector were constructed by lentivirus infection (Fig. 2A). In addition, *BVES-AS1* expression in SW480 cells was knocked down by si-BVES-AS1#1, and si-BVES-AS1#2 (Fig. 2B). Cell Counting Kit-8 and EdU assays showed that *BVES-AS1* overexpression prominently suppressed HT-29 and SW480 cell proliferation while silencing *BVES-AS1* promoted SW480 cell viability (Fig. 2C–F, Supplementary Fig. 1A–C). Transwell and wound healing assay results indicated that the migration and invasion abilities of CRC cells were significantly suppressed by upregulated *BVES-AS1* (Fig. 3A,C, Supplementary Fig. 1D–G). In contrast, the migration and invasion abilities of SW480 cells were enhanced by *BVES-AS1* knockdown (Fig. 3B,D). Meanwhile, western blot analysis revealed that *BVES-AS1* upregulation significantly downregulated *N-cadherin* and *vimentin* levels while silencing *BVES-AS1* produced

the opposite effects (Fig. 4E,F). Flow cytometry apoptosis assays indicated that the overexpression of *BVES-AS1* contributed to SW480 and HT-29 cell apoptosis (Fig. 4A,B, Supplementary Fig. 1H,I). *BVES-AS1* downregulation inhibited SW480 cell apoptosis (Fig. 4C,D). In general, *BVES-AS1* acted as a tumor suppressor gene to inhibit CRC cell biological roles in vitro.

BVES-AS1 functions as a sponge for miR-1269a and miR-1269b

To clarify the mechanism of *BVES-AS1*, we employed nuclear-cytoplasmic fractionation and FISH assays and observed that *BVES-AS1* was mainly distributed in the cytoplasm of HT-29 and SW480 cells (Fig. 5A,B). Next, we used the miRDB and LncBase databases to predict miRNAs that may bind to *BVES-AS1*. The predicted results revealed that *BVES-AS1* contained *miR-1269a* and *miR-1269b* binding sites (Fig. 5C). Unexpectedly, the seed sequences of *miR-1269a* and *miR-1269b* were identical (Fig. 5J). The study also found that compared with normal colorectal tissue, the *miR-1269a* and *miR-1269b* levels in CRC were upregulated (Fig. 5D,F). Correlation analysis demonstrated that *miR-1269a* and *miR-1269b* expression had a negative correlation with *BVES-AS1* expression in CRC (Fig. 5E,G). In addition, overexpression of *miR-1269a* and *miR-1269b* in HT-29 and SW480 cells significantly downregulated *BVES-AS1* mRNA levels (Fig. 5H,I). To further explain the relationship between *miR-1269a*, *miR-1269b* and *BVES-AS1*, the WT and Mut dual-luciferase reporter gene plasmids of *BVES-AS1* were constructed and synthesized. (Fig. 5J). The *miR-1269a* mimics, *miR-1269b* mimics or NC mimics were cotransfected with WT or Mut plasmids into HT-29 and SW480 cells to detect luciferase activity. The results indicated that the *miR-1269a* or *miR-1269b* mimics could significantly inhibit luciferase activity in the WT group compared with the NC mimics. In contrast, the luciferase activity in the Mut group was not significantly different (Fig. 6A–D). Biotinylated *miR-1269a* mimic and *miR-1269b* mimic WT probes, and Mut probes were designed and synthesized for a biotin-coupled microRNA capture assay. The results indicated that *BVES-AS1* in the WT probe group was significantly enriched in HT-29 cells (Fig. 6E,F). In addition, RIP experiments further found that compared with the immunoglobulin G (IgG) group, the enrichment of *BVES-AS1*, *miR-1269a* and *miR-1269b* was significantly higher (Fig. 6G). Our data suggested that *BVES-AS1* may function as a sponge for *miR-1269a* and *miR-1269b* in CRC cells.

BVES-AS1 reverses the oncogenic effect of miR-1269a and miR-1269b

To evaluate whether *BVES-AS1* can inhibit the biological function of CRC cells by sponging *miR-1269a* or *miR-1269b*, rescue experiments were performed. The results
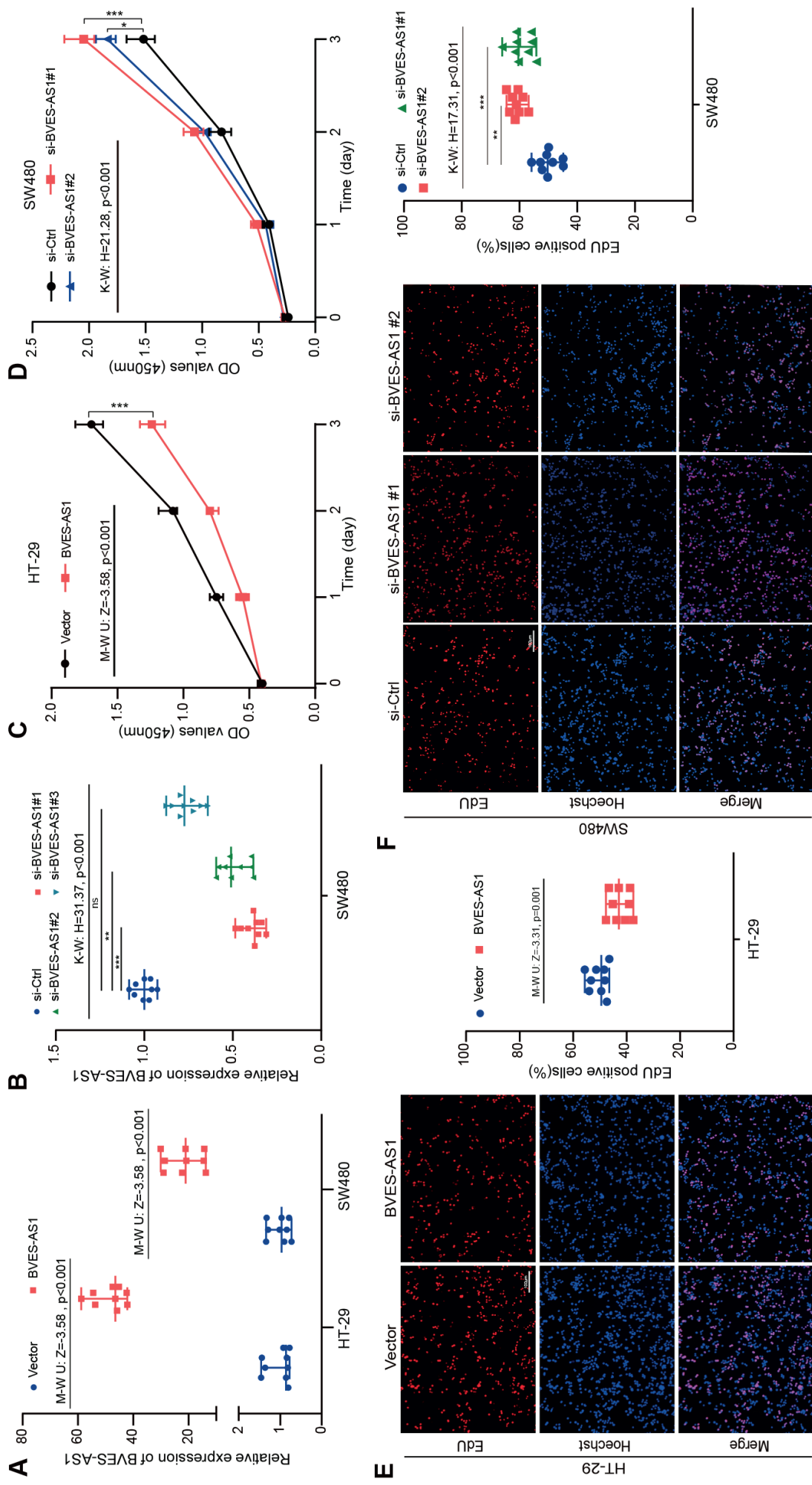
Fig. 2. *BVES-AS1* inhibits CRC cell proliferation in vitro. A,B. *BVES-AS1* overexpression and downregulation were verified with qualitative real-time polymerase chain reaction (qPCR); C,D. The proliferation curves of colorectal cancer (CRC) cells with upregulation or knockdown of *BVES-AS1* were detected using the Cell Counting Kit-8 (CCK-8) assay at 0 h, 24 h, 48 h, and 72 h; E,F. 5-Ethynyl-2′-deoxyuridine (EdU) assay was conducted to evaluate the proliferation ability of CRC cells after overexpression or silencing *BVES-AS1*; A,C,E. The results were statistically analyzed using the Mann–Whitney U test (n = 9); B,D,F. The results were analyzed using the Kruskal–Wallis test with Dunn's post hoc test (n = 9). *p < 0.05, **p < 0.01, ***p < 0.001. The data are presented as median with range. All assays were conducted in triplicate
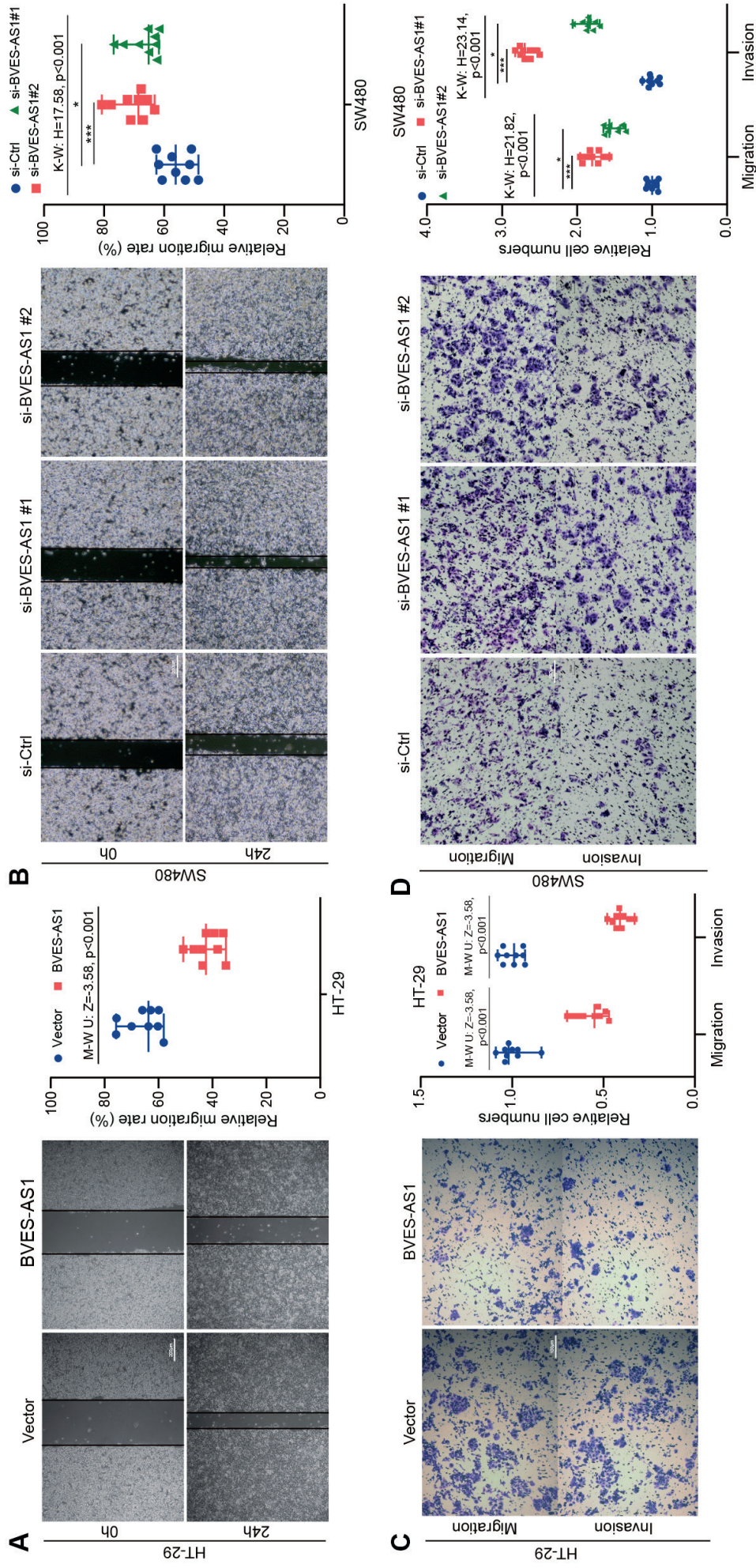
Fig. 3. *BVES-AS1* inhibits colorectal cancer (CRC) cell migration and invasion in vitro. A,B. Wound healing assays were used to estimate CRC cells migration abilities after transfecting the *BVES-AS1* lentivirus or siRNA; C,D. Transwell assays were used to evaluate CRC cells migration and invasion abilities; A,C. The results were statistically analyzed using the Mann–Whitney U test (n = 9); B,D. The results were analyzed using the Kruskal–Wallis test with Dunn's post hoc test (n = 9). *p < 0.05, **p < 0.01, ***p < 0.001. The data are presented as median with range. All assays were conducted in triplicate
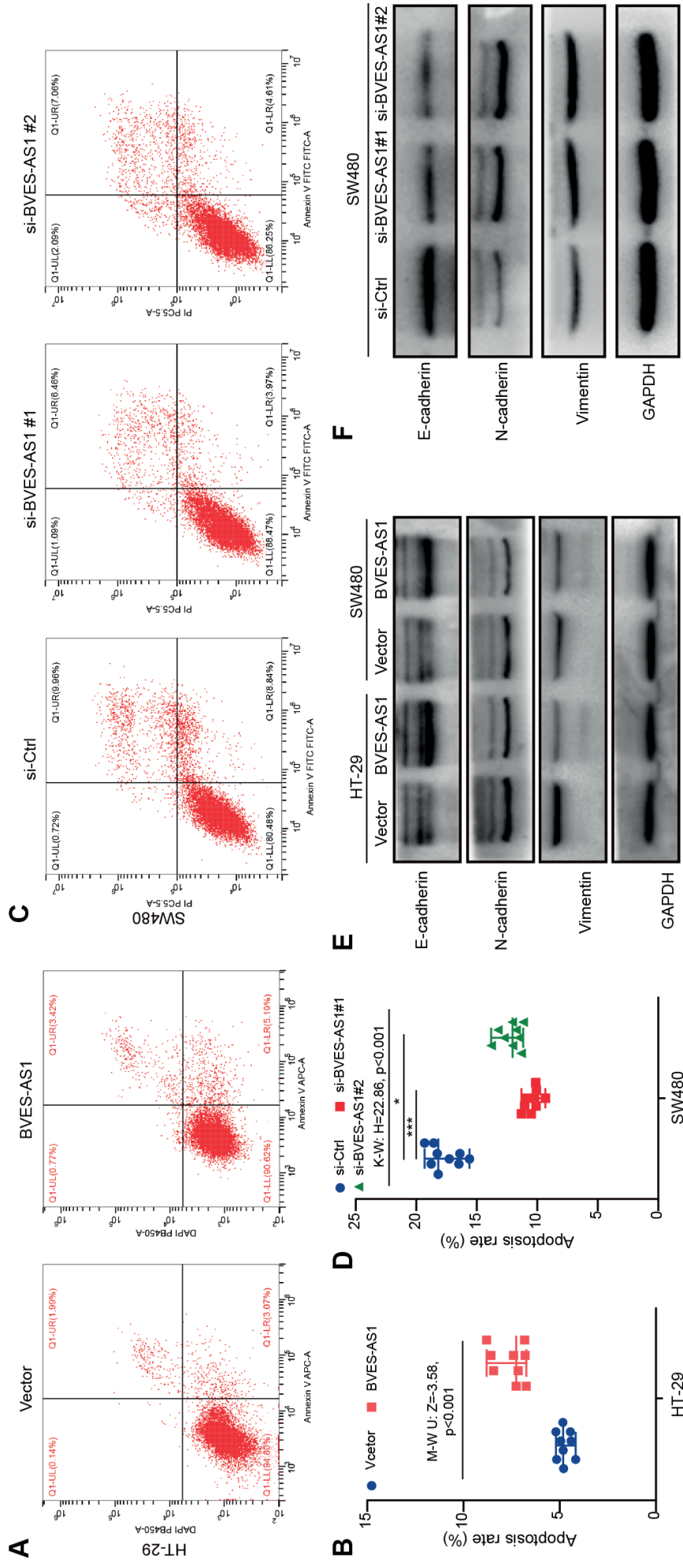
Fig. 4. *BVES-AS1* induces the apoptosis and suppresses epithelial-mesenchymal transition (EMT) of colorectal cancer (CRC) cells in vitro. A–D. Apoptosis of CRC cells silenced and overexpressed *BVES-AS1*; it was detected using flow cytometry; E,F. EMT markers (*E-cadherin, N-cadherin,* and *vimentin*) were detected with western blot after *BVES-AS1* overexpression or downregulation; B. The results were statistically analyzed using the Mann–Whitney U test (n = 9); C. The results were analyzed using the Kruskal–Wallis test with Dunn's post hoc test (n = 9). *p < 0.05, **p < 0.01, ***p < 0.001. The data are presented as median with range. All assays were conducted in triplicate

Fig. 5. The correlation of *BVES-AS1* with *miR-1269a* and *miR-1269b*. A. Fluorescence in situ hybridization (FISH) was used to detect the localization of *BVES-AS1* in HT-29 and SW480 cells. The nucleus was stained with 4',6-diamidino-2-phenylindole (DAPI); B. The level of *BVES-AS1* in nuclear and cytoplasmic mRNA of HT-29 and SW480 cells was analyzed with quantitative real-time polymerase chain reaction (qPCR); C. Forty-four potential target miRNAs of *BVES-AS1* were predicted using miRDB and LncBase; D.F. Expression of *miR-1269a* and *miR-1269b* in 96 colorectal cancer (CRC) tissues and paired adjacent tissues (Wilcoxon signed-rank test, n = 96); E.G. Correlation analysis showed that the expressions of *BVES-AS1* and *miR-1269a* or *miR-1269b* were negatively correlated in 96 CRC tissues (Spearman's correlation coefficient, n = 96); H.I. The change of *BVES-AS1* after the upregulation of *miR-1269a* or *miR-1269b* (Mann–Whitney U test); J. Schematic diagram of *BVES-AS1* wild-type (WT) and mutant (Mut) luciferase reporter gene vectors. The data are presented as median with range, and all assays were performed in triplicate

Fig. 6. *BVES-AS1* functions as a sponge for *miR-1269a* and *miR-1269b*. A–D. Wild-type (WT) or mutant (Mut) *BVES-AS1* luciferase reporter gene vectors were co-transfected with *miR-1269a* or *miR-1269b* mimics, and the luciferase activity was determined (Mann–Whitney U test, n = 9); E,F. Biotin-labeled miRNA pulldown assay showed the enrichment level of *BVES-AS1* captured by biotinylated *miR-1269a/b* mimics or negative control (NC) mimics (Kruskal–Wallis test with Dunn's post hoc test, n = 9; ***p < 0.001); G. RNA immunoprecipitation (RIP) assay showed the fold enrichment of *BVES-AS1*, *miR-1269a*, and *miR-1269b* in HT-29 cells (Mann–Whitney U test, n = 9). The data are presented as median with range, and all assays were performed in triplicate

1228

J. Yang et al. BVES-AS1 suppresses the colorectal cancer

indicated that the *miR-1269a* and *miR-1269b* mimics promoted CRC cell proliferation and vitality while transfecting the *BVES-AS1* plasmid partially eliminated the proliferation ability induced by *miR-1269a* mimics or *miR-1269b* mimics (Supplementary Fig. 2A–D). Transwell and wound healing assays indicated that compared with NC mimics, the overexpression of *miR-1269a* and *miR-1269b* advanced CRC cell migration and invasion ability. The migration and invasion mediated by *miR-1269a* and *miR-1269b* mimics were also attenuated by upregulated *BVES-AS1* (Supplementary Fig. 2E–I). Western blot analysis showed that *E-cadherin* levels were partially downregulated in CRC cells after cotransfecting with *miR-1269a* mimics, *miR-1269b* mimics and *BVES-AS1*. In contrast, *N-cadherin* and *vimentin* protein levels showed the opposite results (Supplementary Fig. 2L). Furthermore, inhibition of apoptosis induced by *miR-1269a* mimics or *miR-1269b* mimics was also reversed by upregulated *BVES-AS1* (Supplementary Fig. 2J,K). In summary, these results demonstrate that *BVES-AS1* can reverse the oncogenic effect of *miR-1269a* and *miR-1269b* in CRC cells.

SVEP1 is the common downstream target of *miR-1269a* and *miR-1269b*

To further elucidate how *BVES-AS1* regulated CRC cell function through *miR-1269a* and *miR-1269b*, we performed RNA-seq on HT-29 cells transfected with *BVES-AS1* overexpression plasmid and vector plasmid. The results showed that compared with the vector group, 35 upregulated genes and 59 downregulated genes were detected in the *BVES-AS1* overexpression group ($|log2$-fold change$|{\geq}1$, $p < 0.05$) (Fig. 7A, Supplementary Table 4). The TargetScan database and RNA-seq data were applied to prognosticate the target genes of *miR-1269a* and *miR-1269b*. The predicted results indicated that *SVEP1* had binding sites for *miR-1269a* and *miR-1269b* (Fig. 7B). In the TCGA database, *SVEP1* was significantly downregulated in CRC tissue (Fig. 7C). The qPCR detection of 96 CRC samples and matched adjacent samples suggested that the mRNA level of *SVEP1* in CRC was also decreased (Fig. 7D). Correlation analysis indicated that *SVEP1* in CRC tissues was significantly positively correlated with *BVES-SA1* (R = 0.615) (Fig. 7E). In contrast, *SVEP1* was negatively correlated with *miR-1269a* (R = 0.545) and *miR-1269b* (R = 0.545) in CRC (Fig. 7F,G). The qPCR and western blotting indicated that *SVEP1* was upregulated at the mRNA and protein levels by *BVES-AS1* overexpression in CRC cells (Fig. 7I,K). As expected, *miR-1269a* and *miR-1269b* mimics in CRC cells significantly downregulated the expression of *SVEP1* (Fig. 7H,J). To verify the relationship among *SVEP1*, *miR-1269* and *miR-1269b*, we constructed *SVEP1* 3'-UTR WT and Mut dual-luciferase reporter gene plasmids (Fig. 8A,B). The luciferase assay revealed that the luciferase activity of CRC cells transfected with the *SVEP1* WT plasmid was inhibited by *miR-1269a* and

miR-1269b mimics. In contrast, no significant difference was detected in the *SVEP1*-Mut plasmid (Fig. 8C–F). These results indicated that *SVEP1* is the common target gene of *miR-1269a* and *miR-1269b*.

SVEP1 suppresses the function of CRC cells through the *PI3K/AKT* pathway

The biological role of *SVEP1* in CRC is still unknown. We performed functional experiments in CRC cells by knocking down *SVEP1* with siRNA to elucidate the role of *SVEP1* (Fig. 9A, Supplementary Fig. 3A). Subsequently, EdU and CCK-8 assays indicated that compared with si-Ctrl transfection, *SVEP1* knockdown promoted HT-29 and SW480 cell proliferation (Fig. 9B–E). The si-SVEP1#1 and si-SVEP1#2 also enhanced CRC cell migration and invasion (Fig. 9F–H, Fig. 10A, Supplementary Fig. 3B). Western blot analysis indicated that *SVEP1* knockdown in CRC cells significantly promoted EMT (Fig. 10C). Moreover, downregulating *SVEP1* also inhibited the apoptosis of CRC cells (Fig. 10B, Supplementary Fig. 3C). The results demonstrated that *SVEP1* has a tumor suppressor function in CRC cells.

A previous study mentioned that *SVEP1* knockdown promoted proliferation, bone infiltration and lung metastasis of HCC cells by activating the *PI3K/AKT* pathway.[18] Therefore, we discussed whether *BVES-AS1* could regulate the *PI3K/AKT* pathway through the *miR-1269a/miR-1269b-SVEP1* axis in CRC cells. Western blotting revealed that *BVES-AS1* upregulation decreased the levels of phosphorylated *AKT* and *PI3K* in CRC cells (Fig. 10D). In CRC cells, transfection of *miR-1269a* and *miR-1269b* mimics also upregulated p-*AKT* and p-*PI3K* levels (Fig. 10E). Furthermore, *SVEP1* silencing significantly enhanced the levels of phosphorylated *AKT* and *PI3K* in CRC cells (Fig. 10F). Rescue experiments showed that *miR-1269a* or *miR-1269b* could partially restore the downregulation of phosphorylated *AKT* and *PI3K* caused by the upregulation of *BVES-AS1* (Fig. 10G). Silencing *SVEP1* also partially restored the decrease in p-*AKT* and p-*PI3K* in CRC caused by overexpression of *BVES-AS1* (Fig. 10H). The data indicated that *BVES-AS1* regulated the *PI3K/AKT* pathway through the *miR-1269a/miR-1269b-SVEP1* axis (Fig. 11G).

BVES-AS1 inhibits the proliferation of CRC cells in vivo

To verify the impact of *BVES-AS1* on CRC cell proliferation in vivo, HT-29 cells stably overexpressing *BVES-AS1* or the vector were xenografted into nude mice by right axilla subcutaneous injection to form an animal model. The size of the xenograft tumor was measured 5, 10, 15, 20, and 25 days after tumor cell injection. The xenograft tumors were harvested on the 25th day (Fig. 11A). Compared with the vector group, the *BVES-AS1* group had smaller tumor volumes and slower tumor growth in xenografts (Fig. 11B–D).

Fig. 7. The correlation of *SVEP1* with *miR-1269a* and *miR-1269b*.

A. The cluster heatmap showing the top 20 upregulated and top 20 downregulated mRNA of RNA-sequencing ("edgeR" package of R, n = 6); B. Four potential target mRNAs of *miR-1269a* and *miR-1269b* were predicted using RNA-sequencing and Targetscan; C. Expression of *SVEP1* in colorectal cancer (CRC) samples and paired normal samples in The Cancer Genome Atlas (TCGA) database (paired Student's t-test; n = 47); D. Expression of *SVEP1* in CRC tissues and matched adjacent tissues (Wilcoxon signed-rank test, n = 96); E. The correlation analysis of *BVES-AS1* level and *SVEP1* level in CRC tissues (Spearman's correlation coefficient, n = 96); F.G. The correlation analysis of *miR-1269a* or *miR-1269b* level and *SVEP1* level in CRC tissues (Spearman's correlation coefficient, n = 96); H–K. The mRNA and protein level of *SVEP1* after *BVES-AS1*, *miR-1269a*, or *miR-1269b* overexpression (Mann–Whitney U test and Kruskal–Wallis test with Dunn's post hoc test, n = 9; *p < 0.05, ***p < 0.01, ***p < 0.001). The data are presented as median with range. All assays were conducted in triplicate
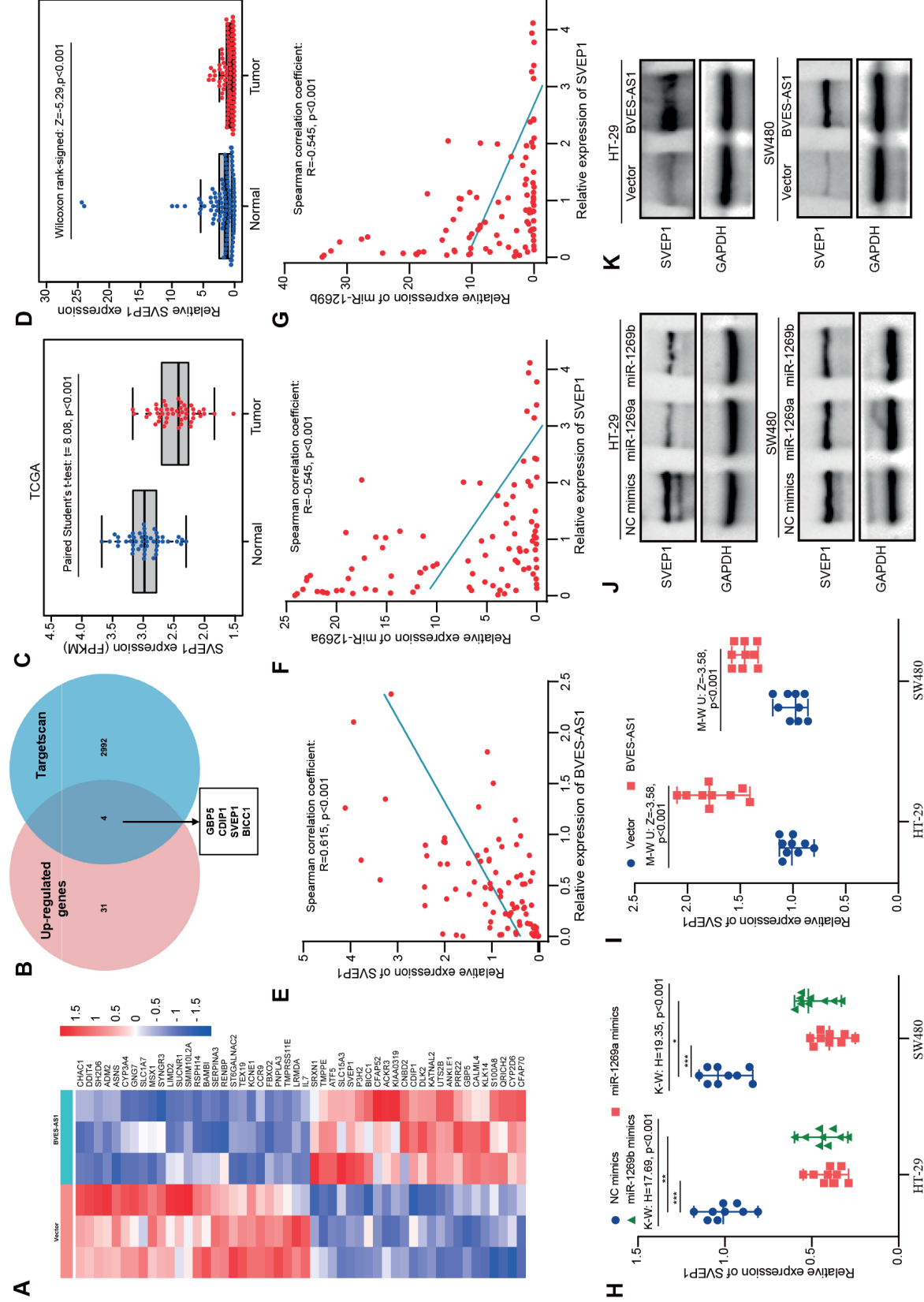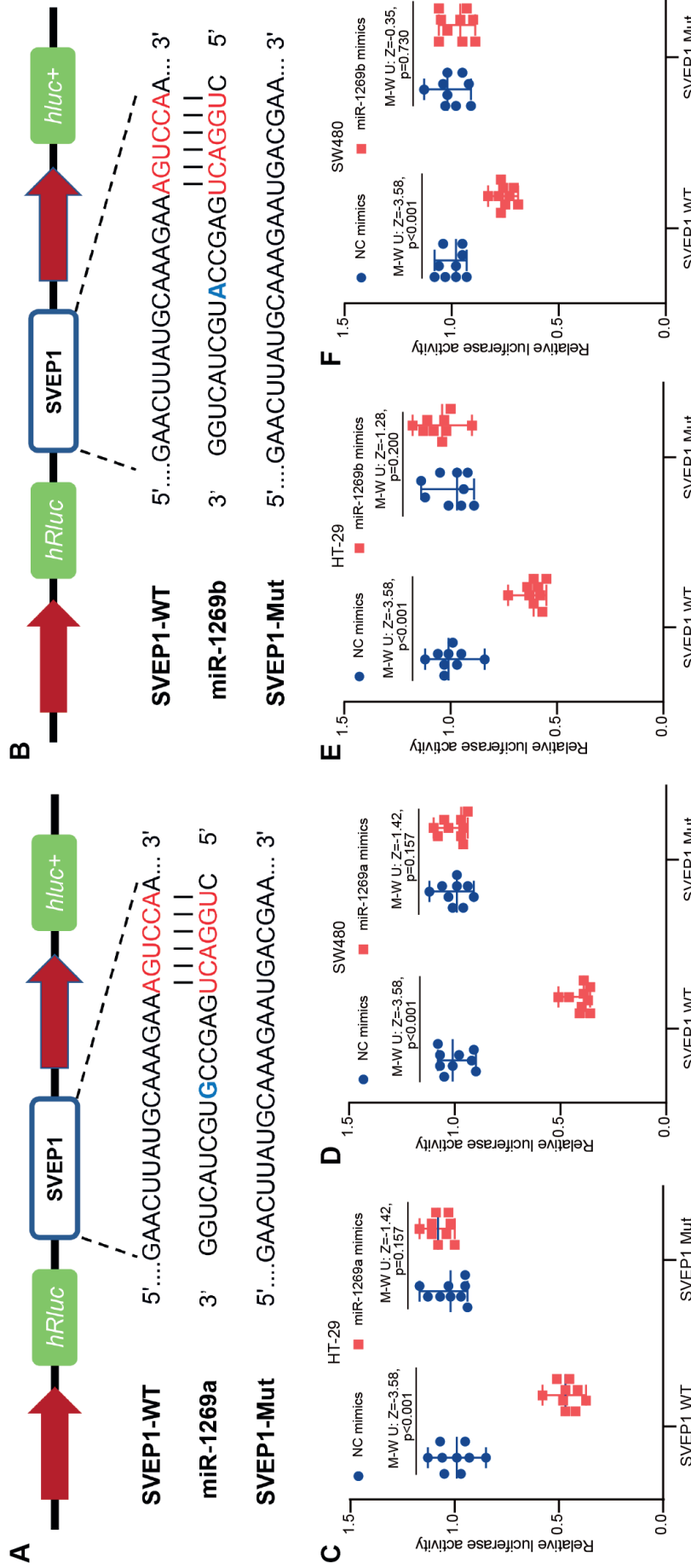
Fig. 8. *SVEP1* is the common downstream target of *miR-1269a* and *miR-1269b*. A,B. Schematic diagram of *SVEP1* 3'-UTR and mutant (Mut) luciferase reporter gene vectors; D–F. Luciferase assay in colorectal cancer (CRC) cells co-transfected WT or Mut *SVEP1* plasmid together with *miR-1269a* mimics or *miR-1269b* mimic or negative control (NC) mimics (Mann–Whitney U test, n = 9). The data are presented as median with range. All assays were conducted in triplicate

Fig. 9. SVEP1 suppresses the proliferation, migration and invasion of colorectal cancer (CRC) cells in vitro. A. Quantitative real-time polymerase chain reaction (qPCR) was used to detect the expression of SVEP1 after transfecting siRNA; B–E. The proliferation of CRC cells transfected siRNA was accessed using Cell Counting Kit-8 (CCK-8) assay and 5-Ethynyl-2'-deoxyuridine (EdU) assay; F–H. The migration and invasion capability of HT-29 and SW480 cells after silencing SVEP1 was evaluated with transwell and wound healing assays. A–C, E,G,H.* p < 0.05, ***p < 0.01, ***p < 0.001; Kruskal–Wallis test with Dunn's post hoc test (n = 9). The data are presented as median with range, and all assays were performed in triplicate
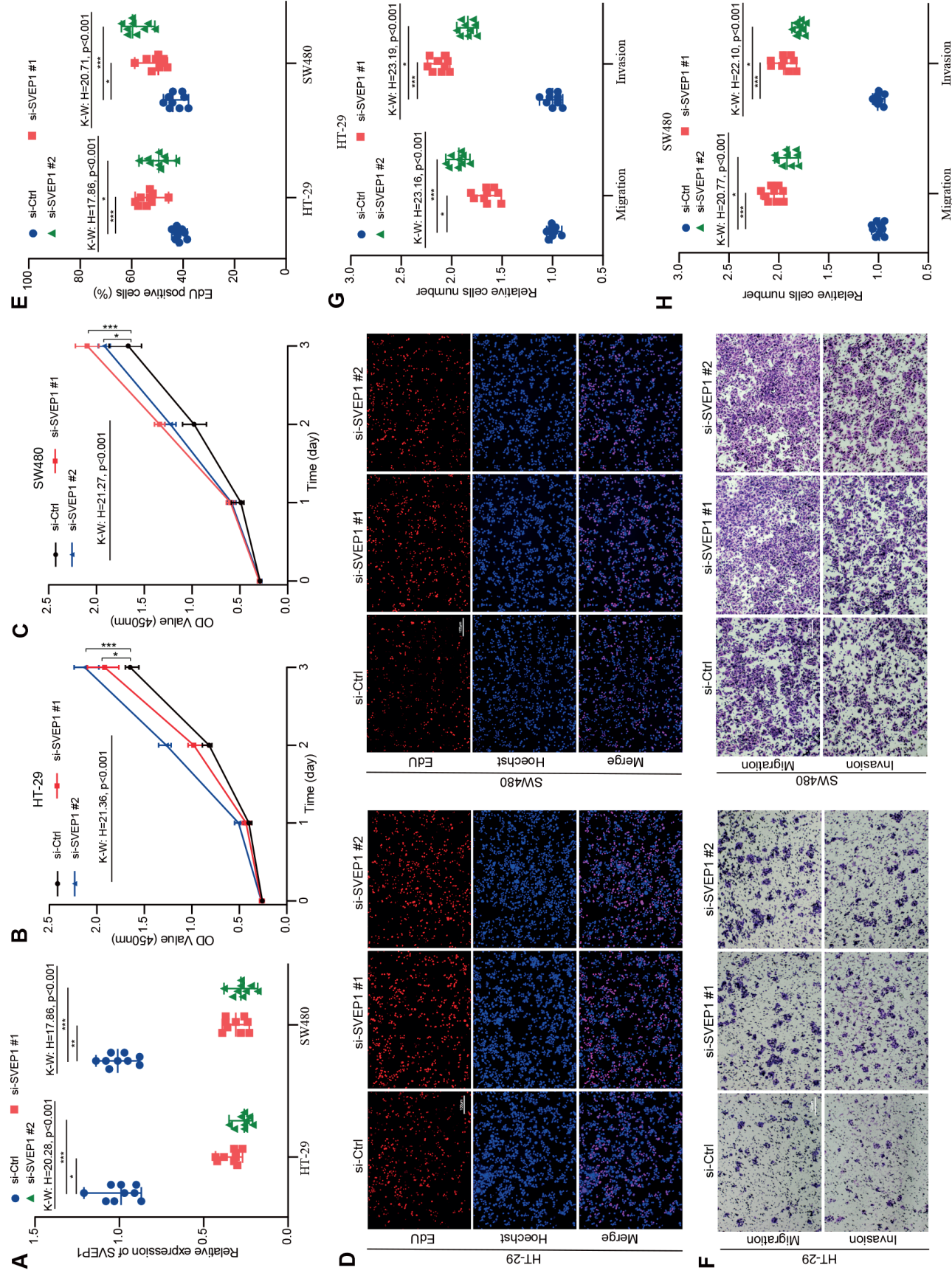
Fig. 10. *BVES-AS1* suppresses the *PI3K/AKT* pathway by *miR-1269a/miR-1269b* and *SVEP1*.
A. Wound healing assays was used to estimate colorectal cancer (CRC) cells migration abilities after knocking down *SVEP*. B. Flow cytometry was used to detect the apoptosis of CRC cells after downregulating *SVEP1*; C. Western blot was used to estimate the relative protein levels of EMT markers (*E-cadherin, N-cadherin,* and *vimentin*) in CRC cells transfected with siRNA; D–F. The protein levels of *PI3K, p-PI3K, AKT,* and *p-AKT* in CRC cells with *BVES-AS1, miR-1269a/b* overexpression or *SVEP1* silence were detected with western blot; G,H. The protein levels of *PI3K, p-PI3K, AKT,* and *p-AKT* were detected with western blot after transfection of *miR-1269a/b* mimic or *SVEP1* siRNA in *BVES-AS1* overexpressed CRC cells. A,B. *p < 0.05, ***p < 0.01, ***p < 0.001; Kruskal–Wallis test with Dunn's post hoc test (n = 9). The data are presented as median with range, and all assays were performed in triplicate
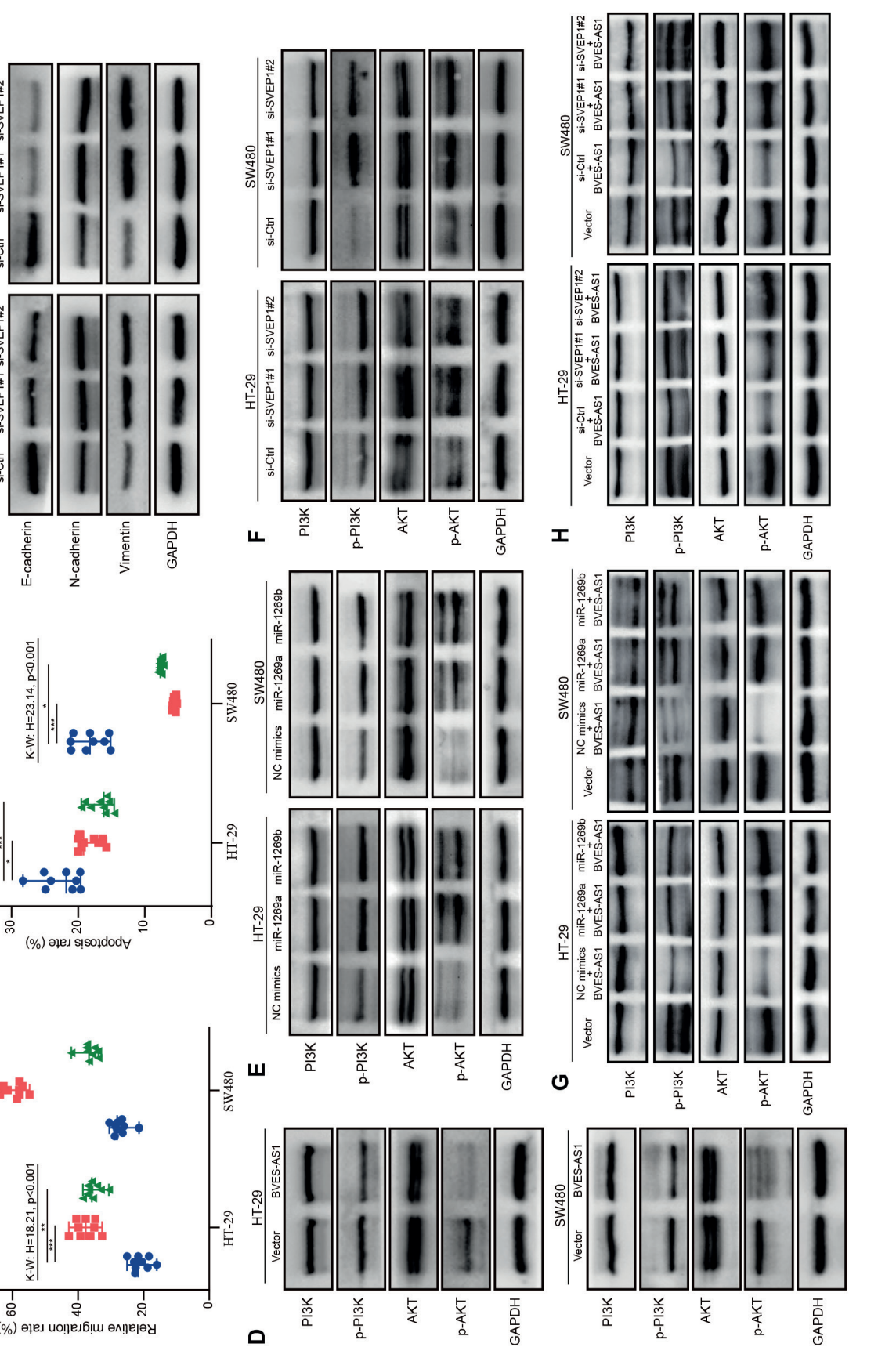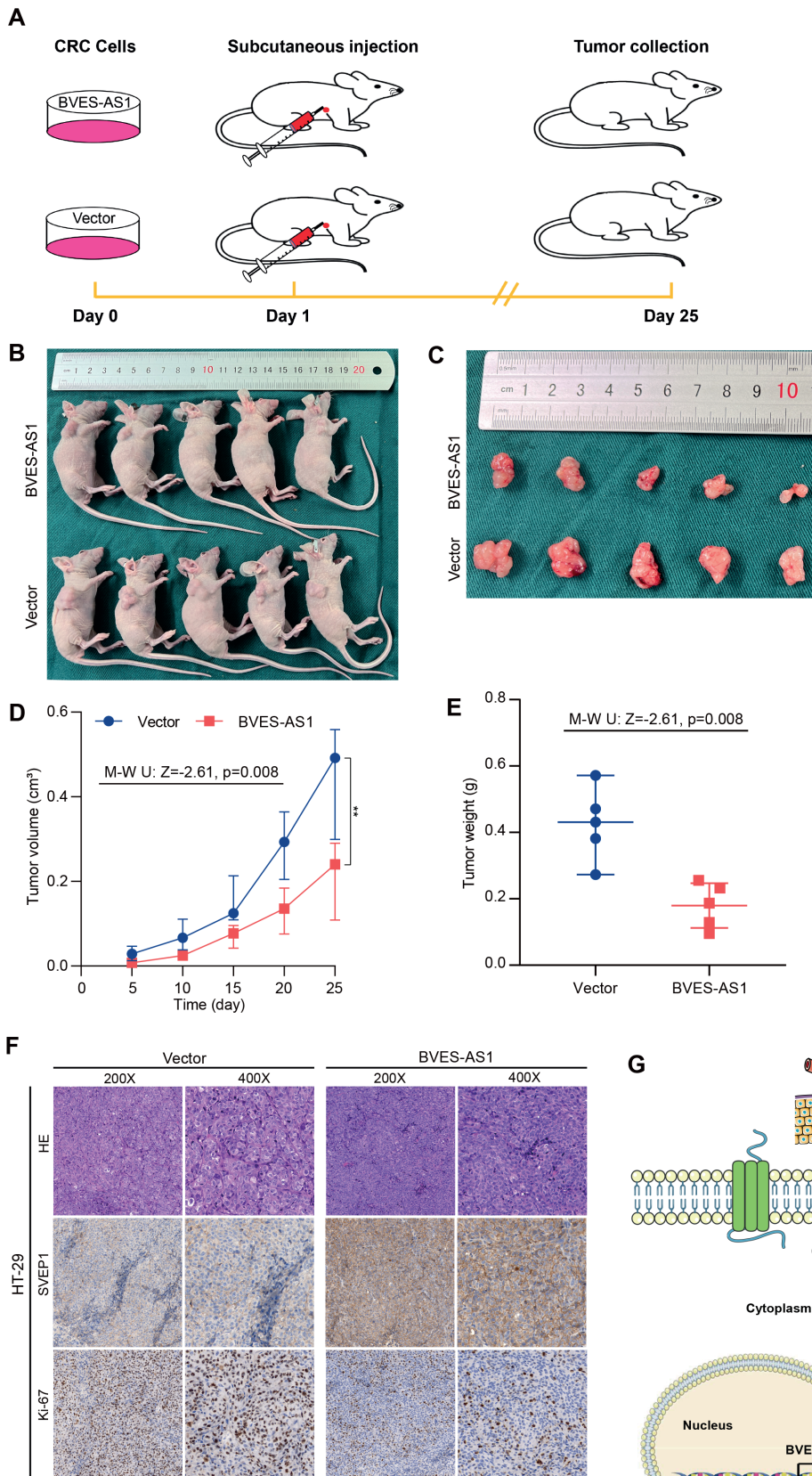
Fig. 11. *BVES-AS1* inhibits the proliferation of colorectal cancer (CRC) cells in vivo. A. Schematic diagram of the subcutaneous xenograft tumor model in BALB/c nude mice; B,C. Images of subcutaneous xenograft tumors; D. The tumor growth curve was measured every 5 days after injection (Mann–Whitney U test, n = 5; **p < 0.01); E. The tumor weights of the subcutaneous xenografts (Mann–Whitney U test, n = 5); F. Staining and immunohistochemistry (IHC) analysis of *Ki 67* and *SVEP1* expression in subcutaneous xenograft tumors; G. Schematic illustration of the mechanism of *BVES-AS1* in CRC. *BVES-AS1* served as a sponge of *miR-1269a/miR-1269b* to promote the expression of *SVEP1* and then inhibited *PI3K/ATK* pathway. Therefore, *BVES-AS1*, *miR-1269a/miR-1269b*, *SVEP1*, and *PI3K/AKT* formed an axis to regulate CRC cell proliferation, migration and invasion. The data are presented as median with range, and all assays were performed in triplicate

The xenograft tumor weight of the *BVES-AS1* group was lower than that of the vector group (Fig. 11E). To evaluate the ability of *BVES-AS1* to induce tumor growth inhibition, H&E staining and IHC (*Ki-67, SVEP1*) were performed on subcutaneous xenograft tumors. The results showed that in xenograft tumors with *BVES-AS1* upregulation, *Ki-67* expression was decreased, and *SVEP1* expression was increased (Fig. 11F). Consistent with the in vitro experiments, the xenograft tumor assay indicated that *BVES-AS1* could suppress CRC cell growth in vivo.

Discussion

To further understand the role of lncRNAs in the progression of CRC, we conducted bioinformatics analysis using TCGA data on paired tumor tissues and adjacent normal tissues from CRC patients. Our study revealed that *BVES-AS1* expression was significantly downregulated in human CRC. The low expression of *BVES-AS1* was associated with tumor infiltration depth and lymph node positivity in CRC patients. The overexpression of *BVES-AS1* suppresses the proliferation, invasion and EMT capability of CRC cells. *BVES-AS1* functioned as a sponge for *miR-1269a* and *miR-1269b*, regulating the expression of *SVEP1*. Additionally, *SVEP1* inhibits CRC cell proliferation and metastasis through the *PI3K/AKT* pathway. Ultimately, our study uncovered a complex regulatory network involving *BVES-AS1*, *miR-1269a/b*, *SVEP1*, and the *PI3K/AKT* pathway, collectively governing CRC progression.

BVES-AS1 belongs to the antisense lncRNA family derived from the *BVES* antisense strand. LncRNAs can mediate biological functions through epigenetic, transcriptional and post-transcriptional regulation. The subcellular localization of lncRNAs determines their biological roles. LncRNAs localized in the cytoplasm regulate target genes mainly through competitive binding to miRNAs.[6,23,24] The results indicated that most of *BVES-AS1* was distributed in the SW480 and HT-29 cytoplasm, indicating that *BVES-AS1* can regulate the function of CRC through the ceRNA (competing for endogenous RNA) mechanism. Bioinformatics analysis showed that *miR-1269a* and *miR-1269b* shared the same seed region sequence and had potential binding sites to *BVES-AS1*. The *miR-1269a* expression was reportedly elevated in various cancers, and *miR-1269a* overexpression promoted tumor cell proliferation, metastasis and EMT.[25–28] Bu et al. revealed that *miR-1269a* enhanced the *TGF-β* signaling pathway by competitively binding to *HOXD10* and *Smad7*, and *miR-1269a-HOXD10/Smad7-TGF-β* built a positive feedback loop promoting CRC growth and metastasis.[29] *CircASS1* can sponge *miR-1269a* to regulate *VASH1* expression, inhibiting CRC cells growth and invasion ability.[30] Similarly, *miR-1269b* was upregulated in HCC, lung cancer and oropharyngeal squamous cell cancer.[18,31,32] However, overexpression of *miR-1269b* induced downregulation of *METTL3*, suppressing

stomach cancer cell proliferation and invasion.[33] Notably, there was no report on the expression and function of *miR-1269b* in CRC. Our experimental data indicated that *miR-1269a* and *miR-1269b* were elevated in CRC and had a negative relationship with *BVES-AS1* expression. Furthermore, as verified through molecular interaction experiments, *BVES-AS1* could serve as a miRNA sponge to interact with *miR-1269a* and *miR-1269b*.

As ceRNAs, lncRNAs perform biological functions mainly by targeting downstream mRNAs. We conducted RNA-seq, and the RNA-seq data indicated that *BVES-AS1* overexpression markedly upregulated *SVEP1* expression in CRC cells. The online database and dual-luciferase experiments predicted and validated that *SVEP1* was the common target of *miR-1269a* and *miR-1269b*. *SVEP1* is an extracellular matrix protein associated with epidermal differentiation and lymphatic vessel development and can act as a cell adhesion molecule involved in intercellular adhesion.[34] Its silencing enhanced cell chemotaxis and decreased epithelial marker expression and cell adhesion capacity.[16,35] Cell adhesion molecule degradation reduces the tumor adhesion ability, contributing to tumor cell separation from the primary region and metastasis.[36] *SVEP1* was expressed at relatively low levels in liver cancer and corresponded with invasion and metastasis. The proliferation, metastasis, bone invasion, and lung metastasis abilities were promoted by *SVEP1* downregulation in liver cancer cells.[18,19] We first revealed the biological function of *SVEP1* in CRC cells. The results suggested that *SVEP1* downregulation promoted CRC cell proliferation, migration, invasion, and EMT. The *PI3K/AKT* pathway is crucial in the proliferation, invasion, and apoptosis of various cancers.[37] *SVEP1* knockdown induced the upregulation of phosphorylated *AKT*, thus promoting HCC cell proliferation and metastasis.[18] Our research also demonstrated that *SVEP1* downregulation could activate p-*PI3K* and p-*AKT* expression. In addition, overexpression of *BVES-AS1* partially reversed the upregulation of phosphorylated *PI3K* and *AKT* induced by *SVEP1* silencing. These data suggested that *BVES-AS1* overexpression suppressed CRC cell proliferation and invasion by sponging *miR-1269a/miR-1269b* to upregulate *SVEP1* expression and inhibit the activation of the *PI3K/AKT* pathway.

Limitations

Although the tumor suppressive effect and mechanism of *BVES-AS1* were revealed in CRC, some limitations must be considered. First, the study showed that *BVES-AS1* was expressed in the nucleus and cytoplasm of CRC cells. We only investigated the molecular mechanism of *BVES-AS1* in the cytoplasm; the function of nuclear *BVES-AS1* needs to be further verified. Second, *BVES-AS1* was able to serve as a ceRNA to sponge *miR-1269a* and *miR-1269b*. However, in CRC cells, the relationship between *miR-1269a* and *miR-1269b* remains unclear. Finally, we suggest that *SVEP1* knockdown contributes to the activation

of the *PI3K/AKT* pathway. Nevertheless, the specific mechanism by which *SVEP1* regulates the *PI3K/AKT* pathway needs to be further elucidated.

Conclusions

This study suggests that *BVES-AS1* functions as a tumor suppressor gene inhibiting the growth and metastasis of CRC cells in vivo and in vitro. Mechanistically, *BVES-AS1* acts as a miRNA sponge, attenuating the effects of *miR-1269a* and *miR-1269b* on *SVEP1*, which in turn inhibits the *PI3K/AKT* pathway. Therefore, our study reveals that the *BVES-AS1-miR-1269a/b-SVEP1-PI3K/AKT* axis is a key regulator in suppressing CRC progression. These findings provide new insights for potential treatment strategies in CRC.

Supplementary data

The supplementary materials are available at https://doi.org/10.5281/zenodo.10069707. The package contains the following files:

Supplementary Table 1. Sequences of oligonucleotides and probes used in this study.

Supplementary Table 2. Primer sequences.

Supplementary Table 3. Clinical characteristics of colorectal cancer patients.

Supplementary Table 4. Differentially expressed genes in RNA-seq.

Supplementary Table 5. Results of normality test.

Supplementary Table 6. Statistical analysis results of models.

Supplementary Table 7. Results of Levene's test.

Supplementary Fig. 1. *BVES-AS1* inhibits CRC cell proliferation, migration and invasion in vitro.

Supplementary Fig. 2. *BVES-AS1* reverses the oncogenic effect of *miR-1269a* or *miR-1269b*.

Supplementary Fig. 3. *SVEP1* inhibits CRC cell proliferation, migration, and invasion in vitro.

Data availability

The datasets generated and/or analyzed during the current study are available from the corresponding author on reasonable request.

Consent for publication

Not applicable.

ORCID iDs

Jianguo Yang https://orcid.org/0000-0000-0000-0000
Qican Deng https://orcid.org/0000-0003-4233-970X
Zhenzhou Chen https://orcid.org/0000-0002-4324-5388
Yajun Chen https://orcid.org/0000-0002-4059-6561
Zhongxue Fu https://orcid.org/0000-0001-8160-2975

References

1. Sung H, Ferlay J, Siegel RL, et al. Global cancer statistics 2020: GLOBOCAN estimates of incidence and mortality worldwide for 36 cancers in 185 countries. *CA A Cancer J Clin*. 2021;71(3):209–249. doi:10.3322/caac.21660

2. Lu B, Li N, Luo CY, et al. Colorectal cancer incidence and mortality: The current status, temporal trends and their attributable risk factors in 60 countries in 2000–2019. *Chin Med J (Engl)*. 2021;134(16):1941–1951. doi:10.1097/CM9.0000000000001619

3. Xie YH, Chen YX, Fang JY. Comprehensive review of targeted therapy for colorectal cancer. *Sig Transduct Target Ther*. 2020;5(1):22. doi:10.1038/s41392-020-0116-z

4. Maeda H, Kashiwabara K, Aoyama T, et al. Hazard rate of tumor recurrence over time in patients with colon cancer: Implications for postoperative surveillance from three Japanese Foundation for Multidisciplinary Treatment of Cancer (JFMC) clinical trials. *J Cancer*. 2017;8(19):4057–4064. doi:10.7150/jca.21365

5. Statello L, Guo CJ, Chen LL, Huarte M. Gene regulation by long noncoding RNAs and its biological functions. *Nat Rev Mol Cell Biol*. 2021;22(2):96–118. doi:10.1038/s41580-020-00315-9

6. Kopp F, Mendell JT. Functional classification and experimental dissection of long noncoding RNAs. *Cell*. 2018;172(3):393–407. doi:10.1016/j.cell.2018.01.011

7. Wang X, Cheng H, Zhao J, et al. Long noncoding RNA DLGAP1-AS2 promotes tumorigenesis and metastasis by regulating the Trim21/ELOA/LHPP axis in colorectal cancer. *Mol Cancer*. 2022;21(1):210. doi:10.1186/s12943-022-01675-w

8. Shi K, Yang S, Chen C, et al. RNA methylation-mediated LINC01559 suppresses colorectal cancer progression by regulating the miR-106b-5p/PTEN axis. *Int J Biol Sci*. 2022;18(7):3048–3065. doi:10.7150/ijbs.70630

9. Wang L, Cho KB, Li Y, Tao G, Xie Z, Guo B. Long noncoding RNA (lncRNA)-mediated competing endogenous RNA networks provide novel potential biomarkers and therapeutic targets for colorectal cancer. *Int J Mol Sci*. 2019;20(22):5758. doi:10.3390/ijms20225758

10. Xu W, Zhou G, Wang H, et al. Circulating lncRNA SNHG11 as a novel biomarker for early diagnosis and prognosis of colorectal cancer. *Int J Cancer*. 2020;146(10):2901–2912. doi:10.1002/ijc.32747

11. Nikolaou S, Qiu S, Fiorentino F, Rasheed S, Tekkis P, Kontovounisios C. Systematic review of blood diagnostic markers in colorectal cancer. *Tech Coloproctol*. 2018;22(7):481–498. doi:10.1007/s10151-018-1820-3

12. Gilgès D, Vinit MA, Callebaut I, et al. Polydom: A secreted protein with pentraxin, complement control protein, epidermal growth factor and von Willebrand factor A domains. *Biochem J*. 2000;352(Pt 1):49–59. PMID:11062057. PMCID:PMC1221431.

13. Sato-Nishiuchi R, Nakano I, Ozawa A, et al. Polydom/SVEP1 is a ligand for integrin α9β1. *J Biol Chem*. 2012;287(30):25615–25630. doi:10.1074/jbc.M112.355016

14. Karpanen T, Padberg Y, Van De Pavert SA, et al. An evolutionarily conserved role for Polydom/Svep1 during lymphatic vessel formation. *Circ Res*. 2017;120(8):1263–1275. doi:10.1161/CIRCRESAHA.116.308813

15. Morooka N, Futaki S, Sato-Nishiuchi R, et al. Polydom is an extracellular matrix protein involved in lymphatic vessel remodeling. *Circ Res*. 2017;120(8):1276–1288. doi:10.1161/CIRCRESAHA.116.308825

16. Samuelov L, Li Q, Bochner R, et al. SVEP 1 plays a crucial role in epidermal differentiation. *Exp Dermatol*. 2017;26(5):423–430. doi:10.1111/exd.13256

17. Glait-Santar C, Pasmanik-Chor M, Benayahu D. Expression pattern of SVEP1 alternatively-spliced forms. *Gene*. 2012;505(1):137–145. doi:10.1016/j.gene.2012.05.015

18. Chen L, Liu D, Yi X, et al. The novel miR-1269b-regulated protein SVEP1 induces hepatocellular carcinoma proliferation and metastasis likely through the PI3K/Akt pathway. *Cell Death Dis*. 2020;11(5):320. doi:10.1038/s41419-020-2535-8

19. Gong WC, Han ZQ, Guo MX, et al. Decreased expression of SVEP1 is closely related to a cancer stem cell-like phenotype and poor prognosis in hepatocellular carcinoma. *Neoplasma*. 2022;69(5):1209–1216. doi:10.4149/neo_2022_220614N629

20. Wu J, Cai Y, Zhao G, Li M. A ten N6-methyladenosine-related long non-coding RNAs signature predicts prognosis of triple-negative breast cancer. *Clin Lab Anal*. 2021;35(6):e23779. doi:10.1002/jcla.23779

21. Xing Y, Zhao Z, Zhu Y, Zhao L, Zhu A, Piao D. Comprehensive analysis of differential expression profiles of mRNAs and lncRNAs and identification of a 14-lncRNA prognostic signature for patients with colon adenocarcinoma. *Oncol Rep*. 2018;39(5):2365–2375. doi:10.3892/or. 2018.6324

22. Lu S, Han L, Hu X, et al. N6-methyladenosine reader IMP2 stabilizes the ZFAS1/OLA1 axis and activates the Warburg effect: Implication in colorectal cancer. *J Hematol Oncol*. 2021;14(1):188. doi:10.1186/s13045-021-01204-0

23. Yao RW, Wang Y, Chen LL. Cellular functions of long noncoding RNAs. *Nat Cell Biol*. 2019;21(5):542–551. doi:10.1038/s41556-019-0311-8

24. Salmena L, Poliseno L, Tay Y, Kats L, Pandolfi PP. A ceRNA hypothesis: The Rosetta Stone of a hidden RNA language? *Cell*. 2011;146(3):353–358. doi:10.1016/j.cell.2011.07.014

25. Cho HJ, Baek GO, Seo CW, et al. Exosomal microRNA-4661-5p-based serum panel as a potential diagnostic biomarker for early-stage hepatocellular carcinoma. *Cancer Med*. 2020;9(15):5459–5472. doi:10.1002/cam4.3230

26. Guo X, Dai X, Liu J, Cheng A, Qin C, Wang Z. Circular RNA circREPS2 acts as a sponge of miR-558 to suppress gastric cancer progression by regulating RUNX3/β-catenin signaling. *Mol Ther Nucleic Acids*. 2020;21:577–591. doi:10.1016/j.omtn.2020.06.026

27. Zhang K, Zhang L, Mi Y, et al. A ceRNA network and a potential regulatory axis in gastric cancer with different degrees of immune cell infiltration. *Cancer Sci*. 2020;111(11):4041–4050. doi:10.1111/cas.14634

28. Zhao Y, Xu L, Wang X, Niu S, Chen H, Li C. A novel prognostic mRNA/miRNA signature for esophageal cancer and its immune landscape in cancer progression. *Mol Oncol*. 2021;15(4):1088–1109. doi:10.1002/1878-0261.12902

29. Bu P, Wang L, Chen KY, et al. miR-1269 promotes metastasis and forms a positive feedback loop with TGF-β. *Nat Commun*. 2015;6(1):6879. doi:10.1038/ncomms7879

30. Xiong HL, Zhong XH, Guo XH, Liao HJ, Yuan X. circASS1 overexpression inhibits the proliferation, invasion and migration of colorectal cancer cells by regulating the miR-1269a/VASH1 axis. *Exp Ther Med*. 2021;22(4):1155. doi:10.3892/etm.2021.10589

31. Yang W, Xiao W, Cai Z, Jin S, Li T. miR-1269b drives cisplatin resistance of human non-small cell lung cancer via modulating the PTEN/PI3K/AKT signaling pathway. *Onco Targets Ther*. 2020;13:109–118. doi:10.2147/OTT.S225010

32. Chen HC, Tseng YK, Chi CC, et al. Genetic variants in microRNA-146a (C > G) and microRNA-1269b (G > C) are associated with the decreased risk of oral premalignant lesions, oral cancer, and pharyngeal cancer. *Arch Oral Biol*. 2016;72:21–32. doi:10.1016/j.archoralbio.2016.08.010

33. Kang J, Huang X, Dong W, Zhu X, Li M, Cui N. MicroRNA-1269b inhibits gastric cancer development through regulating methyltransferase-like 3 (METTL3). *Bioengineered*. 2021;12(1):1150–1160. doi:10.1080/21655979.2021.1909951

34. Morris GE, Denniff MJ, Karamanavi E, et al. The integrin ligand SVEP1 regulates GPCR-mediated vasoconstriction via integrins α9β1 and α4β1. *Br J Pharmacol*. 2022;179(21):4958–4973. doi:10.1111/bph.15921

35. Nakada TA, Russell JA, Boyd JH, Thair SA, Walley KR. Identification of a nonsynonymous polymorphism in the *SVEP1* gene associated with altered clinical outcomes in septic shock. *Crit Care Med*. 2015;43(1):101–108. doi:10.1097/CCM.0000000000000604

36. Özkan E, Chia PH, Wang RR, et al. Extracellular architecture of the SYG-1/SYG-2 adhesion complex instructs synaptogenesis. *Cell*. 2014;156(3):482–494. doi:10.1016/j.cell.2014.01.004

37. Koveitypour Z, Panahi F, Vakilian M, et al. Signaling pathways involved in colorectal cancer progression. *Cell Biosci*. 2019;9(1):97. doi:10.1186/s13578-019-0361-4

Parthenolide induces ROS-dependent cell death in human gastric cancer cell

*Dandan Han[1,B,D], *Wenhao Zhu[2,B,D], Yang Chen[1,B,E], Huiru Wang[1,A,C,E,F]

[1] Department of Transfusion, The First Affiliated Hospital of University of Science and Technology of China (USTC), Division of Life Sciences and Medicine, University of Science and Technology of China, Hefei, China

[2] Institute of Integrated Medicine, School of Basic Medicine, Qingdao University, China

A – research concept and design; B – collection and/or assembly of data; C – data analysis and interpretation;
D – writing the article; E – critical revision of the article; F – final approval of the article

Address for correspondence
Huiru Wang
E-mail: wanghuiru@ustc.edu.cn

Abstract

Background. Parthenolide (PN), a key active ingredient of feverfew, has been used to treat gastrointestinal disorders. However, the mechanism of the cytotoxic effect exerted by PN on tumor cells has not been elucidated.

Objectives. To study the cytotoxic effect of PN on human gastric cancer cells, the specific death mode, and gene expression changes induced by PN.

Materials and methods. In this study, MGC-803 cells were used to study PN-induced cytotoxicity as a gastric cancer cell line. Assays of cell proliferation, cell cycle distribution, apoptosis, and reactive oxygen species (ROS) were performed using a Cell Counting Kit-8 (CCK-8) assay and a flow cytometer. MGC-803 cells treated with and without PN were separately subjected to high-throughput RNA sequencing. Western blotting was used to investigate the expression of some important proteins.

Results. Parthenolide exposure elicited cell proliferation inhibition in a dose- and time-dependent manner. Parthenolide induced cell cycle arrest at the G1 and S stages. Parthenolide-induced caspase-dependent apoptosis and necroptosis were caused by the activation of RIP, RIP3 and MLKL. MGC-803 cells showed a response to ROS and oxidative stress after PN treatment. Moreover, ROS and cytotoxicity induced by PN were significantly attenuated by a ROS scavenger catalase.

Conclusions. Parthenolide-induced gastric cancer cell death is a complex ROS-dependent process different from ordinary apoptosis and necrosis, suggesting that PN is a potential treatment option for gastric cancer.

Key words: cytotoxicity, reactive oxygen species, apoptosis, gastric cancer, parthenolide

1238

D. Han et al. Parthenolide kills gastric cancer cells

Background

Parthenolide (PN), a sesquiterpene lactone derived from feverfew, which is the traditional herbal medicine, has been found to exert multiple pharmacological effects such as antimicrobial, anti-inflammatory and anti-cancer effects.[1–3] These biological properties of PN may be attributed to its α-methylene-γ-lactone moiety.[4] At present, strong inhibition of nuclear factor NF-κB (nuclear factor kappa-light-chain-enhancer of activated B cells) along the NF-κB signaling pathway in multiple steps makes PN the inhibitor of NF-κB.[5] However, the underlying mechanisms in the cytotoxic effect of PN on tumor cells are still not fully elucidated.

Several recent studies indicate that apoptosis and autophagy are involved in PN-induced cell death in tumor cells. However, it is unclear whether other cell death forms are involved in PN-induced cell death.[6–8] To differ from the old and inappropriate definition of cell death formulated from the morphological perspective, regulated cell death (RCD) is newly classified into multiple forms including apoptosis, pathanatos, necroptosis, pyroptosis, and ferroptosis.[9]

Reactive oxygen species (ROS), a heterogeneous group of oxygen-containing radical species, participates in a wide range of biochemical processes in tumor cells.[10] The function of ROS is decided by its level. For instance, persistently high levels of ROS could be beneficial to tumorigenesis and metastasis.[11] Reactive oxygen species participate in the initiation, progression and metastasis of gastric cancer cells. However, further exposure to higher ROS induces serious oxidative stress which facilitates cell death.[12] Thus, induction of oxidative damage may be a therapeutic approach for gastric cancer.[13] It has been reported that PN causes oxidative stress by inducing ROS generation; however, ROS and PN-induced cell death are not well understood.[14,15]

Objectives

To study the cytotoxic effect of PN on human gastric cancer cells, the specific death mode and gene expression changes induced by PN.

Materials and methods

Reagents

Parthenolide, Z-VAD-fmk, AG14361, and Nec-1 were all supplied by Selleck (Houston, USA). Catalase and dimethyl sulfoxide (DMSO) were supplied by Beyotime Biotechnology (Shanghai, China).

Cell culture and treatment

The MGC-803 cell line was purchased from the National Infrastructure of Cell Line Resource (Beijing, China) and cultured at 37°C, 5% CO_2 in Dulbecco's modified Eagle's medium (DMEM)/high glucose supplemented with 10% fetal bovine serum (FBS; Gibco, Waltham, USA). We incubated cells in 96-well plates ($1×10^4$ cells/well) and 6-cm dishes ($6×10^5$ cells/dish) for 24 h. Then, MGC-803 was treated with PN at indicated concentrations for the indicated time with or without 1 h pretreatment with Z-VAD-fmk, AG14361, Nec-1, and catalase. We followed the methods of the previous study.[16]

Cell cycle assay

Cell cycles were identified using a cell cycle assay kit (Beyotime Biotechnology). MGC-803 cells were harvested after treatment and washed with phosphate-buffered saline (PBS), then fixed with 70% ethanol overnight at 4°C. For staining, cells were incubated at room temperature with 40 mg/mL propidium iodide (PI), followed by 30 min at room temperature in the dark, and then analyzed using a flow cytometer (BD Accuri C6; BD Biosciences, Franklin Lakes, USA).

Colony formation assay

MGC-803 cells were plated into the 6-well plate ($2×10^3$ cells/well) with treatment or control and grown for 2 weeks at 37°C, 5% CO_2. The cell colonies were stained with crystal violet and the colony numbers were recorded.

ROS assay

An ROS assay kit was used to measure the intracellular ROS levels (Beyotime Biotechnology). After treatment, cells were harvested and washed with PBS, and then incubated with dichlorodihydrofluorescein diacetate (DCFH-DA) (50 µM) containing PBS solution for 30 min at 37°C in the dark and analyzed with a flow cytometer.

Cell apoptosis assay

The annexin-V/PI staining kit (EpiZyme Biotech, Cambridge, USA) was used to identify cell apoptosis. Cells were harvested, washed with PBS, stained with 10 µM annexin-V and 5 µM PI in the dark for 15 min at 37°C, and then analyzed with a flow cytometer.

RNA sequencing (RNA-seq)

MGC-803 cells treated with DMSO or PN (40 µM) for 24 h were collected and the RNA samples were isolated with Trizol according to the manufacturer's instructions. After the cDNA was synthesized, the library was sequenced using Illumina NovaSeq6000 platform (Illumina, San Diego, USA). The abundance of genes was estimated using featureCounts program (https://subread.sourceforge.net). Differentially expressed genes between

DMSO-treated and DMSO-treated MGC-823 cells were identified using DEseq2. Original RNA-seq data have been deposited in the National Center for Biotechnology Information Gene Expression Omnibus repository (GSE217526). Differentially expressed genes (DEGs) were defined as genes with a p-value >0.05 and absolute fold change >2. Gene Ontology (GO) functional enrichment analysis was used to identify significantly enriched GO terms in DEGs.

Western blot analysis

Radioimmunoprecipitation assay (RIPA) lysis buffer was used for total protein extraction and a BCA assay was applied to identify protein concentrations. Samples (40 µg each) were separated using 10–15% sodium dodecyl-sulfate polyacrylamide gel electrophoresis (SDS-PAGE) and transferred to polyvinylidene difluoride (PVDF) membranes. The membranes were incubated with specific primary antibodies after blocking. The antibodies against p53, cyclin D1, cyclin E1, p21$^{WAF1/CIP1}$, p27^{KIP1}, caspase-3, caspase-9, caspase-8, c-FLIP, poly(ADP-ribose)polymerase 1 (PARP-1), BCL2, BAX, BAK, p-receptor-interacting serine/threonine kinase (pRIP), RIP, p-RIP3, RIP3, and p-mixed lineage kinase domain-like pseudo kinase (MLKL) were obtained from Cell Signaling Technology (CST; Danvers,

USA; 1:1,000 dilution), and β-actin was obtained from ABclonal Biotech (1:5,000 dilution; Wuhan, China). The protein bands were visualized using chemiluminescent detection.

Statistical analyses

GraphPad Prism 7 software (GraphPad Software, San Diego, USA) and IBM SPSS v. 22 (IBM Corp., Armonk, USA) was used to perform the statistical analysis. Data are shown as data points with the median and analyzed using 2-sided Wilcoxon rank-sum test (2 groups) or Kruskal–Wallis tests and the post hoc Dunn's test (more than 2 groups). A p-value of <0.05 and 0.05 < p < 0.1 are considered statistically significant and marginally statistically significant, respectively. The original data analysis was shown in the Supplementary material.

Results

The growth of human gastric cancer cell MGC-803 was inhibited after PN treatment

To explore the effect of PN on tumor cell growth, CCK-8 was used to detect cell viability. As shown in Fig. 1A, PN exposure inhibited cell viability in a dose- and time-dependent
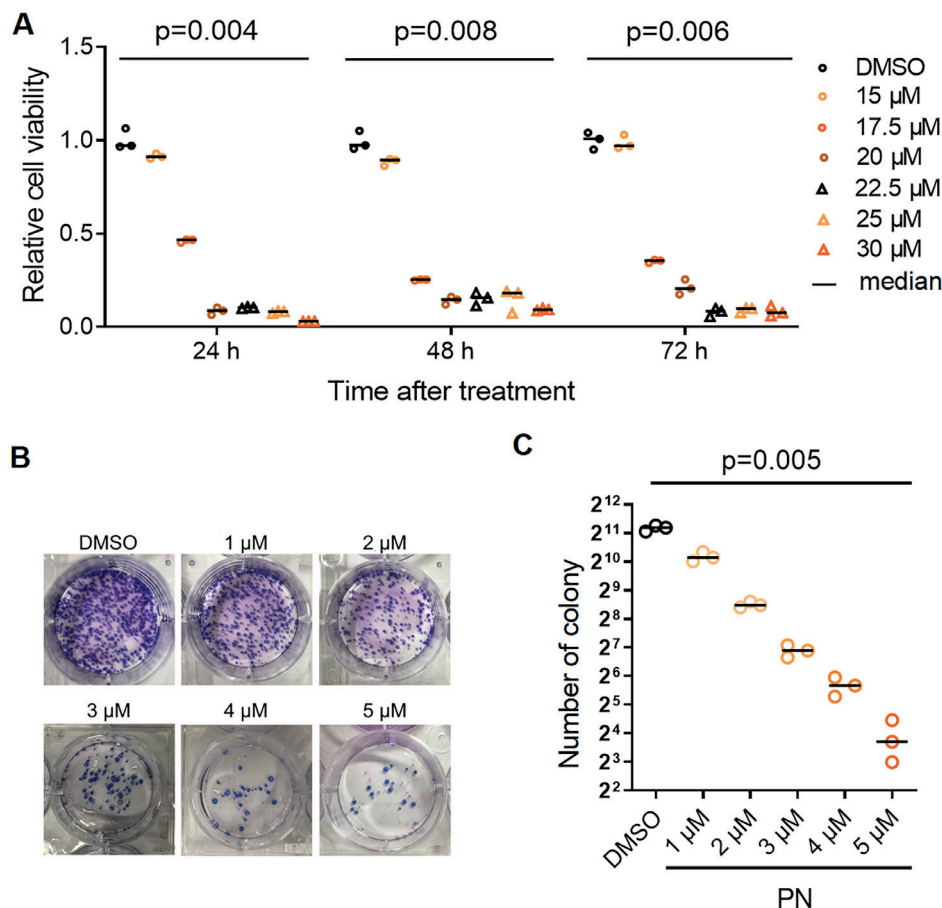
Fig. 1. The growth of human gastric cancer cell MGC-803 was inhibited after parthenolide (PN) treatment. A. MGC-803 cells were treated with dimethyl sulfoxide (DMSO) and PN (15, 17.5, 20, 22.5, 25 µM) for 24 h, 48 h and 72 h, and then the cell viability was measured using Cell Counting Kit-8 (CCK-8) assay. Three culture plates were used in total and in each plate 3 culture replicates per condition were set up. After 24 h of culture, CCK-8 was added to the 1st culture plate and proliferation was evaluated based on the optical density (OD) values. After incubation for 48 h and 72 h, the 2nd and 3rd culture plates were removed, and proliferation was detected in a similar manner; B, C. MGC-803 cells were treated with DMSO and PN (1, 2, 3, 4, 5 µM) for 2 weeks and then colony numbers were recorded. Each experimental group was equipped with 3 repeated wells. Each dot or triangle represents each well. Representative images of cell clonal staining (B) and statistical analysis of colony numbers (C) were shown. A, C. Data points with the median. A. Kruskal–Wallis test, 24 h: p = 0.004, H = 18.327, df = 6; 48 h: p = 0.008, H = 18.327, df = 6; 72 h: p = 0.006, H = 18.327, df = 6. C. Kruskal–Wallis test, p = 0.005, H = 18, df = 5

manners (Kruskal–Wallis test, 24 h: p = 0.004, H = 18.327, df = 6; 48 h: p = 0.008, H = 18.327, df = 6; 72 h: p = 0.006, H = 18.327, df = 6). Compared with the control, when PN was used at a concentration of 20 μM, the growth of half of the cells was inhibited (Supplementary Table 1). Moreover, the results of the colony formation assay showed that the growth of MGC-803 cells exposed to PN for 2 weeks was inhibited in a dose-dependent manner (Fig. 1B,C, Supplementary Table 2, Kruskal–Wallis test, p = 0.005, H = 18, df = 5).

MGC-803 showed G1 and S phase cell cycle arrest after PN treatment

Since the cell cycle plays an important role in the development of cancer, we use PI staining to identify the effects of PN on the cell cycle of MGC-803 cells. As shown in Fig. 2A,B, the cell cycle of MGC-803 cells exposed to PN showed a strong tendency to be selectively arrested at the G_1 and S phases (2-sided Wilcoxon rank-sum test, p = 0.081, T = 6). Furthermore, PN exposure induced the increase of protein levels of p53, p21$^{WAF1/CIP1}$ and p27^{KIP1}, while the protein levels of cyclin D1 and cyclin E1 were decreased (Fig. 2C), indicating that PN may induce G_1 and S cell cycle arrest.

The expression of apoptosis and necrosis related proteins in MGC-803 cells increased after PN treatment

We used annexin-V/PI staining to identify whether PN induced apoptosis in MGC-803 cells. Parthenolide exposure elicited a marginal statistically significant increase in the apoptotic cell population (Fig. 3A, 2-sided Wilcoxon rank-sum test, p = 0.081, T = 6), indicating that apoptosis occurred after PN treatment. Furthermore, as shown in Fig. 3B, PN exposure elicited an increase in cleaved caspase-3 (19 kDa and 17 kDa), cleaved caspase-9 (37 kDa, 35 kDa), cleaved caspase-8 (43 kDa), and cleaved PARP1 (87 kDa), indicating that PN exposure activated caspase-3, caspase-9, caspase-8, and PARP1 in MGC-803 cells. Furthermore, both protein levels of c-FLIP$_L$ and c-FLIPs, 2 isoforms of c-FLIP (cellular FLICE-like inhibitory proteins) endowed with inhibitory activity in caspase-8 activation, appeared to decrease over time after PN treatment, indicating that extrinsic apoptosis propagated by caspase-8 was involved in PN-induced cell death in MGC-803 cells. On the other hand, after PN exposure, both the protein levels of BAX and BAK which were implicated in intrinsic apoptosis appeared to increase over time, while BCl2 protein levels appeared unchanged, indicating that intrinsic apoptosis was also involved in PN-induced cell death in MGC-803 cells (Fig. 3C).
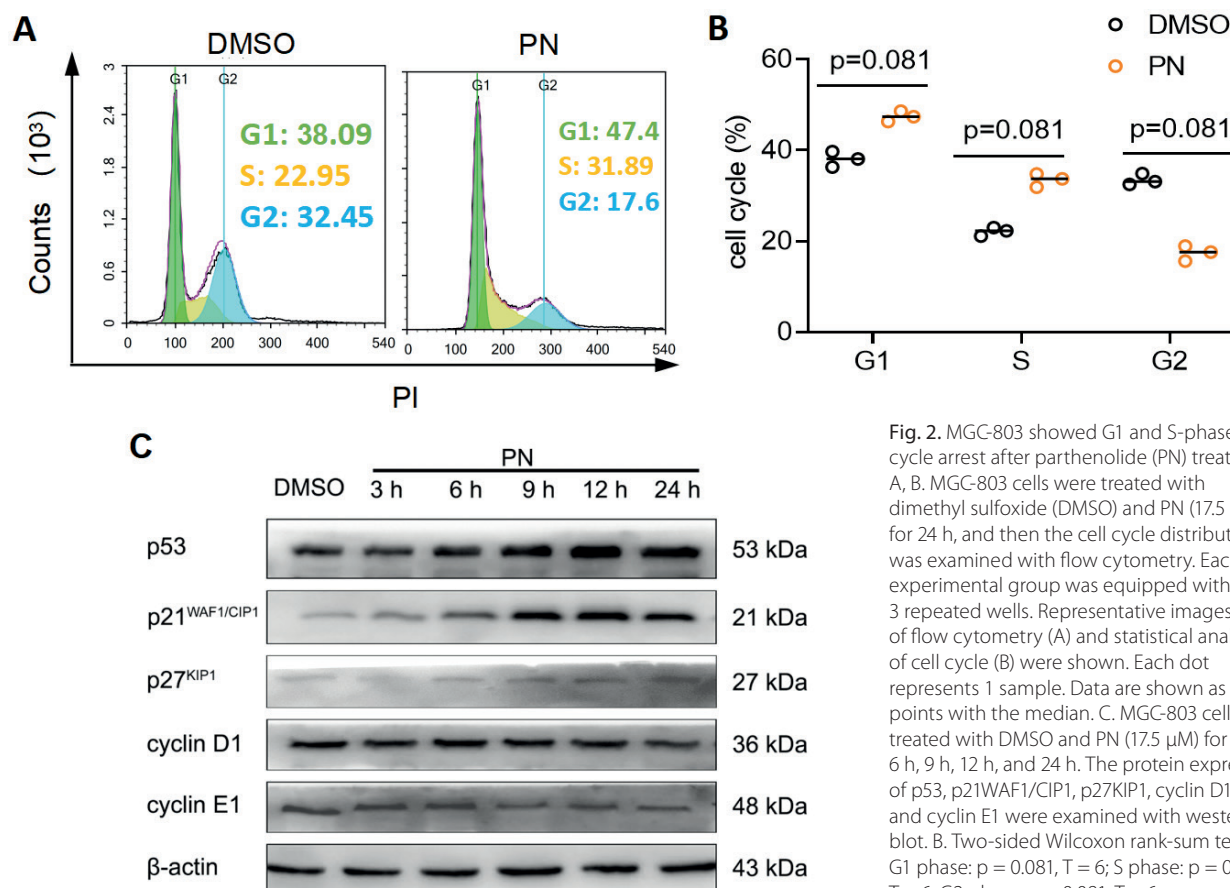
Fig. 2. MGC-803 showed G1 and S-phase cell cycle arrest after parthenolide (PN) treatment. A, B. MGC-803 cells were treated with dimethyl sulfoxide (DMSO) and PN (17.5 μM) for 24 h, and then the cell cycle distribution was examined with flow cytometry. Each experimental group was equipped with 3 repeated wells. Representative images of flow cytometry (A) and statistical analysis of cell cycle (B) were shown. Each dot represents 1 sample. Data are shown as data points with the median. C. MGC-803 cells were treated with DMSO and PN (17.5 μM) for 3 h, 6 h, 9 h, 12 h, and 24 h. The protein expression of p53, p21WAF1/CIP1, p27KIP1, cyclin D1, and cyclin E1 were examined with western blot. B. Two-sided Wilcoxon rank-sum test, G1 phase: p = 0.081, T = 6; S phase: p = 0.081, T = 6; G2 phase: p = 0.081, T = 6
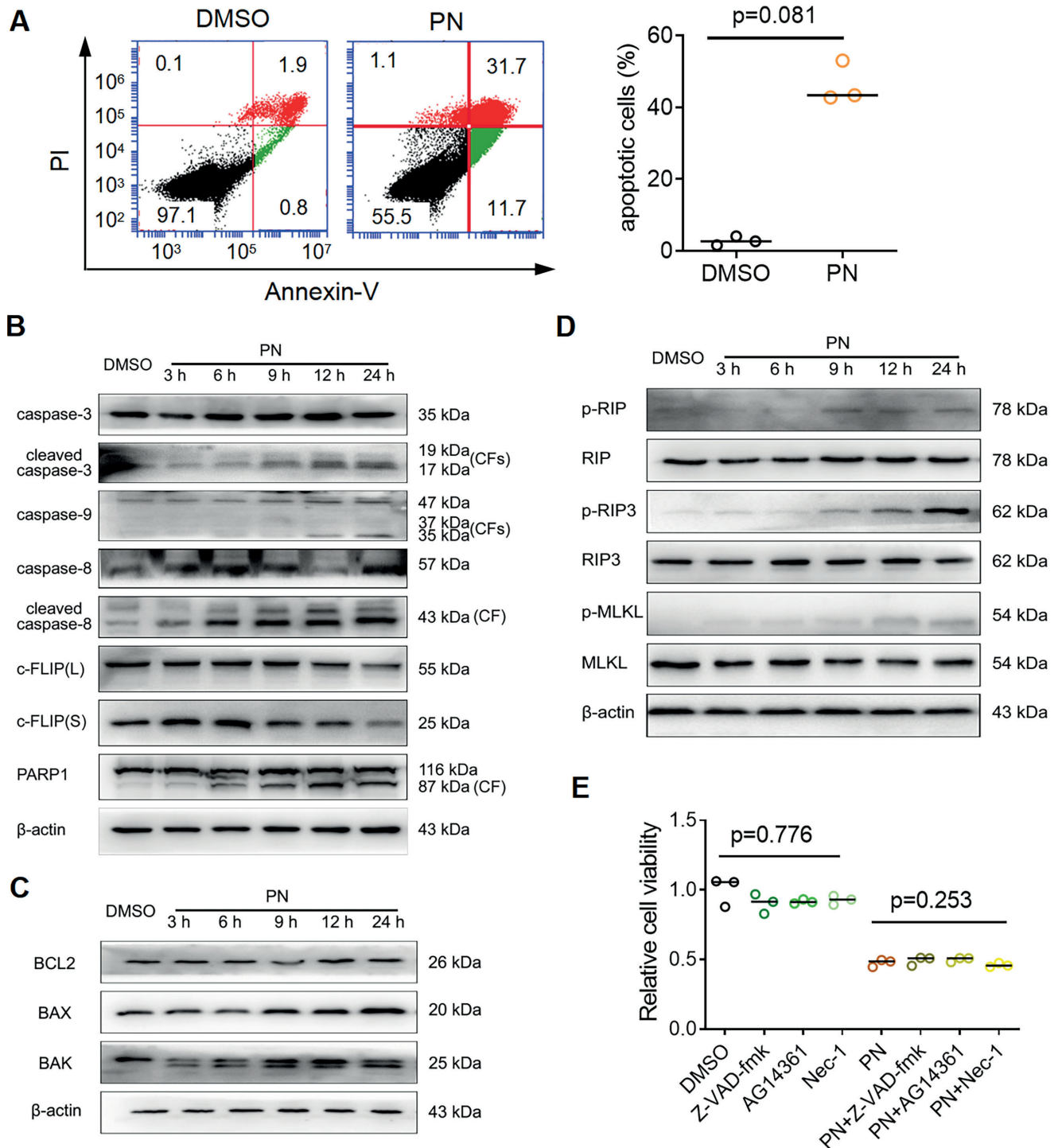
Fig. 3. The expression of apoptosis- and necrosis-related proteins in MGC-803 cells increased after parthenolide (PN) treatment. A. MGC-803 cells were treated with DMSO and PN (17.5 µM) for 3 h, 6 h, 9 h, 12 h, and 24 h. The cell apoptotic population was examined with flow cytometry after annexin-V/PI staining. Representative images of flow cytometry (left panel) and statistical analysis of apoptosis (right panel) were shown. Each experimental group was equipped with 3 repeated wells. Each dot represents 1 sample; B. The protein levels of caspase-3, caspase-8, caspase-9, PARP-1, and c-FLIP were examined using western blot after treatment; C. The protein levels of BCL2, BAX and BAK were examined with western blot after treatment; D. The protein levels of p-RIP, RIP, p-RIP3, RIP3, p-MLKL, and MLKL were examined with western blot; E. MGC-803 cells were treated with PN (17.5 µM) with or without 1 h pretreatment with Z-VAD-fmk (100 µM), AG14361 (50 µM) or Nec-1 (50 µM). Cell viability was measured using Cell Counting Kit-8 (CCK-8) assay after culture for 24 h. Data are shown as data points with the median (A, E). A. Two-sided Wilcoxon rank-sum test, p = 0.081, T = 6. E, Kruskal–Wallis test, p = 0.776, H = 1.333, df = 3; p = 0.253, H = 4, df = 3

We also examined whether necroptosis was induced by PN exposure in human gastric cancer cells. Necroptosis is an RCD type that involves the activation of RIP, RIP3 and MLKL. As shown in Fig. 3D, PN exposure elicited an increase in RIP phosphorylation (Ser166), RIP3 phosphorylation (Ser227) and MLKL phosphorylation (Ser358), indicating that PN may induce necroptosis in human gastric cancer cells. Next, we used Z-VAD-fmk (pan-caspase

1242

D. Han et al. Parthenolide kills gastric cancer cells

inhibitor), AG14361 (PARP1 inhibitor) and Nec-1 (RIP1 inhibitor) to detect whether apoptosis and necroptosis induced by PN can be inhibited. As shown in Fig. 3E, pretreatment of all 3 inhibitors in MGC-803 cells could not mitigate PN-induced cytotoxicity, indicating that PN-induced cytotoxicity was a complicated process (Kruskal–Wallis test, p = 0.776, H = 1.333, df = 3; p = 0.253, H = 4, df = 3).

High-throughput sequencing showed that the oxidative stress response was enhanced after PN treatment

To comprehensively analyze the changes in cancer cells caused by PN treatment, the transcriptomes of PN-treated MGC-803 cells with control (DMSO-treated) were profiled using RNA-Seq. Heat maps were drawn based on FPKM

(fragments per kilobase million) values for hundreds of DEGs identified between the groups (Fig. 4A). Collectively, the upregulation of expression of 832 unique transcripts and downregulation of 1,278 transcripts was evident in the transcriptional profiles of PN-treated MGC-803 cells compared to the control (Fig. 4B). Next, we found that "response to oxidative stress" and "response to reactive oxygen species" were enriched at the top of GO Biological Process terms enrichment (Fig. 4C). These results indicated that response to ROS may be involved in cytotoxicity induced by PN.

Cytotoxicity induced by PN was attenuated by catalase in MGC-803

Since the sequencing results suggested that ROS are closely related to cell death induced by PN, we also used
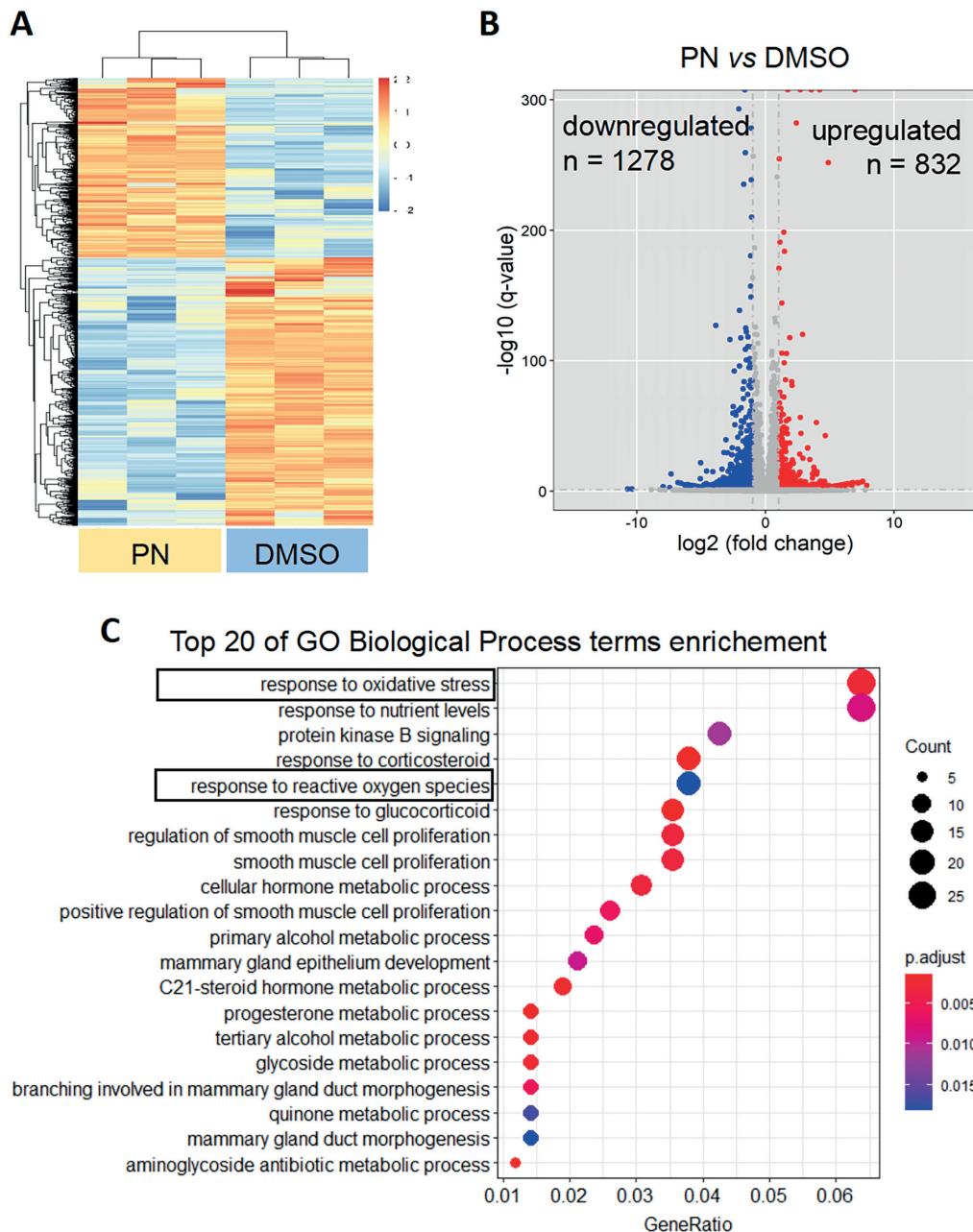
Fig. 4. High-throughput sequencing showed that the oxidative stress response was enhanced after parthenolide (PN) in MGC-803. A. The differentially expressed genes (DEGs) (fold change >2 and p-value <0.05) of MGC-803 cells treated with dimethyl sulfoxide (DMSO) compared with their counterparts treated with PN for 24 h were selected for heat map analysis. Each column represents 1 sample (n = 3 per group); B. DEGs, including upregulated genes (n = 832) and downregulated genes (n = 1,278), were illustrated using a volcano plot: PN treatment compared to DMSO treatment; C. Top 20 biological processes obtained with GO enrichment of DEGs
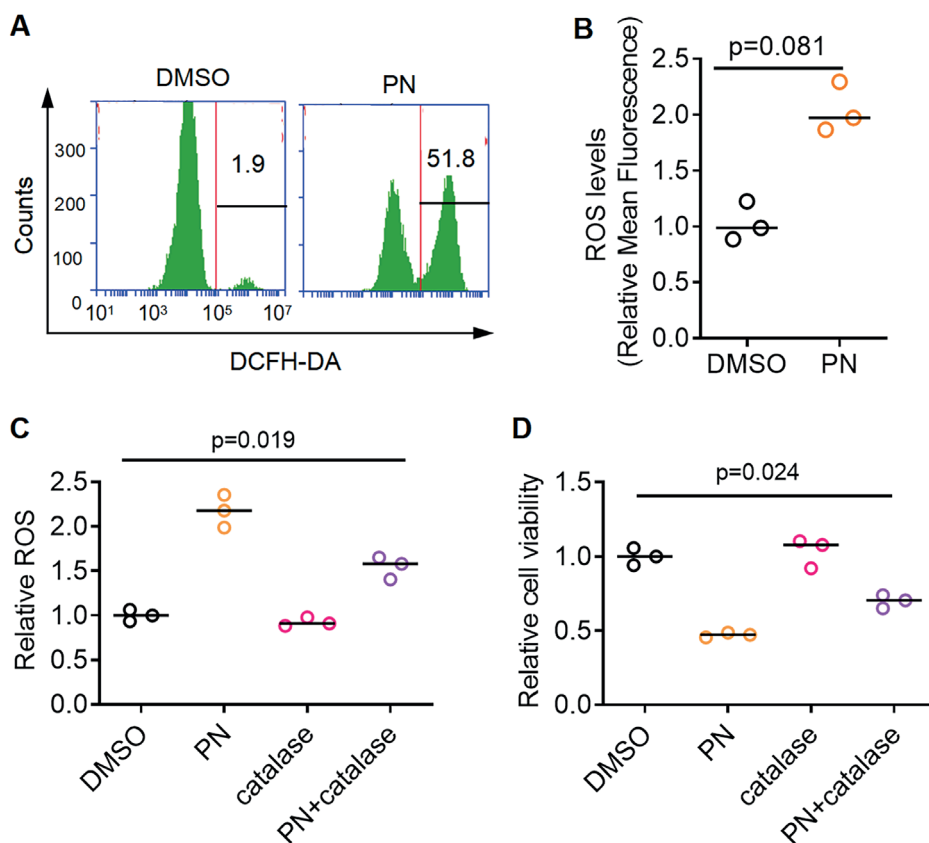
Fig. 5. Cytotoxicity induced by parthenolide (PN) was attenuated using catalase in MGC-803. A. The intracellular reactive oxygen species (ROS) levels of MGC-803 cells treated with dimethyl sulfoxide (DMSO) and PN (17.5 µM) for 24 h were measured using flow cytometry; B. Quantification of relative mean fluorescence of ROS level; C, D. The relative intracellular ROS and viability of MGC-803 cells treated with DMSO, PN (17.5 µM), catalase (2,000 U/mL), or co-treatment with PN and catalase was measured with flow cytometry and Cell Counting Kit-8 (CCK-8) assay. Each experimental group was equipped with 3 repeated wells. Data are shown as data points with the median. B. Two-sided Wilcoxon rank-sum test, p = 0.081, T = 6. C. Kruskal–Wallis test, p = 0.019, H = 9.974, df = 3. D, Kruskal–Wallis test, p = 0.024, H = 9.462, df = 3

DCFH-DA staining to determine ROS levels. As shown in Fig. 5A,B, PN exposure elicited a marginal statistically significant increase in ROS levels in MGC-803 cells (2-sided Wilcoxon rank-sum test, p = 0.081, T = 6). Furthermore, the ROS quencher catalase was used to identify the role of ROS in PN-induced cytotoxicity, and the results showed that pretreatment of catalase significantly attenuated the increase of ROS levels (Fig. 5C, Supplementary Table 3, Kruskal–Wallis test: p = 0.019, H = 9.974, df = 3; post hoc Dunn's test, DMSO compared to PN + catalase: p = 0.258) and cell death (Fig. 5D, Supplementary Table 4, Kruskal–Wallis test: p = 0.024, H = 9.462, df = 3; post hoc Dunn's test, DMSO compared to PN + catalase: p = 0.174) induced by PN, indicating that ROS may be critical in PN-induced cytotoxicity.

Discussion

Parthenolide, a sesquiterpene lactone derived from feverfew, has shown cytotoxic activity in multiple human cancer cells, such as glioblastoma cells,[17] breast cancer cells,[18] renal cell carcinoma,[19] and colorectal cancer.[20] There has not yet been a complete explanation of the mechanism behind PN-induced cell death. In this study, the biological effects of PN were investigated in human gastric cancer cells MGC-803.

In our study, PN inhibited cell growth in a dose- and time-dependent manner, demonstrating its cytotoxic effect. In addition, we demonstrated that PN can induce tumor cell arrest in G1 and S phases, which is consistent with some other studies.[21,22] There are various types of cyclins, cyclin-dependent kinases and other regulatory proteins that regulate cell cycle progression. Among them, p53 controls 3 cell cycle checkpoints. For G1 to S, cyclin D1 and cyclin E1 are the positive regulators, and p21$^{WAF1/CIP1}$ and p27^{KIP1} are the negative regulators.[23] In this study, PN treatment upregulated the p53 protein levels in MGC-803 cells compared with those in DMSO-treated cells, indicating that PN may activate p53. In addition, PN exposure downregulated the protein levels of cyclin D1 and cyclin E1 in MGC-803 cells, indicating that PN may induce G1 phase arrest. Moreover, the present study also examined 2 negative regulators, p21$^{WAF1/CIP1}$ and p27^{KIP1}, which restraint G1-S progression, and the results showed that PN exposure upregulated the protein levels of p21^{CIP1} and p27^{KIP1} in MGC-803 cells compared with those in DMSO-treated cells, confirming that PN induced G1 and S-phase arrest.

Cytotoxicity of PN involves several RCD types; among them, apoptosis serves a very essential part in PN-induced cell death in several cancer cells models.[24,25] Likewise, our results show that PN exposure elicited a significant increase in the apoptotic cell population in MGC-803 cells. BCL2 and BAX mediate irreversible mitochondrial outer membrane permeabilization (MOMP), an essential step in mitochondrial-dependent intrinsic apoptosis.[26,27] In the present study, both the protein levels of BAX and

BAK in MGC-803 cells treated with PN increased over time, while BCl2 protein levels appeared unchanged, suggesting that intrinsic apoptosis may be involved in PN-induced cell death. Extrinsic apoptosis was propagated by caspase-8 and precipitated by executioner caspases, mainly caspase-3. In the present study, PN exposure activated caspase-8 and downregulated the protein levels of caspase-8 inhibitors, c-FLIP, indicating that extrinsic apoptosis may be also involved in PN-induced cell death in MGC-803 cells.[28] Moreover, we also found that PN exposure elicited an increase of cleaved PARP1, indicating that PARP1 was activated. PARP1 activation can occur in response to DNA damage, leading to Δψm dissipation and MOMP.[29]

Necroptosis is a type of RCD that manifests a necrotic morphotype. Its main mechanism is the sequential activation of RIP, RIP3 and MLKL.[30,31] Our results show that in MGC-803 cells, PN exposure elicited an increase of RIP, RIP3 and MLKL phosphorylation, indicating that RIP, RIP3 and MLKL may be activated by PN exposure to precipitate necroptosis.

A lot of evidence suggests that for the processes that are referred to as necessary steps for the execution of cell death, pharmacologic inhibition only changes its biochemical and morphological manifestations, but could not effectively prevent cell death.[32–34] For example, although the inhibitors of caspase, PARP1 and RIP can significantly block the activation of caspases, PARP1 and RIP induced by pharmacologic interventions, cell death remain unchanged.[35] Likewise, our results show that Z-VAD-fmk, AG14361 or Nec-1 failed to protect MGC-803 cells from cell death.

In the whole process of RCD, the reverse of early-phase biochemical changes such as decreasing ATP levels and oxidative stress could restore cellular homeostasis.[32] Our results show that in MGC-803 cells, PN exposure elicited a significant increase in ROS, while pretreatment of the ROS scavenger catalase significantly attenuated this effect. Moreover, pretreatment of catalase effectively inhibited the decrease of cell viability induced by PN exposure, indicating that PN-induced cytotoxicity is ROS-dependent.

Limitations

Due to the poor solubility of PN, more improvements in the dosage form are needed for its clinical application in the future. Similarly, the forms of drug dosage also limit experiments on animals.

Conclusions

Parthenolide-induced gastric cancer cell death is a complex ROS-dependent process different from ordinary apoptosis and necrosis, suggesting that PN is a potential treatment option for gastric cancer.

Supplementary data

The Supplementary materials are available at https://doi.org/10.5281/zenodo.10066470. The package includes the following files:

Supplementary Table 1. Post hoc Dunn's test for the effect of PN on the cell viability of MGC-803 cell.

Supplementary Table 2. Post hoc Dunn's test for the effect of PN on the cell colonies of MGC-803 cells.

Supplementary Table 3. Post hoc Dunn's test for the effect of PN and catalase on ROS Generation of MGC-803 cells.

Supplementary Table 4. Post hoc Dunn's test for the effect of PN and catalase on cell viability of MGC-803 cells.

Supplementary Table 5. Original data. Parthenolide induces ROS-dependent cell death in human gastric cancer cellanalysis.

Supplementary Table 6. Gene sample count from MGC-803 cells treated with DMSO compared with counterparts treated with PN.

Data availability

The datasets generated and/or analyzed during the current study are available from the corresponding author on reasonable request.

Consent for publication

Not applicable.

ORCID iDs

Dandan Han   https://orcid.org/0000-0003-0000-5541
Wenhao Zhu   https://orcid.org/0009-0008-0460-2283
Yang Chen   https://orcid.org/0000-0002-9449-3699
Huiru Wang   https://orcid.org/0000-0003-3026-6005

References

1. Liu L, Liu N, Zhang H, Li D. Exploring and validating the metastasis mechanism of pathenolide interfering with cutaneous melanoma through ER stress-dependent apoptosis based on the network pharmacology. *Phytochem Anal*. 2023;34(7):745–754. doi:10.1002/pca.3193

2. Zhang Y, Feng W, Peng X, et al. Parthenolide alleviates peritoneal fibrosis by inhibiting inflammation via the NF-κB/TGF-β/Smad signaling axis. *Lab Invest*. 2022;102(12):1346–1354. doi:10.1038/s41374-022-00834-3

3. Liu M, Xiao C, Sun M, Tan M, Hu L, Yu Q. Parthenolide inhibits STAT3 signaling by covalently targeting Janus kinases. *Molecules*. 2018; 23(6):1478. doi:10.3390/molecules23061478

4. Tyagi V, Alwaseem H, O'Dwyer KM, et al. Chemoenzymatic synthesis and antileukemic activity of novel C9- and C14-functionalized parthenolide analogs. *Bioorg Med Chem*. 2016;24(17):3876–3886. doi:10.1016/j.bmc.2016.06.028

5. Li Y, Xu H, Tan X, et al. Parthenolide inhibits proliferation of cells infected with Kaposi's sarcoma-associated herpesvirus by suppression of the NF-κB signaling pathway. *Arch Virol*. 2023;168(2):39. doi:10.1007/s00705-022-05626-0

6. Yi J, Gong X, Yin XY, et al. Parthenolide and arsenic trioxide co-trigger autophagy-accompanied apoptosis in hepatocellular carcinoma cells. *Front Oncol*. 2022;12:988528. doi:10.3389/fonc.2022.988528

7. Cui M, Wang Z, Huang LT, Wang JH. Parthenolide leads to proteomic differences in thyroid cancer cells and promotes apoptosis. *BMC Complement Med Ther*. 2022;22(1):99. doi:10.1186/s12906-022-03579-0

8. Hu B, Zhen D, Bai M, et al. Ethanol extracts of *Rhaponticum uniflorum* (L.) DC flowers attenuate doxorubicin-induced cardiotoxicity via alleviating apoptosis and regulating mitochondrial dynamics in H9c2 cells. *J Ethnopharmacol*. 2022;288:114936. doi:10.1016/j.jep.2021.114936

9. Galluzzi L, Vitale I, Aaronson SA, et al. Molecular mechanisms of cell death: Recommendations of the Nomenclature Committee on Cell Death 2018. *Cell Death Differ*. 2018;25(3):486–541. doi:10.1038/s41418-017-0012-4

10. Dickinson BC, Chang CJ. Chemistry and biology of reactive oxygen species in signaling or stress responses. *Nat Chem Biol*. 2011;7(8):504–511. doi:10.1038/nchembio.607

11. Moloney JN, Cotter TG. ROS signalling in the biology of cancer. *Semin Cell Dev Biol*. 2018;80:50–64. doi:10.1016/j.semcdb.2017.05.023

12. Cui Q, Wang JQ, Assaraf YG, et al. Modulating ROS to overcome multidrug resistance in cancer. *Drug Resist Updat*. 2018;41:1–25. doi:10.1016/j.drup.2018.11.001

13. Slika H, Mansour H, Wehbe N, et al. Therapeutic potential of flavonoids in cancer: ROS-mediated mechanisms. *Biomed Pharmacother*. 2022;146:112442. doi:10.1016/j.biopha.2021.112442

14. Flores-Lopez G, Moreno-Lorenzana D, Ayala-Sanchez M, et al. Parthenolide and DMAPT induce cell death in primitive CML cells through reactive oxygen species. *J Cell Mol Med*. 2018;22(10):4899–4912. doi:10.1111/jcmm.13755

15. Zhu J, Tang C, Cong Z, et al. ACT001 reverses resistance of prolactinomas via AMPK-mediated EGR1 and mTOR pathways. *Endocr Relat Cancer*. 2022;29(2):33–46. doi:10.1530/ERC-21-0215

16. Liu N, Li Y, Chen G, Ge K. Evodiamine induces reactive oxygen species-dependent apoptosis and necroptosis in human melanoma A-375 cells. *Oncol Lett*. 2020;20(4):121. doi:10.3892/ol.2020.11983

17. Hou Y, Sun B, Liu W, et al. Targeting of glioma stem-like cells with a parthenolide derivative ACT001 through inhibition of AEBP1/PI3K/AKT signaling. *Theranostics*. 2021;11(2):555–566. doi:10.7150/thno.49250

18. Sufian HB, Santos JM, Khan ZS, et al. Parthenolide reverses the epithelial to mesenchymal transition process in breast cancer by targeting TGFbeta1: In vitro and in silico studies. *Life Sci*. 2022;301:120610. doi:10.1016/j.lfs.2022.120610

19. Liu D, Han Y, Liu L, et al. Parthenolide inhibits the tumor characteristics of renal cell carcinoma. *Int J Oncol*. 2020;58(1):100–110. doi:10.3892/ijo.2020.5148

20. Liu X, Wang C, Li S, et al. Parthenolide derivatives as PKM2 activators showing potential in colorectal cancer. *J Med Chem*. 2021;64(23):17304–17325. doi:10.1021/acs.jmedchem.1c01380

21. Kouhpaykar H, Sadeghian MH, Rafatpanah H, et al. Synergy between parthenolide and arsenic trioxide in adult T-cell leukemia/lymphoma cells in vitro. *Iran J Basic Med Sci*. 2020;23(5):616–622. doi:10.22038/ijbms.2020.40650.9610

22. Jorge J, Neves J, Alves R, Geraldes C, Gonçalves AC, Sarmento-Ribeiro AB. Parthenolide induces ROS-mediated apoptosis in lymphoid malignancies. *Int J Mol Sci*. 2023;24(11):9167. doi:10.3390/ijms24119167

23. Malumbres M, Barbacid M. Cell cycle, CDKs and cancer: A changing paradigm. *Nat Rev Cancer*. 2009;9(3):153–166. doi:10.1038/nrc2602

24. Ding Y, Chen X, Liu C, et al. Identification of a small molecule as inducer of ferroptosis and apoptosis through ubiquitination of GPX4 in triple negative breast cancer cells. *J Hematol Oncol*. 2021;14(1):19. doi:10.1186/s13045-020-01016-8

25. Karam L, Abou Staiteieh S, Chaaban R, et al. Anticancer activities of parthenolide in primary effusion lymphoma preclinical models. *Mol Carcinog*. 2021;60(8):567–581. doi:10.1002/mc.23324

26. Delbridge ARD, Grabow S, Strasser A, Vaux DL. Thirty years of BCL-2: Translating cell death discoveries into novel cancer therapies. *Nat Rev Cancer*. 2016;16(2):99–109. doi:10.1038/nrc.2015.17

27. Czabotar PE, Lessene G, Strasser A, Adams JM. Control of apoptosis by the BCL-2 protein family: Implications for physiology and therapy. *Nat Rev Mol Cell Biol*. 2014;15(1):49–63. doi:10.1038/nrm3722

28. Park EJ, Chauhan AK, Min KJ, Park DC, Kwon TK. Thymoquinone induces apoptosis through downregulation of c-FLIP and Bcl-2 in renal carcinoma Caki cells. *Oncol Rep*. 2016;36(4):2261–2267. doi:10.3892/or.2016.5019

29. Fatokun AA, Dawson VL, Dawson TM. Parthanatos: Mitochondrial-linked mechanisms and therapeutic opportunities. *Br J Pharmacol*. 2014;171(8):2000–2016. doi:10.1111/bph.12416

30. Yang Y, Chen Y, Wu JH, et al. Targeting regulated cell death with plant natural compounds for cancer therapy: A revisited review of apoptosis, autophagy-dependent cell death, and necroptosis. *Phytother Res*. 2023;37(4):1488–1525. doi:10.1002/ptr.7738

31. Holmgren C, Sunström Thörnberg E, Granqvist V, Larsson C. Induction of breast cancer cell apoptosis by TRAIL and Smac mimetics: Involvement of RIP1 and cFLIP. *Curr Issues Mol Biol*. 2022;44(10):4803–4821. doi:10.3390/cimb44100327

32. Galluzzi L, Bravo-San Pedro JM, Vitale I, et al. Essential versus accessory aspects of cell death: Recommendations of the NCCD 2015. *Cell Death Differ*. 2015;22(1):58–73. doi:10.1038/cdd.2014.137

33. Huang Z, Xia H, Cui Y, Yam JWP, Xu Y. Ferroptosis: From basic research to clinical therapeutics in hepatocellular carcinoma. *J Clin Transl Hepatol*. 2022;11(1):207–218. doi:10.14218/JCTH.2022.00255

34. Scimeca M, Rovella V, Palumbo V, et al. Programmed cell death pathways in cholangiocarcinoma: Opportunities for targeted therapy. *Cancers*. 2023;15(14):3638. doi:10.3390/cancers15143638

35. Steinhart L, Belz K, Fulda S. Smac mimetic and demethylating agents synergistically trigger cell death in acute myeloid leukemia cells and overcome apoptosis resistance by inducing necroptosis. *Cell Death Dis*. 2013;4(9):e802. doi:10.1038/cddis.2013.320

B10 cells: Development, phenotype, and function in cancer

Dandan Li[D], Yunfeng Ma[A,D–F]

Department of Pathogenic Biology and Immunology, School of Basic Medical Sciences, Xi'an Jiaotong University Health Science Centre, China

A – research concept and design; B – collection and/or assembly of data; C – data analysis and interpretation;
D – writing the article; E – critical revision of the article; F – final approval of the article

Address for correspondence
Yunfeng Ma
E-mail: fanxin199@163.com

Conflict of interest
None declared

Abstract

B10 cells, a specialized subset of regulatory B cells, have been identified in both mice and humans. These cells are characterized by their regulatory impact on immune dynamics, principally through their secretion of interleukin-10 (IL-10), a cytokine known for its anti-inflammatory properties. The pivotal role of immune mediators such as B10 cells is to maintain a delicate equilibrium between antitumor immunity and tumor-promoting responses. Emerging studies have cast B10 cells as key suppressors in the antitumor immune arsenal. They operate in synergy with a spectrum of immune cells within the innate and adaptive spectrums, contributing to a milieu that favors tumor progression and metastatic spread. In this comprehensive review, we will discuss the ontogeny, phenotype and effector functions of B10 cells in murine systems. We will also review the role of B10 cells in oncological models in animal studies and extend these findings to the human clinical context, elucidating their role in facilitating tumor immune evasion. A thorough understanding of these processes is imperative for the strategic targeting and attenuation of B10 cell activity, which is anticipated to be a cornerstone in the advancement of effective cancer immunotherapy strategies.

Key words: cancer, IL-10, tumor immunology, B10 cells

Introduction

B cells (Bregs) have undergone extensive research due to their diverse roles in antigen presentation, T cells activation, and secretion of antibodies, cytokines, and proteases.[1–6] B cell development originates from hematopoietic stem cells in bone marrow. Immature transitional B cells leave the bone marrow and circulate through the peripheral immune organs, where they further mature into naïve B cells. Upon stimulation by specific antigens, naïve B cells proliferate in lymphoid follicles and form the germinal center (GC). Here, activated B cells differentiate into short-lived plasmablasts that secrete antibodies, as well as long-lived plasma cells and memory cells. Each subset has distinct phenotypes, and they all function as effector cells in humoral immune responses (Table 1).[7–13] In recent years, many studies have described the role of B cells with immunosuppressive functions in regulating antitumor immune responses. Regulatory B cells were originally used by Mizoguchi et al. to refer to B lymphocytes that prevent inflammatory bowel disease (IBD) from progression in mouse models,[14,15] mainly by suppressing and/ or modulating immune responses by producing the potent anti-inflammatory cytokine interleukin 10 (IL-10).[16] To date, the unique phenotype of B cells has not been determined, and for clarity, the subset of regulatory B cells with the function to express IL-10 is referred to as B10 cells. We use the term "B10 cell" to denote B cells capable of expressing IL-10 in vitro. Due to the ability of B10 cells to induce a tolerogenic environment and increase the number and activity of immunosuppressive cells, increasing evidence supports a role of B10 cells in tumor immunity to promote tumor progression.

Objectives

In this review, we discuss the identification, distribution and development of B10 cells. We provide a summary of the functions of key surface molecules in B10 cells. Additionally, we analyze the phenotypes and functions of B10 cells in both human and animal models of solid malignancies (Table 2). We also discuss therapeutic options that could be used to reduce B10 cell activity and boost antitumor reactions.

Materials and methods

Data for this review were collected in January 2023. The search strategy involved searching the PubMed database using the keywords "B10 cells", "regulatory B cells" and "IL-10-producing B cells". During the 2nd round of data collection, more precise keywords were used: "development", "function", "toll-like receptors", "cytokine", "inflammation", "tumor", "T cells", and "IL-10". This more focused search produced 91 articles. Articles were selected based on their relevance to our objectives.

Results

Identification, distribution and surface markers

The identification of B10 cells was studied in mice using a contact hypersensitivity (CHS) model.[16] In this model, CD19$^{-/-}$ mice (B10 cells in the spleen: 1–2%) exhibited an increased T-cell-dependent inflammatory response resulting in ear thickness augmentation, compared to wild-type mice (B10 cells in the spleen: absent). Conversely, CD19 transgenic (CD19Tg) mice (B10 cells in the spleen: ~10%) exhibited reduced inflammation. Previous research has indicated that B cell-mediated IL-10 secretion ability parallels the CHS response inhibition in CD19$^{-/-}$, WT and CD19Tg mice.[16] It has been shown that transplanting IL-10-producing B cells from wild-type mice into CD19$^{-/-}$ mice may decrease inflammation in the CD19$^{-/-}$ mice, and that this reduction is dependent on the generation of IL-10 in the B cells. In addition, CD19Tg mice showed aberrant B-1 subset development, altered antibody and autoantibody production, and alterations in the T-cell compartment.[16] Therefore, the production of the powerful inhibitory cytokine IL-10

Table 1. B cell subsets in mice and humans

Subsets	Mouse phenotype	Human phenotype	Reference
Transitional	CD19$^+$B220$^+$CD24$^+$	CD19$^+$CD24^{hi}CD38^{hi}	7
Mature naïve	FO-B: B220$^+$IgM^{lo}IgD^{hi}CD21^{int} CD23$^+$	CD19$^+$CD20$^+$CD27 CD24^{int}CD38^{int}CD21$^+$CD10$^-$IgD$^+$IgM$^-$	8–10
	MZ-B: IgM^{hi}IgD^{lo}CD21^{hi}CD23$^-$CD1d^{hi}		
Germinal center	CD19$^+$CD38^{lo}PNA$^+$GL7$^+$FAS$^+$	CD19$^+$CD10$^+$CD20$^+$CD27$^+$CD38$^+$FAS$^+$IgDBR3$^+$	10, 11
Memory	CD19$^+$B220$^+$CD38$^+$ and/or CD80$^+$ and/or PD-L2$^+$ and/or CD73$^+$	CD19$^+$CD27$^+$CD38$^-$	7
Antibody-secreting cells	plasmablasts: CD19$^{lo/-}$CD138$^+$CD93$^+$MHCII$^+$Ki-67$^+$	plasmablasts: CD19$^+$IgD$^-$CD27^{hi}CD38^{hi}CD138$^-$	12, 13
	plasma cells: CD19$^{lo/-}$CD138$^+$CD93$^+$MHCII$^+$Ki-67$^+$	plasma cells: CD19$^+$IgD$^-$CD27^{hi}CD38^{hi}CD138$^+$	

FO-B – follicular B cells; MZ-B – marginal zone B cells.

led to the functional definition of this distinct regulatory subgroup as the B10 cell. Because of their small population size, IL-10-producing B cells (also known as "B10 effector cells") can be difficult to detect in vivo. However, the ability of B10 effector cells (B10eff) to produce IL-10 can be tested in vitro. B10 cells can be detected using flow cytometry after being stimulated with PMA (phorbol 12-myristate 13-acetate), ionomycin and monensin (PIM) for 5 h ex vivo.[16–18] In addition, increased IL-10 production after co-culturing B10 with lipopolysaccharide (LPS) or CpG compared to stimulation with PMA and ionomycin alone suggests that B10 are more likely to be antigen-experiencing cells.[19–21]

B10 cells comprised between 1% and 2% of spleen B cells and over 40% of peritoneal cavity B cells of wild-type mice.[16] These cells are also detected in various tissues, including blood, lymph nodes, Peyer's patches, intestinal tissues, and the central nervous system, albeit at extremely low levels.[19,22,23] When compared to non-B10 cells, B10 cells from untreated mice exhibit elevated levels of immunoglobulin M (IgM), CD19, CD5, CD24, CD43, and MHCII, along with reduced IgD and CD23 expression.[23] Phenotypically, spleen B10 cells resemble various distinct B cell subsets and can be further categorized based on cell surface marker expression into transitional cells, marginal zone (MZ) cells, marginal zone precursor cells, and memory cells.[16,24–26] The specific marker for spleen B10 cells is CD19hiCD1dhiCD5+.[16,24,27,28] However, B10 cells also occur in low frequencies among other spleen B cells populations, such as those marked CD1dlo and CD5− population B cells.[29] B10 cells from the peritoneal cavity and spleen share similar phenotypes, despite the absence of CD1dhi or CD21hi B cells in the peritoneum.[23] Based on surface molecule expression, peritoneal cavity B10 cells can be further subdivided into B1a (CD5+CD11b+) and B1b (CD5−CD11b+).[23]

Low but detectable numbers of B10 cells are present in human peripheral blood, averaging around $1.9 \pm 0.3 \times 10^3$ B10 cells/mL. These cells are also sporadically found in the spleen, tonsils and umbilical cord blood.[17] In human adult blood, B10 cells display elevated levels of CD19, as well as activation and memory markers such as CD27, CD48 and CD148. The expression of the memory markers, CD48 and CD148, suggests prior antigenic encounters in vivo.[17] Unlike immature or transitional B cells, B10 cells lack CD10 expression and have lower IgM levels. Levels of CD5, CD20, CD21, CD22, CD23, CD25, CD28, and CD40 expression are similar between B10 and typical B cells.[17] B10 cells are enriched within the CD24hi CD27+ B cell subset, making up about 25% of all B cells in healthy individuals' blood. This subsets has a tenfold higher proportion of B10 cells compared to the CD24loCD27− subpopulation.[17] Additional studies have identified IL-10-producing human B cells with markers CD25hiCD27hiCD86hiCD1dhi B cells[30] and CD19+CD24hiCD38hi B cells.[31]

Development of B10 cell

Upon antigen-BCR binding, a cascade of appropriate signaling pathways is activated, leading B cells to release IL-10 These B cells are referred to as B10 cells (Fig. 1A).[32] A subpopulation of B cells, termed progenitor B10 cells (B10pro), receives the requisite signals for IL-10 production but has not yet attained full IL-10 secretory capability. Notably, B10pro cells lack definitive markers for identification. In the absence of specific stimulatory signals such as LPS or the CD40L/CD40 axis, these cells are incapable of IL-10 secretion. However, intracellular IL-10 production can be detected upon PIM stimulation. The transition from B10pro to fully functional B10 cells can be induced by a 48-h incubation with either CD40 monoclonal antibody (mAb) or LPS.[19] In human samples, B10pro cells constitute about 7% of peripheral B cells,[33] while in murine spleens, they generally represent 3–8% of the B cell population.[19] Importantly, studies indicate that B10pro cell frequencies remain stable in murine models during inflammatory and autoimmune conditions,[16,19,22,24,27] but show a marked upregulation in human samples.[17] This discrepancy suggests that the functional response of B10pro cells to inflammatory cues may be species-specific.

B10 cells that initiate IL-10 secretion are termed B10eff cells, although they are extremely rare in vivo. There is evidence that BCR-antigen interactions and BCR-mediated signaling are critical for normal B10 cell functionality.[19] For differentiation into IL-10-secreting B10eff cells, B10 cells require additional stimuli, potentially including CD40 signaling, IL-21, LPS or CpG.[19,28] Further studies indicate that B-lymphocyte stimulator (BlyS), also known as BAFF, significantly influences both the differentiation into B10 cells and their capacity to release IL-10.[28] Splenic B cells are cocultured with NIH-3T3 cells expressing CD40L (CD154) and BAFF in the presence of IL-4 for 4 days. The old NIH-3T3-CD40L/BAFF cells are then replaced with fresh cells and IL-21 is added, this process is continued for another 5 days of co-culture, resulting in a 4 million fold increase in the number of B10 cells.[28] Some B10eff cells lose their IL-10-producing capability after transient in vivo expression, subsequently upregulating plasma cell-associated transcription factors like IRF4, PRDM1 and XBP1. This enables these B10eff cells to differentiate into plasma cells capable of generating polyreactive or autoreactive antibodies.[26] The regulatory implications of antibody production by B10eff cells remain unclear. Further research is being undertaken to understand the alternative fates of B10eff cells post-IL-10 secretion.

B10pro cells can develop normally in the absence of T cells, as evidenced by their presence in T cell-deficient nude mice.[19] Nevertheless, the interplay between B10 cells and CD4+ T cells is essential for IL-10-mediated suppression of inflammation in vivo. Utilizing germline B-cell receptors (BCRs), antigen-specific B10 cells can capture antigens and present them to cognate CD4+ T cells. This
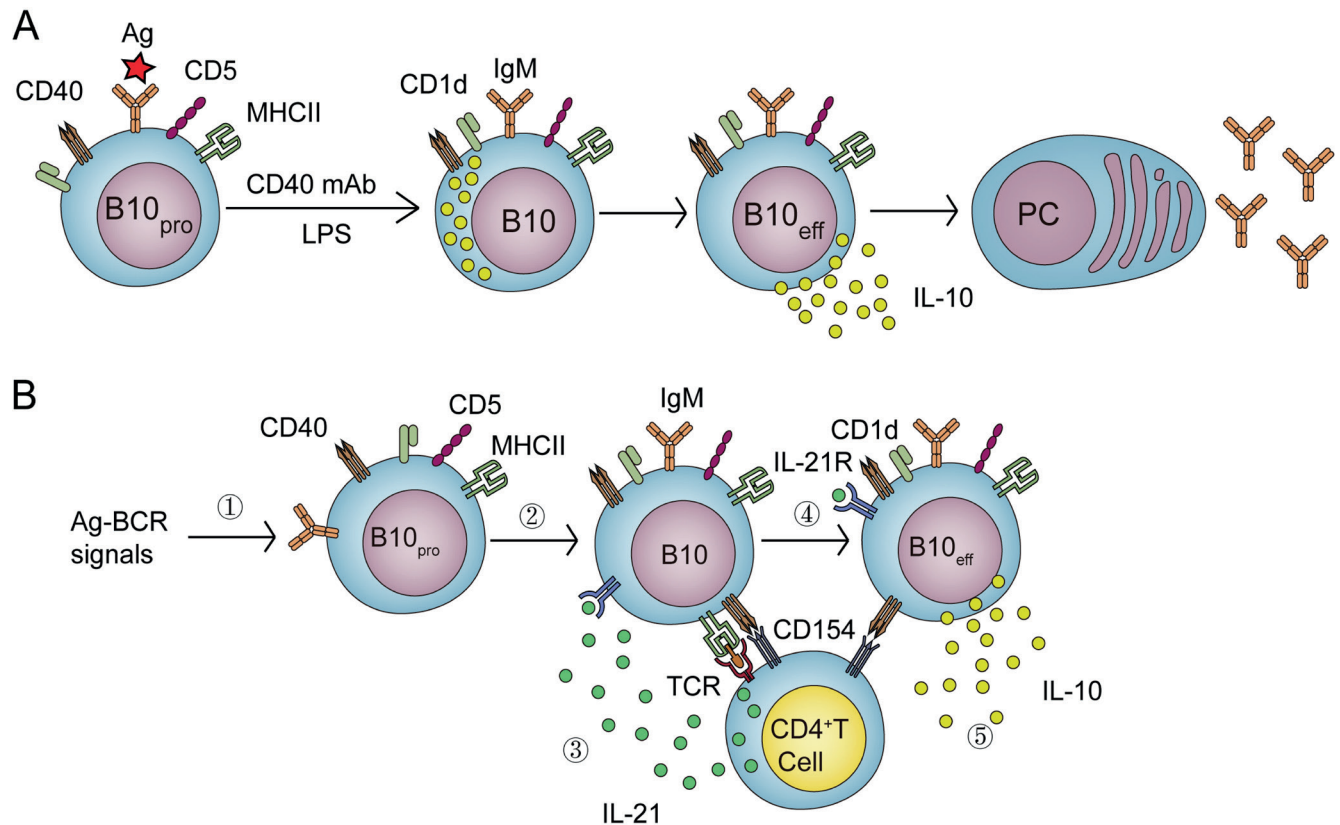
Fig. 1. Mouse B10 cell development A. B cells acquire interleukin 10 (IL-10) activity. After B cells interact with specific antigens in vivo, appropriate levels of B-cell receptor (BCR) signaling induce a small proportion of B cells to become B10pro cells. IL-10 is not expressed by B10pro cells. However, when CD40 is ligated to B10pro cells ex vivo, the B10pro cells mature into fully functional B10 cells. Addition of PMA, ionomycin, and monensin (PIM) during the last 5 h of culture, mature B10pro cells and B10 cells were induced to express cytoplasmic IL-10. B10 cells that begin to secrete IL-10 become B10eff cells and can secrete IL-10 for 24–48 h in vivo. Upon termination of IL-10 transcription, a small number of B10eff cells differentiate into antibody-secreting plasma cells (PC) in vivo; B. The interaction between B10 cells and CD4+ T cells. B cells capture antigens that trigger appropriate BCR signals (step 1) and promote the development of B10pro cells with IL-10 activity (step 2). B10pro presents antigenic peptides to antigen-specific T cells and induces T cell activation to produce IL-21 through homologous interaction and CD40/CD154 interaction (step 3). IL-21 binds to IL-21R in B10 cells (step 4) and promotes IL-10 production by B10 effector (B10eff) cells to negatively regulate antigen-specific T cell function (step 5). In this figure, mouse spleen B10 cells are shown as an example

B10pro – progenitor B10 cell; B10eff – B10 effector cell; PC – plasma cell.

contact is dependent on MHCII and CD40 molecules. Synchronized engagement between T cells and B10pro cells may expedite B10 cell maturation and promote T cell secretion of IL-21, which directly stimulates B10 cells to produce IL-10 in the local milieu.[28] The functions of proximal, homologously activated CD4+ T cells and effector cells are dampened by antigen-specific B10 effector cells. Consequently, B10 cells lacking MHCII, CD40, IL-21R, or IL-10 are ineffective in mitigating autoimmune and inflammatory reactions. This crosstalk between B10 and T cells elucidates the antigen-specific regulatory roles of B10 cells in vivo.

Function of receptors on B10 cell

Inflammation is a prerequisite for the in vivo proliferation and functionality of B10 cells. In both colitis and experimental autoimmune encephalomyelitis (EAE) models, B10 cells localize to the draining lymph nodes adjacent to inflamed tissues.[27] The ability of B10 cells to secrete IL-10 is determined by the inflammatory microenvironment; this was corroborated by the observation that splenectomy in an EAE animal model did not impede B10 cell development or IL-10 secretion at these inflammatory sites.[24] The presence of various inflammatory mediators enhances B10 cell numbers and triggers IL-10 secretion. Similar dynamics can be observed in malignancies with an inflammatory component, such as colorectal cancer. Although the precise mechanism by which inflammatory signals drive B10 cell proliferation and IL-10 production remains unknown, it is likely linked to the high density of specific receptors on B10 cell surfaces. These receptors, in conjunction with inflammatory factors, may be responsible for B10 development and differentiation in tissue. Subsequently, we will discuss the relevance of selected B10 cell surface receptors and their functional implications.

B-cell receptor

The BCR plays a role in inhibiting pro-inflammatory responses in both inflammation and cancer, as shown by studies in autoimmune disease models. Transgenic MD4 mice expressing a fixed BCR display a compromised ability

to prevent myelin oligodendrocyte glycoprotein (MOG)-induced autoimmune encephalomyelitis.[34] Results showed that B cell-derived IL-10 is pivotal for EAE amelioration. Under homeostatic conditions, MD4 mice exhibit a significantly reduced population of IL-10^{+} B cells in the spleen, indicating the importance of BCR specificity and signaling in B10 genesis.[19] Additionally, the development of B10 cells is independent of MHCII, CD40, MyD88, or IL-10 receptor expressions on B-cells, underlining the critical role of BCR signaling in conferring IL-10 competence.[19]

B10 cells, localized in the spleen and peritoneal cavity, express a wide variety of BCR genes, majority of which are germline and devoid of somatic mutations.[23,26] This indicates that BCR specificity plays a crucial role on shaping B10 cell development and Ag-specific regulatory function.[16,19,28] B10 cell number can be significantly influenced by receptors or pathways that either positively or negatively affect BCR signaling, such as CD19, CD22 and CD40.[23] Interestingly, the number of IL-10-expressing B cells in both the peritoneum and the spleen diminishes when BCRs are robustly cross-linked with anti-IgM antibodies.[19] This suggests that a certain fraction of B cells may be primed to transition induced into B10pro and subsequently IL-10-competent B10 cells under low-affinity or persistent Ag-BCR signaling. Conversely, strong BCR signals could reroute B10pro cells towards alterative functional pathways.[32] Therefore, the specificity and strength of the BCR signal could enable B10 cells to swiftly react to both foreign and self-antigens, serving as an initial immunological defense while concurrently inhibiting autoantibody generation and safeguarding self-tissues.

Toll-like receptors

Toll-like receptors (TLRs) are a group of proteins that can recognize specific molecular patterns on invading bacteria and viruses. Various TLRs are expressed on the surface of B10 cells, which regulate IL-10 secretion by the cells during inflammation. Through a MyD88-dependent mechanism, TLRs modulate B10 regulatory functions by enhancing IL-10 expression. This is evident when TLR2, TLR4 or TLR9 agonists stimulate splenic B10 cells in vitro.[19,35,36] In mice, LPS can induce the differentiation of spleen B10pro into B10 effector cells. Interestingly MyD88 is dispensable for B10 cell development in vivo.[17] Although various other signaling pathways can induce B10 cell activation, proliferation and effector function, BCR-associated signals appear to predominantly program B10 cells for IL-10 competence.

Intestinal IL-10-producing B cells are activated by resident enteric bacteria via TLR2, MyD88 and PI3K pathways,[36] subsequently dampening colonic T cell activation and maintaining mucosal homeostasis. Although the role of TLRs in tumor-associated B10 cell activation is unclear, it is possible that TLR signaling is activated by cancer-related byproducts. Exosomes from patients with esophageal squamous cell carcinoma contain mRNAs that can activate TLR4 and MAPK signaling pathways, thereby promoting the differentiation of CD19^{+} B cells into B10 cells in the peripheral blood.[37] In a separate study, Xiao et al. identified a novel pro-tumorigenic PD-1^{hi} B10 cell subpopulation in human hepatocellular carcinoma (HCC).[38] The HCC-derived soluble factors activate TLR4 and elevate B-cell PD-1 expression. Significantly, these PD-1^{hi} B cells acquire regulatory functions, suppressing tumor-specific T cell immunity in an IL-10-dependent manner. In addition, the TLR4-mediated BCL6 upregulation in the HCC microenvironment also resulted in the accumulation of PD-1^{hi} B cells.[38] Moreover, intestinal extracts from mice with pancreatic cancer contain high concentration of TLR ligands that regulate B cell function by receptors binding, affecting disease progression.[39,40] Surface TLRs on B cells can regulate the cell's response to damage-related molecular patterns (DAMPs) produced during treatments like radiation and chemotherapy. Therefore, future research should investigate the effect of TLR function on tumor-associated B-cell behavior.[41] Animal models with conditional knockdowns of molecules like TLRs and MyD88 could offer valuable insights into B cell regulation in cancer.

CD40

Although CD40 is not essential for IL-10 expression in B cells, its overexpression significantly increases the production of IL-10^{+} B cells.[19] B10pro cells can mature to B10 cells in vitro by CD40 signal activation.[19] The role of CD40 signaling in specific B cell subsets within disease contexts remains unclear. In MC38 tumor-bearing mice lacking B-cell CD40, tumor growth was comparable to that in wild-type mice, indicating that CD40 on the surface of B cells is not necessary for tumor growth.[42] However, CD40L^{+} EL4 thymoma cells co-cultured with wild-type B cells produced markedly more IL-10 compared to their interaction with CD40^{−/−}B cells, indicating the effect may be model-specific.[42,43] In a mouse model of lupus, CD40 agonists induced B cell IL-10 secretion, thereby reducing inflammation and inhibiting disease progression. CD40 antibody treatment significantly improved survival rates in MRL/lpr lupus mice.[44] Additionally, it has been discovered that CD24^{+}CD38^{+} B cells engage with cancer cells via CD40 and CD40L interaction, leading to IL-10 and tumor growth factor beta (TGF-β) secretion, which in turn promotes tumor progression.[45] Given that both IL-10 production and B cell differentiation into antibody-producing cells are heavily influenced by CD40, further investigation into the molecular mechanisms governing B cell fate in response to CD40 signaling is imperative.

Cytokine receptor

Even though B10 cells express IL-21R on their surface, incubating most B cells with IL-21 does not increase

IL-10 secretion.[28] The response of B cells to IL-21 varies according to their developmental stage and the presence of other costimulatory signals. Notably, IL-21 can induce apoptosis in addition to proliferation, survival, plasma cell differentiation, or isotype conversion of B cells.[46,47] However, IL-21R and IL-21 are required for B10 cell growth and the activation of IL-10-secreting B10 effector cell during the initiation of autoimmunity.[28] In the MOG-induced EAE mouse model, mice receiving IL-21R-deficient B cells showed enhanced MOG-TCR CD4+ T cells proliferation and exacerbated disease symptoms compared to those receiving B cells from wild-type mice. This suggests that IL-21 can potentially suppress autoreactive T cells in vivo via a B cell-mediated mechanism.[28] Additionally, in tumorigenesis, IL-21 in tumor tissues can induce the generation of a population of CD38+CD1d+IgM+CD147+ regulatory B cells, characterized by their granzyme B (GrB) secretion, thus designated GrB+ B cells.[48] A significant subset of these GrB+ B cells produce IL-10, highlighting that regulatory B cells in tumor milieu expressed both IL-10 and GrB.[48] Additionally, IL-21 activated B cells have demonstrated IL-10+CD25+ regulatory phenotypes across various human tumor types.[48]

B10 cells, which express multiple inflammatory cytokine receptors including IL-21R, are directly regulated by proinflammatory cytokines.[49] This was evidenced in a mouse model of inflammatory arthritis, where elevated IL-6 and IL-1β levels fostered the expansion of B10 cells that limited the activity of autoreactive T cells.[49] In the context of oncogenesis, pro-inflammatory cytokines are critical in recruiting cells that support angiogenesis and tumor growth.[50] Both autocrine and paracrine effects of these cytokines are observed in the tumor microenvironment. Animal models of pancreatic cancer showed that blocking IL-1β production in the tumor reduced IL-10-secreting CD-1d^{hi}CD5+ B cells and amplified interferon gamma (INF-γ) and GrB-producing CD8+ T cells, resulting in a stronger antitumor immune response and reduced tumor growth.[51] Furthermore, administration of a neutralizing IL-1β antibody to animals carrying pancreatic tumors produced similar results and, when synergized with α-PD-1 therapy, significantly decreased the tumor burden.[51] This data suggest that the pro-tumorigenic activities of B10 cells, driven by inflammatory cytokines, could promote their own proliferation and IL-10 production, thus hindering the immune system's attack on the tumor.[51,52] As a result, cytokines can variably regulate B10 cell proliferation and IL-10 secretion in vivo.

Mechanisms underlying B10 cell-mediated suppression of antitumor responses

Cancer-related B10 cell immunoregulatory mechanisms have been gradually revealed. The equilibrium of all tumor infiltrating cells determines the nature of the relationship between immune cells, tumor cells and stromal cells in the tumor microenvironment. Multiple studies have recognized IL-10-producing B cells in tumor models; however, few have linked these properties to distinct B cell subsets (Table 2).[38,53–61]

B10 cells inhibit antitumor responses by interacting with different tumor-infiltrating immune cells. Moreover, B10 cells can participate in tumor progression by producing specific antibodies (Fig. 2).

Table 2. IL-10-producing B-cell phenotype and mechanism of action in human and mouse cancer

Phenotype	Species	Cancer type	Location	Mechanism	Reference
CD19+CD1d^{hi}CD5+	mouse	non-Hodgkin lymphoma	spleen	IL-10-mediated suppression of macrophages activity	53
IgA+CD19+	mouse	colorectal tumor	tumors	high expression of PD-L1, secretion of IL-10 and TGF-β, mediated inhibition of CD8+ T cells, proliferation and activation	54
CD19+CD5+CD43+	mouse	melanoma	tumors	IL-10 mediated suppression IFN-γ and TNF-α by CD8+ T cells	55
CD5^{hi}CD24$^{-/+}$CD27$^{hi/+}$CD38^{dim}	human	HCC	tumors and PB	IL-10-mediated inhibition of CD8+T cells	38
CD19+CD1d^{hi}CD5+	human	cervical cancer and cervical intraepithelial neoplasia	PB	IL-10-mediated suppression perforin and GrB by CD8+ T cells	56
CD19^{lo}CD27^{hi}TIM-1^{hi}	human	colorectal cancer	tumors	IL-10-mediated the suppression of IFN-γ and TNF-α secretion by T cells	57
CD19+CD24^{hi}CD38^{hi}	human	GC	tumors and PB	IL-10-mediated the suppression of IFN-γ and TNF-α secretion by CD4+ T cells	58
CD19+CD27+CD10$^-$	human	GC	tumors and PB	IL-10-mediated inhibition of IFN-γ, TNF-α, and IL-17 secretion by CD8+ and CD4+ T cells	59
CD19+IL-10+	human	ovarian cancer	abdominal cavity	IL-10-mediated induction of T cells	60
CD19+IL-10+	human	TSCC	tumors	IL-10-mediated induction of T cells	61

GrB – granzyme B; HCC – hepatocellular carcinoma; HPV – human papillomavirus; TSCC – tongue squamous cell carcinoma; GC – gastric cancer; PB – peripheral blood; TSCC – tongue squamous cell carcinoma; IFN-γ – interferon gamma; TNF-α – tumor necrosis factor alpha.
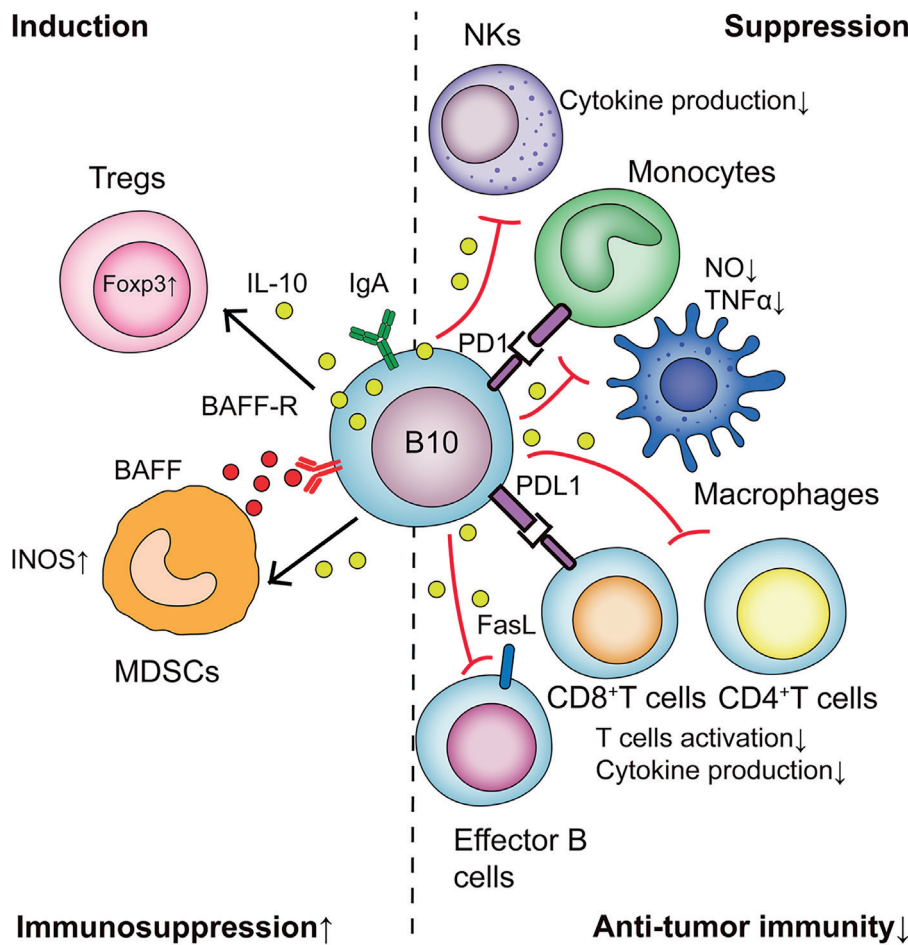
Fig. 2. Regulatory pathways and multifaceted interactions of B10 cells in the immune response. The dual role of B10 cells includes the induction and suppression mechanisms within the immune system. Induction pathways: 1. T cells: B10 cells participate in the proliferation and differentiation of T cells by secreting interleukin 10 (IL-10); 2. MDSCs: B10 cells and myeloid-derived suppressor cells (MDSCs) interact via BAFF and its receptor (BAFF-R), leading to increased expression of inducible nitric oxide synthase (INOS). Suppression pathways: 1. Natural killer (NK) cells: Interactions with B10 cells lead to reduced cytokine production by NK cells, indicating a possible suppression or modulation of NK cell responses in the presence of IL-10; 2. Monocytes and macrophages: B cells induce the generation of B10 cells by binding to monocyte PD-L1. B10 cells inhibit NO and tumor necrosis factor alpha (TNF-α) production by monocytes and macrophages by secreting IL-10 and impair macrophage-mediated antitumor activity; 3. T cells: The activation of both CD8+ cytotoxic T cells and CD4+ helper T cells is notably diminished in the presence of B10 cells. The production of effector cytokines by these T cells is also reduced, highlighting the significant role of B10 cells in regulating T cell-mediated immune responses; 4. Effector B cells: Effector B cells can directly eliminate tumor cells by expressing FasL. B10 can inhibit the function of effector B cells through the secretion of IL-10

Effect of innate immune cells activation

B10 cells play a crucial role in controlling the immune system's antitumor response. Rituximab is highly effective in treating non-lymphoma Hodgkin's and chronic lymphocytic leukemia (CLL), despite a high relapse rate.[62] A study has indicated that endogenous B cells, particularly CD1d^{hi}CD5$^+$ B cells that produce IL-10 in CD20$^{-/-}$ mice, diminish the efficacy of CD20 mAb treatment.[53] In experiments, syngeneic Burkitt-like lymphoma-injected mice demonstrated a substantial increase in tumor size after receiving CD20$^{-/-}$CD1d^{hi}CD5$^+$IL-10$^+$ B cells prior to anti-CD20 therapy, while IL-10-deficient CD1d^{lo}CD5$^+$ B cells transfer had no impact.[53] Co-culture of CD1d^{hi}CD5$^+$ B cells with macrophages revealed that CD1d^{hi}CD5$^+$ B cells could inhibit macrophage production of nitric oxide and TNF-α in response to LPS, as well as downregulate the expression of MHC II molecules and co-stimulatory molecules, impairing macrophage-mediated antitumor activity. Interleukin 10 from CD1d^{hi}CD5$^+$ B cells is essential to this inhibitory mechanism.[53] Natural killer (NK) cells, key components of the innate immune system's host defense, can directly lyse pathogen-infected or damaged cells and are actively involved in caner immunology, particularly in directly lysing tumor cells.[63,64] Research using a B cell knockout mouse model with tumor showed that

the interaction between tumor cells and B cells via CD40L-CD40 can promote the production of a large amount of interleukin IL-10, which in turn hinders NK cells secretion of IFN-γ and GrB, and subsequently impedes the antitumor function of NK cells.[43]

B10 cells not only impede the antitumor actions of innate immune cells but also promote their suppressive functions. For example, in the 4T1 breast cancer model, myeloid-derived suppressor cells (MDSCs) were observed to facilitate the proliferation of PD1$^-$PDL1$^+$CD19$^+$ IL-10-secreting B cells in the spleen, which in turn suppressed the expansion and IFN-γ production of effector T cells.[65] This effect is actually reciprocal, as B10 cells can lead to immune escape in cervical cancer by enhancing the suppressive function of MDSCs. Furthermore, MDSCs can drive the differentiation of B cells into IL-10-rich B10 cells via BAFF/BAFF-R signaling, which, in turn, activates the STAT3 pathway in MDSCs, creating a self-amplifying loop. These activated MDSCs can suppress CD8$^+$ T cells through the release of inducible nitric oxide synthase (INOS) and other immunoregulatory factors.[66]

Suppression of effector T cell

B10 cells not only diminish the antitumor functions of innate immune cells, but also impair the antitumor

effects of adaptive immune cells. One crucial mechanism of B10 cells' impact on the antitumor response is direct suppression of effector T cell activity. In cervical cancer, CD19+CD5+CD1d+ B cells produce IL-10, hindering CD8+ T cells infiltration and subsequently reducing the fraction of cells producing perforin and GrB. The fraction of perforin- and GrB-producing CD8+ T cells in tumor tissues can be restored with IL-10 blocking antibodies. B10 cells present in ascites drastically limit the number of IFN-γ-secreting CD8+ T cells in ovarian cancer.[60] Elevated levels of TIM-1-expressing CD19loCD27hi B cells in colorectal cancer suppress IFN-γ and TNF-α production by T cells via an IL-10-dependent mechanism.[57] Patients with gastric cancer (GC) exhibit a heightened frequency of IFN-γ+ and TNF-α+CD4+ T cells in the peripheral blood, correlating with a scarcity of IL-10-producing CD19+CD24hiCD38hiB cells.[59] Co-culturing of CD27+CD10− B10 cells with autologous T cells from the peripheral blood or tumor tissues of patients markedly inhibits the capacity of CD4+ T cells to express IFN-γ, TNF- α and IL-17, as well as the ability of CD8+ T cells to generate IFN-γ and TNF-α. These findings are corroborated by animal studies,[67] with reports indicating that B1a cells (CD19+CD5+CD43+) use IL-10 to inhibit IFN-γ and TNF-α production by tumor-infiltrating CD8+ T cells, thereby exerting a negative regulation on tumor immunity in melanoma.[55] Furthermore, several studies demonstrate that B cells secreting IL-10 within tumors express PD-1 at high levels.[37,38] These PD-1hi B cells facilitate the depletion and dysfunction of CD8+ T cells through IL-10, particularly upon activation via PD-L1 signaling in mice with hepatoma. This evidence underscores the role of PD-1/PD-L1 interactions in the suppressive functions of B10 cells within tumor environments.

Induction of regulatory T cells

B10 cells not only modulate immune responses by controlling effector T cells but also promote the generation and/or maintenance of T cells, thereby contributing to an immunosuppressive microenvironment. Previous studies have postulated that B cells facilitate the conversion of resting CD4+ T cells into T cells predominantly via TGF-β, rather than IL-10.[68] However, evidence from several disease models suggests that a deficiency of B cell-specific IL-10 also correlates with reduced T cell numbers.[33,69] This implicates an involvement of IL-10 in T cell development, potentially explaining the observed correlation between increased T cell populations and accelerated cancer progression. B cells that produce IL-10 are present in the tumors in ovarian cancer and tongue squamous cell carcinoma.[60,61] These cells are not only inversely associated with disease prognosis but also positively correlated with the fraction of T cells (Foxp3+CD4+ T cells) and inversely with the frequency of IFN-γ+CD8+ T cells.[60,61] In vitro studies involving co-culture of tumor-derived CD19+IL-10+ B cells with autologous CD4+CD25− T cells from patients with tongue

squamous cell carcinoma have shown that these T cells can differentiate into T cells through an IL-10 dependent mechanism provided by CD19+IL-10+ B cells.[61] These results reveal that B10 cells may facilitate T cell development within the tumor microenvironment. Nevertheless, further investigation is needed to fully understand the mechanism behind this T cell induction by B10 cells in the tumor context. Conversely, regulatory T cells may also enhance the proliferation and differentiation of B10 cells in tumors. A newly identified T cell subset, follicular regulatory T cells (Tfr), has been shown to induce IL-10 production in B cells within the context of breast cancer [70]

Other tumor-infiltrating targets of B10 cells

B cells have both antitumor and pro-tumor effects. Tao et al. have shown that effector B cells from tumor-draining lymph nodes (TDLNs) express Fas ligand (FasL) in vitro, which can directly eliminate 4T1 tumor cells. This suggests that the adoptive transfer of TDLN B cells could enhance their therapeutic effect. However, IL-10-producing B cells within TDLNs may suppress the antitumor functions of these effector B cells.[71] Remarkably, depletion of IL-10 from B-cell adoptive transfers significantly enhances CTL activity within the recipient's peripheral blood mononuclear cells (PBMCs) and splenic cells, as well as B-cell function.[71]

B cells may also facilitate tumor growth by producing specific antibodies, yet the role of B10 cells in tumor suppression via this mechanism remains to be verified. The current consensus posits that antibody-secreting B cells, especially those producing IgA, regulate T cell-mediated antitumor immunity in 1 of 2 major ways: either through the expression of immune checkpoint molecules like PDL1 or by releasing inhibitory cytokines such as IL-10. These mechanisms, which can occur via direct contact or indirectly, ultimately contribute to the diminished effectiveness of T cells in eliciting an antitumor immune response.[54,72] The presence of IgA+PD-L1+IL-10+ plasma cells in prostate cancer tissues has been shown to contribute to chemotherapy resistance.[72] The underlying mechanism involves chemotherapeutic agents like oxaliplatin promoting plasma cell migration into tumors, where these cells express PDL1 and produce TGF-β and IL-10, thereby dampening CD8+ T cell activation. This means that IgA expression alone does not account for the immune suppression observed. The ablation of IgA+PD-L1+IL-10+ plasma cells could increase the activity of CD8+T cells and restore the oxaliplatin-mediated regression of tumors. In a mouse model of colorectal cancer, tumor-infiltrating IgA+ B cells release a high number of immunoregulatory molecules (PD-L1, IL-10 and TGF-β), which restrain CD8+ T cells limiting the proliferation.[54] Reducing the presence of IgA+ B cells in colorectal tumors correlates with extended patient survival. These findings bolster the hypothesis that

antibody-secreting B cells are integral in promoting tumor growth by inhibiting cytotoxic T cell responses.

Recent research largely supports the notion that B10 facilitate tumor progression and metastasis. However, B10 cells may also serve a protective role in oncogenesis. For example, Melcher et al. found that B cell-derived IL-10 can regulate chronic intestinal inflammation but not colitis-associated colorectal cancer (CAC). Upon differentiation into plasma cells, B cells cease IL-10 production and begin the secretion IgAthat modulates the gut microbiota composition and potentially guards against CAC development.[73] Similarly, patients infected with *Heliobacter pylori* exhibiting elevated high levels of IL-10-secreting B cells are less prone to developing gastric cancer. It is proposed that B cells may downregulate tissue-damaging proinflammatory responses triggered by bacterial infection, thereby creating an environment that hinders tumor progression.[74] These observations add another level of complexity to the biology of B10 cells in cancer.

Discussion

Targeting B10 cells

There is growing evidence that B10 cells play an immunosuppressive role in cancer, even though their suppression is typically beneficial in autoimmune disease.[75,76] The benefits of entirely eliminating B cells for cancer patients remain uncertain. While studies on certain cancers, such as colon cancer and melanoma, have shown that the widespread reduction of CD20^{+} cells using anti-CD20 antibodies can be beneficial, other studies report no benefit or even harmful effects.[77–82] This discrepancy may reflect the dual regulatory roles played by B cells in tumor development. Presently, several therapies focus on the selective reduction of B10 cell populations.[83,84] Small molecule inhibitors targeting B10 cell activity may also prove beneficial.[84] In cancer mouse models, MAP kinase pathway inhibitor and BTK inhibitor selectively suppress IL-10 production and the proliferation of CD1d^{hi}CD5^{+}, TIM-1^{+} and CD21^{+}CD23^{+}CD24^{+} B cell subsets without impacting other B cell subsets.[52,83] Total glucoside of paeony (TGP) demonstrates antitumor effects in rat HCC by reducing the number of B10 cells in the spleen of treated rats.[84] Lipoxin A4, also known as LXA4, is an anti-inflammatory lipid mediator derived from arachidonic acid that can reshape the tumors immune microenvironment and confer antitumor properties.[85] Lipoxin A4 inhibited B10 cell induction in tumor-bearing mice, which decreased T cell numbers in both lymph node draining and tumor tissue while enhancing cytotoxic T cell activity.[85] Intriguingly, LXA4 can specifically suppress B10 cell generation without interfering with the proliferation, differentiation, or germinal center formation of conventional B cells.[85] Furthermore, studies have shown that targeting IL-10R1 selectively to B cells with CD19 single chain antibody can decrease the number of B10 cells and T cells, augment the activity of cytotoxic CD8^{+} T cells, and inhibit the progression of HCC.[86] The oncogenic function of CXCL13 across diverse desmoplastic mouse tumor models has been elucidated. Shen et al. found that within the tumor microenvironment (TME), tumor-associated fibroblasts secrete CXCL13, which is pivotal for the recruitment and subsequent differentiation of B cells into IL-10^{+}CD1d^{+}CD5^{+}CD138^{+}CD19^{+} cells. The inhibition of CXCL13 has been shown to curtail tumor progression.[87] These findings underscore the potential of B10 cell blockade as an effective approach to impede cancer metastasis. Further investigations are imperative to devise a cancer treatment strategy that targets B10 cells.

The exploitation of immune checkpoints, specifically the PD-1 and PD-L1 pathways, by tumors facilitates immune evasion by attenuating the activation of immune cells.[88] The presence of PD-1 is notable on a spectrum of activated immune cells – ranging from monocytes to T cells – and is indicative of the receptor's regulatory role. PD-L1, correspondingly upregulated within the tumor milieu on both tumor and presenting cells, becomes a focal point for therapeutic intervention.[89] Disruption of the PD-1–PD-L1 interaction has yielded significant tumor regression and prolonged survival in both clinical and preclinical settings.[88] It has been previously observed that B cells with concurrent PD-1 or PD-L1 and IL-10 expression attenuate CD4^{+} and CD8^{+} T cell functions following PD-1/PD-L1 signal activation, which implies a potential inducement of IL-10 by PD-1/PD-L1 pathways.[37,38,65,72,75,90,91] This is exemplified by IL-10^{+}PD-L1^{+} B cells in mouse pancreatic cancer models, where they diminish T cell viability – an effect reversible by PD-L1 inhibition.[90] Additionally, IgA[+]PD-L1^{+} B cells, which are capable of secreting IL-10, were discovered in models of both liver and prostate cancer. These B cells were found to be responsible for promoting chemoresistance, a process that can be reversed by PD-L1 targeting.[72,91] These insights reinforce the influential role of B cells in the milieu of PD-1/PD-L1-targeted therapies and suggest that targeting PD-1 and PD-L1 on B cells harbors therapeutic potential. There is an ongoing need to unravel the intricacies of immune checkpoint therapy-driven antitumor responses to refine immunotherapeutic strategies.

Limitations

B10 cell biology has advanced significantly in recent years, but the specifics of their development, phenotypic, functional, and suppressive mechanisms remain unanswered. To begin, B10 cells are found beyond the spleen, in the abdominal cavity, lymph nodes, and other organs. However, it is unclear whether IL-10 production mechanisms are consistent across these varied locations. The second issue is that B10 cells are known for IL-10 secretion, but it is uncertain if they exert regulatory role through other cell surface molecules, such as co-stimulatory molecules.

Furthermore, the role of B10 cells in the tumor micro-environment is crucial to understand, specifically, how they facilitate tumor growth while dampening inflammation. Unraveling this could improve antitumor immunity by targeting B10 cells in cancer. The complex processes of B10 cell generation and activation, especially in cancer progression, warrant in-depth investigation.

Conclusions

B10 cells are a subset of B cells that regulate immune responses, such as inflammation and tumor suppression. B10 cells perform their functions by interacting with other immune cells and secreting cytokines. The proliferation and function of B10 cells rely on the existence of cancer-induced inflammation. B10 cells within the TME hinder antitumor immunity by suppressing effector T and B cells, inducing regulatory T cells, and impairing other tumor-infiltrating immune cells including NK cells and macrophages. B10-generated antibodies are also implicated in tumor immune escape mechanisms (Fig. 2). Moving forward, research in B10-based immunotherapies should prioritize identifying the surface markers expressed on B10 cells.

ORCID iDs

Dandan Li https://orcid.org/0009-0003-9797-621X
Yunfeng Ma https://orcid.org/0000-0002-7699-473X

References

1. LeBien TW, Tedder TF. B lymphocytes: How they develop and function. *Blood*. 2008;112(5):1570–1580. doi:10.1182/blood-2008-02-078071
2. Li Q, Teitz-Tennenbaum S, Donald EJ, Li M, Chang AE. In vivo sensitized and in vitro activated B cells mediate tumor regression in cancer adoptive immunotherapy. *J Immunol*. 2009;183(5):3195–3203. doi:10.4049/jimmunol.0803773
3. Li Q, Lao X, Pan Q, et al. Adoptive transfer of tumor reactive B cells confers host T-cell immunity and tumor regression. *Clin Cancer Res*. 2011;17(15):4987–4995. doi:10.1158/1078-0432.CCR-11-0207
4. Liu Y, Wu Y, Ramarathinam L, et al. Gene-targeted B-deficient mice reveal a critical role for B cells in the CD4 T cell response. *Int Immunol*. 1995;7(8):1353–1362. doi:10.1093/intimm/7.8.1353
5. Mauri C, Ehrenstein MR. The 'short' history of regulatory B cells. *Trends Immunol*. 2008;29(1):34–40. doi:10.1016/j.it.2007.10.004
6. Bao Y, Cao X. The immune potential and immunopathology of cytokine-producing B cell subsets: A comprehensive review. *J Autoimmun*. 2014;55:10–23. doi:10.1016/j.jaut.2014.04.001
7. Upasani V, Rodenhuis-Zybert I, Cantaert T. Antibody-independent functions of B cells during viral infections. *PLoS Pathog*. 2021;17(7): e1009708. doi:10.1371/journal.ppat.1009708
8. Cerutti A, Cols M, Puga I. Marginal zone B cells: Virtues of innate-like antibody-producing lymphocytes. *Nat Rev Immunol*. 2013;13(2): 118–132. doi:10.1038/nri3383
9. Pillai S, Cariappa A. The follicular versus marginal zone B lymphocyte cell fate decision. *Nat Rev Immunol*. 2009;9(11):767–777. doi:10.1038/nri2656
10. Sarvaria A, Madrigal JA, Saudemont A. B cell regulation in cancer and anti-tumor immunity. *Cell Mol Immunol*. 2017;14(8):662–674. doi:10.1038/cmi.2017.35
11. Nojima T, Haniuda K, Moutai T, et al. In-vitro derived germinal centre B cells differentially generate memory B or plasma cells in vivo. *Nat Commun*. 2011;2(1):465. doi:10.1038/ncomms1475
12. Shen P, Fillatreau S. Antibody-independent functions of B cells: A focus on cytokines. *Nat Rev Immunol*. 2015;15(7):441–451. doi:10.1038/nri3857
13. Kaminski DA, Wei C, Qian Y, Rosenberg AF, Sanz I. Advances in human B cell phenotypic profiling. *Front Immunol*. 2012;3:302. doi:10.3389/fimmu.2012.00302
14. Mizoguchi E, Mizoguchi A, Preffer FI, Bhan AK. Regulatory role of mature B cells in a murine model of inflammatory bowel disease. *Int Immunol*. 2000;12(5):597–605. doi:10.1093/intimm/12.5.597
15. Mizoguchi A, Mizoguchi E, Takedatsu H, Blumberg RS, Bhan AK. Chronic intestinal inflammatory condition generates IL-10-producing regulatory B cell subset characterized by CD1d upregulation. *Immunity*. 2002;16(2):219–230. doi:10.1016/S1074-7613(02)00274-1
16. Yanaba K, Bouaziz JD, Haas KM, Poe JC, Fujimoto M, Tedder TF. A regulatory B cell subset with a unique CD1dhiCD5+ phenotype controls T cell-dependent inflammatory responses. *Immunity*. 2008;28(5): 639–650. doi:10.1016/j.immuni.2008.03.017
17. Iwata Y, Matsushita T, Horikawa M, et al. Characterization of a rare IL-10-competent B-cell subset in humans that parallels mouse regulatory B10 cells. *Blood*. 2011;117(2):530–541. doi:10.1182/blood-2010-07-294249
18. Matsushita T, Tedder TF. Identifying regulatory B cells (B10 cells) that produce IL-10 in mice. In: Cuturi MC, Anegon I, eds. *Suppression and Regulation of Immune Responses*. Vol. 677. Methods in Molecular Biology. Totowa, USA: Humana Press; 2010:99–111. doi:10.1007/978-1-60761-869-0_7
19. Yanaba K, Bouaziz JD, Matsushita T, Tsubata T, Tedder TF. The development and function of regulatory B cells expressing IL-10 (B10 cells) requires antigen receptor diversity and TLR signals. *J Immunol*. 2009;182(12):7459–7472. doi:10.4049/jimmunol.0900270
20. Brummel R, Lenert P. Activation of marginal zone B cells from lupus mice with type A(D) CpG-oligodeoxynucleotides. *J Immunol*. 2005; 174(4):2429–2434. doi:10.4049/jimmunol.174.4.2429
21. Gray M, Miles K, Salter D, Gray D, Savill J. Apoptotic cells protect mice from autoimmune inflammation by the induction of regulatory B cells. *Proc Natl Acad Sci U S A*. 2007;104(35):14080–14085. doi:10.1073/pnas.0700326104
22. Matsushita T, Horikawa M, Iwata Y, Tedder TF. Regulatory B cells (B10 cells) and regulatory T cells have independent roles in controlling experimental autoimmune encephalomyelitis initiation and late-phase immunopathogenesis. *J Immunol*. 2010;185(4):2240–2252. doi:10.4049/jimmunol.1001307
23. Maseda D, Candando KM, Smith SH, et al. Peritoneal cavity regulatory B cells (B10 cells) modulate IFN-γ+CD4+ T cell numbers during colitis development in mice. *J Immunol*. 2013;191(5):2780–2795. doi:10.4049/jimmunol.1300649
24. Matsushita T, Yanaba K, Bouaziz JD, Fujimoto M, Tedder TF. Regulatory B cells inhibit EAE initiation in mice while other B cells promote disease progression. *J Clin Invest*. 2008;118(10):3420–3430. doi:10.1172/JCI36030
25. Evans JG, Chavez-Rueda KA, Eddaoudi A, et al. Novel suppressive function of transitional 2 B cells in experimental arthritis. *J Immunol*. 2007;178(12):7868–7878. doi:10.4049/jimmunol.178.12.7868
26. Maseda D, Smith SH, DiLillo DJ, et al. Regulatory B10 cells differentiate into antibody-secreting cells after transient IL-10 production in vivo. *J Immunol*. 2012;188(3):1036–1048. doi:10.4049/jimmunol.1102500
27. Haas KM, Watanabe R, Matsushita T, et al. Protective and pathogenic roles for B cells during systemic autoimmunity in NZB/W F1 mice. *J Immunol*. 2010;184(9):4789–4800. doi:10.4049/jimmunol.0902391
28. Yoshizaki A, Miyagaki T, DiLillo DJ, et al. Regulatory B cells control T-cell autoimmunity through IL-21-dependent cognate interactions. *Nature*. 2012;491(7423):264–268. doi:10.1038/nature11501
29. Ding Q, Yeung M, Camirand G, et al. Regulatory B cells are identified by expression of TIM-1 and can be induced through TIM-1 ligation to promote tolerance in mice. *J Clin Invest*. 2011;121(9):3645–3656. doi:10.1172/JCI46274
30. Kessel A, Haj T, Peri R, et al. Human CD19+CD25high B regulatory cells suppress proliferation of CD4+ T cells and enhance Foxp3 and CTLA-4 expression in T-regulatory cells. *Autoimmun Rev*. 2012;11(9):670–677. doi:10.1016/j.autrev.2011.11.018
31. Blair PA, Noreña LY, Flores-Borja F, et al. CD19+CD24hiCD38hi B cells exhibit regulatory capacity in healthy individuals but are functionally impaired in systemic lupus erythematosus patients. *Immunity*. 2010;32(1):129–140. doi:10.1016/j.immuni.2009.11.009

32. DiLillo DJ, Matsushita T, Tedder TF. B10 cells and regulatory B cells balance immune responses during inflammation, autoimmunity, and cancer. *Ann N Y Acad Sci*. 2010;1183(1):38–57. doi:10.1111/j.1749-6632.2009.05137.x

33. Carter NA, Rosser EC, Mauri C. Interleukin-10 produced by B cells is crucial for the suppression of Th17/Th1 responses, induction of T regulatory type 1 cells and reduction of collagen-induced arthritis. *Arthritis Res Ther*. 2012;14(1):R32. doi:10.1186/ar3736

34. Fillatreau S, Sweenie CH, McGeachy MJ, Gray D, Anderton SM. B cells regulate autoimmunity by provision of IL-10. *Nat Immunol*. 2002; 3(10):944–950. doi:10.1038/ni833

35. Lampropoulou V, Hoehlig K, Roch T, et al. TLR-activated B cells suppress T cell-mediated autoimmunity. *J Immunol*. 2008;180(7):4763–4773. doi:10.4049/jimmunol.180.7.4763

36. Mishima Y, Oka A, Liu B, et al. Microbiota maintain colonic homeostasis by activating TLR2/MyD88/PI3K signaling in IL-10-producing regulatory B cells. *J Clin Invest*. 2019;129(9):3702–3716. doi:10.1172/JCI93820

37. Mao Y, Wang Y, Dong L, et al. Circulating exosomes from esophageal squamous cell carcinoma mediate the generation of B10 and PD-1high Breg cells. *Cancer Sci*. 2019;110(9):2700–2710. doi:10.1111/cas.14122

38. Xiao X, Lao XM, Chen MM, et al. PD-1hi identifies a novel regulatory B-cell population in human hepatoma that promotes disease progression. *Cancer Discov*. 2016;6(5):546–559. doi:10.1158/2159-8290.CD-15-1408

39. Riquelme E, Zhang Y, Zhang L, et al. Tumor microbiome diversity and composition influence pancreatic cancer outcomes. *Cell*. 2019; 178(4):795–806.e12. doi:10.1016/j.cell.2019.07.008

40. Pushalkar S, Hundeyin M, Daley D, et al. The pancreatic cancer microbiome promotes oncogenesis by induction of innate and adaptive immune suppression. *Cancer Discov*. 2018;8(4):403–416. doi:10.1158/2159-8290.CD-17-1134

41. Ochi A, Nguyen AH, Bedrosian AS, et al. MyD88 inhibition amplifies dendritic cell capacity to promote pancreatic carcinogenesis via Th2 cells. *J Exp Med*. 2012;209(9):1671–1687. doi:10.1084/jem.20111706

42. Shah S, Divekar AA, Hilchey SP, et al. Increased rejection of primary tumors in mice lacking B cells: Inhibition of anti-tumor CTL and TH1 cytokine responses by B cells. *Int J Cancer*. 2005;117(4):574–586. doi:10.1002/ijc.21177

43. Inoue S, Leitner WW, Golding B, Scott D. Inhibitory effects of B cells on antitumor immunity. *Cancer Res*. 2006;66(15):7741–7747. doi:10.1158/0008-5472.CAN-05-3766

44. Blair PA, Chavez-Rueda KA, Evans JG, et al. Selective targeting of B cells with agonistic anti-CD40 is an efficacious strategy for the generation of induced regulatory T2-like B cells and for the suppression of lupus in MRL/*lpr* mice. *J Immunol*. 2009;182(6):3492–3502. doi:10.4049/jimmunol.0803052

45. Shao Y, Lo CM, Ling CC, et al. Regulatory B cells accelerate hepatocellular carcinoma progression via CD40/CD154 signaling pathway. *Cancer Lett*. 2014;355(2):264–272. doi:10.1016/j.canlet.2014.09.026

46. Ettinger R, Sims GP, Fairhurst AM, et al. IL-21 induces differentiation of human naive and memory B cells into antibody-secreting plasma cells. *J Immunol*. 2005;175(12):7867–7879. doi:10.4049/jimmunol.175.12.7867

47. Ozaki K, Spolski R, Feng CG, et al. A critical role for IL-21 in regulating immunoglobulin production. *Science*. 2002;298(5598):1630–1634. doi:10.1126/science.1077002

48. Lindner S, Dahlke K, Sontheimer K, et al. Interleukin 21-induced granzyme B-expressing B cells infiltrate tumors and regulate T cells. *Cancer Res*. 2013;73(8):2468–2479. doi:10.1158/0008-5472.CAN-12-3450

49. Rosser EC, Oleinika K, Tonon S, et al. Regulatory B cells are induced by gut microbiota-driven interleukin-1β and interleukin-6 production. *Nat Med*. 2014;20(11):1334–1339. doi:10.1038/nm.3680

50. Dranoff G. Cytokines in cancer pathogenesis and cancer therapy. *Nat Rev Cancer*. 2004;4(1):11–22. doi:10.1038/nrc1252

51. Das S, Shapiro B, Vucic EA, Vogt S, Bar-Sagi D. Tumor cell-derived IL1β promotes desmoplasia and immune suppression in pancreatic cancer. *Cancer Res*. 2020;80(5):1088–1101. doi:10.1158/0008-5472.CAN-19-2080

52. Das S, Bar-Sagi D. BTK signaling drives CD1dhiCD5⁺ regulatory B-cell differentiation to promote pancreatic carcinogenesis. *Oncogene*. 2019;38(17):3316–3324. doi:10.1038/s41388-018-0668-3

53. Horikawa M, Minard-Colin V, Matsushita T, Tedder TF. Regulatory B cell production of IL-10 inhibits lymphoma depletion during CD20 immunotherapy in mice. *J Clin Invest*. 2011;121(11):4268–4280. doi:10.1172/JCI59266

54. Liu R, Lu Z, Gu J, et al. MicroRNAs 15A and 16–1 activate signaling pathways that mediate chemotaxis of immune regulatory B cells to colorectal tumors. *Gastroenterology*. 2018;154(3):637–651.e7. doi:10.1053/j.gastro.2017.09.045

55. Kobayashi T, Oishi K, Okamura A, et al. Regulatory B1a cells suppress melanoma tumor immunity via IL-10 production and inhibiting T helper type 1 cytokine production in tumor-infiltrating CD8⁺ T cells. *J Invest Dermatol*. 2019;139(7):1535–1544.e1. doi:10.1016/j.jid.2019.02.016

56. Chen Z, Zhu Y, Du R, et al. Role of regulatory B cells in the progression of cervical cancer. *Mediators Inflamm*. 2019;2019:6519427. doi:10.1155/2019/6519427

57. Mao H, Pan F, Wu Z, et al. Colorectal tumors are enriched with regulatory plasmablasts with capacity in suppressing T cell inflammation. *Int Immunopharmacol*. 2017;49:95–101. doi:10.1016/j.intimp.2017.05.018

58. Wang W, Yuan X, Chen H, et al. CD19⁺CD24hiCD38hiBregs involved in downregulate helper T cells and upregulate regulatory T cells in gastric cancer. *Oncotarget*. 2015;6(32):33486–33499. doi:10.18632/oncotarget.5588

59. Hu HT, Ai X, Lu M, Song Z, Li H. Characterization of intratumoral and circulating IL-10-producing B cells in gastric cancer. *Exp Cell Res*. 2019;384(2):111652. doi:10.1016/j.yexcr.2019.111652

60. Wei X, Jin Y, Tian Y, et al. Regulatory B cells contribute to the impaired antitumor immunity in ovarian cancer patients. *Tumor Biol*. 2016; 37(5):6581–6588. doi:10.1007/s13277-015-4538-0

61. Zhou X, Su YX, Lao XM, Liang YJ, Liao GQ. CD19⁺IL-10⁺ regulatory B cells affect survival of tongue squamous cell carcinoma patients and induce resting CD4⁺ T cells to CD4⁺Foxp3⁺ regulatory T cells. *Oral Oncol*. 2016;53:27–35. doi:10.1016/j.oraloncology.2015.11.003

62. Smith MR. Rituximab (monoclonal anti-CD20 antibody): Mechanisms of action and resistance. *Oncogene*. 2003;22(47):7359–7368. doi:10.1038/sj.onc.1206939

63. Bi J, Wang X. Molecular regulation of NK cell maturation. *Front Immunol*. 2020;11:1945. doi:10.3389/fimmu.2020.01945

64. Konjević GM, Vuletić AM, Mirjačić Martinović KM, Larsen AK, Jurišić VB. The role of cytokines in the regulation of NK cells in the tumor environment. *Cytokine*. 2019;117:30–40. doi:10.1016/j.cyto.2019.02.001

65. Shen M, Wang J, Yu W, et al. A novel MDSC-induced PD-1⁻ PD-L1⁺ B-cell subset in breast tumor microenvironment possesses immuno-suppressive properties. *OncoImmunology*. 2018;7(4):e1413520. doi:10.1080/2162402X.2017.1413520

66. Jianyi D, Haili G, Bo Y, et al. Myeloid-derived suppressor cells cross-talk with B10 cells by BAFF/BAFF-R pathway to promote immunosuppression in cervical cancer. *Cancer Immunol Immunother*. 2023;72(1): 73–85. doi:10.1007/s00262-022-03226-0

67. Bodogai M, Moritoh K, Lee-Chang C, et al. Immunosuppressive and prometastatic functions of myeloid-derived suppressive cells rely upon education from tumor-associated B cells. *Cancer Res*. 2015; 75(17):3456–3465. doi:10.1158/0008-5472.CAN-14-3077

68. Olkhanud PB, Damdinsuren B, Bodogai M, et al. Tumor-evoked regulatory B cells promote breast cancer metastasis by converting resting CD4⁺ T cells to T-regulatory cells. *Cancer Res*. 2011;71(10):3505–3515. doi:10.1158/0008-5472.CAN-10-4316

69. Das A, Ellis G, Pallant C, et al. IL-10-producing regulatory B cells in the pathogenesis of chronic hepatitis B virus infection. *J Immunol*. 2012;189(8):3925–3935. doi:10.4049/jimmunol.1103139

70. Song H, Liu A, Liu G, Wu F, Li Z. T follicular regulatory cells suppress Tfh-mediated B cell help and synergistically increase IL-10-producing B cells in breast carcinoma. *Immunol Res*. 2019;67(4–5):416–423. doi:10.1007/s12026-019-09090-y

71. Tao H, Lu L, Xia Y, et al. Antitumor effector B cells directly kill tumor cells via the Fas/FasL pathway and are regulated by IL-10. *Eur J Immunol*. 2015;45(4):999–1009. doi:10.1002/eji.201444625

72. Shalapour S, Font-Burgada J, Di Caro G, et al. Immunosuppressive plasma cells impede T-cell-dependent immunogenic chemotherapy. *Nature*. 2015;521(7550):94–98. doi:10.1038/nature14395

73. Melcher C, Yu J, Duong VHH, et al. B cell-mediated regulatory mechanisms control tumor-promoting intestinal inflammation. *Cell Rep*. 2022;40(2):111051. doi:10.1016/j.celrep.2022.111051

74. Zhang H, Yue R, Zhao P, et al. Proinflammatory follicular helper T cells promote immunoglobulin G secretion, suppress regulatory B cell development, and correlate with worse clinical outcomes in gastric cancer. *Tumour Biol*. 2017;39(6):101042831770574. doi:10.1177/1010428317705747

75. Candando KM, Lykken JM, Tedder TF. B10 cell regulation of health and disease. *Immunol Rev*. 2014;259(1):259–272. doi:10.1111/imr.12176

76. Tedder TF. B10 cells: A functionally defined regulatory B cell subset. *J Immunol*. 2015;194(4):1395–1401. doi:10.4049/jimmunol.1401329

77. Bodogai M, Lee Chang C, Wejksza K, et al. Anti-CD20 antibody promotes cancer escape via enrichment of tumor-evoked regulatory B cells expressing low levels of CD20 and CD137L. *Cancer Res*. 2013;73(7):2127–2138. doi:10.1158/0008-5472.CAN-12-4184

78. Barbera-Guillem E, Nelson MB, Barr B, et al. B lymphocyte pathology in human colorectal cancer: Experimental and clinical therapeutic effects of partial B cell depletion. *Cancer Immunol Immunother*. 2000;48(10):541–549. doi:10.1007/PL00006672

79. Winkler JK, Schiller M, Bender C, Enk AH, Hassel JC. Rituximab as a therapeutic option for patients with advanced melanoma. *Cancer Immunol Immunother*. 2018;67(6):917–924. doi:10.1007/s00262-018-2145-9

80. Pinc A, Somasundaram R, Wagner C, et al. Targeting CD20 in melanoma patients at high risk of disease recurrence. *Mol Ther*. 2012;20(5):1056–1062. doi:10.1038/mt.2012.27

81. Theurich S, Schlaak M, Steguweit H, et al. Targeting tumor-infiltrating B cells in cutaneous T-cell lymphoma. *J Clin Oncol*. 2016;34(12):e110–e116. doi:10.1200/JCO.2013.50.9471

82. Aklilu M, Stadler WM, Markiewicz M, et al. Depletion of normal B cells with rituximab as an adjunct to IL-2 therapy for renal cell carcinoma and melanoma. *Ann Oncol*. 2004;15(7):1109–1114. doi:10.1093/annonc/mdh280

83. Yarchoan M, Mohan AA, Dennison L, et al. MEK inhibition suppresses B regulatory cells and augments anti-tumor immunity. *PLoS One*. 2019;14(10):e0224600. doi:10.1371/journal.pone.0224600

84. Song SS, Yuan PF, Li PP, et al. Protective effects of Total Glucosides of Paeony on N-nitrosodiethylamine-induced hepatocellular carcinoma in rats via down-regulation of regulatory B cells. *Immunol Invest*. 2015;44(6):521–535. doi:10.3109/08820139.2015.1043668

85. Wang Z, Cheng Q, Tang K, et al. Lipid mediator lipoxin A4 inhibits tumor growth by targeting IL-10-producing regulatory B (Breg) cells. *Cancer Lett*. 2015;364(2):118–124. doi:10.1016/j.canlet.2015.04.030

86. Zhao R, Liu M, Li X, et al. A strategy of targeting B10 cell by CD19scFv-IL10R for tumor therapy. *Biochem Biophys Res Commun*. 2018;506(4):990–996. doi:10.1016/j.bbrc.2018.10.191

87. Shen L, Li J, Liu Q, et al. Nano-trapping CXCL13 reduces regulatory B cells in tumor microenvironment and inhibits tumor growth. *J Control Release*. 2022;343:303–313. doi:10.1016/j.jconrel.2022.01.039

88. Hashimoto M, Kamphorst AO, Im SJ, et al. CD8 T cell exhaustion in chronic infection and cancer: Opportunities for interventions. *Annu Rev Med*. 2018;69(1):301–318. doi:10.1146/annurev-med-012017-043208

89. Sharpe AH, Pauken KE. The diverse functions of the PD1 inhibitory pathway. *Nat Rev Immunol*. 2018;18(3):153–167. doi:10.1038/nri.2017.108

90. Zhao Y, Shen M, Feng Y, et al. Regulatory B cells induced by pancreatic cancer cell-derived interleukin-18 promote immune tolerance via the PD-1/PD-L1 pathway. *Oncotarget*. 2018;9(19):14803–14814. doi:10.18632/oncotarget.22976

91. Shalapour S, Lin XJ, Bastian IN, et al. Inflammation-induced IgA+ cells dismantle anti-liver cancer immunity. *Nature*. 2017;551(7680):340–345. doi:10.1038/nature24302

Metabolic encephalopathies in children: A pragmatic diagnostic approach based on literature analysis

Dariusz Rokicki[A–F]

Children's Memorial Health Institute, Warsaw, Poland

A – research concept and design; B – collection and/or assembly of data; C – data analysis and interpretation;
D – writing the article; E – critical revision of the article; F – final approval of the article

Address for correspondence
Dariusz Rokicki
E-mail: d.rokicki@ipczd.pl

Abstract

Inborn errors of metabolism (IEM) in the general population are rare diseases. However, from the perspective of general pediatrics and pediatric intensive care units (PICUs), they are becoming a significant challenge both diagnostically and therapeutically. Clinically, there is a useful division of IEMs with neurological manifestations into 2 categories: acute and progressive encephalopathies. The extent of individual IEMs in these 2 groups varies, requiring different diagnostic strategies. Despite progress in development of diagnostic tools in IEM, initial diagnosis is made on the basis of basic laboratory tests, neuroradiological findings and metabolic screening. In settings of shortage of diagnostic resources and under time pressure, rational decisions should be made based on available clinical data. The text discusses diagnostic aspects of IEM presenting as metabolic encephalopathies, highlighting their significance in the context of general pediatric care and intensive care units (ICUs), and the challenges associated with diagnosis. It should be noted that the paper does not include a discussion of epileptic encephalopathies of IEM etiology, although some cases of metabolic encephalopathies may also present initially as epileptic encephalopathy.

Key words: inborn errors of metabolism, metabolic encephalopathy, metabolic screening

Introduction

In the general population, inborn errors of metabolism (IEM) are rare diseases. However, from the perspective of general pediatrics and pediatric intensive care units, they are becoming a significant challenge both diagnostically and therapeutically. Clinically, there is a useful division of IEMs with neurological manifestations into 2 categories: acute and progressive encephalopathies. The extent of individual IEMs in these 2 groups varies, requiring different diagnostic strategies. The text discusses diagnostic aspects of IEM presenting as metabolic encephalopathies, highlighting their significance in the context of pediatric care and the challenges associated with diagnosis.

It should be noted that the paper does not include a discussion of epileptic encephalopathies of IEM etiology, although some cases of metabolic encephalopathies may also present initially as epileptic encephalopathy.

Metabolic encephalopathy: Definition and scale of the problem

Encephalopathy is a non-specific term that generally refers to disorders of central nervous system (CNS) function. These disorders are usually characterized by symptoms such as impaired consciousness and cognitive abilities, and may be accompanied by symptoms related to the pyramidal, extrapyramidal or seizure systems.

Etiologically, 2 main groups of encephalopathies can be distinguished: acquired and inborn, while from a clinical perspective, we distinguish acute and chronic encephalopathies. Metabolic encephalopathies result from inborn metabolic errors, which manifest themselves in both acute and chronic, progressive forms.

The overall incidence of IEM is 50.9 cases per 100,000 live births, with a higher prevalence in Middle Eastern countries. The approximate mortality rate in this group of patients averages 33%, but with significant differences depending on the level of national income. In highly developed countries, the rate fluctuates between 2% and 23%.[1] There are no separate data on the proportion of cases manifested by acute or chronic encephalopathy in the total number of IEM cases. An attempt to estimate the epidemiological size of this phenomenon in the context of acute encephalopathies is provided by information on the percentage of patients with IEM hospitalized in intensive care units (ICUs).

In a study conducted by Maksoud et al., in a group of 30 patients with encephalopathy of unknown cause admitted to the ICU within a year, it was found that 10 of them showed abnormal biochemical test results indicative of IEM. Of these cases, 4 hospitalized patients (13.3%) had organic aciduria, 4 (13.3%) had probable mitochondrial disease, 1 (3.3%) had a urea cycle defect, and 1 (3.3%) had non-ketotic hyperglycemia.[2] In contrast, in a study by Magdy et al. of 308 infants with initial suspected IEM, a metabolic defect was eventually confirmed in 93 patients (30.2%).[3]

A large study by Lipari et al. involving analysis of 4,459 pediatric ICU admissions over a 10-year period found that IEM accounted for 2% of hospitalizations (88 cases in 65 children). Of these cases, 62 admissions (70.4%) were associated with metabolic decompensation, which manifested clinically as encephalopathy. There were 8 deaths in this group of patients.[4] Results similar to these were also described by Couce et al., who observed 31 cases of patients with IEM out of 1,104 admissions to the pediatric ward over an 8-year period, accounting for 1.63% of all hospitalizations. Of these cases, 18 required intensive care, and 12 patients had a clinical picture of acute encephalopathy that did not require ICU care. The mortality rate among patients with IEM was 10.3%.[5] It is noteworthy that both of these latter analyses are from highly developed countries where there is a well-developed IEM diagnostic base based on population-based screening, which may influence the lower reported rate of cases leading to metabolic decompensation.

Metabolic encephalopathies can manifest themselves at any stage of life, but most often are observed in the first few years. As symptoms appear later, cases are more likely to fall into the group of chronic, progressive diseases associated with a defect in the metabolism of complex molecules. In the study by Lipari et al., the average age of patients with IEM hospitalized in the acute-onset state was 3 years (ranging from 3 days old to 21 years), with the average age of diagnosis at 3 months.[4]

In the context of acute encephalopathy, from a clinical perspective, it is useful to divide the disease into 2 main groups:

1. Intoxication group (organic acidurias, urea cycle defects);
2. Energy failure group (fatty acid oxidation disorders, mitochondrial diseases).

In the available studies, the syndromes of intoxication (IG) and energy production disorders (EFG) represent comparable numerical groups of hospitalized patients. In a study by Lipari et al., the numbers of patients admitted were 23 and 21, respectively, out of 65 hospitalized for encephalopathy.[4] Similar proportions of patients with IG and EFG are reported in other studies: 5 and 6 out of 11 hospitalized with IEM, respectively[6] and 5 and 4 out of 10 hospitalized with IEM.[1]

Clinical picture

In IG, disorders of consciousness (coma) are the leading symptom, which affects almost all patients. Disorders of consciousness are usually preceded by the onset of infection and vomiting. More than half of the patients have seizures, 20% patients have hypotonia and 10% have muscular hypertonia.[1]

In EFG, due to impaired fatty acid oxidation, the clinical presentation at the onset of encephalopathy is similar to IG. In Polish conditions, most patients at the time of admission already have a confirmed diagnosis (screening).

In the case of mitochondrial diseases, the clinical picture is richer, and the course of the disease itself is an exacerbation of the course rather than a sudden manifestation of the encephalopathy – respiratory failure or respiratory disorders of the hyperventilation type, dehydration, heart failure in patients with developmental problems, hypotonia and muscle weakness. The course of the disease is most often exacerbated by infections. From the point of view of physicians working in pediatric wards, it is important to report that the most common symptom in this group of patients on admission was fever.[8]

In view of the highly non-specific clinical picture of a patient with acute metabolic encephalopathy (this problem does not, of course, apply to those with already diagnosed metabolic disease), the correct diagnosis of the causes of the encephalopathy can be guided by basic tests.[9,10] The most common abnormalities found in this group of patients are metabolic acidosis (75–78% of patients), lactic acidosis (50–66%), hyperammonemia (33–62.5% of patients), and ketonuria (22–37% of patients).[8,11] Hypoglycemia as an abnormality in metabolic encephalopathies was reported in only 1 study (37.5%) with a comparable percentage of hyperglycemia (25%).[8] The same study also reported a high percentage of hyperuricemia in acute metabolic encephalopathies (87.5%). A high value for this parameter also occurred among acute non-metabolic conditions (30.8%), indicating the severity of catabolism in a given patient regardless of its cause. Metabolic acidosis is equally non-specific, occurring in a significant percentage of patients referred to ICUs. The laboratory examinations listed above should also be performed when patients are hospitalized already with a diagnosis of any of the diseases from the group of intoxication syndrome. The occurrence of the above abnormalities indicates a metabolic breakthrough or a significant risk of its occurrence.

Neuroimaging studies are an integral part of diagnosing encephalopathies. In the case of metabolic encephalopathies, computed tomography (CT) or magnetic resonance imaging (MRI) scans often reveal changes, but practically only in 2 cases led to the suspicion of specific diseases: glutaric aciduria type 1 and Leigh syndrome.[12]

A CT scan of the head often reveals cerebral edema and atrophy, with total abnormalities found in 68% of studies.[2] A brain MRI provides more informative results: atrophic lesions (44%), white matter lesions (19%) and lesions in the basal nuclei (7%). Abnormalities were present in 44% of all patients.[2]

Neuroimaging studies are important in the differential diagnosis of encephalopathies and in making initial therapeutic decisions, but when analyzed in a specific clinical context, they can help in the metabolic diagnosis. Of the other imaging studies, we should consider evaluation of the heart for cardiomyopathy (mitochondrial diseases), the presence of pericardial fluid and arrhythmias (fatty acid oxidation disorders) or abdominal ultrasound – hepatomegaly.

The basis of metabolic diagnosis in encephalopathies of unknown cause are metabolic screening tests:

1. Profile of acylcarnitines in dry blood drop using tandem mass spectrometry (MSMS) method;
2. Urine organic acid profile using gas chromatography-mass spectrometry (GCMS) method;
3. Plasma aminoacidogram.

The above tests make it possible to diagnose syndromes of intoxication, listed as following:

1. Organic aciduria;
2. Defects of the urea cycle;
3. Disorders of fatty acid and ketone metabolism;
4. Disorders of amino acid metabolism;
5. Exacerbation of the course of mitochondrial diseases.

In the case of mitochondrial encephalopathy exacerbation, these tests do not allow a confident diagnosis; there is no unequivocal biochemical marker in mitochondrial diseases. The lactic acidosis associated with these diseases occurs in about 60% of cases and is usually associated with hyperalaninemia.

Results of metabolic screening tests are necessary to conduct targeted treatment in IEM. The problem lies in the rapid availability of the tests. Most hospitals lack adequate diagnostic facilities and samples must be sent to other centers. Samples for testing should be secured immediately after the child's hospitalization, even in the case of newborns who have already undergone population screening and whose test results are still unavailable. It is possible that the tested disease markers have not yet accumulated in sufficient quantity to give a positive screening result.[13] Widespread genetic testing such as targeted gene sequencing panels and whole exome sequencing (WES) are currently not applicable to the clinical practice for differential diagnosis of acute metabolic encephalopathies. This limitation is primarily due to the time factor – the result is obtained too late to affect therapeutic decisions by causing a change in perspective.

Nevertheless, in any case of acute encephalopathy of unknown cause, a DNA sample should be secured for such testing, in case of an unsuccessful course of the disease and for subsequent confirmation of the diagnosis.[14]

Chronic metabolic encephalopathies

Chronic metabolic encephalopathies (CME) are a group of diseases that are the domain of pediatric departments (except for exacerbations of mitochondrial diseases) and should be diagnosed according to the standards of classical differential diagnosis. Chronic metabolic encephalopathies are characterized by:

1. Progressive neurological deterioration; the period of observation can vary depending on the disease. Generally, the older the age of first manifestation, the slower the disease progression. An important element of follow-up is the progression of changes on brain MRI;
2. Gradual loss of cognitive or psychomotor abilities;

3. The appearance of additional neurological symptoms;

4. Lack of external causes of encephalopathy (inflammatory, traumatic, toxic).

The magnitude of the CME is represented by the percentage of IEM diagnoses among patients with progressive encephalopathies. In 2 cross-sectional studies, the percentage of IEM among CME was 75%[15] and 62.5%.[16] In 1 study, the percentage was as high as 88.9%.[17] In a study by Stromme et al., the percentage of IEM among patients with encephalopathy was 33.3% (88 patients were identified), giving an incidence of 2.14/100,000. However, this study analyzed all encephalopathies, including those with acute manifestations.[18]

The spectrum of IEM with neurological manifestations, including CME, is considerable, some with multi-organ manifestations. The exception is protein glycosylation diseases, where CNS dysfunction is rarely progressive, although the course can be extremely severe from the perinatal period onward, with significant mortality also from extracerebral causes (cardiac and hematologic).[19,20]

There are no data on the age distribution of CME manifestation. The data that Stromme et al. cite in their paper are cumulative data, which also include encephalopathies classified as acute in this study. In such a compilation, the percentage of age-related encephalopathies is 45.5% for 1 month-olds, 21.8% for infancy, 27.2% for 1–5 years, and 5.5% for 6–12 years.[18] The reported data indicate a significant percentage of acute encephalopathies in young children, as, for example, the age of manifestations of the most common lysosomal diseases among CME is 2 years.[21]

In the analysis of 2,152 reports from PubMed on progressive cognitive and neurological disorders, 85 cases had a metabolic basis, of which 34/85 (40%) were specifically lysosomal diseases, 15/85 (17.6%) diseases from the group of disorders of metabolism of nitrogen-containing molecules (organic acidurias, urea cycle defects – encephalopathies with acute presentation), 15/85 (17.6%) disorders of vitamin, cofactor and metal metabolism, 14/85 (16.5%) mitochondrial diseases, 2/85 peroxisomal diseases, and 2/85 disorders of lipid metabolism with 1 case each of glycosylation, carbohydrate and tetrapyrrole disorders.[22] Regardless of the methodology of analysis, the most common causes of CME are lysosomal diseases followed by mitochondrial disorders, peroxisomal disorders, congenital disorders of glycosylation, and disorders of purine and pyrimidine metabolism.

The clinical presentation of CME is included in the above criteria. The most commonly associated neurological symptoms are epilepsy (79%) and psychomotor or intellectual developmental delay (39%). Disorders of muscle tone, nystagmus, and sensory or movement disorders are also observed. In some diseases, extra-neurological symptoms are also present, which, for example, in some mucopolysaccharidoses precede neurological symptoms and are often the starting point of diagnosis.

Of the neuroimaging studies, MRI provides the most information. The result of the study in individual cases may indicate a specific diagnosis such as glutaric aciduria type 1 or X-linked adrenoleukodystrophy (XALD). Receiving such suggestions also depends on the experience of the radiologist and the collaboration with the patient's treating physician, which means that tests should not be evaluated in a clinical vacuum. In other cases, MRI guides the diagnosis of diseases with predominant involvement of the white matter, gray matter or basal nuclei. According to Wenger et al., a metabolic background of the disease is indicated by symmetrical changes in brain MRI, especially with associated features[23]:

1. Pattern of change characteristic of the IEM;

2. Brain MRI does not correspond with hypoxic-ischemic changes;

3. Isolated or dominant cerebellar or brainstem involvement;

4. Freshly revealed acute or chronic lesions;

5. In newborns, congenital lesions and/or reduced brain volume;

6. Progressive brain atrophy;

7. Malformations with acquired lesions.

White matter involvement is frequently observed in CME, which is consistent with the predominance of lysosomal diseases in this group of patients. However, it should be remembered that lysosomal diseases are a large group of genetic metabolic disorders with heterogeneous clinical presentation and patterns of CNS involvement.

In an analysis of 5,166 MRI images with white matter involvement, leukodystrophy was present in 5% of all images. Autoimmune diseases predominated (23%) and often required differentiation from IEM.[23]

Nonspecific lesions may be a problem in patients who have undergone testing for causes other than CME (18%). In the absence of a complete clinical analysis, they may be the cause for further unnecessary and traumatizing diagnosis.

Characteristically, in the cited study, all instances of white matter involvement in this group of patients were located supratentorially.[23] If leukodystrophy is found, further radiological analysis should differentiate between hypomyelination, demyelination and dysmyelination. The presence of additional changes such as cysts, contrast enhancement or involvement of the nucleus accumbens can further guide the diagnosis.[24,25] Magnetic resonance spectroscopy reveals nonspecific lesions and indicates the diagnosis only in the case of deficits in creatine synthesis and transport.[27]

Baseline tests in CME are mostly not diagnostic. However, in rare cases they may be the basis for diagnosis, such as low copper and ceruloplasmin levels in the Menkes disease or low uric acid and homocysteine levels in molybdenum cofactor deficiency.

These useful metabolic screening tests are also rarely diagnostic in CME, but are nevertheless necessary since patients in between acute episodes of intoxication

demonstrate chronic symptoms, including consequences of past exacerbations. In view of the prevalence of lysosomal disease in CME, tests of lysosomal enzyme activity in a dry blood spot or whole blood, supported by assessment of oligosaccharide or glucosamine excretion, are most useful. The above does not cover the full spectrum of tests available for the diagnosis of lysosomal diseases, but from a clinical point of view, it is a good diagnostic starting point.

The desirable situation is the suspicion of a specific IEM. When peroxisomal diseases are suspected, of great value as a first-line test is the concentration of very long-chain fatty acids, useful in the most common diseases of this group such as XALD and disorders of peroxisome biogenesis.

Confirmation of the diagnosis is provided with genetic testing, especially next-generation sequencing (NGS), in the absence of a specific suspicion or narrowing the suspicion to a group of diseases. In a study by Salman et al., out of 126 genetic tests performed in suspected IEM, positive WES results helped establish the diagnosis in 22/45 patients (48.9%), panel testing in 8/13 (62%), and targeted genetic testing in 50/67 (75%), indicating the role of precise clinical analysis in ordering this type of testing.[27] For neurogenetic diseases in general, the reported efficiency of WES ranges from 16 to 68%, depending on the study.[28] It is interesting to compare the efficiency of diagnosing IEM using WES (whole exome sequencing) and MSMS as first-line methods. The study was performed on samples from 4.5 million newborns. The sensitivity of WES was 88% with 98.4% specificity compared to the 99% sensitivity and 99% specificity of the MSMS method.[29]

Summary

Inborn errors of metabolism in the general population are rare diseases, but from the perspective of general pediatrics or ICUs, they are already a significant epidemiological problem. There is a lack of epidemiological data for Poland, partly due to the lack of a rare disease registry. Estimates based on literature reports put the percentage of IEM at 1.63–2% of those hospitalized in ICUs. In clinical practice, these are patients with acute metabolic decompensation or acute encephalopathy. These data come from highly developed countries with a well-developed screening system for inborn metabolic diseases.

A separate issue is the percentage of progressive encephalopathies of metabolic origin that usually do not require acute hospitalization. Data report 33.3–89.8% of all progressive encephalopathies, with a frequency in the general population of 2.14/100,000 people, making CME a significant problem in the practice of metabolic or neurological departments.

Inborn errors of metabolism with acute encephalopathy manifestations are primarily disorders of small molecule metabolism and they include organic acidurias (OA), urea cycle defects (UCD) and fatty acid oxidation disorders (FAOD). Of these diseases, OA and FAOD are largely covered by screening. In practice, this means that the preponderance of patients in these groups are newborns with early manifestations of the disease (before screening results are available) and children with an already established diagnosis and disease exacerbation. In the case of UCD in Poland, screening includes patients associated with increased levels of citrulline (2 enzymatic defects), which does not allow neonatal screening to identify ornithine transcarbamylase deficiency, the most common enzymatic defect in UCD.

Baseline laboratory investigations can give important clues to the metabolic background of the disease. The most common abnormalities include hyperammonemia, acidosis, lactic acidosis, and hyperketonemia. The clinical presentation of acute encephalopathy and the above abnormalities require consideration of IEM in therapeutic management.

Considering the IEM as the cause of acute encephalolpathies, the basis for the diagnosis is the profile of acylcarnitines in a dry blood drop using MSMS, the profile of urinary organic acids by GCMS and the plasma amino acids profile. The latter test is crucial in the differential diagnosis of UCD. These tests should also be performed in any acute encephalopathy, despite a negative screening result.

Lysosomal diseases account for the largest percentage of CME. The most common of these are neuronal ceroid lipofuscinosis (CLN), Niemann–Pick disease type C (NPC), mucopolysaccharidosis type 3 (MPS3), and metachromatic leukodystrophy (MLD).[30] Lysosomal diseases account for the largest percentage of CME. The most common of these are CLN, NPC, MPS3, and MLD. The basic biochemical diagnostic methods for lysosomal diseases include the measurement of enzyme activity, substrate concentrations and alternative reaction products for particular diseases.

The choice of test depends on the patient's clinical evaluation and radiographic findings and can be made after consultation with a metabolic pediatric specialist. A summary of tests necessary for the diagnosis of metabolic encephalopathies is given in Table 1.

Broad-spectrum genetic testing plays an important role in CME. However, its efficiency in diagnosing progressive metabolic encephalopathy, a component of most IEMs, remains lower than targeted genetic testing, emphasizing the importance of clinical analysis of the disease course.

For acute presentations of IEM, there are attempts to use rapid WES diagnostic techniques, but metabolic studies are still the basis of diagnostic decision-making. The exception are mitochondrial diseases, in which genetic testing is the first choice in the absence of clear biochemical markers.

Applications

- Inborn errors of metabolism that present as encephalopathies are rare diseases in the general population, but are a significant concern in pediatric departments and ICUs.

Table 1. The usefulness of biochemical tests in the diagnosis of different groups of IEM

Type of test	Acute metabolic encephalopathies	Progressive metabolic encephalopathies
Urine		
Ketones	+	−
Organic acid profile method – GCMS	++	−/+
Glycosaminoglycans	−	+
Oligosaccharides	−	+
Profile of purines and pyrimidines	−	+
Blood		
Ammonia, gasometry, lactic acid	++	−/+
Profile of acylcarnitines in a dry blood drop method – MSMS	++	−/+
Aminoacidogram	++	−/+
Homocysteine	−/+	+
Transferrin isoforms	−	+
VLCFA	−	+

IEM – inborn errors of metabolism; GCMS – gas chromatography-mass spectrometry; MSMS – tandem mass spectrometry; VLCFA – very long-chain fatty acids.

• In every case of encephalopathy of unknown origin, metabolic background of the disease should be considered. The extent of first-line metabolic testing should vary between acute and chronic encephalopathy patient groups.

• Baseline laboratory investigations often reveal key abnormalities such as hyperammonemia, acidosis, lactic acidosis, and hyperketonemia. If these abnormalities coincide with the symptoms of acute encephalopathy, it's worth considering IEM as a part of therapeutic management.

• Diagnosis of acute metabolic encephalopathies relies on specific tests, including profiling acylcarnitines in dry blood drops using MSMS, urinary organic acid profiling with GCMS and plasma amino acid profiling. These tests are essential even if screening results are negative.

• Broad-spectrum genetic testing (WES, NGS) plays a crucial role in diagnosing CME. However, its efficiency is still lower than targeted genetic testing, emphasizing the importance of clinical analysis. In acute presentations of IEM, metabolic studies remain the primary diagnostic tool, except in mitochondrial diseases, where genetic testing takes precedence.

ORCID iDs

Dariusz Rokicki ⓘ https://orcid.org/0000-0002-9736-2838

References

1. Waters D, Adeloye D, Woolham D, Wastnedge E, Patel S, Rudan I. Global birth prevalence and mortality from inborn errors of metabolism: A systematic analysis of the evidence. *J Glob Health*. 2018;8(2):021102. doi:10.7189/jogh.08.021102

2. Abdel Maksoud M, Elsayed S, Shatla RH, et al. Frequency of inborn errors of metabolism screening for children with unexplained acute encephalopathy at an emergency department. *Neuropsychiatr Dis Treat*. 2018;14:1715–1720. doi:10.2147/NDT.S165833

3. Magdy RM, Abd-Elkhalek HS, Bakheet MA, Mohamed MM. Selective screening for inborn errors of metabolism by tandem mass spectrometry at Sohag University Hospital, Egypt. *Arch Pediatr*. 2022; 29(1):36–43. doi:10.1016/j.arcped.2021.11.002

4. Lipari P, Shchomak Z, Boto L, et al. Inborn errors of metabolism in a tertiary pediatric intensive care unit. *J Pediatr Intensive Care*. 2022; 11(3):183–192. doi:10.1055/s-0040-1721738

5. Couce ML, Baña A, Bóveda MD, Pérez-Muñuzuri A, Fernández-Lorenzo JR, Fraga JM. Inborn errors of metabolism in a neonatology unit: Impact and long-term results. *Pediatr Int*. 2011;53(1):13–17. doi:10.1111/j.1442-200X.2010.03177.x

6. Kamate M, Chetal V, Kulgod V, Patil V, Christopher R. Profile of inborn errors of metabolism in a tertiary care centre PICU. *Indian J Pediatr*. 2010;77(1):57–60. doi:10.1007/s12098-010-0008-2

7. Martín-Rivada Á, Cambra Conejero A, Martín-Hernández E, et al. Newborn screening for propionic, methylmalonic acidemia and vitamin B12 deficiency: Analysis of 588,793 newborns. *J Pediatr Endocrinol Metabol*. 2022;35(10):1223–1231. doi:10.1515/jpem-2022-0340

8. Singhal K, Bothra M, Kapoor S, Jhamb U, Mishra D. Metabolic disorders among children presenting with acute encephalopathy. *Indian J Pediatr*. 2022;89(7):665–672. doi:10.1007/s12098-022-04087-2

9. Surtees R, Leonard JV. Acute metabolic encephalopathy: A review of causes, mechanisms and treatment. *J Inherit Metab Dis*. 1989; 12(Suppl 1):42–54. doi:10.1007/BF01799285

10. Leonard JV. Acute metabolic encephalopathy: An introduction. *J Inherit Metab Dis*. 2005;28(3):403–406. doi:10.1007/s10545-005-8047-y

11. El-Nawawy A, Dawood M, Omar O. A retrospective study of small molecule disorder types of metabolism in paediatric patients in intensive care. *East Mediterr Health J*. 2018;24(11):1103–1111. doi:10.26719/emhj.18.056

12. Lai LM, Gropman AL, Whitehead MT. MR neuroimaging in pediatric inborn errors of metabolism. *Diagnostics*. 2022;12(4):861. doi:10.3390/diagnostics12040861

13. Chakrapani A, Cleary MA, Wraith JE. Detection of inborn errors of metabolism in the newborn. *Arch Dis Child Fetal Neonatal Ed*. 2001; 84(3):F205–F210. doi:10.1136/fn.84.3.F205

14. Navarrete R, Leal F, Vega AI, et al. Value of genetic analysis for confirming inborn errors of metabolism detected through the Spanish neonatal screening program. *Eur J Hum Genet*. 2019;27(4):556–562. doi:10.1038/s41431-018-0330-0

15. Keene DL, Sutcliffe T, Harman P, Grenier D. Surveillance for progressive intellectual and neurological deterioration in the Canadian paediatric population. *Can J Neurol Sci*. 2004;31(2):220–224. doi:10.1017/S0317167100053865

16. Nunn K, Williams K, Ouvrier R. The Australian Childhood Dementia Study. *Eur Child Adolesc Psychiatry*. 2002;11(2):63–70. doi:10.1007/s007870200012

17. Verity C, Winstone AM, Will R, et al. Surveillance for variant CJD: Should more children with neurodegenerative diseases have autopsies? *Arch Dis Child*. 2019;104(4):360–365. doi:10.1136/archdischild-2018-315458

18. Stromme P, Kanavin OJ, Abdelnoor M, et al. Incidence rates of progressive childhood encephalopathy in Oslo, Norway: A population based study. *BMC Pediatr.* 2007;7(1):25. doi:10.1186/1471-2431-7-25

19. Paprocka J, Jezela-Stanek A, Tylki-Szymańska A, Grunewald S. Congenital disorders of glycosylation from a neurological perspective. *Brain Sci.* 2021;11(1):88. doi:10.3390/brainsci11010088

20. Greczan M, Rokicki D, Wesół-Kucharska D, Kaczor M, Rawiak A, Jezela-Stanek A. Perinatal manifestations of congenital disorders of glycosylation: A clue to early diagnosis. *Front Genet.* 2022;13:1019283. doi:10.3389/fgene.2022.1019283

21. Chen X, Qiu W, Ye J, Han L, Gu X, Zhang H. Demographic characteristics and distribution of lysosomal storage disorder subtypes in Eastern China. *J Hum Genet.* 2016;61(4):345–349. doi:10.1038/jhg.2015.155

22. Warmerdam HAG, Termeulen-Ferreira EA, Tseng LA, et al. A scoping review of inborn errors of metabolism causing progressive intellectual and neurologic deterioration (PIND). *Front Neurol.* 2020;10:1369. doi:10.3389/fneur.2019.01369

23. Wenger KJ, Koldijk CE, Hattingen E, Porto L, Kurre W. Characterization of MRI white matter signal abnormalities in the pediatric population. *Children (Basel).* 2023;10(2):206. doi:10.3390/children10020206

24. Schiffmann R, Van der Knaap MS. Invited Article: An MRI-based approach to the diagnosis of white matter disorders. *Neurology.* 2009;72(8):750–759. doi:10.1212/01.wnl.0000343049.00540.c8

25. Parikh S, Bernard G, Leventer RJ, et al. A clinical approach to the diagnosis of patients with leukodystrophies and genetic leukoencephalopathies. *Mol Genet Metab.* 2015;114(4):501–515. doi:10.1016/j.ymgme.2014.12.434

26. Van De Kamp J, Mancini G, Pouwels P, et al. Clinical features and X-inactivation in females heterozygous for creatine transporter defect. *Clin Genet.* 2011;79(3):264–272. doi:10.1111/j.1399-0004.2010.01460.x

27. Salman DO, Mahfouz R, Bitar ER, Samaha J, Karam PE. Challenges of genetic diagnosis of inborn errors of metabolism in a major tertiary care center in Lebanon. *Front Genet.* 2022;13:1029947. doi:10.3389/fgene.2022.1029947

28. Shakiba M, Keramatipour M. Effect of whole exome sequencing in diagnosis of inborn errors of metabolism and neurogenetic disorders. *Iran J Child Neurol.* 2018;12(1):7–15. PMID:29379558. PMCID:5760669.

29. Adhikari AN, Gallagher RC, Wang Y, et al. The role of exome sequencing in newborn screening for inborn errors of metabolism. *Nat Med.* 2020;26(9):1392–1397. doi:10.1038/s41591-020-0966-5

30. Poupětová H, Ledvinová J, Berná L, Dvořáková L, Kožich V, Elleder M. The birth prevalence of lysosomal storage disorders in the Czech Republic: Comparison with data in different populations. *J Inherit Metab Dis.* 2010;33(4):387–396. doi:10.1007/s10545-010-9093-7

CBCT and modern intraoral scanners as tools for developing comprehensive, interdisciplinary treatment plans

Wojciech Frąckiewicz[B–D,F], Aleksandra Jankowska[B–D,F], Monika E. Machoy[A,E,F]

Department of Periodontology, Faculty of Medicine and Dentistry, Pomeranian Medical University in Szczecin, Poland

A – research concept and design; B – collection and/or assembly of data; C – data analysis and interpretation;
D – writing the article; E – critical revision of the article; F – final approval of the article

Address for correspondence
Monika E. Machoy
E-mail: m.machoy@gmail.com

Abstract

The aim of this narrative literature review is to present the possibilities of using cone beam computed tomography (CBCT) and 3D dental scanners to prepare comprehensive, interdisciplinary treatment plans. Scanners are instruments whose usage seems to be a key element of modern digital dentistry. Their importance in orthodontic treatment with overlay appliances, planning modern prosthetic treatments (CAD/CAM) and implantology cannot be overestimated. These scanners allow for accurate imaging of the tooth structures and their positioning independently in the maxilla and mandible as well as in the occlusion. As a result, dentists can plan treatment, e.g., in the case of the need to implant dental implants, prosthetic crowns or orthodontic braces. Dentistry was revolutionized to a similar extent by the introduction of CBCT to everyday diagnostics, which is the most advanced imaging technology that provides even more detailed images in 3 dimensions. Its use has enabled a wider and more precise range of diagnostics, which in turn has improved the quality of multidisciplinary treatment planning. This paper explains how scanners and CBCT can be used in orthodontics and prosthetics based on the articles found in 3 databases: PubMed, Scopus and Embase. The review included 28 articles on the aforementioned topics and was presented with a brief description of the content of each article.

Key words: orthodontics, prosthodontics, CBCT, scanners, modern dentistry

Introduction

Modern dentistry provides many new tools for carrying out diagnostics allowing for the preparation of the safest, interdisciplinary treatment plans. They include, e.g., cone-beam computed tomography (CBCT) and modern intraoral scanners.[1]

Cone beam computed tomography can be used in almost every field of dentistry as it allows for determining the spatial conditions of the jaw bones, which is used, among others, in dental surgery, orthodontics and maxillofacial surgery, but also enables precise assessment of alveolar processes, the quality and density of their bones, the course of individual tooth structures, such as root canals, which greatly facilitates endodontic treatment or endodontic re-treatment, and also makes it possible to detect even the smallest periapical inflammatory foci or external and internal resorption[2]. In orthodontics, CBCT makes it possible to assess bone conditions and plan the range of possible tooth movements while avoiding complications such as fenestrations, dehiscences or recessions.[3]

In implant prosthetics, CBCT can be used to assess the possibility of implantation without additional procedures, such as sinus floor elevation or bone grafting, and if the procedure is necessary, to design its scope and architectonics.[4] After the initial planning of the implant insertion position and path, another digital element facilitating the complicated implantation procedure is the use of a Dynamic Navigation system or specially prepared surgical templates in CAD/CAM technology.[5] Cone beam computed tomography also increases the safety of performed procedures, allowing for precise determination of the location of individual nerve canals, which are anatomically variable.[6]

In addition to CBCT, 3D scanners are also widely used in today's dentistry. Intraoral scanners make it possible to reproduce the patient's occlusion without the use of impression materials.[7] This ensures accurate mapping of the mutual arrangement of teeth, which is necessary for proper diagnosis before orthodontic treatment and assessment of the correctness of the treatment effects, as well as minimizes the impression-taking procedure, which is unpleasant for patients. As a result, it is also possible to avoid distortions in models cast from impressions, when they are stored under inappropriate physical conditions. Owing to scanners, this problem can also be eliminated in prosthetics. They enable to accurately map the tooth preparation border for permanent restorations (inlays, onlays, crowns) directly in the patient's oral cavity, or indirectly, by applying extraoral scanners used in prosthetic laboratories.[8] Using special computer software, it is possible to determine the insertion path, and then fabricate the finished prosthetic appliance (e.g., in CAD/CAM technology) and transfer it into the patient's mouth.

Nowadays, CBCT and scanners are auxiliary tools commonly used in various fields of dentistry, which is the aim of this article. It presents their principles, types, and applications based on academic knowledge and provides the current knowledge contained in articles from the last 5 years available in the US National Library of Medicine National Institutes of Health (PubMed), as well as Scopus and Web of Science databases. The last search was performed on May 10, 2023. Two authors selected and described the articles (WF, AJ), and the 3rd author reviewed them in accordance with the guidelines (MM). The results of their review are presented later in the article.

Objectives

The aim of this study was to present the advantages and possibilities of using CBCT and intraoral scanners in clinical practice during dental procedures, to show their usefulness in planning prosthetic and orthodontic procedures as a tool of modern digital dentistry.

Materials and methods

The present systematic review was conducted in accordance with the Preferred Reporting Items for Systematic Reviews and Meta-Analyses (PRISMA) statement.[9] The study took into account articles from 3 databases: PubMed, Scopus and Web of Science. The initial search took place on March 15, 2023, and included a total of 421 articles. After removing duplicates, 273 articles advanced to the next stage. Articles had to meet criteria such as being written in English and not being older than 5 years. After a deeper analysis, 214 articles were excluded due to a topic other than the main one discussed by the authors. Overall, 28 articles were included for the final description in the review if they met all the criteria, i.e., they referred to CBCT and/or dental scanners used in dentistry. A PRISMA 2022 Flow Diagram representing the study selection process is presented in Fig. 1.

Cone beam tomography in dentistry

It is very interesting to observe how innovative technologies are increasingly applied in dentistry and orthodontics. Cone beam computed tomography, in particular, is becoming the imaging technique of choice in comprehensive orthodontic treatment.[10]

Over the past 2 decades, CBCT, a versatile 3D X-ray imaging technique, has become increasingly popular in the field of dental radiology.[11] Since the development of the first CBCT device specifically for maxillofacial imaging in 1998, the variety of models has increased significantly, especially in the last 10 years.[12]

The CBCT technology uses a conical source of ionizing radiation and a 2-dimensional (2D) monitor.[13] It offers

Identification of studies via databases and registers

Identification

Records identified from*:
Pubmed (n = 214)
Embase (n = 123)
Web of Science (n = 84)

Records removed before screening:
Duplicate records removed
(n = 148)
Records marked as ineligible
by automation tools (n = 0)
Records removed for other reasons
(n = 0)

Screening

Records screened
(n = 273)

Records excluded (completely
different subject, other reviews)
(n = 214)

Reports sought for retrieval
(n = 59)

Reports not retrieved (access
denied due to unavailable database)
(n = 0)

Reports assessed for eligibility
(n = 59)

Reports excluded:
Reason 1 – studies concentrating on others
features of dental scanners (n = 16)
Reason 2 – studies not related to cone
beam tomography (n = 15)

Included

Studies included in review (n = 28)
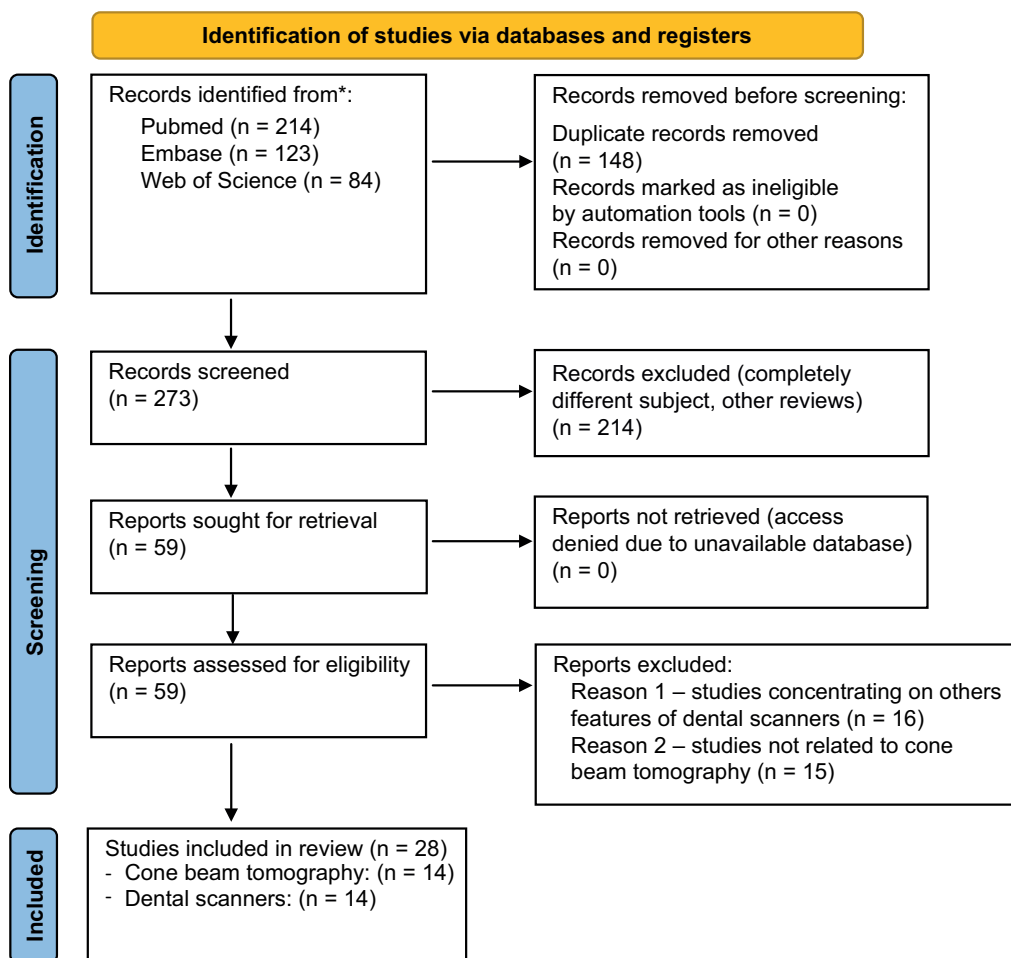- Cone beam tomography: (n = 14)
- Dental scanners: (n = 14)

Fig. 1. Search strategy
– Preferred Reporting Items for
Systematic Reviews and Meta-
Analyses (PRISMA) flow diagram

dimensionally accurate multi-dimensional images for diagnosis and treatment planning. The isotropic voxels (volume elements) in these images provide accurate multiplanar images in any direction.[14] Each volume element has equal dimensions in each of the 3 perpendicular planes.

Principles of CBCT

The principle of CBCT scanning is based on the rotation of a gantry with an X-ray tube and an image detector. The X-ray cone beam is attenuated by the patient's tissues and the imaging area is exposed during scanning. Partial tissue exposure occurs in a rotating region around the imaging area, as the X-ray beam cone sweeps the necessary angular range to obtain the raw projection images used to reconstruct the final 3D CBCT images.[15]

Radiation doses from CBCT devices can be determined using an optically stimulated luminescence dosimeter (OSLD) or the Monte Carlo method. In the first method, a phantom simulating human body tissues in the maxillofacial area was equipped with OSLD and subjected to 4 different test conditions using 2 different devices. The irradiated portion of the skin, lymph nodes and muscles of the head and neck area was estimated to be 5%, and the irradiated portion of the esophagus was estimated at 10%. In both cases, the oral mucosa and salivary glands were the most frequently irradiated organs.[16]

The use of CBCT in prosthetics and orthodontics

The digitization of orthodontic and prosthetics procedures is increasing due to the use of the latest technologies. Currently, better and more individualized treatment planning is possible, largely due to the use of overlays, digital dental models and wider access to CBCT images.[17]

In addition, CBCT offers applications for surgical procedures, such as conducting CT scans with computer-generated surgical templates used in implant prosthetics, as well as enhanced in-office diagnostic capabilities. Current practice requires a thorough understanding of the basics of CBCT science and the ability to accurately and fully interpret images.[18]

The tables below summarize the potential applications and current knowledge on some types and selected properties of CBCT, which is increasingly used in dental prosthetics (Table 1) and orthodontics (Table 2).

Table 1. The use of cone beam computed tomography in prosthodontics in the last 5 years of publications

Number	Author and year	Title	Significance
1.	Al-Humairi et al., 2022[19]	Visual grading experiments and optimization in CBCT dental implantology imaging: Preliminary application of integrated visual grading regression	Optimization of the radiation dose used in the examination in dental implantology – CBCT was used as a tool for visualizing a human skull phantom using a real skull as bone and a plexiglass-like material as soft tissues. Using integrated visual grading regression (IVGR), it was assessed whether it was possible to reduce the amount of radiation during the examination without significantly affecting the image quality. The dose reduction was estimated at 31%, proving that IVGR can be an effective tool to determine reduction not only in CBCT but also in computed tomography (CT) – but more research is needed to confirm it.
2.	Chandran et al., 2022[20]	Guided implant surgery with R2Gate®: A multicenter retrospective clinical study with 1 year of follow-up	Cone beam computed tomography was used to study the patient's anatomy and bone condition before planning implant treatment. The prosthetic laboratory, based on Digital Imaging and Communications in Medicine (DICOM) files, made surgical guides without a guide sleeve in a new, keyless system.
3.	Derksen et al., 2019[21]	The accuracy of computer-guided implant surgery with tooth-supported, digitally designed drill guides based on CBCT and intraoral scanning. A prospective cohort study	Implantation using surgical templates – the initial qualification of patients included 68 study participants. Based on CBCT results, 2 patients were excluded due to insufficient bone width and the need for horizontal bone augmentation. Cone beam computed tomography was also used to determine the standard deviation of the implant position. Digitally designed and printed 3D drill guides/surgical templates were created based on both (intra-oral scans (IOS) and CBCT data.
4.	Horsch et al., 2021[22]	Predictability and image quality of low-dose cone-beam computed tomography in computer-guided implantology: An experimental study	The study was designed to test the predictability and image quality of low-dose cone beam computed tomography (LD-CBCT). The aim was to reduce the radiation dose without compromising image quality and its usefulness in clinical analysis. The apex deflection and deflection angle of LD-CBCT were greater than in the case of high-definition cone beam computed tomography (HD-CBCT), whereas no significant differences were noticed in entry point deviation. Despite the differences, the authors claimed that the advantages of HD-CBCT could be balanced with a higher radiation dose.
5.	Kauling et al., 2019[23]	Can lithium disilicate ceramic crowns be fabricated on the basis of CBCT data?	The fit of lithium disilicate CAD/CAM crowns fabricated on the basis of direct (IOS), indirect (CBCT) digitization of impressions and indirect digitization of plaster cast (extraoral scanners (EOS)) was assessed. Unfortunately, although the marginal fit of CBCT is within the clinically acceptable range, it is significantly inferior to EOS and IOS.
6.	Leisner et al., 2022[24]	Measuring peri-implant bone lesions using low-dose cone-beam computed tomography	The aim of this study was to determine whether peri-implant bone changes could be accurately measured with LD-CBCT, even when the influence of surrounding tissues was taken into account. Although the surrounding tissue degrades the quality of CBCT with an LD image, the differences between the 2 technologies in terms of absolute differences are negligible. Taking into account the limitations of the in vitro study, LD-CBCT may become a useful imaging technique for tracking peri-implantation lesions while exposing patients to much less radiation.
77.	Mauad et al., 2021[25]	Quantitative assessment of artefacts and identification of gaps in prosthetic crowns: A comparative in vitro study between periapical radiography and CBCT images	Determination of the diagnostic precision of CBCT scans and periapical radiographs in identifying gaps in prosthetic crowns and the number of artifacts produced in vitro by 2 separate regenerating materials. Periapical radiography remained the most economical method of identifying the maladjustment of prosthetic restorations. CBCT examinations, although more expensive than ordinary radiovisiography (RVG), did not increase the accuracy of identifying defects in prosthetic crowns. However, they can serve as an additional diagnostic tool.
8.	Polara et al., 2022[26]	Digital immediate tooth restoration: Fabricating acrylic resin interim crowns from CBCT scans for immediate implant-supported prostheses: A case series	The purpose of this clinical study was to describe a method for creating a temporary acrylic resin crown using CBCT information. Using the technique of rapid implant placement and provisional restoration, information from CBCT scans resulted in temporary acrylic resin crowns, which required fewer corrections, thus shortening the time of performing the procedure.

Scanners in dentistry

Intraoral scanners are used to visualize the maxillary and mandibular dental processes together with their soft tissues.[33] They allow for digitization of dental arches to create virtual models that replace conventional dental impressions.

The scanner works by projecting a light source in the form of a laser or structured light to capture 2D images of the object being scanned. The scanner software then processes the captured 2D images to create point clouds, which are triangulated to create a 3D surface model (mesh) of the scanned object.[34]

The history of intraoral scanners dates back to 1985, when a scanner called CEREC 1 was developed by Dentsply Sirona. However, the system created over 30 years ago had its limitations – it provided a 2D view of scanned images and was only used to create posts for immediate cementation.[35]

Table 2. The use of cone beam computed tomography in orthodontics in the last 5 years of publications

Number	Author and year	Title	Significance
1.	Alsino et al., 2022[27]	The diagnostic accuracy of cone-beam computed tomography (CBCT) imaging in detecting and measuring dehiscence and fenestration in patients with class I malocclusion: A surgical-exposure-based validation study	The authors of the article intended to check how CBCT could increase the rate of fenestration and dehiscence detection among patients. Unfortunately, no study evaluated diagnostic accuracy, so pre-orthodontic status was assessed against the gold standard, i.e., actual clinical detection of bone defects during surgical exposure. Compared to the gold standard, the crack detection percentage was 2.5 times higher, and the fenestration detection rate was almost 3 times higher.
2.	Chun et al., 2022[28]	Skeletal and alveolar changes in conventional rapid palatal expansion (RPE) and mini-screw-assisted RPE (MARPE): A prospective randomized clinical trial using low-dose CBCT	Cone beam computed tomography was used to define and visualize skeletal and alveolar changes in conventional rapid palatal expansion (RPE) and mini-screw-assisted RPE (MARPE). The main outcome of this study was the opening of the mid-palatal suture, and the secondary findings were the assessment of the skeleton, dento-alveoli and periodontium, imaged with CBCT.
3.	Halim et al., 2021[29]	Preliminary study: Evaluating the reliability of CBCT images for tongue space measurements in the field of orthodontics	The aim of the study was to assess the accuracy of tongue space measurement, including tongue volume and oral air volume, using CBCT. According to the earliest findings of the study, the landmarks used to calculate the total language space are repeatable and easy to detect using CBCT.
4.	Ruetters et al., 2022[30]	Low-dose CBCT imaging of alveolar buccal bone adjacent to mandibular anterior teeth: A pilot study	The aim of the study was to assess whether CBCT could be used to measure the thickness of the buccal bone in the mandible and in the anterior segment, which would be useful during orthodontic and periodontal treatment. It was noted that low-dose cone beam computed tomography (LD-CBCT) is a sufficiently accurate and practical method for measuring the bone of the buccal alveolar process adjacent to the anterior teeth of the human lower jaw.
5.	van Bunningen et al., 2022[31]	Precision of orthodontic cephalometric measurements on ultra-low dose-low dose CBCT reconstructed cephalograms	The authors of the study aimed to assess whether the use of CBCT could replace the standard radiovisiography (RVG) image/radiograph during cephalometric measurements. Low-dose CBCT was used for this purpose. It turned out that CBCT allows for cephalometric measurements with small differences. However, the significant advantage is the avoidance of a high radiation dose, so using it for these purposes should be considered by orthodontists in the future.
6.	Wang et al., 2021[32]	Multiclass CBCT image segmentation for orthodontics with deep learning	The study describes the use of CBCT for maxillary and mandibular segmentation, necessary to plan the correct orthodontic treatment. This is usually a long-term process performed manually/semi-automatically by the physician, which is why the authors are looking for a new method of segmentation. The study used a new MS-D network (multi-class segmentation) for CBCT scans of the jaw, teeth and background – it achieved segmentation accuracy comparable to binary segmentation, i.e., the one used by default.

Since then, the shortcomings of the scanner have been removed and the device has been improved. The current version of the system is CEREC 3D, and there is a whole list of intraoral scanners available on the market. These include, i.a., Trios 3 and Trios 4, iTero Element, iTero 2, iTero 5D Element, Dental Wings, Panda, Medit i500, Planmeca Emerald™ and Aoralscan. Of these, the Trios series shows the highest scanning accuracy. It should be noted that regardless of the type of scanner used, moving the device away from the scanned image has a negative effect and reduces the accuracy of measurements. The same happens when scanning from a different angle. It has been shown that diagonal scanning reduces the precision of mapping, so it should always be done carefully and in accordance with the manufacturer's recommendations.[36]

In addition to the scanning technique, the operator's experience is important. The more experienced the operator and the smaller the area to be scanned, the more precise the effect is.[37]

Orthodontic scanners are used at the beginning, during and after treatment. There is often a need to obtain an image of full dental arches together with the fixed orthodontic appliances. There may be doubts about the accuracy of the obtained scan. Studies have shown that the presence of orthodontic brackets has no clinically significant effect on the scanning precision.[38]

The use of scanners in prosthetics and orthodontics

For prosthetic reconstruction planning or malocclusion diagnosis, it is important to register occlusal contacts. The intraoral scanner minimizes the need to use occluding papers for this purpose, because the interocclusal record made with intraoral scanners is more accurate than the measurement using traditional physical methods.[39]

An important procedure in both prosthetics and orthodontics is reporting the mutual position of the maxilla and mandible at various stages of treatment. In the case of conventional methods, such registration may give false measurement results due to the deformation of the materials

Table 3. The use of scanners in prosthodontics in the last 5 years of publications

Number	Author and year	Title	Significance
1.	Ashraf et al., 2022[41]	Influence of preparation type and tooth geometry on the accuracy of different intraoral scanners	In the case of complex tooth preparations and non-standard geometries, scanning accuracy decreases. The type of scanner also affects precision – when comparing the 3 Shape Trio, Medit i500 and Cerec Omnicem, there were no significant differences between the first 2, but they showed significantly higher accuracy than Cerem Omnicem, even when the preparation was simple.
2.	Fraile et al., 2022[42]	Clinical study comparing the accuracy of interocclusal records, digitally obtained by three different devices	When comparing the accuracy of occlusal contact measurements made with the intraoral scanner, the extraoral scanner and the T-Scan III system, it was found that the intraoral scanner was the most accurate. The intraoral scanner can be successfully used to examine occlusal contacts.
3.	Park et al., 2021[43]	A digital approach to the evaluation of mandibular position by using a virtual articulator	The use of an intraoral scanner together with CBCT makes it possible to assess the centric relation occlusion (CRO) and the maximal intercuspal position (MIP). This eliminates the need to wear a facebow.
4.	Park et al., 2020[44]	Clinical evaluation of time efficiency and fit accuracy of lithium disilicate single crowns between conventional and digital impression	The impression of abutments for lithium silicate crowns was made by conventional and digital methods using 2 scanners – AEGIS, PO and CEREC Omnicam. The scanning time was shorter compared to the traditional method of taking impressions, which made it possible to make a single crown during one visit. The difference in the accuracy of fitting between the 2 mentioned methods was not statistically significant.
5.	Ren et al., 2020[45]	Accuracy of virtual interocclusal records for partially edentulous patients	The study showed that the intraoral scanner in a partially edentulous arch can be used without fear of a decrease in the accuracy of the virtual record when a single tooth in the posterior segment is missing. When the edentulous area is more extended (3 or more teeth in the anterior and posterior parts of the arch), the record accuracy decreases.
6.	Son et al., 2021[46]	Comparison of intaglio surface adjustment in the oral cavity for lithium disilicate crowns fabricated using different scanners	The intra-oral fitting of crowns made on the basis of a scan taken with 3 scanners was compared with crowns made on the basis of conventional impressions. Intraoral scanners can be used to make fitted crowns instead of the conventional method. However, the study proved that those prepared with impressions require fewer intraoral adjustments.

used. Intraoral scanners overcome this problem – there is no need for materials, so there is no deformation and the results become repeatable.[40]

The following tables summarize the current knowledge on the selected types as well as properties of scanners used in prosthetics (Table 3) and orthodontics (Table 4).

Discussion

Three-dimensional models designed on the basis of CBCT can be used to perform various types of procedures, such as crown lengthening, making a surgical template, or redesigning the patient's occlusion using specialized software. This is possible by converting CBCT images from Digital Imaging and Communications in Medicine (DICOM) files to STL, which in turn can be applied to stereolithographic (STL) files from intraoral scans, and then, using 3D printers, a specific drill guide can be prepared.[55,56] Cone beam computed tomography is also helpful in implant prosthetics. The accuracy of imaging of bone defects around implants using CBCT was assessed by Song et al.[57] The study showed that CBCT is more accurate and reliable than intraoral imaging in detecting, classifying and measuring peri-implant bone defects. Based on the data obtained, it is possible

to take actions whose righteousness could not be confirmed with intraoral imaging alone.

Cone beam computed tomography tools also have their drawbacks as their accuracy can be affected by factors such as patient's movement, metal artifacts, device-specific exposure parameters, software, and manual and automated procedures.[58] They can reduce the precision and reliability of linear measurements in CBCT images.

The development of CBCT and CAD/CAM technologies has made it possible to create partial dentures and single crowns with precise mapping of tooth, arch and bone anatomy. Direct transfer of CBCT data to CAM software can eliminate a number of manufacturing processes. After tooth preparation, crowns can be restored directly on the prepared natural teeth, without the need to take final intraoral impressions thanks to CBCT with a voxel size of 0.125 mm, which is necessary for diagnosis and/or treatment planning.[59] However, CAD/CAM technology is not without its disadvantages, because prosthetic restorations are milled from large blocks and about 90% of the prefabricated blocks are lost during their machining.[60]

Intraoral scanners have significantly shortened the time from the patient's first visit to the completion of treatment. Omitting the stage of making a conventional impression shortens the time needed to send it to the prosthetic

Table 4. The use of scanners in orthodontics in the last 5 years of publications

Number	Author and year	Title	Significance
1.	Burzynski et al., 2018[47]	Comparison of digital intraoral scanners and alginate impressions: Time and patient satisfaction	An intraoral scanner can be a solution for patients who experience discomfort and pain when using standard alginate masses.
2.	Ferraro et al., 2022[48]	Accuracy of three-dimensional printed models derived from cone-beam computed tomography	Intraoral scanners and cone beam computed tomography (CBCT) can be used to measure tooth width and intercanine molar width, giving clinically insignificant discrepancy in results. Most deviations are noted in the area of the molars.
3.	Koch et al., 2022[49]	Accuracy of indirect bonding trays – a measurement algorithm	TRIOS® 3 Shape was used to make a transfer splint, which turned out to be a digital alternative to the conventional one.
4.	Pellitteri et al., 2022[50]	Comparative analysis of intraoral scanners accuracy using 3D software: An in vivo study	An intraoral scanner provides information about the shape and width of dental arches. Among CS3600, CEREC Omnicam and Trios 3Shape, the latter reproduces single teeth most accurately. Comparing the use of scanners to conventional impressions, it can be observed that scanners deform the molar area more than conventional impressions.
5.	Pellitteri et al., 2021[51]	Comparison of the accuracy of digital face scans obtained by two different scanners	The Face Hunter extraoral scanner gives the opportunity to compare key parameters before and after treatment, which is why it is a very good clinical tool for routine assessment of treatment effectiveness. It can also replace the X-ray in the youngest patients. The image obtained from this scanner can be compared with the image of hard tissues obtained from computed tomography.
6.	Sfondrini et al., 2018[52]	Computerized casts for orthodontic purpose using powder-free intraoral scanners: Accuracy, execution time, and patient feedback	Intraoral scanners show accuracy comparable to alginate impressions. They can be used to reduce the waiting time for the final product to be picked up from the lab. Scanning takes less time than taking a conventional impression, which is especially important for patients with a gag reflex.
7.	Schnailendran et al., 2022[53]	Accuracy and reliability of tooth widths and Bolton ratios measured by ClinCheck Pro	The Clincheck Pro scanner was used to measure the tooth width and Bolton ratio. This scanner, compared to the 3D OP and a calibrated digital caliper, underestimates the tooth width.
8.	Song and Kim, 2020[54]	Accuracy on scanned images of full arch models with orthodontic brackets by various intraoral scanners in the presence of artificial saliva	The accuracy of mapping full arches with 3 types of brackets – ceramic, metal, resin, and without brackets using CS3600, i500, Trios3 was compared. Metal or resin brackets showed greater discrepancies. Regardless of the bracket type, CS3600 and Trios3 gave more accurate results than i500.

laboratory, as well as the time needed for corrections caused by a communication error between the doctor and the technician.[61] Regarding the aforementioned communication, the scanner is also a tool that helps in mutual understanding between the doctor and the patient. Presentation of a prosthetic or orthodontic problem by means of a scan displayed on the monitor screen better illustrates the scale of the problem to the patient and makes it possible to avoid misunderstandings resulting in the failure to meet the patient's expectations or irreversible damage to the patient's tissues. In the patient–doctor–technician relationship, the mapping of the patient's oral tissues using a scanner instead of conventional impressions reduces the risk of cross-infection, which is important given the existing problem of unsatisfactory awareness of dental technicians about infection control.[62] Al-Mortadi et al. assessed the knowledge of dental technicians in Jordan about infection control and their practice of disinfection.[63] Over 40% of laboratories admitted that they did not adequately disinfect both alginate and silicone impressions. Most (more than half) of the laboratory owners believe that disinfection of impressions is only the dentist's responsibility before sending them to laboratory, and 38%

of the respondents declared that they did not use gloves in the laboratory.

Specialists from all fields of dentistry, especially orthodontics and prosthetics, would not be able to fully solve the patient's problems without imaging. Scanners are a very good clinical tool for routine assessment of treatment effectiveness. Due to the fact that data are collected in files on a computer, there is no problem with the lack of space for the required storage of plaster models for 20 years after treatment. Nevertheless, the CBCT scanner is quite large, which is its disadvantage, as is its price.[64]

Scanned images provide essential information needed for digitally assisted design and even fabrication of full dentures. Data obtained with scanners are often more precise and accurate than those obtained with analogue impressions.[65] Al-Atyaa and Majeed proved that the impression technique had a significant impact on the marginal and internal seal of CAD/CAM monolithic zirconia crowns.[66]

Differences in mean values of marginal fissures caused by the impression technique were statistically significant. Zirconium oxide crowns made using an intraoral scanner showed a better marginal and internal fit than crowns made

with conventional impression techniques. The authors also noted that, among conventional impressions, a better fit of the crowns is obtained with the use of a two-step rather than one-step impression-taking method. In turn, when comparing the discrepancy in the marginal seal of lithium disilicate crowns made in CAD/CAM technology using conventional impressions and with the use of intraoral scanners, it was found[67] that there is no statistically significant difference in the effects between the above-mentioned impression techniques.

A similar level of accuracy is achieved in the case of crowns made using conventional and digital impressions.

In reviews with meta-analyses performed by other authors, we can find information that IOSs are precise enough to provide full-arch digital impressions that meet clinical requirements. The accuracy of IOS's for complete arches can change depending on the clinical situation. Based on information from articles examined in another systematic review, objectives could not be precisely and objectively defined. The authors do not know which implant impression approach results in a superior passive fit of the superstructure.[68,69]

Limitations

When scanners and CBCT are used, we can count on more accurate imaging of tissues and anatomical structures within the patient's head, but unfortunately there are also limitations to this technology. A large number of studies indicate the advantages of using these devices in everyday clinical practice.

However, taking into account the opinion of many prosthetic technicians working in prosthetic laboratories, it can be noticed that not all scans allow for as accurate reflection of the patient's oral cavity conditions as impressions taken, e.g., with silicone or polyether masses. They believe that impressions prepared with the use of scanners often need additional corrections, which extends the treatment time and causes additional visits to the dentist's office.[46]

In the case of CBCT, the main limitations that may occur during the examination are the high cost of the device, which translates into a higher cost of the examination, limited access to the radiology laboratory, and exposure of the patient to ionizing radiation.[14] The limitation for the physician is mainly the additional need for training, which also generates costs for the office.

Conclusions

Cone beam computed tomography is a tool for in vivo and in vitro examinations of oral cavity tissues. Despite the existing doubts and discussions regarding the safe dose of radiation, it has been proven that cone beam tomography can be applied in various fields of dentistry, from maxillofacial surgery through prosthetics to orthodontics.

Early detection of changes in the bone and its more accurate image help to plan a safe range of tooth movements and to notice early periapical changes that are a contraindication to moving the teeth.

Intraoral scanners allow for hard tissue imaging, which can be useful in prosthetics to determine the margin of preparation during tooth preparation procedures for permanent restorations, and in both prosthetics and orthodontics to determine and design the occlusion.

Despite the discussed applications for both tools, there are still many fields of dentistry and other applications that have not been described so far, and future research may enable their widespread use in everyday dentistry.

ORCID iDs

Wojciech Frąckiewicz   https://orcid.org/0009-0007-0394-820X
Aleksandra Jankowska   https://orcid.org/0009-0006-5268-301X
Monika E. Machoy   https://orcid.org/0000-0001-5787-222X

References

1. Mangano FG, Admakin O, Lerner H, Mangano C. Artificial intelligence and augmented reality for guided implant surgery planning: A proof of concept. *J Dent*. 2023;133:104485. doi:10.1016/j.jdent.2023.104485
2. Setzer FC, Lee SM. Radiology in endodontics. *Dent Clin North Am*. 2021;65(3):475–486. doi:10.1016/j.cden.2021.02.004
3. Kapila SD, Nervina JM. CBCT in orthodontics: Assessment of treatment outcomes and indications for its use. *Dentomaxillofac Radiol*. 2015;44(1):20140282. doi:10.1259/dmfr.20140282
4. Jacobs R, Salmon B, Codari M, Hassan B, Bornstein MM. Cone beam computed tomography in implant dentistry: Recommendations for clinical use. *BMC Oral Health*. 2018;18(1):88. doi:10.1186/s12903-018-0523-5
5. Panchal N, Mahmood L, Retana A, Emery R. Dynamic navigation for dental implant surgery. *Oral Maxillofac Surg Clin North Am*. 2019;31(4):539–547. doi:10.1016/j.coms.2019.08.001
6. Del Lhano NC, Ribeiro RA, Martins CC, Assis NMSP, Devito KL. Panoramic versus CBCT used to reduce inferior alveolar nerve paresthesia after third molar extractions: A systematic review and meta-analysis. *Dentomaxillofac Radiol*. 2020;49(4):20190265. doi:10.1259/dmfr.20190265
7. Abduo J. Accuracy of intraoral scanners: A systematic review of influencing factors. *Eur J Prosthodont Restor Dent*. 2018;(26):101–121. doi:10.1922/EJPRD_01752Abduo21
8. Memari Y, Mohajerfar M, Armin A, Kamalian F, Rezayani V, Beyabanaki E. Marginal adaptation of CAD/CAM All-ceramic crowns made by different impression methods: A literature review. *J Prosthodont*. 2019;28(2):e536–e544. doi:10.1111/jopr.12800
9. Page MJ, McKenzie JE, Bossuyt PM, et al. The PRISMA 2020 statement: An updated guideline for reporting systematic reviews. *BMJ*. 2021;372:n71. doi:10.1136/bmj.n71
10. Machado GL. CBCT imaging: A boon to orthodontics. *Saudi Dent J*. 2015;27(1):12–21. doi:10.1016/j.sdentj.2014.08.004
11. Kaasalainen T, Ekholm M, Siiskonen T, Kortesniemi M. Dental cone beam CT: An updated review. *Phys Med*. 2021;88:193–217. doi:10.1016/j.ejmp.2021.07.007
12. Gaêta-Araujo H, Leite AF, Vasconcelos KDF, Jacobs R. Two decades of research on CBCT imaging in DMFR: An appraisal of scientific evidence. *Dentomaxillofac Radiol*. 2021;50(4):20200367. doi:10.1259/dmfr.20200367
13. De Vos W, Casselman J, Swennen GRJ. Cone-beam computerized tomography (CBCT) imaging of the oral and maxillofacial region: A systematic review of the literature. *Int J Oral Maxillofac Surg*. 2009;38(6):609–625. doi:10.1016/j.ijom.2009.02.028
14. Abdelkarim A. Cone-beam computed tomography in orthodontics. *Dent J*. 2019;7(3):89. doi:10.3390/dj7030089
15. Kiljunen T, Kaasalainen T, Suomalainen A, Kortesniemi M. Dental cone beam CT: A review. *Phys Med*. 2015;31(8):844–860. doi:10.1016/j.ejmp.2015.09.004

16. Lee C, Yoon J, Han SS, et al. Dose assessment in dental cone-beam computed tomography: Comparison of optically stimulated luminescence dosimetry with Monte Carlo method. *PLoS One*. 2020;15(3): e0219103. doi:10.1371/journal.pone.0219103

17. Bianchi J, Mendonca G, Gillot M, et al. Three-dimensional digital applications for implant space planning in orthodontics: A narrative review. *J World Fed Orthod*. 2022;11(6):207–215. doi:10.1016/j.ejwf. 2022.10.006

18. Greenberg AM. Cone beam computed tomography scanning and diagnosis for dental implants. *Oral Maxillofac Surg Clin North Am*. 2015;27(2):185–202. doi:10.1016/j.coms.2015.01.002

19. Al-Humairi A, Ip RHL, Spuur K, Zheng X, Huang B. Visual grading experiments and optimization in CBCT dental implantology imaging: Preliminary application of integrated visual grading regression. *Radiat Environ Biophys*. 2022;61(1):133–145. doi:10.1007/s00411-021-00959-x

20. Chandran S, Sers L, Picciocchi G, et al. Guided implant surgery with R2Gate®: A multicenter retrospective clinical study with 1 year of follow-up. *J Dent*. 2022;127:104349. doi:10.1016/j.jdent.2022.104349

21. Derksen W, Wismeijer D, Flügge T, Hassan B, Tahmaseb A. The accuracy of computer-guided implant surgery with tooth-supported, digitally designed drill guides based on CBCT and intraoral scanning: A prospective cohort study. *Clinical Oral Implants Res*. 2019;30(10): 1005–1015. doi:10.1111/clr.13514

22. Horsch L, Labis C, Trebing CT, et al. Predictability and image quality of low-dose cone-beam computed tomography in computer-guided implantology: An experimental study. *J Dent*. 2021;112:103744. doi:10.1016/j.jdent.2021.103744

23. Kauling AEC, Keul C, Erdelt K, Kühnisch J, Güth JF. Can lithium disilicate ceramic crowns be fabricated on the basis of CBCT data? *Clin Oral Invest*. 2019;23(10):3739–3748. doi:10.1007/s00784-019-02802-6

24. Leisner LC, Tasaka A, Trebing CT, et al. Measuring peri-implant bone lesions using low-dose cone-beam computed tomography. *J Prosthodont Res*. 2022;66(2):326–332. doi:10.2186/jpr.JPR_D_20_00110

25. Mauad LQ, Doriguêtto PVT, Almeida DD, Fardim KAC, Machado AH, Devito KL. Quantitative assessment of artefacts and identification of gaps in prosthetic crowns: A comparative in vitro study between periapical radiography and CBCT images. *Dentomaxillofac Radiol*. 2021;50(3):20200134. doi:10.1259/dmfr.20200134

26. Polara G, Pistone F, Giorgio Alfredo S. Digital immediate tooth restoration: Fabricating acrylic resin interim crowns from CBCT scans for immediate implant-supported prostheses. A case series. *J Prosthet Dent*. 2022;127(4):578–584. doi:10.1016/j.prosdent.2020.09.042

27. Alsino HI, Hajeer MY, Alkhouri I, Murad RMT. The diagnostic accuracy of cone-beam computed tomography (CBCT) imaging in detecting and measuring dehiscence and fenestration in patients with class malocclusion: A surgical-exposure-based validation study. *Cureus*. 2022;14(3):e22789. doi:10.7759/cureus.22789

28. Chun JH, De Castro ACR, Oh S, et al. Skeletal and alveolar changes in conventional rapid palatal expansion (RPE) and miniscrew-assisted RPE (MARPE): A prospective randomized clinical trial using low-dose CBCT. *BMC Oral Health*. 2022;22(1):114. doi:10.1186/s12903-022-02138-w

29. Halim IA, Park JH, Liou EJW, Zeinalddin M, Al Samawi YS, Bay RC. Preliminary study: Evaluating the reliability of CBCT images for tongue space measurements in the field of orthodontics. *Oral Radiol*. 2021;37(2):256–266. doi:10.1007/s11282-020-00443-0

30. Ruetters M, Gehrig H, Kronsteiner D, et al. Low-dose CBCT imaging of alveolar buccal bone adjacent to mandibular anterior teeth: A pilot study. *Clin Oral Invest*. 2022;26(5):4173–4182. doi:10.1007/s00784-022-04389-x

31. Van Bunningen RH, Dijkstra PU, Dieters A, Van Der Meer WJ, Kuijpers-Jagtman AM, Ren Y. Precision of orthodontic cephalometric measurements on ultra low dose-low dose CBCT reconstructed cephalograms. *Clin Oral Invest*. 2022;26(2):1543–1550. doi:10.1007/s00784-021-04127-9

32. Wang H, Minnema J, Batenburg KJ, Forouzanfar T, Hu FJ, Wu G. Multiclass CBCT image segmentation for orthodontics with deep learning. *J Dent Res*. 2021;100(9):943–949. doi:10.1177/00220345211005338

33. Goodacre B, Goodacre C, Baba N. Using intraoral scanning to capture complete denture impressions, tooth positions, and centric relation records. *Int J Prosthodont*. 2018;31:377–381. doi:10.11607/ijp.5741

34. Osman RB, Alharbi NM. Influence of scan technology on the accuracy and speed of intraoral scanning systems for the edentulous maxilla: An in vitro study [published online ahead of print on December 26, 2022]. *J Prosthet Dent*. 2022. doi:10.1111/jopr.13633

35. Sannino G, Germano F, Arcuri L, Bigelli E, Arcuri C, Barlattani A. CEREC CAD/CAM chairside system. *Oral Implantol (Rome)*. 2014;7(3):57–70. PMID:25992260. PMCID:PMC4402686.

36. Amornvit P, Rokaya D, Sanohkan S. Comparison of accuracy of current ten intraoral scanners. *Biomed Res Int*. 2021;2021:2673040. doi:10.1155/2021/2673040

37. Kustrzycka D, Marschang T, Mikulewicz M, Grzebieluch W. Comparison of the accuracy of 3D images obtained from different types of scanners: A systematic review. *J Healthcare Eng*. 2020;2020:8854204. doi:10.1155/2020/8854204

38. Kang SJ, Kee YJ, Lee KC. Effect of the presence of orthodontic brackets on intraoral scans. *Angle Orthod*. 2021;91(1):98–104. doi:10.2319/040420-254.1

39. Solaberrieta E, Otegi JR, Goicoechea N, Brizuela A, Pradies G. Comparison of a conventional and virtual occlusal record. *J Prosthet Dent*. 2015;114(1):92–97. doi:10.1016/j.prosdent.2015.01.009

40. Li J, Galli M, Chen Z, Venezia P, Mangano F, Lepidi L. A novel digital technique for maintaining maxillomandibular relations in fixed prosthetic rehabilitations. *J Dent*. 2021;114:103798. doi:10.1016/j.jdent.2021.103798

41. Ashraf Y, Sabet A, Hamdy A, Ebeid K. Influence of preparation type and tooth geometry on the accuracy of different intraoral scanners. *J Prosthodont*. 2020;29(9):800–804. doi:10.1111/jopr.13202

42. Fraile C, Ferreiroa A, Romeo M, Alonso R, Pradíes G. Clinical study comparing the accuracy of interocclusal records, digitally obtained by three different devices. *Clin Oral Invest*. 2022;26(2):1957–1962. doi:10.1007/s00784-021-04174-2

43. Park JH, Lee GH, Moon DN, Kim JC, Park M, Lee KM. A digital approach to the evaluation of mandibular position by using a virtual articulator. *J Prosthet Dent*. 2021;125(6):849–853. doi:10.1016/j.prosdent.2020.04.002

44. Park JS, Lim YJ, Kim B, Kim MJ, Kwon HB. Clinical evaluation of time efficiency and fit accuracy of lithium disilicate single crowns between conventional and digital impression. *Materials (Basel)*. 2020;13(23): 5467. doi:10.3390/ma13235467

45. Ren S, Morton D, Lin WS. Accuracy of virtual interocclusal records for partially edentulous patients. *J Prosthet Dent*. 2020;123(6):860–865. doi:10.1016/j.prosdent.2019.08.013

46. Son K, Yu B, Lee J, Son Y, Lee K. Comparison of Intaglio surface adjustment in the oral cavity for lithium disilicate crowns fabricated using different scanners. *J Prosthodont*. 2021;30(3):276–281. doi:10.1111/jopr.13259

47. Burzynski JA, Firestone AR, Beck FM, Fields HW, Deguchi T. Comparison of digital intraoral scanners and alginate impressions: Time and patient satisfaction. *Am J Orthod Dentofacial Orthop*. 2018;153(4): 534–541. doi:10.1016/j.ajodo.2017.08.017

48. Ferraro JM, Falter J, Lee S, et al. Accuracy of three-dimensional printed models derived from cone-beam computed tomography. *Angle Orthod*. 2022;92(6):722–727. doi:10.2319/021122-128.1

49. Koch P, Albrecht M, Lin W, Jost-Brinkmann P. Accuracy of indirect bonding trays: A measurement algorithm. *Int J Comput Dent*. 2022; 25(3):295–302. doi:10.3290/j.ijcd.b2599775

50. Pellitteri F, Albertini P, Vogrig A, Spedicato GA, Siciliani G, Lombardo L. Comparative analysis of intraoral scanners accuracy using 3D software: An in vivo study. *Prog Orthod*. 2022;23(1):21. doi:10.1186/s40510-022-00416-5

51. Pellitteri F, Brucculeri L, Spedicato GA, Siciliani G, Lombardo L. Comparison of the accuracy of digital face scans obtained by two different scanners. *Angle Orthod*. 2021;91(5):641–649. doi:10.2319/092720-823.1

52. Sfondrini MF, Gandini P, Malfatto M, Di Corato F, Trovati F, Scribante A. Computerized casts for orthodontic purpose using powder-free intraoral scanners: Accuracy, execution time, and patient feedback. *Biomed Res Int*. 2018;2018:4103232. doi:10.1155/2018/4103232

53. Shailendran A, Weir T, Freer E, Kerr B. Accuracy and reliability of tooth widths and Bolton ratios measured by ClinCheck Pro. *Am J Orthod Dentofacial Orthop*. 2022;161(1):65–73. doi:10.1016/j.ajodo.2020.06.048

54. Song J, Kim M. Accuracy on scanned images of full arch models with orthodontic brackets by various intraoral scanners in the presence of artificial saliva. *Biomed Res Int*. 2020;2020:2920804. doi:10.1155/2020/2920804

55. Gialain IO, Pinhata-Baptista OH, Cavalcanti MGP, Cortes ARG. Computer-aided design/computer-aided manufacturing milling of allogeneic blocks following three-dimensional maxillofacial graft planning. *J Craniofac Surg*. 2019;30(5):e413–e415. doi:10.1097/SCS.0000000000005353

56. Passos L, Soares FP, Choi IGG, Cortes ARG. Full digital workflow for crown lengthening by using a single surgical guide. *J Prosthet Dent*. 2020;124(3):257–261. doi:10.1016/j.prosdent.2019.06.027

57. Song D, Shujaat S, De Faria Vasconcelos K, et al. Diagnostic accuracy of CBCT versus intraoral imaging for assessment of peri-implant bone defects. *BMC Med Imaging*. 2021;21(1):23. doi:10.1186/s12880-021-00557-9

58. Fokas G, Vaughn VM, Scarfe WC, Bornstein MM. Accuracy of linear measurements on CBCT images related to presurgical implant treatment planning: A systematic review. *Clinical Oral Implants Res*. 2018;29(S16):393–415. doi:10.1111/clr.13142

59. Şeker E, Ozcelik TB, Rathi N, Yilmaz B. Evaluation of marginal fit of CAD/CAM restorations fabricated through cone beam computerized tomography and laboratory scanner data. *J Prosthet Dent*. 2016;115(1):47–51. doi:10.1016/j.prosdent.2015.08.006

60. Wang W, Yu H, Liu Y, Jiang X, Gao B. Trueness analysis of zirconia crowns fabricated with 3-dimensional printing. *J Prosthet Dent*. 2019;121(2):285–291. doi:10.1016/j.prosdent.2018.04.012

61. Mangano F, Gandolfi A, Luongo G, Logozzo S. Intraoral scanners in dentistry: A review of the current literature. *BMC Oral Health*. 2017;17(1):149. doi:10.1186/s12903-017-0442-x

62. Al-Aali K, Binalrimal S, AlShedokhi A, Al Saqer E, AlHumaid M. Infection control awareness level among dental laboratory technicians, Riyadh, Saudi Arabia. *J Family Med Prim Care*. 2021;10(4):1540. doi:10.4103/jfmpc.jfmpc_2258_20

63. Al Mortadi N, Al-Khatib A, Alzoubi KH, Khabour OF. Disinfection of dental impressions: Knowledge and practice among dental technicians. *Clin Cosmet Investig Dent*. 2019;11:103–108. doi:10.2147/CCIDE.S205144

64. Nasseh I, Al-Rawi W. Cone beam computed tomography. *Dent Clin North Am*. 2018;62(3):361–391. doi:10.1016/j.cden.2018.03.002

65. Impellizzeri A, Horodynski M, De Stefano A, et al. CBCT and intra-oral scanner: The advantages of 3D technologies in orthodontic treatment. *Int J Environ Res Public Health*. 2020;17(24):9428. doi:10.3390/ijerph17249428

66. Al-Atyaa TZ, Majeed AM. Comparative evaluation of the marginal and internal fitness of monolithic CAD/CAM zirconia crowns fabricated from different conventional impression techniques and digital impression using silicone replica technique (an in vitro study). *Biomed Pharmacol J*. 2018;11(1):477–490. doi:10.13005/bpj/1397

67. Abdel-Azim T, Rogers K, Elathamna E, Zandinejad A, Metz M, Morton D. Comparison of the marginal fit of lithium disilicate crowns fabricated with CAD/CAM technology by using conventional impressions and two intraoral digital scanners. *J Prosthet Dent*. 2015;114(4):554–559. doi:10.1016/j.prosdent.2015.04.001

68. García-Gil I, Cortés-Bretón-Brinkmann J, Jiménez-García J, Peláez-Rico J, Suárez-García M. Precision and practical usefulness of intraoral scanners in implant dentistry: A systematic literature review. *J Clin Exp Dent*. 2020;12(8):e784–e793. doi:10.4317/jced.57025

69. Vitai V, Németh A, Sólyom E, et al. Evaluation of the accuracy of intraoral scanners for complete-arch scanning: A systematic review and network meta-analysis. *J Dent*. 2023;137:104636. doi:10.1016/j.jdent.2023.104636

Current role of intravascular imaging in percutaneous treatment of calcified coronary lesions

Oscar Rakotoarison[1,2,A–F], Tomasz Roleder[3,4,A,E,F], Wojciech Zimoch[1,2,E,F],
Wiktor Kuliczkowski[1,2,E,F], Krzysztof Reczuch[1,2,E,F], Piotr Kübler[1,2,A,C,E,F]

[1] Institute of Heart Diseases, Wroclaw Medical University, Poland

[2] Institute of Heart Diseases, Jan Mikulicz-Radecki University Hospital, Wrocław, Poland

[3] Department of Cardiology, J. Gromkowski Regional Specialist Hospital, Wrocław, Poland

[4] Department of Cardiology and Structural Heart Diseases, Medical University of Silesia, Katowice, Poland

A – research concept and design; B – collection and/or assembly of data; C – data analysis and interpretation;
D – writing the article; E – critical revision of the article; F – final approval of the article

Abstract

Percutaneous treatment of calcified coronary lesions is still a challenge in modern interventional cardiology practice. Coronary angiography is limited to the precise and quantitative assessment of calcium in coronary arteries. Intracoronary imaging (ICI) modalities, including optical coherence tomography (OCT) and intravascular ultrasound (IVUS), produce a very detailed image of calcifications and could help in proper percutaneous treatment. Intracoronary imaging indicates the need to use additional tools and improves the final effect of an intervention. Drawing on the already published literature, the authors focused on the qualification of patients to the procedure, conduct and result of interventional procedures involving calcified lesions supported by ICI. The article shows the advantages and disadvantages of both ICI methods in general and especially in calcified lesions. Currently available tools dedicated to dealing with coronary calcium and helping to meet optimal stent implantation criteria are also described. This article reviews the data on ICI implementation in daily clinical practice to improve the results of percutaneous interventions, and indicates further directions.

Key words: coronary artery disease, percutaneous coronary intervention, coronary stenosis

1278

O. Rakotoarison et al. Intravascular imaging of coronary calcium

Background

Coronary artery disease (CAD) is one of the most common conditions in the current population. Coronary atheroma is composed of lipid-rich and calcified lesions. Detection and appropriate modification of coronary artery calcification (CAC) remain one of the last unmet clinical needs in interventional cardiology. Coronary artery calcification is a frequent problem encountered during percutaneous coronary intervention (PCI) in various patient populations.[1] Among the 8,582 patients included in the multicenter ADAPT-DES study focused on the drug-eluting stent (DES), calcifications were present in 30.8% of patients,[2] and similar frequency was reported in many other publications.[3] Age, hypertension, hyperlipidemia, nicotinism, insulin-dependent diabetes mellitus, hemodialysis, and peripheral artery disease were independent predictors of coronary calcification.[2]

Coronary artery calcification may lead to unsatisfying results of stent implantation, causing its underexpansion,[4] assymetry[5] and inappropriate struts apposition[6] despite using special tools for calcium modification. Even nowadays the treatment of this population is very difficult, as was reported in a meta-analysis[7] of 2,361 patients with new-generation DES. Patients with moderate/severe calcifications had higher rate of target-lesion failure (13.5% vs 8.4%; p = 0.003) and stent thrombosis (2.1% vs 0.2%; p < 0.0001). Bourantas et al.[8] found a lower rate of complete revascularization (48% vs 55.6%; p < 0.001) among 6,269 patients with severe calcifications. Moreover, patients with severe calcifications had a higher mortality rate compared to those without calcifications (10.8% vs 4.4%; p < 0.001). Another large meta-analysis[3] of 18 randomized DES trials confirmed worse PCI outcomes for moderately/severely calcified coronary lesions. The 5-years risk of a composite endpoint including death, myocardial infarction, revascularization (adjusted HR: 1.12; 95% CI: 1.05–1.20), target lesion failure (adjusted HR: 1.21; 95% CI: 1.09–1.34), as well as death, myocardial infarction, and ischemia-driven target lesion revascularization was higher in patients with severe CAC.

As technology has advanced, interventional cardiology has been equipped with advanced tools for detecting and assessing CAC and thus for planning interventions in CAC such as intracoronary imaging (ICI). Intravascular ultrasound (IVUS) and optical coherence tomography (OCT) are nowadays widely employed in catheterization laboratories. Intracoronary imaging helps to assess the burden of CAC and choose appropriate treatment strategy at a time when multiple dedicated calcium management tools are available. This article presents how ICI facilitates the management of CAC during PCI.

Objectives

The aim of this review was to provide comprehensive information about the use of ICI in percutaneous treatment of calcified coronary lesions.

Formation and histology of coronary calcifications

The process of calcium formation is not fully understood and involves multiple factors and cells. Nowadays, arterial mineralization process is considered to be the main driver of lesion calcification. The loss of function of osteopontin, fetuin, gamma-carboxyglutamic acid and Gia protein, which inhibits mineralization and the induction of osteogenesis by osteoblast-like cells, is the beginning of CAC formation.[9] Vascular smooth muscle cells are induced to an osteoblastic phenotype. Residual pericytes and circulating stem cells are activated to osteochondrogenic phenotype. Furthermore, the process is associated with oxidative stress, inflammation and lipids. There are 2 types of CAC: intimal (also called: vascular, atherosclerotic) and medial. In the 1st type, the intima thickens as a response to the following clinical risk factors: advanced age, diabetes mellitus, dyslipidemia, hypertension, male sex, nicotinism, and hyperphosphatemia. The 2nd type is connected with the thickening of the medial layer of the artery, and is more common in patients of advanced age with diabetes mellitus, lower glomerular filtration rate, hypercalcemia, hyperphosphatemia, and long duration of dialysis.[10] An analysis of 902 histological cross-sections from 44 cadavers revealed 4 types of calcifications – superficial (158 (18%)), deep intimal (20 (13%)), scattered (30 (19%)), and calcified nodules (CN) (3 (2%)).[11] Chronic coronary syndrome is connected with extensive calcium formation.[12] Statin therapy reduces fibrofatty tissue volume, but promotes the increase of calcium volume in atherosclerotic plaques.[13] However, about 5% of cases of acute coronary syndrome (ACS) are caused by eruptive CN. This mechanism was described by Torii et al., who suggested that fragmentation of the necrotic core causes CN disruption and formation of thrombosis.[14]

Intracoronary imaging

General information

Both IVUS and OCT probes are monorail catheters inserted into the coronary vessels using a conventional 0.014″ guidewire. Optical coherence tomography uses near-infrared light waves (wavelength of approx. 1,300 nm), whereas IVUS imaging relies on emission and detection of 20–60 MHz sound waves bouncing back from the artery wall. Multiple advantages and disadvantages of different ICI modalities result from their physical principles (Table 1).[15–17]

Intracoronary imaging for PCI in general

Traditional coronary angiography (CA) is a standard for lesions assessment and PCI guidance. Unfortunately, the 2-dimensional lumenogram has too many limitations to give appropriate insight into 3-dimensional (3D) structures.

Table 1. Advantages and disadvantages of OCT and IVUS

ICI	Advantages	Disadvantages
OCT	• high resolution (axial 12–15 µm; lateral 20–40 µm) • better tissue characterization (more details visualized: malapposition, dissection, thrombus, tissue protrusion) • easier to interpretate • calcium thickness assessment possible • long and fast pull-back	• flushing required (poor flushing interrupts/impedes image interpretation), low likelihood of dissection, hematoma • additional contrast injection • low penetration (1.0–2.5 mm) • difficult probe delivery in complex lesions • less research data in comparison with IVUS
IVUS	• deep penetration (>5 mm: to adventitia) • flushing is not necessary: lower likelihood of dissection, hematoma • long and fast pull-back • more research data in comparison with OCT	• inferior resolution (axial – 100–300 µm, up to 22 µm (60 MHz); lateral 150–300 µm, 50–140 µm) • worse detection of tissue details • limited tissue interpretation • calcium thickness assessment impossible • difficult probe delivery in complex lesions

ICI – intracoronary imaging; IVUS – intravascular ultrasound; OCT – optical coherence tomography.

Technological progress has provided modern cardiology new, immensely helpful and accurate tools to meet current requirements. Intracoronary imaging has become a method that broadens insight into plaque morphology, often changing clinical decisions during percutaneous procedures. Intravascular ultrasound and OCT are increasingly popular instruments used in catheter laboratories worldwide. Other ICI methods, i.e., near-infrared spectroscopy or virtual-histology IVUS, are dedicated to evaluate lipid-rich plaques and are therefore not described in this article.

A meta-analysis conducted by Darmoch et al.[18] clearly showed the superiority of IVUS-guided compared to CA-guided PCIs in the reduction of cardiovascular death (risk ratio (RR): 0.63; 95% CI: 0.54–0.73), myocardial infarction (RR: 0.71; 95% CI: 0.58–0.86), target lesion revascularization (RR: 0.81; 95% CI: 0.70–0.94), and stent thrombosis (RR: 0.57; 95% CI: 0.41–0.79). Three-year results from the ULTIMATE trial[19] (CA vs IVUS-guided PCI) demonstrated a lower rate of target vessel failure (47 vs 76; p = 0.01) and stent thrombosis (0.1% vs 1.1%; p = 0.02) in the IVUS group. Procedural data presented possible explanation for the difference in 3-year outcomes.[20] Patients in the IVUS-guided group received longer (49.99 ±25.10 mm vs 47.38 ±22.42 mm; p = 0.02) and larger (3.14 ±0.51 mm vs 2.97 ±0.48 mm; p < 0.001) stents, and post-dilatation, larger non-compliant balloon catheters (3.73 ±0.56 mm vs 3.51 ±0.53 mm; p < 0.001) were used at higher pressures (19.7 ±3.7 atm vs 19.0 ±3.7 atm; p < 0.001). Same as with IVUS-guided PCI, studies on OCT-guided PCI demonstrated superiority in relation to CA-guidance alone.

Kuku et al.,[21] in their meta-analysis, showed results from 1,753 percutaneous procedures and found lower rates of MACE (odds ratio (OR): 0.70 (0.49, 1.00) p = 0.05) and cardiac deaths (OR: 0.40 (0.18, 0.90) p = 0.03). Furthermore, they compared results from OCT and IVUS-guided PCIs, and did not conclude that either method is superior.

A large observational study on Pan-London PCI cohort[22] included 87,166 patients who underwent CA-guided PCI (75,046; 86.1%), IVUS (10,539; 12.6%) and OCT (1,149;1.3%). All-cause mortality was established as primary endpoint at median follow up of 4.8 years. The results clearly showed the superiority of OCT guidance in terms of lowering incidence rate of the primary endpoint (7.7%) compared with IVUS (12.2%) or CA (15.7%; p < 0.0001) in general, as well as in chronic (p < 0.0001) and acute coronary syndrome patients (p < 0.0024). Procedural details revealed that the group of OCT patients had longer and bigger stents (25.8 ±13.9 mm; 3.48 ±2.43) than the IVUS group (23.5 ±13.5 mm; 3.59 ±3.46) and the CA group (21.0 ±11.9 mm; 3.20 ±3.23).

A detailed analysis of various aspects imaged using different modalities presents a possible mechanism for their advantages and disadvantages. The OPUS-CLASS study[23] proved the accuracy of the intracoronary OCT diameter measurements, which were equal to the phantom diameters. A large, prospective, 3-arm, single-blinded, multicenter ILUMIEN III trial[24] was designed to establish whether OCT-guidance has any advantage in terms of minimal stent area (MSA) achieved during PCI over the IVUS and/or CA guidance. A total of 450 patients were randomly allocated to the OCT (158 (35%)), IVUS (146 (32%)) and CA-alone (146 (32%)) groups, and the results did not demonstrate OCT to be superior to IVUS. However, post-PCI findings showed lower rate of untreated major dissections (OCT 14% vs IVUS 26% vs CA 19%; for OCT vs IVUS p = 0.009, for OCT vs CA p = 0.25) and major malappositions (OCT 11% vs IVUS 21% vs CA 31%; for OCT vs IVUS p = 0.02, for OCT vs CA p < 0.0001) among OCT-group patients in comparison to IVUS and CA patients. Twelve-month observation of the ILUMIEN III trial population[25] did not show significant clinical results.

Recently published ILUMIEN IV trial[26] indicated larger MSA in OCT-guided PCI group in comparison to angiography guidance group (5.72 ±2.04 mm^2 vs 5.36 ±1.87 mm^2; 95% CI 0.21–0.51; p < 0.001). There was no difference in incidence of target-vessel failure at 2 years observation in both groups.

Intracoronary imaging for calcified lesions

Intracoronary imaging presents CAC in a distinct way due to its physical principles. Optical coherence

tomography depicts a calcified plaque as a sharp, well-demarcated, bordered, signal-poor region (Fig. 1), and CN as a protruding area of calcium, which could be connected to an overlying thrombus and/or fibrous cap disruption (Fig. 2).[27] Intravascular ultrasound, on the other hand, shows CAC as a bright echo with shadowing caused by impermeability of ultrasounds through calcium. Due to the good penetration of ultrasounds, the leading edge of the acoustic shadow in the shallow half (superficial CAC) (Fig. 1,3), as well as in the deeper half of the vessel (deep CAC), can be detected (Fig. 4).[28] In comparison with CA, IVUS detects calcium more often (38% vs 73%; p < 0.0001).[29] Greater arc, length, as well as superficial location, concordant distribution (CAC within 45° to the max. plaque thickness) were associated with better detection of CAC in CA. Another study, published by Wang et al.,[30]

confirmed the superiority of IVUS in terms of calcium detection (82.7% (364 of 440)) in relation to CA (40.2% (177 of 440)) and OCT (76.8% (338)). Coronary angiography has a high specificity in identifying OCT CAC of 95.1% and IVUS CAC of 98.7%, but low sensitivity – 50.9% and 48.4%, respectively. A detailed analysis clarifies why 26 calcified lesions were detected only with IVUS in this study: plaque attenuation in 15 superficial CACs concealed the morphology in OCT, and 11 were located too deep for OCT penetration. Furthermore, the researchers presented values that predict visible calcification of CA: 110° maximum calcium

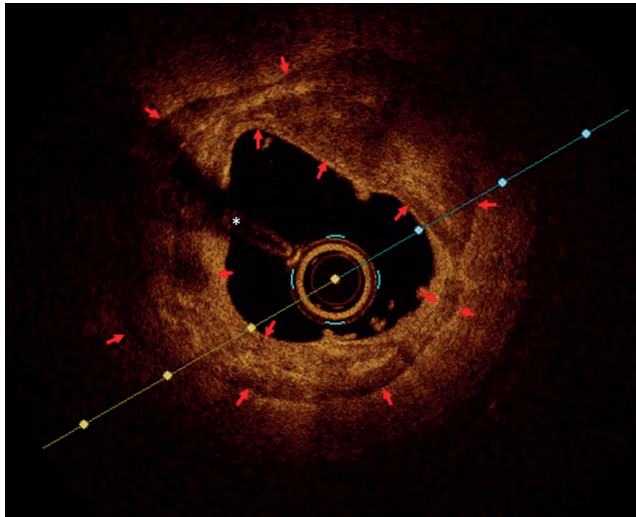**Fig. 3.** Superficial, 360° calcification, wire artifact (white asterisk) – intravascular ultrasound

Fig. 1. Coronary calcification – sharp, well-demarcated, bordered, signal-poor region, superficial, 360° (red arrows), wire artifact (white asterisk) – optical coherence tomography
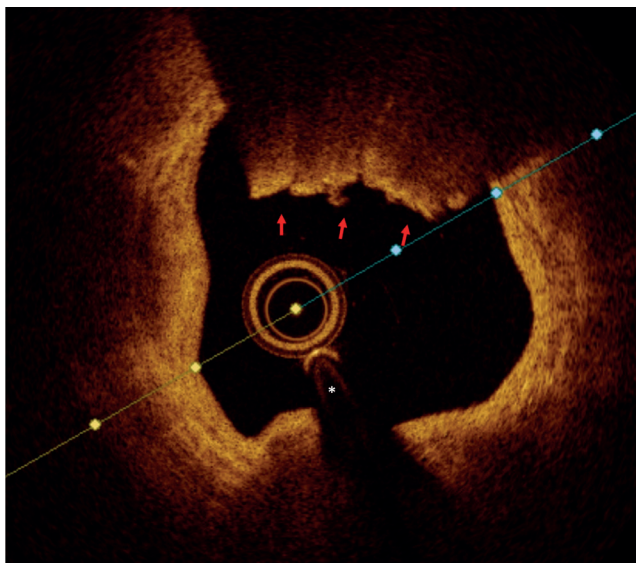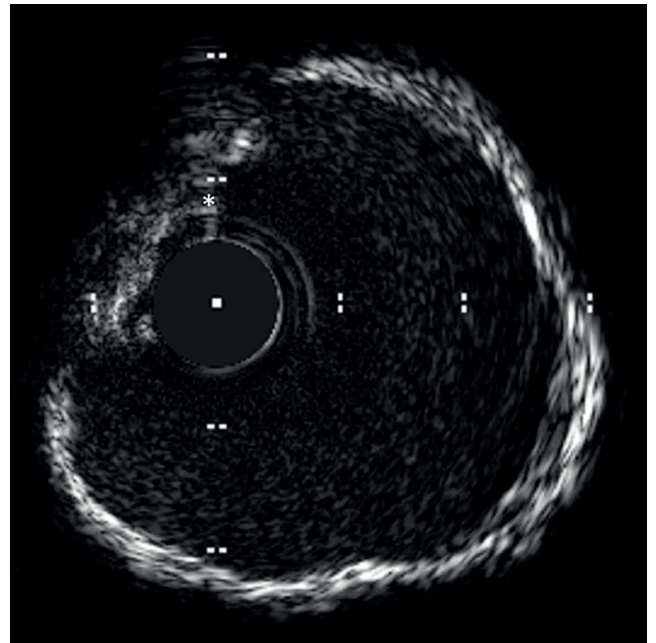

Fig. 2. Protruding calcified nodule (red arrow), wire artifact (white asterisk) – optical coherence tomography
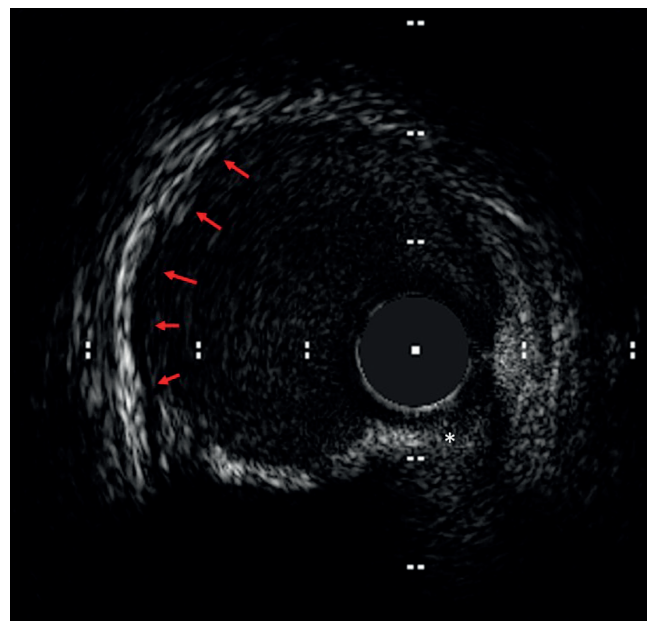

Fig. 4. Deep calcification (red arrows), wire artifact (white asterisk) – intravascular ultrasound

angle in IVUS (area under curve (AUC): 0.80, 95% CI: 0.76–0.83; p < 0.0001) and for OCT, calcium angle of 101° (AUC: 0.78, 95% CI: 0.73–0.81; p < 0.0001), 4.0 mm length (AUC: 0.81, 95% CI: 0.77–0.84; p < 0.0001), and 0.57 mm thickness (AUC: 0.80, 95% CI: 0.76–0.84; p < 0.0001). Mintz et al.[29] classified CAC visible in CA as non/mild, moderate (radiopacities visible only during cardiac motion) or severe (radiopacities on both sides of the vessel, visible without cardiac motion), and IVUS CAC intensity was correlated with this classification.

The next step for the proper treatment of a calcified lesion is adequate evaluation of its burden. Intravascular ultrasound, due to impermeability of ultrasounds through calcium, cannot image more than its proximal border, causing an underestimation of the calcium area in relation to histology and OCT.[31] There was a strong correlation between the lumen and the arc of calcification measured using OCT, IVUS and histology. The accuracy of OCT assessment of CAC was also investigated on cadaveric coronary arteries in a more recent study by Mehanna et al.,[32] in which 1,285 cryo-images were compared with 257 OCT images. The study results prove a high agreement between both methods. Mean calcium depth (0.25 ±0.09 mm vs 0.26 ±0.12 mm; p = 0.742; R = 0.90) and mean calcium angle (35.33 ±21.86° vs 39.68 ±26.61°; p = 0.207; R = 0.90) were similar. There was a limitation in the evaluation of calcium volume only in the case of inability to visualize its distal border, which required trace interpolation and turned out to under-report CAC volume (3.11 ±2.14 vs 4.58 ±3.39 mm; p = 0.001). Intracoronary imaging is very helpful to plan PCI, but OCT and IVUS probes in particularly severely calcified, tight and tortuous lesions can be uncrossable before initial preparation.

Dedicated tools for the treatment of calcifications

Modern interventional cardiology has several instruments for treating coronary calcifications. These range from "gentle" devices such as the non-compliant high and very-high pressure balloon catheters, through scoring balloon (SB)/cutting balloon (CB), to more aggressive methods such as rotational/orbital atherectomy (OA) and intravascular lithotripsy (IVL). Non-compliant balloon catheters were designed to avoid the uncontrolled expansion of the well-known semi-compliant ones, which may lead to vessel dissection and/or perforation, especially in calcified lesions, due to easier expansion in lower resistance regions. Higher pressures can be used with the non-compliant catheters with rated burst pressure (usually about 20 atm). Special, ultra-high-pressure non-compliant balloons have a rated burst pressure of 35 atm; it is effective and safe in treatment of severely calcified lesions, which was demonstrated in OCT multicenter registry.[33] There is always a safety concern when using high pressure so as not to damage the vessel. Plenty of lesions remain resistant to high pressure inflations. The next step and more aggressive tools are SB and CB. The former is an encased spiral with wires on the balloon, while the latter is longitudinally covered with 3 or 4 blades, which are designed to damage coronary calcium and allow full balloon expansion before stent implantation. Cutting balloons have worse deliverability due to their larger crossing profile and low vulnerability of blades, especially in tight lesions, sometimes located distally and/or in angulated vessels. Both types have proven effective in better stent expansion.[34,35] Nevertheless, everyday practice shows that even these tools are insufficient when dealing with severe CAC.

The next step in the treatment of CAC is atherectomy. Currently, there are 2 methods available: rotational and orbital atherectomy. Rotational atherectomy (RA) has been known since 1988. This method uses olive-shape diamond coated burr between 1.25 and 2.5 mm in size. The procedure is conducted in burr runs, which can last up to 30 s, when the burr is gently moved forward-backward (pecking motion) on a RotaWire (Boston Scientific, Boston, USA) to modify calcium. The technique employs the new RotaPRO system (Boston Scientific), as opposed to the previous ROTABLATOR system (Boston Scientific). The new system is easier to use and more operator-friendly. The technique can be used in both stable CAD and ACS.[36,37] European,[38] North American[39] and Japanese[40] consensus documents describe how to safely and effectively use this tool. Two large, randomized trials assessing RA before stent implantation strategy were conducted. The PREPARE-CALC study[41] compared RA with the cutting and scoring balloons, whereas the RO-TAXUS study[42] compared RA with the standard therapy. Both trials proved the safety and feasibility of RA, as well as higher strategy success. Rotablation leaves behind specific calcium modifications such as semicircular marks in the exact size of the burr used (Fig. 5), sometimes combined with white thrombi (Fig. 6), fractures (Fig. 7,8) and dissections (Fig. 9). Combination of RA and CB results in better acute lumen gain and stent expansion compared to RA or SB/CB alone.[43]

Still under development, the OA technique introduced in 2013 uses a 1.25 mm diamond-coated crown mounted eccentrically and proximally to the tip of the shaft. Depending on the speed of the crown, it can be used in the treatment of vessels from 2.5 to 4 mm. In contrast to RA, OA provides bidirectional atherectomy. This method, like RA, ensures good PCI outcomes and procedure safety.[44] Rotablation and OA have never been directly compared in a reliable multicenter trial, so there is no way of knowing which atherectomy type is better or which exact type of lesion is better for which method. One small, nonrandomized study[45] compared 30 RA and 30 OA PCIs and showed a trend toward more frequent calcium modification with OA, especially in larger vessels, but it did not affect OCT results for the procedure.
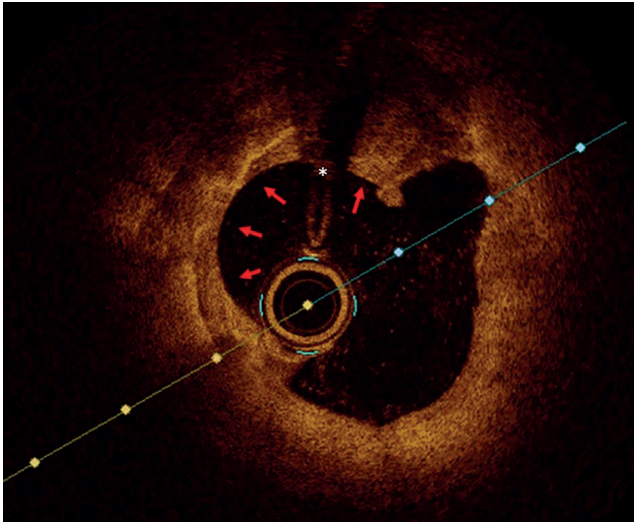
Fig. 5. Burr mark (red arrows) after 1.75 rotational atherectomy, wire artifact (white asterisk) – optical coherence tomography
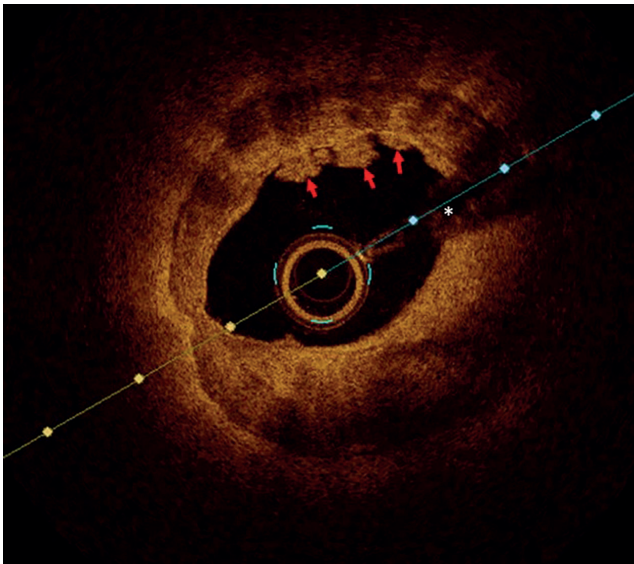

Fig. 7. Calcification fractures (red arrows), wire artifact (white asterisk) – optical coherence tomography

Fig. 6. White thrombi (red arrows) after rotational atherectomy, wire artifact (white asterisk) – optical coherence tomography

Fig. 8. Calcification fractures (red arrows), wire artifact (white asterisk) – intravascular ultrasound

The latest tool invented for dealing with CAC uses a well-known technique for treating nephrolithiasis. The Shockwave Intravascular Lithotripsy System (Shockwave Medical, Fremont, USA) employs ultrasounds to deliver sonic pressure waves that crush calcium located even in the deep layer of the artery. The crossing profile of IVL balloon catheters ranges from 0.043 to 0.046 inches (depending on the diameter – from 2.5 to 4.0 mm), which makes it useful in larger vessels. Its high efficacy and safety were shown in the Disrupt CAD III study.[46] Delivery of IVL catheter to tight as well as tortuous lesions is demanding and sometimes even unreachable. It could potentially be used to treat stent underexpansion[47] and stent restenosis associated with the formation of calcified plaque (Fig. 10).
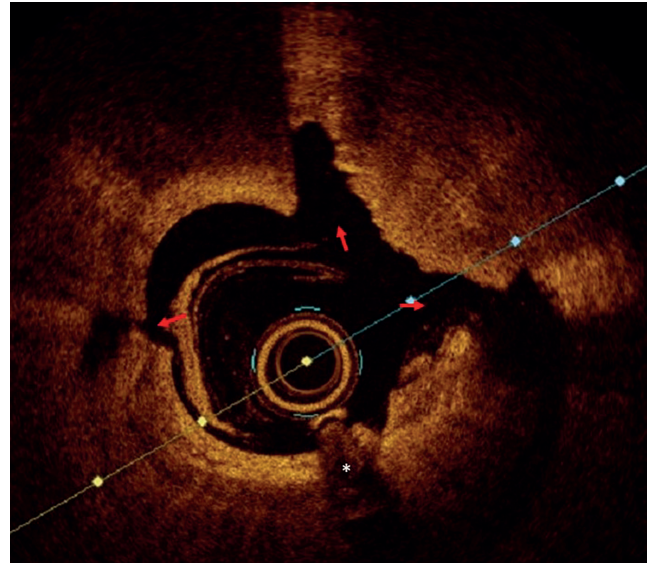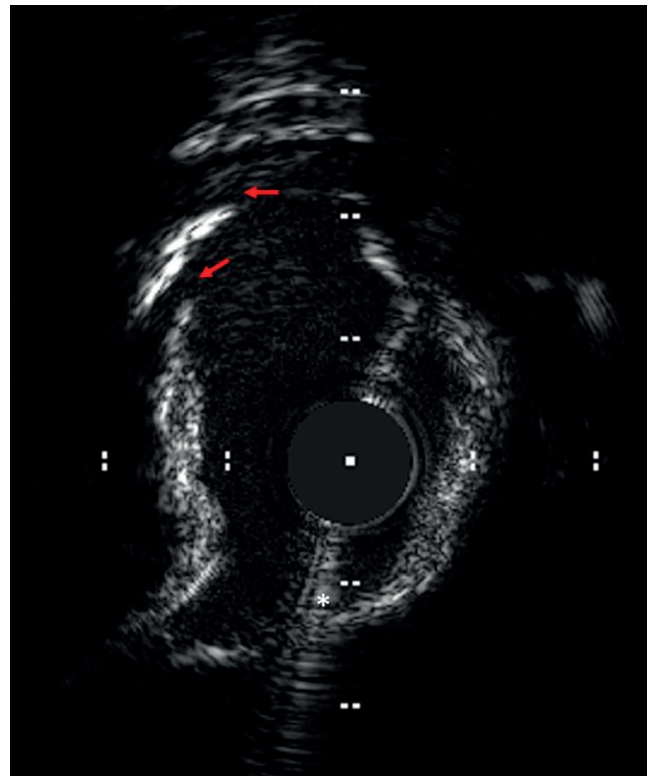
There is one more tool, i.e., coronary laser atherectomy catheter, which is sometimes considered for the treatment of CAC. It is rather helpful in the delivery of RA, OA and IVL[48] catheters, especially in tight stenoses, when wires cannot pass beyond the lesion. The manufacturer of the device predicts that it will be able to deal with moderately calcified stenoses.
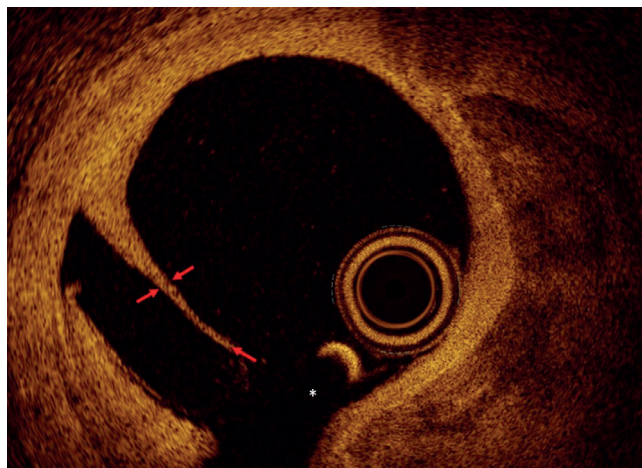
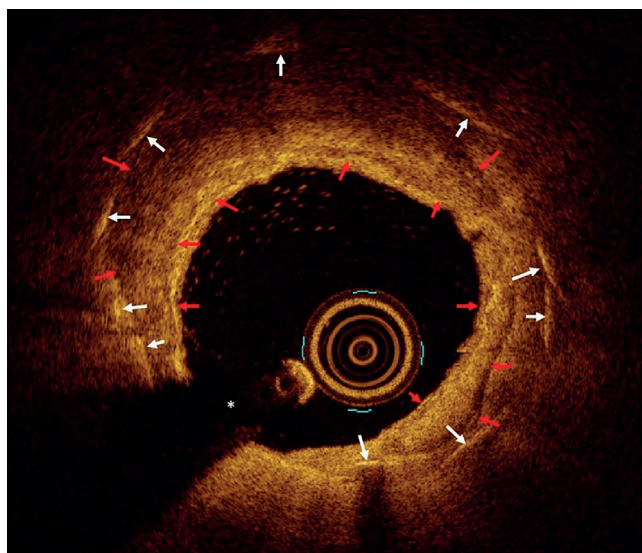Fig. 9. Dissection flap (red arrows), wire artifact (white asterisk)

Fig. 10. Calcified in-stent restenosis (red arrows), stent struts (white arrows), wire artifact (white asterisk) – optical coherence tomography

Percutaneous coronary intervention of calcified coronary lesions supported by ICI

Intracoronary imaging modalities provide a lot of data, which help to optimize percutaneous interventions. Calcium burden, its localization and diameters influence the final effect of PCI. Many papers demonstrated worse results of CAC procedures with higher rate of stent underexpansion,[4] stent apposition,[6] target vessel failure, stent thrombosis,[7] incomplete revascularization, mortality,[8] and major adverse cardiac events (MACE).[3] A recently published European consensus statement for heavily calcified coronary stenoses management,[38] as well as a document issued by the Japanese Association of Cardiovascular Intervention and Therapeutics (CVIT) on RA,[40] and the North American Expert Review of Rotational Atherectomy,[39] clearly advise to use ICI during PCI of calcified lesions. The researchers were looking for specific calcium parameters that

lead to worse outcomes. Henneke et al.[49] already in 1999 presented such a parameter, stent asymmetry, among patients with >180° IVUS calcium angle, in comparison with non-calcified lesions (p < 0.05). Another ultrasound-based study has shown less frequent proper stent apposition and higher rate of periprocedural non-Q-wave myocardial infarct among ≥270° angle calcified lesions than among <270° angle calcium lesions.[50] The next paper, published in 2014, using OCT measurements, pointed to the arc and area of the calcification as a predictor of stent expansion.[51] Patients with a greater arc of calcium had lower percentage of predicted minimal stent diameter and area (respectively, r = −0.37, p < 0.01; and r = −0.33, p < 0.02). Larger calcium area turned out to affect only the predicted minimal stent diameter (r = −0.38, p < 0.01), but not the minimal stent area (r = −0.26, p = 0.07). Lesions with >90° arc and >1.58 mm² calcium area had lower minimal stent diameter on the final OCT.

An innovative approach to assessing lesion calcium burden was introduced by Fujino et al.[52] The authors established OCT-based scale regarding 3 parameters: the arc of calcium, its length and thickness. A lesion is scored as follows: 2 points for >180° arc and 1 for >5 mm length, and one for ≥0.5 mm thickness of calcium. An analysis showed that the 4-point lesions indicate the worst stent expansion and seem to require specific plaque modification before stent implantation. Zhang et al.[53] published an IVUS-based scoring system for predicting stent underexpansion. The scale awarded 1 point for each >5 mm length of >270° calcium, the presence of CN and <3.5 mm vessel diameter. The cutoff that predicts underexpansion was 2 points, so ≥2 point lesions should be considered for preparation with dedicated devices for calcium modification. The abovementioned studies are in line with conclusions made by Wang et al.,[30] according to which minor calcifications did not affect the final stent expansion during PCI, and only major calcium burden requires additional tools to improve PCI outcomes.

Lesions that require additional tools have been described, but it is also important to know what can be achieved using them. Maejima et al.[54] assessed OCT images after rotablation and inflation of balloon catheter in 37 calcified coronary lesions. Results showed better stent expansion when OCT imaging revealed the presence of calcium fractures before stenting. Lesions with calcium fractures achieved greater stent cross-sectional area (7.38 ±1.92 mm² vs 7.13 ±1.68 mm²; p = 0.035) and lumen gain (3.89 ±1.53 mm² vs 3.40 ±1.46 mm²; p < 0.001). According to this study, the optimal calcium arc and thickness for predicting formation of fractures is 227° and 0.67 mm, respectively. The group of lesions with OCT fractures had thinner calcium (0.53 ±0.28 mm vs 1.02 ±0.42 mm; p < 0.001) with a larger arc (360°, interquartile range (IQR): 246–360° vs 147°, IQR: 118–199°; p < 0.001), which was also affirmed by Fujino et al.[52] An OCT-based study[55] on a new tool, IVL device, dedicated to calcified lesions, confirmed the link

between calcium burden and fracture formation. Another paper[56] indicated better stent expansion (minimal stent area of 5.02 ±1.43 mm^2 vs 4.33 ±1.22 mm^2; p = 0.047) when OCT calcium fractures were achieved. Moreover, it showed smaller angiographic diameter stenosis (19 ±27% vs 38 ±38%; p = 0.030), lower frequency of binary restenosis (14% vs 41%; p = 0.024) and ischemia-driven target lesion revascularization (7% vs 28%; p = 0.046) at 10-month follow-up in the group with primary fracture formation. Kobayashi et al.[57] similarly demonstrated that greater calcium damage resulted in better stent expansion. The formation of dissections was a predictor of greater MSA when RA was performed. Moreover, the minimal thickness of CAC in multivariable analysis turned out to be crucial for larger final MSA.

Furthermore, ICI provides other data to optimize PCI in calcified lesions. Intravascular ultrasound might help in the choice of the RotaWire: extra support or floppy in preparation for the rotablation.[58] Unlike angiography alone, the IVUS probe can show the precise position of the wire and its contact with the vessel structures. It is particularly helpful when dealing with angulated lesions. The fibrofatty and/or necrotic core component of the target plaque imaged by IVUS before intervention[59] and ineffective probe delivery through CAC[60] determine a higher probability of slow/no flow during PCI. Intracoronary imaging provides a lot of useful data about the treated vessel such as plaque morphology, calcium burden and vessel diameters, determining the intervention strategy and often identifying the need to change it during the procedure. Especially with regard to CAC, as one of the most complex problems in CAD treatment, there are benefits to the use of ICI. Roy et al.[61] showed that during IVUS-guided PCI with DES implantation, operators choose RA and CB more often than during CA-guided PCI alone. Moreover, ICI-guided RA PCI lowers 1-year MACE compared with CA-guided PCI (28.9 vs 4.3%; OR: 9.06, 95% CI: 3.82–21.52; p < 0.001), which is driven by the reduction of all-cause death (OR: 8.19, 95% CI: 2.15–31.18; p = 0.002), myocardial infarction (OR: 6.13, 95% CI: 2.05–18.3; p = 0.001) and target vessel revascularization (OR: 3.67, 95% CI: 1.13–11.96; p = 0.031). Procedural data analysis

shows that ICI guidance increases the number of burrs used (1.210 ±0.42 vs 1.070 ±0.31; p = 0.005) and the final diameter (1.50 mm (1.50–1.75) vs 1.50 mm (1.25–1.50); p = 0.001), as well as the length of the implanted stent (38.0 mm (30.0–53.7) vs 33.0 mm (22.0–49.0); p = 0.004) and its diameter 3.00 mm (3.00–3.50) vs. 2.75 mm (2.50–3.50); p < 0.001).[62]

Interventional cardiologists have multiple parameters to consider during CAC PCI, which are summarized in Table 2. Two studies on OCT vs IVUS-guided RA PCI showed better results using the former modality. Kobayashi et al.[63] analyzed 88 RA PCI, and the percentage of stent expansion was established as the primary endpoint. The OCT group achieved significantly better expansion (83 ±15% vs 72 ±16%; p = 0.0004) and outcomes due to frequent burr upsizing (55% vs 32%; p = 0.001), larger final burr (1.75 mm (1.50–1.75) vs 1.50 mm (1.50–1.75); p < 0.001) and more burrs used (2.0 mm (1.00–2.00) vs 2.0 mm (1.00–2.00); p < 0.001). Another smaller but also valuable study[64] compared 18 OCT and IVUS images taken after stent implantation in lesions requiring RA PCI. The results indicated better detection of stent malapposition and its extent (20% vs 6%; p < 0.001) in the OCT group, which led to additional post-dilatation and better final MSA (8.15 ±1.90 vs 7.30 ±1.62 mm^2; p < 0.05). In conclusion, the authors want to point to OCT as a method supported by literature for guiding PCI of calcified lesions, because it shows more details of the calcified plaque, has the above-mentioned scale established to predict the need to use an additional tool dedicated to calcified lesions, and better assesses results of such an intervention. Figure 11 presents a practical algorithm for the treatment of calcified lesions based on ICI.

Imaging-guided optimal stent implantation

Optimal stent implantation is the final step of PCI, and its outcome affects the patient's further prognosis. Intracoronary imaging provides very precise data about stent deployment and related complications. The European Intracoronary Imaging Consensus[17] established several points which should be assessed before and after stent implantation. When preparing for deployment, the operator

Table 2. Deciding parameters visualized with OCT and IVUS during CAC PCI

ICI	Primary imaging	Imaging before stent implantation
OCT	• calcium length ≥5 mm, arc ≥180° and thickness ≥0.5 mm: qualification for calcium modification tools, atherectomy or IVL • probe uncrossable lesion and/or fibrofatty/necrotic core component: slow/no flow suspected • determination of wire bias before atherectomy	calcium fractures, dissections: predicts good stent expansion
IVUS	• ≥2 of >5 mm calcium length, arc >270°, presence of CN, <3.5 mm vessel diameter >qualification for calcium modification tools, atherectomy or IVL • probe uncrossable lesion and/or fibrofatty/necrotic core component: slow/no flow suspected • determination of wire bias before atherectomy	calcium fractures, dissections: predicts good stent expansion

ICI – intracoronary imaging; OCT – optical coherence tomography; IVUS – intravascular ultrasound; CAC – coronary artery calcification; PCI – percutaneous coronary intervention; IVL – intravascular lithotripsy.
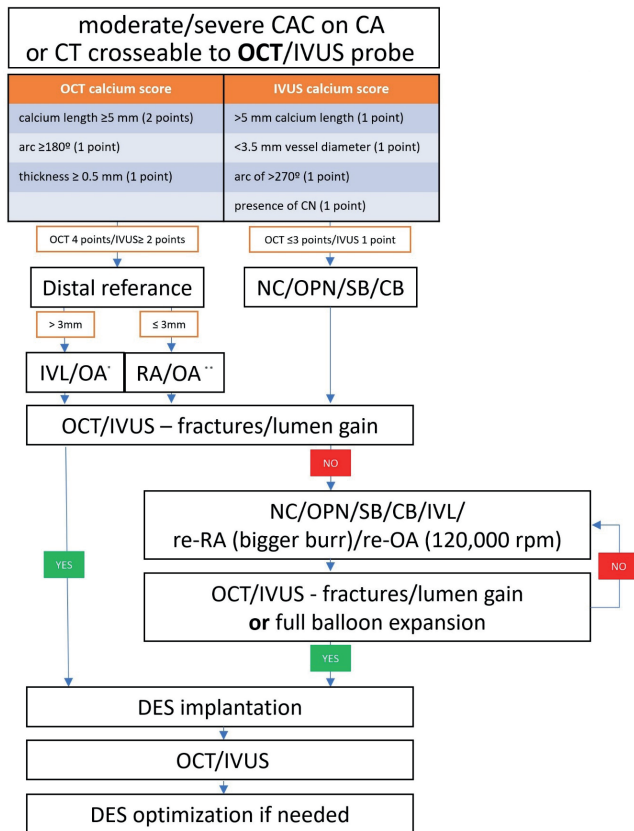
Fig. 11. Practical algorithm for the treatment of calcified lesions based on intracoronary imaging

CA – coronary angiography; CAC – coronary artery calcification; CB – cutting balloon; CN – calcified nodule; CT – computed tomography; DES – drog eluted stent; JVL – intravascular lithotripsy; IVUS – intramuscular ultrasound; NC – non-compliant balloon; OA – orbital atherectomy; OCT – optical coherence tomography; OPN – ultra-high-pressure non-compliant balloon; RA – rotational atherectomy; SB – scoring balloon; * 120,000 rpm; ** 80,000 rpm

ought to choose a proper landing zone. It cannot be located in a lipid-rich region, and the plaque burden cannot exceed 50%. Stent diameter sizing should depend on the distal reference measured with an external elastic membrane (EEM) or, if it cannot be sufficiently visualized (<180% of the EEM is invisible), a lumen-based diameter should be used. Stent size is selected based on the diameter of the EEM with rounding down to the nearest 0.25 mm or rounding up if only the lumen-based approach is viable. In cases of CAC and advanced atherosclerotic lesions, the EEM-based approach is usually not possible. Optimal stent deployment should provide >80% expansion (MSA/average reference lumen area) with MSA >5.5 mm^2 (on OCT) or >4.5 mm^2 (on IVUS) in a location other than the left main. Important aspects that were found to require further optimization are acute malapposition of the stent struts (exceeding >0.4 mm axially and > 1 mm in length), late-acquired malapposition, tissue prolapse (especially in ACS lesions), and dissection localized on the distal stent edge (>60° and >2 mm longitudinally with the involvement of media), which could be associated with local hematoma formation. The criteria

for proper stent implantation differ depending on the ICI modality. Based on the ULTIMATE trial,[20] the optimal IVUS image after stent deployment should meet the following criteria: >5.0 mm^2 of the minimal lumen area (MLA) or 90% of the distal reference MLA, <50% plaque burden proximally and distally to the stent, and no stent edge dissection longer than 3 mm, including the media layer. In OCT, on the other hand, optimal stent implantation depends on the ILUMIEN IV trial[26] and involves: ≥90% stent expansion in both proximal and distal parts, ≥270° visibility of the vessel EEL at both reference sites, no more than 10% intra-stent plaque protrusion/thrombus (protrusion area/stent area), stent edge dissection (≥60 degrees of the circumference of the vessel and ≥3 mm length), and ≥200 μm stent malaposition associated with unacceptable stent expansion. Obtaining a perfect image after PCI, especially in the case of severely calcified lesions, is usually extremely difficult, and additional post-dilatations to achieve the ideal image can result in vessel dissection and/or perforation. Operators should consider the possible losses and gains associated with attempting to achieve an excellent image.

Limitations

This review has some limitations. There is a lack of randomized studies that compare the results of CAC PCI based on OCT compared to IVUS, a shortage of randomized trials comparing dedicated methods to treat CAC head-to-head, and limited data on the exact goal of CAC preparation before stent implantation.

Conclusions

To sum up, ICI is a very safe and helpful tool during percutaneous treatment of calcified coronary lesions. Intracoronary imaging, and particularly OCT, can identify lesions requiring the use of additional tools dedicated to treating calcifications. During the procedure, ICI indicates the need for further calcium modifications. Moreover, even if an acceptable angiographic result of stenting is achieved, ICI often shows abnormalities requiring further improvement. However, imaging modalities are not free from limitations and lesions can still be over- or underestimated. Further studies are needed to improve imaging capabilities, especially IVUS precision and OCT penetration. Intravascular ultrasound provides good insight into deep structures of the vessel, but cannot show calcium parameters. Optical coherence tomography accurately shows structures, but only those localized not too deep, so it can be problematic to image large vessels, especially the left main stem. Efforts continue to combine OCT and IVUS to take advantage of the strengths of both methods. Further research is needed to advance coronary calcium imaging to improve PCI outcomes. The human factor in the assessment of obtained images certainly has an impact on the course

of treatment. This is the place for artificial intelligence, which will assist us in interpretation and decision making in the future. Furthermore, the combination of imaging and physiological measurements of stenosis will bring percutaneous treatment of CAC to the next level. The course of intervention, the choice of appropriate tools, and the combination of available techniques for dealing with calcium are still not fully explored. This is a major area for future research. In particular, calcium resistance during primary intervention remains a difficult problem for interventional cardiologists, and this topic requires further research.

ORCID iDs

Oscar Rakotoarison https://orcid.org/0000-0003-2971-8086
Tomasz Roleder https://orcid.org/0000-0002-1370-7369
Wojciech Zimoch https://orcid.org/0000-0003-4693-491X
Wiktor Kuliczkowski https://orcid.org/0000-0001-6284-0820
Krzysztof Reczuch https://orcid.org/0000-0002-1699-739X
Piotr Kübler https://orcid.org/0000-0003-2645-0475

References

1. Zimoch WJ, Kubler P, Kosowski M, et al. Patients with acute myocardial infarction and severe target lesion calcifications undergoing percutaneous coronary intervention have poor long-term prognosis. *Kardiol Pol*. 2017;75(9):859–867. doi:10.5603/KP.a2017.0093

2. Généreux P, Redfors B, Witzenbichler B, et al. Two-year outcomes after percutaneous coronary intervention of calcified lesions with drug-eluting stents. *Int J Cardiol*. 2017;231:61–67. doi:10.1016/j.ijcard.2016.12.150

3. Guedeney P, Claessen BE, Mehran R, et al. Coronary calcification and long-term outcomes according to drug-eluting stent generation. *JACC Cardiovasc Interv*. 2020;13(12):1417–1428. doi:10.1016/j.jcin.2020.03.053

4. Hoffmann R, Mintz G, Popma J, et al. Treatment of calcified coronary lesions with Palmaz–Schatz stents: An intravascular ultrasound study. *Eur Heart J*. 1998;19(8):1224–1231. doi:10.1053/euhj.1998.1028

5. Hemetsberger R, Gori T, Toelg R, et al. Optical coherence tomography assessment in patients treated with rotational atherectomy versus modified balloons: PREPARE-CALC OCT. *Circ Cardiovasc Interv*. 2021;14(3):e009819. doi:10.1161/CIRCINTERVENTIONS.120.009819

6. Tanigawa J, Barlis P, Mario CD. Heavily calcified coronary lesions preclude strut apposition despite high pressure balloon dilatation and rotational atherectomy in-vivo demonstration with optical coherence tomography. *Circ J*. 2008;72(1):157–160. doi:10.1253/circj.72.157

7. Hemetsberger R, Abdelghani M, Toelg R, et al. Impact of coronary calcification on clinical outcomes after implantation of newer-generation drug-eluting stents. *J Am Heart Assoc*. 2021;10(12):e019815. doi:10.1161/JAHA.120.019815

8. Bourantas CV, Zhang YJ, Garg S, et al. Prognostic implications of coronary calcification in patients with obstructive coronary artery disease treated by percutaneous coronary intervention: A patient-level pooled analysis of 7 contemporary stent trials. *Heart*. 2014;100(15):1158–1164. doi:10.1136/heartjnl-2013-305180

9. Andrews J, Psaltis PJ, Bartolo BAD, Nicholls SJ, Puri R. Coronary arterial calcification: A review of mechanisms, promoters and imaging. *Trends Cardiovasc Med*. 2018;28(8):491–501. doi:10.1016/j.tcm.2018.04.007

10. Madhavan MV, Tarigopula M, Mintz GS, Maehara A, Stone GW, Généreux P. Coronary artery calcification. *J Am Coll Cardiol*. 2014;63(17):1703–1714. doi:10.1016/j.jacc.2014.01.017

11. Saita T, Fujii K, Hao H, et al. Histopathological validation of optical frequency domain imaging to quantify various types of coronary calcifications. *Eur Heart J Cardiovasc Imaging*. 2016;18(3):342–349. doi:10.1093/ehjci/jew054

12. Ehara S, Kobayashi Y, Yoshiyama M, Ueda M, Yoshikawa J. Coronary artery calcification revisited. *J Atheroscler Thromb*. 2006;13(1):31–37. doi:10.5551/jat.13.31

13. Puri R, Libby P, Nissen SE, et al. Long-term effects of maximally intensive statin therapy on changes in coronary atheroma composition: Insights from SATURN. *Eur Heart J Cardiovasc Imaging*. 2014;15(4):380–388. doi:10.1093/ehjci/jet251

14. Torii S, Sato Y, Otsuka F, et al. Eruptive calcified nodules as a potential mechanism of acute coronary thrombosis and sudden death. *J Am Coll Cardiol*. 2021;77(13):1599–1611. doi:10.1016/j.jacc.2021.02.016

15. García-García H, Alfonso F. Intravascular ultrasound. In: *PCR-EAPCI Textbook*. Toulouse, France: Europa Digital & Publishing; 2020. https://www.pcronline.com/eurointervention/textbook/pcr-textbook/chapter/?chapter_id=89. Accessed February 6, 2022.

16. Prati F, Sticchi A, Regar E. Optical coherence tomography. In: *PCR-EAPCI Textbook*. Toulouse, France: Europa Digital & Publishing; 2021. https://www.pcronline.com/eurointervention/textbook/pcr-textbook/chapter/?chapter_id=90. Accessed February 6, 2022.

17. Räber L, Mintz GS, Koskinas KC, et al. Clinical use of intracoronary imaging. Part 1: Guidance and optimization of coronary interventions. An expert consensus document of the European Association of Percutaneous Cardiovascular Interventions. *Eur Heart J*. 2018;39(35):3281–3300. doi:10.1093/eurheartj/ehy285

18. Darmoch F, Alraies MC, Al-Khadra Y, Moussa Pacha H, Pinto DS, Osborn EA. Intravascular ultrasound imaging-guided versus coronary angiography-guided percutaneous coronary intervention: A systematic review and meta-analysis. *J Am Heart Assoc*. 2020;9(5):e013678. doi:10.1161/JAHA.119.013678

19. Zhang J, Gao X, Kan J, et al. Intravascular ultrasound versus angiography-guided drug-eluting stent implantation. *J Am Coll Cardiol*. 2018;72(24):3126–3137. doi:10.1016/j.jacc.2018.09.013

20. Gao XF, Ge Z, Kong XQ, et al. 3-year outcomes of the ULTIMATE trial comparing intravascular ultrasound versus angiography-guided drug-eluting stent implantation. *JACC Cardiovasc Interv*. 2021;14(3):247–257. doi:10.1016/j.jcin.2020.10.001

21. Kuku KO, Ekanem E, Azizi V, et al. Optical coherence tomography-guided percutaneous coronary intervention compared with other imaging guidance: A meta-analysis. *Int J Cardiovasc Imaging*. 2018;34(4):503–513. doi:10.1007/s10554-017-1272-2

22. Jones DA, Rathod KS, Koganti S, et al. Angiography alone versus angiography plus optical coherence tomography to guide percutaneous coronary intervention. *JACC Cardiovasc Interv*. 2018;11(14):1313–1321. doi:10.1016/j.jcin.2018.01.274

23. Kubo T, Akasaka T, Shite J, et al. OCT compared with IVUS in a coronary lesion assessment. *JACC Cardiovasc Interv*. 2013;6(10):1095–1104. doi:10.1016/j.jcmg.2013.04.014

24. Ali ZA, Maehara A, Généreux P, et al. Optical coherence tomography compared with intravascular ultrasound and with angiography to guide coronary stent implantation (ILUMIEN III: OPTIMIZE PCI): A randomised controlled trial. *Lancet*. 2016;388(10060):2618–2628. doi:10.1016/S0140-6736(16)31922-5

25. Ali ZA, Karimi Galougahi K, Maehara A, et al. Outcomes of optical coherence tomography compared with intravascular ultrasound and with angiography to guide coronary stent implantation: One-year results from the ILUMIEN III: OPTIMIZE PCI trial. *EuroIntervention*. 2021;16(13):1085–1091. doi:10.4244/EIJ-D-20-00498

26. Ali ZA, Landmesser U, Maehara A, et al. Optical coherence tomography–guided versus angiography-guided PCI. *N Engl J Med*. 2023;389(16):1466–1476. doi:10.1056/NEJMoa2305861

27. Kubo T, Tanaka A, Ino Y, Kitabata H, Shiono Y, Akasaka T. Assessment of coronary atherosclerosis using optical coherence tomography. *J Atheroscler Thromb*. 2014;21(9):895–903. doi:10.5551/jat.25452

28. Saito Y, Kobayashi Y, Fujii K, et al. Clinical expert consensus document on intravascular ultrasound from the Japanese Association of Cardiovascular Intervention and Therapeutics (2021). *Cardiovasc Interv Ther*. 2022;37(1):40–51. doi:10.1007/s12928-021-00824-0

29. Mintz GS, Popma JJ, Pichard AD, et al. Patterns of calcification in coronary artery disease: A statistical analysis of intravascular ultrasound and coronary angiography in 1155 lesions. *Circulation*. 1995;91(7):1959–1965. doi:10.1161/01.CIR.91.7.1959

30. Wang X, Matsumura M, Mintz GS, et al. In vivo calcium detection by comparing optical coherence tomography, intravascular ultrasound, and angiography. *JACC Cardiovasc Imaging*. 2017;10(8):869–879. doi:10.1016/j.jcmg.2017.05.014

31. Kume T, Okura H, Kawamoto T, et al. Assessment of the coronary calcification by optical coherence tomography. *EuroIntervention*. 2011;6(6):768–772. doi:10.4244/EIJV6I6A130

32. Mehanna E, Bezerra HG, Prabhu D, et al. Volumetric characterization of human coronary calcification by frequency-domain optical coherence tomography. *Circ J*. 2013;77(9):2334–2340. doi:10.1253/circj.CJ-12-1458

33. Pinilla-Echeverri N, Bossard M, Hillani A, et al. Treatment of calcified lesions using a dedicated super-high pressure balloon: Multicenter optical coherence tomography registry. *Cardiovasc Revasc Med*. 2023;52:49–58. doi:10.1016/j.carrev.2023.02.020

34. De Ribamar Costa J, Mintz GS, Carlier SG, et al. Nonrandomized comparison of coronary stenting under intravascular ultrasound guidance of direct stenting without predilation versus conventional predilation with a semi-compliant balloon versus predilation with a new scoring balloon. *Am J Cardiol*. 2007;100(5):812–817. doi:10.1016/j.amjcard.2007.03.100

35. Tang Z, Bai J, Su SP, et al. Cutting-balloon angioplasty before drug-eluting stent implantation for the treatment of severely calcified coronary lesions. *J Geriatr Cardiol*. 2014;11(1):44–49. doi:10.3969/j.issn.1671-5411.2014.01.012

36. Kübler P, Zimoch W, Kosowski M, Tomasiewicz B, Telichowski A, Reczuch K. Acute coronary syndrome: Still a valid contraindication to perform rotational atherectomy? Early and one-year outcomes. *J Cardiol*. 2018;71(4):382–388. doi:10.1016/j.jjcc.2017.10.012

37. Tomasiewicz B, Kubler P, Zimoch W, et al. Acute angulation and sequential lesion increase the risk of rotational atherectomy failure. *Circ J*. 2021;85(6):867–876. doi:10.1253/circj.CJ-20-1222

38. Barbato E, Gallinoro E, Abdel-Wahab M, et al. Management strategies for heavily calcified coronary stenoses: An EAPCI clinical consensus statement in collaboration with the EURO4C-PCR group. *Eur Heart J*. 2023;44(41):4340–4356. doi:10.1093/eurheartj/ehad342

39. Sharma SK, Tomey MI, Teirstein PS, et al. North American expert review of rotational atherectomy. *Circ Cardiovasc Interv*. 2019;12(5):e007448. doi:10.1161/CIRCINTERVENTIONS.118.007448

40. Sakakura K, Ito Y, Shibata Y, et al. Clinical expert consensus document on rotational atherectomy from the Japanese association of cardiovascular intervention and therapeutics. *Cardiovasc Interv Ther*. 2021;36(1):1–18. doi:10.1007/s12928-020-00715-w

41. Abdel-Wahab M, Toelg R, Byrne RA, et al. High-speed rotational atherectomy versus modified balloons prior to drug-eluting stent implantation in severely calcified coronary lesions: The randomized PREPARE-CALC trial. *Circ Cardiovasc Interv*. 2018;11(10):e007415. doi:10.1161/CIRCINTERVENTIONS.118.007415

42. Abdel-Wahab M, Richardt G, Joachim Büttner H, et al. High-speed rotational atherectomy before paclitaxel-eluting stent implantation in complex calcified coronary lesions. *JACC Cardiovasc Interv*. 2013;6(1):10–19. doi:10.1016/j.jcin.2012.07.017

43. Allali A, Toelg R, Abdel-Wahab M, et al. Combined rotational atherectomy and cutting balloon angioplasty prior to drug-eluting stent implantation in severely calcified coronary lesions: The PREPARE-CALC-COMBO study. *Cathet Cardio Intervent*. 2022;100(6):979–989. doi:10.1002/ccd.30423

44. Chambers JW, Feldman RL, Himmelstein SI, et al. Pivotal trial to evaluate the safety and efficacy of the orbital atherectomy system in treating de novo, severely calcified coronary lesions (ORBIT II). *JACC Cardiovasc Interv*. 2014;7(5):510–518. doi:10.1016/j.jcin.2014.01.158

45. Yamamoto MH, Maehara A, Karimi Galougahi K, et al. Mechanisms of orbital versus rotational atherectomy plaque modification in severely calcified lesions assessed by optical coherence tomography. *JACC Cardiovasc Interv*. 2017;10(24):2584–2586. doi:10.1016/j.jcin.2017.09.031

46. Hill JM, Kereiakes DJ, Shlofmitz RA, et al. Intravascular lithotripsy for treatment of severely calcified coronary artery disease. *J Am Coll Cardiol*. 2020;76(22):2635–2646. doi:10.1016/j.jacc.2020.09.603

47. Wańha W, Tomaniak M, Wańczura P, et al. Intravascular lithotripsy for the treatment of stent underexpansion: The multicenter IVL-DRAGON registry. *J Clin Med*. 2022;11(7):1779. doi:10.3390/jcm11071779

48. Jurado-Román A, García A, Moreno R. ELCA-Tripsy: Combination of laser and lithotripsy for severely calcified lesions. *J Invasive Cardiol*. 2021;33(9):E754–E755. PMID:34473078.

49. Henneke KH, Regar E, König A, et al. Impact of target lesion calcification on coronary stent expansion after rotational atherectomy. *Am Heart J*. 1999;137(1):93–99. doi:10.1016/S0002-8703(99)70463-1

50. Mosseri M, Satler LF, Pichard AD, Waksman R. Impact of vessel calcification on outcomes after coronary stenting. *Cardiovasc Revasc Med*. 2005;6(4):147–153. doi:10.1016/j.carrev.2005.08.008

51. Kobayashi Y, Okura H, Kume T, et al. Impact of target lesion coronary calcification on stent expansion: An optical coherence tomography study. *Circ J*. 2014;78(9):2209–2214. doi:10.1253/circj.CJ-14-0108

52. Fujino A, Mintz GS, Lee T, et al. Predictors of calcium fracture derived from balloon angioplasty and its effect on stent expansion assessed by optical coherence tomography. *JACC Cardiovasc Interv*. 2018;11(10):1015–1017. doi:10.1016/j.jcin.2018.02.004

53. Zhang M, Matsumura M, Usui E, et al. Intravascular ultrasound-derived calcium score to predict stent expansion in severely calcified lesions. *Circ Cardiovasc Interv*. 2021;14(10):e010296. doi:10.1161/CIRCINTERVENTIONS.120.010296

54. Maejima N, Hibi K, Saka K, et al. Relationship between thickness of calcium on optical coherence tomography and crack formation after balloon dilatation in calcified plaque requiring rotational atherectomy. *Circ J*. 2016;80(6):1413–1419. doi:10.1253/circj.CJ-15-1059

55. Ali ZA, Brinton TJ, Hill JM, et al. Optical coherence tomography characterization of coronary lithoplasty for treatment of calcified lesions. *JACC Cardiovasc Imaging*. 2017;10(8):897–906. doi:10.1016/j.jcmg.2017.05.012

56. Kubo T, Shimamura K, Ino Y, et al. Superficial calcium fracture after PCI as assessed by OCT. *JACC Cardiovasc Imaging*. 2015;8(10):1228–1229. doi:10.1016/j.jcmg.2014.11.012

57. Kobayashi N, Ito Y, Yamawaki M, et al. Optical frequency-domain imaging findings to predict good stent expansion after rotational atherectomy for severely calcified coronary lesions. *Int J Cardiovasc Imaging*. 2018;34(6):867–874. doi:10.1007/s10554-018-1300-x

58. Sakakura K, Yamamoto K, Taniguchi Y, Tsurumaki Y, Momomura SI, Fujita H. Intravascular ultrasound enhances the safety of rotational atherectomy. *Cardiovasc Revasc Med*. 2018;19(3):286–291. doi:10.1016/j.carrev.2017.09.012

59. Kume T, Okura H, Kawamoto T, et al. Assessment of the histological characteristics of coronary arterial plaque with severe calcification. *Circ J*. 2007;71(5):643–647. doi:10.1253/circj.71.643

60. Sakakura K, Taniguchi Y, Yamamoto K, et al. Comparison of the incidence of slow flow after rotational atherectomy with IVUS-crossable versus IVUS-uncrossable calcified lesions. *Sci Rep*. 2020;10(1):11362. doi:10.1038/s41598-020-68361-z

61. Roy P, Steinberg DH, Sushinsky SJ, et al. The potential clinical utility of intravascular ultrasound guidance in patients undergoing percutaneous coronary intervention with drug-eluting stents. *Eur Heart J*. 2008;29(15):1851–1857. doi:10.1093/eurheartj/ehn249

62. Wongpraparut N, Bakoh P, Anusonadisai K, et al. Intravascular imaging guidance reduce 1-year MACE in patients undergoing rotablator atherectomy-assisted drug-eluting stent implantation. *Front Cardiovasc Med*. 2021;8:768313. doi:10.3389/fcvm.2021.768313

63. Kobayashi N, Ito Y, Yamawaki M, et al. Optical coherence tomography-guided versus intravascular ultrasound-guided rotational atherectomy in patients with calcified coronary lesions. *EuroIntervention*. 2020;16(4):e313–e321. doi:10.4244/EIJ-D-19-00725

64. Gudmundsdottir I, Adamson P, Gray C, et al. Optical coherence tomography versus intravascular ultrasound to evaluate stent implantation in patients with calcific coronary artery disease. *Open Heart*. 2015;2(1):e000225. doi:10.1136/openhrt-2014-000225